UNIVERSITA' DEGLI STUDI DI NAPOLI "FEDERICO II"

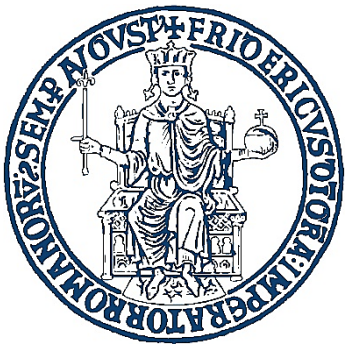

PhD thesis in Industrial Products and Process Engineering
(XXXI cycle)

"TUNEABLE HYDROGEL PLATFORM FOR OLIGONUCLEOTIDE BIOMARKERS DETECTION"

Tania Mariastella Caputo

Supervisors:
Prof. Dr. Paolo Antonio Netti
Prof. Dr. Filippo Causa
Advisor:
Dr. Edmondo Battista

Coordinator:
Prof. Dr. Giuseppe Mensitieri

2015 – 2018

TABLE OF CONTENTS

LIST OF FIGURES ..... **IV**
LIST OF TABLES ..... **VIII**
LIST OF ABBREVIATIONS ..... **X**

CHAPTER 1

ABSTRACT **1**

1. INTRODUCTION 3
   1.1 HYDROGELS IN BIOSENSING 3
      1.1.1. CLASSIFICATION OF HYDROGELS 5
      1.1.2. HYDROGEL MATERIALS 6
   1.2. PROBE IMMOBILIZATION 7
      1.2.1. DOUBLE STRAND PROBE 8
      1.2.2. MOLECULAR BEACON 11
   1.3. HYDROGEL CHARACTERISTICS FOR BIOSENSING 13
2. SYNTHESIS OF HYDROGELS 18
3. BIOMARKERS DESCRIPTION AND DETECTION BY HYDROGELS 21
4. AIM AND OUTLINE OF DISSERTATION 26

REFERENCES 28

CHAPTER 2

"TOEHOLD-MEDIATED STRAND DISPLACEMENT MICROGELS: BIOASSAY FOR CYTOMEGALOVIRUS INFECTION DIAGNOSIS" ***39***

1. INTRODUCTION 40
2. EXPERIMENTAL SECTION 41
   2.1. MATERIALS 41
   2.2. PROBE DESIGN 42
   2.3. MICROGEL SYNTHESIS AND FUNCTIONALIZATION 43
   2.4. FLUORESCENCE MEASUREMENT 43
   2.5. STATISTICAL ANALYSIS 45
3. RESULTS AND DISCUSSION 45
   3.1. PROBE DESIGN 45
   3.2. MICROGEL SYNTHESIS AND FUNCTIONALIZATION 48
   3.3. ASSAY SET-UP 50
4. CONCLUSION 55

REFERENCES 56

CHAPTER 3

"MOLECULAR BEACONS BIO-CONJUGATED MICROGELS: BIOASSAY FOR MIRNA BIOMARKER DETECTION IN CANCER" **60**

1. INTRODUCTION 61
2. EXPERIMENTAL SECTION 63
   - 2.1. MATERIALS 63
   - 2.2. MOLECULAR BEACON DESIGN 63
   - 2.3. MICROGEL SYNTHESIS 64
   - 2.4. MOLECULAR BEACONS CONJUGATION 65
   - 2.5. SPECIFICITY 65
   - 2.6. MICROGEL ASSAY. 66
   - 2.7. HUMAN SERUM ANALYSIS 66
   - 2.8. STATISTICAL ANALYSIS 67
3. RESULTS AND DISCUSSION 67
   - 3.1. MOLECULAR BEACON DESIGN 67
   - 3.2. MICROGEL SYNTHESIS AND BIOCONJUGATION. 71
   - 3.3. ASSAY SENSITIVITY AND KINETICS 72
   - 3.4. ASSAY SPECIFICITY 77
   - 3.5. HUMAN SERUM ASSAY 79
4. CONCLUSION 81

REFERENCES 82

APPENDIX 86

CHAPTER 4

"MICROGELS FOR LONG OLIGONUCLEOTIDE SEQUENCE DETECTION" ***89***

1. INTRODUCTION 90
2. EXPERIMENTAL SECTION 91
   - *2*.1. MATERIALS 91
   - 2.2. PROBE DESIGN 91
   - 2.3. MICROGEL SYNTHESIS AND BIOCONJUGATION 93
   - 2.4. MICROGEL ASSAY 93
   - 2.5. STATISTICAL ANALYSIS 94
3. RESULTS AND DISCUSSION 96
   - 3.1. DOUBLE STRAND-MICROGEL ASSAY 96
   - 3.2. MOLECULAR BEACON-MICROGEL ASSAY 101
4. CONCLUSION 111

REFERENCES 112

CHAPTER 5

"3D-HYDROGEL MICROPARTICLES: MIX-READ BIOASSAY FOR OLIGONUCLEOTIDE DETECTION. CASE STUDY OF MIR-143-3P DETECTION AS EARLY BIOMARKER IN AMYOTROPHIC LATERAL SCLEROSIS" **..... 114**

1. INTRODUCTION 115
2. EXPERIMENTAL SECTION 117
   - 2.1. PROBE DESIGN AND DENSITY 117
   - 2.2. MICROFLUIDIC SYNTHESIS OF 3D-HYDROGEL MICROPARTICLES AND CHARACTERIZATION 119
   - 2.3. ASSAY SET UP IN BUFFER AND HUMAN SERUM 121
   - 2.4. SPECIFICITY ASSAY 121
   - 2.5. STATISTICAL ANALYSIS 121
3. RESULTS AND DISCUSSION 122
   - 3.1. PROBE DESIGN AND DENSITY OPTIMIZATION 122
   - 3.2. THREE-DIMENSIONAL HYDROGEL MICROPARTICLES SYNTHESIS 128
   - 3.3. ASSAY SET-UP AND HUMAN SERUM ANALYSIS 131
   - 3.4. ASSAY SENSITIVITY AND SPECIFICITY 132
4. CONCLUSION 135

REFERENCE 136

CHAPTER 6

CONCLUSIONS AND FUTURE PERSPECTIVES 140

LIST OF FIGURES

CHAPTER 1

Figure 1 Histogram showing the increase in publications related to the keyword “hydrogel” “biosensor” during the past 30 years. PubMed data 4
Figure 2 Classification of hydrogels.....6
Figure 3 Double strand toehold mediated displacement assay. A) double strand probe structure. B) mechanism of displacement mediated by toehold domains; C) Strand displacement rate constant plotted against toehold length and composition (A/C Reprinted from Nat. Chem 2011 reference 38;-Reprinted from J. Am. Chem. Soc. 2009 ref 37;). 9
Figure 4 Constant dissociation Kd predicted from solution-phase thermodynamic parameters(lines) compared with those determined experimentally (empty circle) (Reprinted from Nucleic Acid Research, 1999, reference 42) 10
Figure 5 Acridyte™ group attached to oligonucleotide.....11
Figure 6 Phase transitions of molecular beacons with targets in solution. Phase 1: fluorescent molecular beacon–target duplex; phase 2: nonfluorescent stem–loop hairpin; and phase 3: fluorescent random coil (Reprinted from Springer. 2013, reference 51).....12
Figure 7 Swelling of hydrogel PEGDA microparticles synthetized with different molecular weight of starting monomer (Reprinted from Biomed. Microdevices, 2008, reference 95).....15
Figure 8 Hydrogel particles. A) Core–shell microgels obtained by free-radical polymerization and seeded polymerization (Reprinted by J. Am. Chem. Soc., 2015, reference 41; B) Hydrogel microparticles obtained by droplet generation; C) Flow-focusing microfluidic droplet generation device (Reprinted from Colloids Surf B Biointerfaces, 2016, reference 113); E) Microparticles synthetized by stop-flow lithography technique (Reprinted from Nat. Mater, 2006, 116); F) Janus particles by stop-flow lithography (Reprinted from Appl. Mater. Today, 2017, reference 117); F) Stop flow lithography mechanism (Reprinted from Nat. Mater, 2006, 116).....21
Figure 9 Relation of biomarkers to other technologies and health care (Reprinted from Springer, 2010, reference 120).....22
Figure 10 Circulating DNA is released in the serum of cancer patient by apoptosis, necrosis or secretion from the cancer cells. The DNA circulating in human fluid have different size and is affected by mutation, methylation or alterations. Moreover, viral DNA is also detectable in some tumor caused by virus such as human papillomavirus (HPV), hepatitis B virus (HBV) and Epstein–Barr virus (EBV) (Reprinted from Nat Rev Cancer, 2011, 140)……23

CHAPTER 2

Figure 1 Overview of the assay: A) Double strand probe is designed based on specific biomarker selection. B) Microgel functionalization and fluorescence recovery mechanism involved in target detection. C) Microgels assay working range (nM-aM) and D) LOD tunability is based on the number of microgels used for assay. 45
Figure 2 A) Representation of alignment results for hcmv-miRUS4-5p calculated by mirbase.org B)Fluorescence emission intensity of the tail labelled strand(F, 5nM) and duplex tail-quencher strand (QF, 5nM 1:1 ratio). . C) Fluorescence recovery as a function of time in toehold-mediated strand displacement assay after addition 5nM (empty circle) and 50 nM (full circle) of hcmv-miR-US4-5p target, in homogeneous condition; D) Fluorescence recovery in presence of 10-fold excess of non-matching miRNA alone (black column) and mixed with the target (red column) 46
Figure 3 A-B) Quencher strand (Q) and C) Tail strand (T) folding simulations and their relative free energy.....47
Figure 4 A) Schematic representation of the toehold mediated strand displacement assay on microgel beads; B) Fluorescence intensity measured for 50μg/mL of microgels with different functionalization grade before the quenching step. In the inset, coupling efficiency obtained for a fixed fluorescent tail and microgels amount increasing the EDC concentrations. Data are presented as fluorescence ratio between the reporter (Atto647N) and the reference dye(Rhodamine); C) Quenching efficiency of the above-mentioned functionalised microgels; D) Fluorescence recovery as a function of time in toehold mediated strand displacement assay after addition 5nM (empty circle) and 50 nM (full circle) of hcmv-miR-US4-5p target.....50

Figure 5A) Images collected by CLSM and B) analysed with the software dedicate; Fluorescence intensity recovery, in presence of hcmv-miR-US4-5p (106-10-1 fM) obtained using with 50µg/mL (C), 25µg/mL (D) and 0.5µg/mL(E) of microgels 51
Figure 6 A) Microgels fluorescence recovery measured by spectrofluorometer: using 50 and 25 µg/mL of microgels. B) Comparison between homogenous (5nM of free double strand probe, empty square) and heterogeneous (50µg/mL of functionalised microgels, full black square) assay in human serum in presence of excess of target (50nM); C) Microgel stability measured over a range of 1 years. Black square corresponding to quenched microgels, while red dots to un-quenched microgels. Data are presented as fluorescence intensity ratio between the reporter (Atto647N) and the reference dye(Rhodamine).....52
Figure 7 FACS measurements: A) Microgel without functionalization; B) Unquenched microgel; C) Quenched microgel 54

CHAPTER 3

Figure 1 Folding simulation prediction of MBS5 and MBS6 and predicted thermodynamic parameters.....68
Figure 2 Hybridization kinetics of molecular beacon MBS5 (A) and MBS6(B) in the presence of wild-type target miR-21 in hybridization buffer at rt. 68
Figure 3 Melting and annealing profiles of MBS5(A) and MBS6 (B). Molecular beacons were melted from 20 to 95°C (red circle) and annealed (black square) in hybridization buffer. Moreover, MBS5 and MBS6 were priory melted to 95°C and then annealed until 20°C in presence of 500nM (10fold excess respect to MB) of miR-21 wild type (blue triangle). 69
Figure 4 Hybridization kinetics of molecular beacon MBS5 (A) and MBS6 (B) in the presence of wild-type and mutants miR-21.....69
Figure 5 Melting and annealing profiles of MBS5 (A) and MBS6 (B). Molecular beacons were melted from 20 to 95°C and then annealed until 20°C in presence of 500nM (10fold excess respect to MB) of miR-21 wild type, mutated miR-21 (-1-a, -1-b, -2, -3) and non-matching miR-143. 70
Figure 6 Signal-to-noise ratio of MBS5 (A) and MBS6(B) at different functionalization degree.....72
Figure 7 MBS5-microgels (red) and MB6-microgels (green) assay performances. A -B) microgels coupled with 1nmol, C-D) 0.5nmol and E-F) 0.1nmol of molecular beacons.....73
Figure 8 Target detection performances of mb-microgels with concentration scaled to 0.5ug/mL.....74
Figure 9 MBS5-(A) and MBS6-(B) microgels kinetic of hybridizations measured by spectrofluorometer.....75
Figure 10 MBS5(A) and MBS6(B) kinetic of hybridizations measured by confocal microscope.....76
Figure 11 MBS5-microgels specificity tested towards wild-type miR-21, four mutated miR-21 sequences and a non-matching sequence (miR-143). 77
Figure 12 MBS6-microgels specificity tested towards wild-type miR-21, four mutated miR-21 sequences and a non-matching sequence (miR-143). 78
Figure 13 Mb-microgels assay in human serum. Fluorescence ATTO 647N intensity value is normalized to the rhodamine intensity.....79
Figure 14 Signal-to-ratio of MBS5-microgels calculated by CLSM in PBS and in serum and by FACS 80

CHAPTER 4

Figure 1 Ds-Probe study: folding simulation (P1-A, P2-B), fluorescence analysis (P1-C, P2-D) and kinetics of hybridizations (P1-E, P2-F).....97
Figure 2 Cross-reactivity experiments: ds-P1 (A) and ds-P2 (B) probes were monitored in presence of the correspondent homologous Target ss P2 and P1(black square). After that, the specific target P1(blue square) and P2 (red square) is added and fluorescence emission collected for the following 24hours.....98
Figure 3 Fluorescence intensity measured by CLSM of quenched and unquenched probe P1 (A) and P2(B).....98
Figure 4 Double strand probe functionalized microgels performance. Fluorescence intensity recovery measure for P1-(A) and P2-microgel -(C) after addition of the target and their correlated percentage of displacement(P1-B/P2-D).....99
Figure 5 Kinetic of displacement of P1- and P2-microgels.....100

Figure 6 Folding simulation of the target ss P1 (A) and P2(B). The arrows indicate the target sequence complementary to the loop of the Molecular Beacon P1(C) and Molecular Beacon P2(D) 101
Figure 7 Melting curve and hybridization kinetics of molecular beacon used in this study. Melting profile of MBP1(A) and MBP2 (C) is obtained plotting the normalized fluorescence intensity as function of the temperature. In the inset is plotted the folded fraction vs the temperature. The melting point (Tm) is the inflection point of the curve. Kinetic of hybridization of MBP1 (B) and MBP2(D). in the inset the melting curve of the solution. 102
Figure 8 Titration curve of MBP1(A) and MBP2 (B). from the fitting of the curve is calculated the specific kd of each molecular beacon. 103
Figure 9 Cross-reactivity experiments: MBP1 (A) and MBP2 (B) probes were monitored in presence of the correspondent homologous Target ss P2 and P1(black square). After that, the specific target P1(blue dots) and P2 (red dots) is added and fluorescence emission collected for the following 24hours. 104
Figure 10 Molecular beacon bioconjugated microgels performances in long oligonucleotide target detection. MBP1- (A) and MBP2- (B) microgel with 0.1nmol functionalization (L); MBP1-(C) and MBP2- (D) microgel with 0.25nmol functionalization (M); MBP1- (E) and MBP2- (F) microgel with 0.5nmol of functionalization (H). 105
Figure 11 Kinetic of hybridization of MBP1 (A) and MBP2(B). Fluorescence recovery of low(L), medium(M) and high(H) functionalized microgels was recorder in the time, mixing 50ug/mL of microgels with 500nM of Target (111nt). 106
Figure 12 Hybridization kinetics and melting curve and of MBP1 and MBP2 in presence of the short Target P1 and P2 106
Figure 13 MBP1-microgels cross-reactivity experiment results (A). Molecular beacon bio-conjugated microgels performances in short oligonucleotide target detection measured for MBP1- (L) 0.1nmol of immobilized probes (B); MBP1- (M) 0.25nmol -(C); and MBP1- (D) 0.5nmol (H). 107
Figure 14 MBP2-microgels cross-reactivity experiment results (A).Molecular beacon bio-conjugated microgels performances in short oligonucleotide target detection measured for MBP1- (L) 0.1nmol of immobilized probes (B) and MBP1- (M) 0.25nmol -(C). D) Folding prediction of the short target P2. 108
Figure 15 Kinetic of hybridization of MBP1 (A) and MBP2(B). Fluorescence recovery of mb-microgels was recorder in the time, mixing 50ug/mL of microgels with 500nM of short Target (P1-24nt; P2 23nt). 109

CHAPTER 5

Figure 1 Folding simulation of the Tail(A) and Quencher(B)r strands using UNAFold and setting 50nM of oligonucleotide, 200mM of NaCl and 25°C as parameters. 122
Figure 2 QF* probe/miR-143-3p kinetic of hybridizations 123
Figure 3 A)Fluorescence quenching titration to calculate kb of the probe. The stoichiometric ratio was determined by the intersection point of two straight lines extended, respectively, from the initial linear part and the plateau part of the titration curve. B) Melting profile, in the inset QF*probe annealing and melting curve 124
Figure 4 Mechanism of target detection used to analyse the probe in solution and in bulk 124
Figure 5 Quenching of fluorescence *QFb in PEGDA 10% (A) and 20% (B). Each step was collected after 3 days of incubation. 125
Figure 6 Kinetic of quenching in PEGDA 10%-15%-20% with several oligonucleotides concentrations: (a) F* 1μM- Q* 1x; (b) F* 1μM- Q* 5x; (c) F* 5μM-Q* 1x; (d) F* 5μM- Q* 5x. 126
Figure 7 Bulk displacement efficiency 127
Figure 8 Target detection mechanism in 3D-hydrogel microparticles 128
Figure 9 A) Schematic representation of microfluidic synthesis set-up for microparticles production; UV free radical photopolymerization between PEGDA and methacrylate oligonucleotide 129
Figure 10 A) Geometry and size of the Dolomite chip; B)Droplet generation by microfluidic T-junction device 129
Figure 11 A)Size distribution of functionalized microparticles (PEGDA 10%, 15%, 20%) w/v); B) Optical image of monodisperse microparticles; Swelling parameters (Q, ξ, Mc) for different polymer concentrations 130
Figure 12 A)Plot profile of fluorescence intensity of Oligonucleotide diffusion in microparticles. B) Time lapse of fluorescence intensity (I/I_{max}) of miR-143-3p and BSA. All values reported show a standard deviation of 10%. 131

Figure 13:(a)Fluorescence intensity measured during the hydrogel based assay setup and (b) the corresponding CLSM images. In particular, the figure shows the fundamental steps involved in the target detection: (I) after the synthesis of functionalized hydrogel; (II) when the fluorescent DNA strand was added; (III) in presence of the target in hybridization buffer and (IV) in human serum.....132
Figure 14 (a) MiR143-3p capture efficiency by Hydrogel beads assay and (b) corresponding fluorescence intensity turn-off (c) Images collected by CLSM for the target concentration analysed (Scale bars: 100 μm). 133
Figure 15 Specificity of 3D-hydrogel microparticles. 134

LIST OF TABLES

CHAPTER 1

Table 1 Hydrogel based bioassays for Nucleic acid detection 25

CHAPTER 2

Table 1 Oligonucleotide sequences used and their thermodynamic parameters (predictions calculated setting: 5nM of DNA, 200mM of Na+, pH 7-8, 5°C). 42
Table 2 Hydrodynamic diameter (Dh) and ζ potential measurement of microgels 49
Table 3 Non-linear regression data analysis for ds displacement assay and microgel-based assay performed in presence of hcmv-miR-US4-5p target.by confocal laser scanner microscopy. 53
Table 4 Non-linear regression data analysis for ds displacement assay and microgel-based assay performed in presence of hcmv-miR-US4-5p target by Fluorimeter 53

CHAPTER 3

Table 1 Molecular beacons and target sequences tested 64
Table 2 Melting temperature (Tm) predicted and calculated of MBS5 and MBS6. The temperatures refer to 50mM of molecular beacons in PBS buffer without the addition of miR or mixed with 500nM miR. 70
Table 3 Data analysis for mb-microgels assay 74
Table 4 Data analysis for mb-microgels assay 75
Table 5 FACS analysis results 80

CHAPTER 4

Table 1 Sequence, length, modifications and thermodynamic parameters of the DNA probes and targets used in microgel assay. All parameters are calculated by IDT-Integrated, D. N. A. "Technologies. OligoAnalyzer 3.1. Web setting respectively 50nM and 200mM as oligonucleotide and Na^+concentration. 95
Table 2 Data analysis of ds-microgel assay 100
Table 3 Data analysis of Molecular Beacon P1-microgel assay. MBP1-microgels (with 0.1nmol (L), 0.25nmol (M) and 0.5nmol (H) bioconjugation density) are tested in presence of long single strand oligonucleotide Target or the correspondent short target 109
Table 4 Data analysis of Molecular Beacon P2-microgel assay. MBP2 microgels (with 0.1nmol (L), 0.25nmol (M) and 0.5nmol (H) bioconjugation density) are tested in presence of long single strand oligonucleotide Target or the correspondent short target. 109

CHAPTER 5

Table 1 Sequence, length, modifications and thermodynamic parameters of the DNA probes and RNA targets used in solution and in 3D-hydrogel microparticles assay. All parameters are calculated by IDT-Integrated, D. N. A.

"Technologies. OligoAnalyzer 3.1. Web setting respectively 50nM and 350mM as oligonucleotide and Na^+concentration. TF/QF*hyb represent the free energy gained from the partially complementary T-DNA/F-DNA or F*probe/Q*probe duplex; FTarthyb/*QTarhyb is the free energy gained from the fully complementary Target/F-DNA or Target/Q*probe duplex; Δdisplacement is the free energy gained after T-DNA/F-DNA de-hybridization and Target/F-DNA hybridization 119

Table 2 Sequence, length, modifications and thermodynamic parameters of the DNA probes and RNA targets used in bulk assay. All parameters are calculated by IDT-Integrated, D. N. A. "Technologies. OligoAnalyzer 3.1. Web, setting respectively 50nM and 350mM as oligonucleotide and Na+ concentration 119

Table 3 Data analysis for 3D-hydrogel microparticles assay 133

CHAPTER 6

Table 1 Technology properties of the hydrogel microparticles proposed in the thesis 142

LIST OF ABBREVIATIONS

POC	Point-Of-Care
PEG	PolyEthylene Glycol
UV	Ultra Violet
DNA	Deoxyribose Nucleic Acid
RNA	Ribose Nucleic Acid
miRNAs	Micro RNA
lncRNA	Long non coding RNA
ctDNA	circulating tumor DNA
MB	molecular beacon
PCR	Polymerase Chain Reaction
qRT-PCR	Quantitative Reverse Transcriptase-PCR
LOD	Limit of detection
LOQ	Limit of quantification
Kd	Constant of dissociation
PDMS	PolyDiMethylSiloxane
EDC	1-ethyl-3-(3-dimethylaminopropyl) carbodiimide
v2	Polymer Volume Fraction
Mc	Molecular weight between crosslinks
ξ	Mesh size
PEGDMA	PolyEthylene Glycol DiMethacrylate
AAc	Acrylic Acid
KPS	Potassium PerSulfate
ΔG_d	Free Energy of displacement
Fluo	Fluoresceine O-methacrylate
PVA	PolyVinyl Alcohol
Rhod	Methacryloxyethyl thiocarbamoyl rhodamine B
DMSO	Dimethyl Sulfoxide
DLS	Dynamic Light Scattering
Dh	Hydrodinamic Diameter

PEGDA	PolyEthylene Glycol DiMethacrylate
BSA	Bovine Serum Albumin
D	Diffusion coefficient
Rh	Hydrodinamic Radius
nt	Nucleotide
mer	Length of oligonucleotide
BHQ	Black Hole Quencher
BBQ	BlackBerry Quencher
Ca	Capillary Number
LMO	Light Mineral Oil
TWEEN 20	Polyethylene glycol sorbitan monolaurate
CLSM	Confocal Laser Scanning Microscope
SEM	Scanning Electron Microscope
λex	Excitation wave length
λem	Emission wave length
PBS	Phosphate Buffered Saline
I	Fluorescence Intensity

ABSTRACT

Early detection of circulating biomarkers in human fluids can improve the quality of life reducing the development of several deadliest diseases. Among the latest and most significant medical concept "Liquid Biopsy" is emerging as non-invasive method of gleaning insight into the dynamics of diseases through a patient fluid sample. Actually many tests have been developed in this context, however, despite all the efforts, the majority are complex, require extensive manipulations and skilled operators, failing for point of care *(POC)* applications.

The main focus of this thesis has been devoted to develop advanced technologies, based on a hydrogel platform, properly designed for biosensing application. In particular, PEG engineered hydrogel microparticles have been synthetized with different chemical strategies and functionalized with oligonucleotide probes to detect circulating biomarker in human serum. In this thesis, the parameters affecting the hydrogel biosensing properties have been carefully evaluated to obtain an accurate functionalized network capable of sensitive and specific biomarker recognition. The developed hydrogel assays are based on the optical fluorescence read out over a single microgel, fixed the number of microgels and sample volume for each test. Therefore, the target concentration is easily quantified comparing the fluorescence observed with a calibration curve.

The thesis starts with the description of a microgel-based bioassay for Cytomegalovirus infection diagnosis (*Chapter 2*). The bioassay is based on microgels, with core-shell architecture, endowed with optical fluorescence probes for the recognition of circulating endogenous viral hcmv-miR-US4-5p. In particular, a double strand is used as probe and the recognition is driven by a toehold strand displacement mechanism whit a consequent fluorescence recovery after target capture. The performances of optical detection in terms of dynamic range and limit of detection are finely tuned changing the number of microgels per assay. As results, the limit of detection (LOD) is tuned from fM to aM by 100-fold decreasing the microgel concentration. The assay results specific for the selected target, suitable for several laboratory equipment, stable over a one-year span time and not affected by the presence of serum. Then, a microgel-based bioassay is described for microRNA biomarker detection in cancer application (*Chapter 3*). In this case, the outmost shell of microgel is functionalized with molecular beacons for circulating miR-21 recognition. The probe design is opportunely projected to reduce the interferences at the surface and the probe density is tuned to minimize the crowding effect. The molecular beacon-microgels assay is resulted very sensitive reaching fM LOD in 3 hours, without preliminary amplification step and using only 20 µL of sample. In addition, the microgel assay is extremely specific towards single mutated targets (SNP). The versatility, the stability in presence of high concentrations of interfering oligonucleotides and capability of work in human serum make the assay very interesting for biosensing application.

Is hydrogel-based technology also suitable for long oligonucleotide sequence detection? Yes, it is, and in *Chapter 4* are elucidated the main parameters taken into consideration to develop sensitive and specific microgel-based assay for long oligonucleotide detection, as lncRNA, mRNA or DNA. In particular, in this study are considered two DNA sequences of 111 nucleotides, with 70% of sequence similarity. Core-shell microgels are functionalized with double strand or molecular beacon probes and their performance compared. Microgels functionalized with molecular beacons have achieved femtomolar LOD, high specificity toward the similar sequence and rapid time of analysis avoiding sample manipulation.
Finally, is described the design of Three-dimensional hydrogel microparticles by microfluidics for the detection of microRNA and in particular is presented a case study of miR-143-3p detection as early biomarker in Amyotrophic lateral sclerosis (*Chapter 5*). The pivotal steps involved in the design of these 3D hydrogels, homogeneously functionalized into their whole volume, are explained. The design of the immobilized DNA probes and their density are opportunely optimized. Furthermore, the diffusion into the polymer network is tuned adjusting the polymer concentration and consequently the characteristic mesh size. Once these parameters have been set, 3D-hydrogels are synthetized in microfluidics, armed with fluorescent probes and then mixed with the sample solution. Target detection is achieved by double strand displacement assay associated with a fluorescence depletion within the hydrogel microparticles. The optimization of synthesis parameters has allowed to obtained 3D-hydrogel microparticles with wide working range, pM LOD and good specificity. Moreover, due to the PEG anti-fouling property, target detection occurs in human serum with performance comparable to those observed in PBS buffer.

Therefore, the biosensing platform obtained using engineered hydrogels can represent a smart technology capable to predict, identify and follow-up several diseases, monitoring free circulating oligonucleotides in body fluids. The flexible use of these engineered hydrogels, which avoid sample manipulation and can be easily integrated in miniaturized device for optical readout, aims to push these technologies as point of care device.

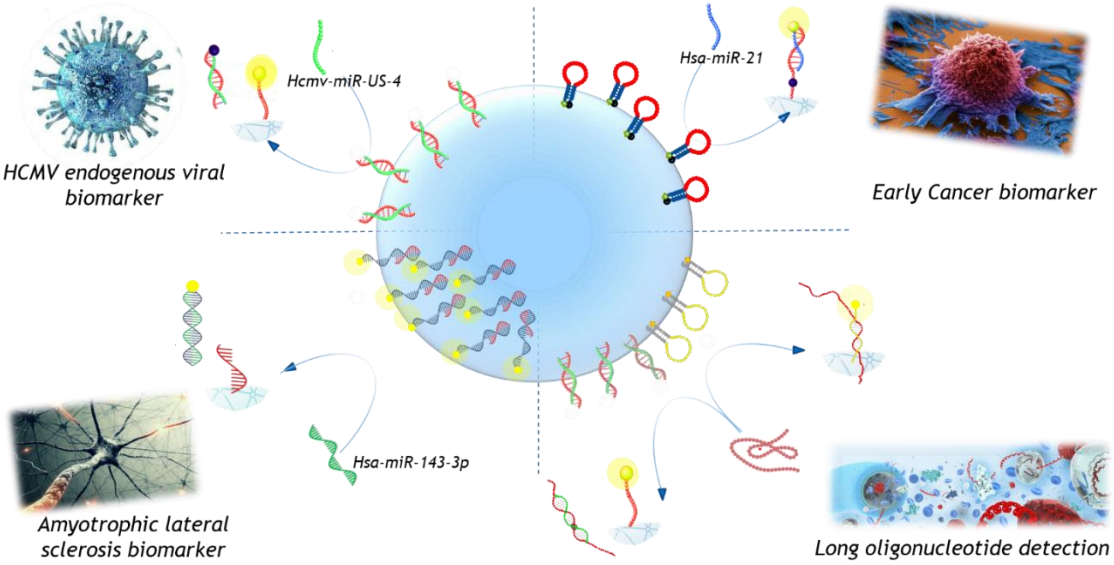

CHAPTER 1

1. INTRODUCTION

Many analytical methods have been developed to identify oligonucleotide biomarkers in human fluids, however, the majority require extensive manipulation of the sample, repeated separation and washing steps resulting time-consuming, expensive and subject to errors. For these reasons, in the last year many *mix & read* assays have been developed through engineered biosensors leading the way toward innovative devices for *liquid biopsy* and *Point of Care* (POC) applications[1,2]. These *mix & read* assays are easily performed by mixing the sample solution with engineered biosensors equipped by signal generator probes and making possible the reading of a detectable signal in solution or on solid surface.

The work presented in this thesis aims to point out the features of this new class of engineered biosensors, characterized by sensitivity, specificity and capability of work directly in human fluids.

In this chapter are briefly discussed the concerns that have led us to develop hydrogels for biosensing application, focusing on: 1) the appealing properties of hydrogels, the importance of the material choice and the strategy of target capture; 2) the methods available to synthetize hydrogels; 3) the clinical importance of oligonucleotides as innovative circulating biomarkers and the innovative highly performant biosensors based on hydrogel recently developed for oligonucleotide detection.

1.1. HYDROGELS IN BIOSENSING

In Biosensor field, hydrogel-based technologies have attracted considerable attention during the last years, as confirmed by the number of studies published (Figure 1). This huge interest is due to hydrophilic, bio-friendly and highly tunable nature of these materials, which make them very suitable in diagnostics[3,4] and in many other biomedical fields such as drug delivery[5], tissue engineering[6] and pharmaceutical applications [7].

Hydrogels are physically or chemically cross-linked materials able to absorb large amounts of water without dissolve. The capacity to absorb and store water within the polymer network makes them distinctive materials[8]. Indeed, they absorb water because of the hydrophilic nature of the functional groups present into the polymer backbone and, at the same time, they are resistant to dissolution since

the cross-links between network chains. In this way, the water within the hydrogel permits the free diffusion of soluble molecules, while the cross-linked network works as support.

Moreover, hydrogels are easily synthetized with a variety of chemical strategies and functionalized with several biological entities such as nucleic acids or proteins. Thus, hydrogels can be engineered for capture and detection of clinically relevant analytes including but not limited to proteins, DNA, mRNA, and microRNA (miRNA)[9].

The main advantages of hydrogels in biosensing consist on their optimal environment for the immobilization, the enhanced molecule permeability, the reduced non-specific interactions with analytes that improve the sensitivity and accuracy, the encoding versatility and the enhanced thermodynamic constant association within the polymeric hydrogel network. However, there are still some limitations that reduce the clinical applications of these hydrogels. In particular, the kinetics of hybridizations are slower compared to free solution probes and the shelf-life of hydrogel biosensors is not well investigated over long period of times. Moreover, it is still necessary to develop sensitive and portable analytic device to ensure the readout of exact measurements.

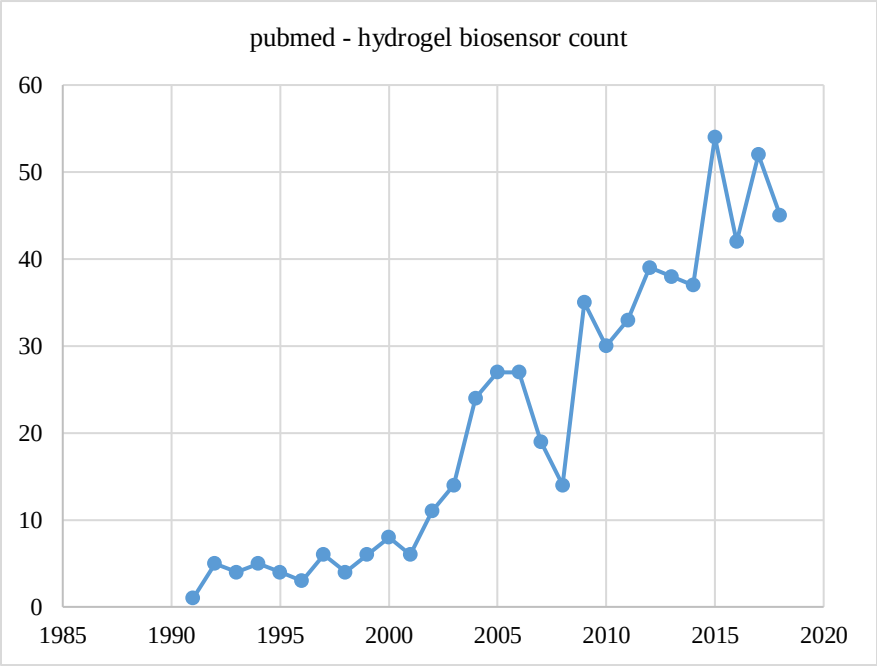

Figure 1 Histogram showing the increase in publications related to the keyword “hydrogel” “biosensor” during the past 30 years (PubMed data)

1.1.1. CLASSIFICATION OF HYDROGELS

Hydrogels are classified based on the origin and ionic charges, the nature of swelling, the technique of preparation, physical properties, and nature of crosslinking (Figure 2).

Firstly, Hydrogels can be classified into two groups based on their natural or synthetic origins[10]. Moreover, they are also divided based on the nature of side groups in neutral or ionic[11]. In neutral hydrogels, the swelling is driven by the contribution of thermodynamic mixing water-polymer, which contributes to the overall free energy, along with elastic polymer contribution. In ionic hydrogels, the swelling is also affected by the ionic interactions between charged polymers and free ions[12]. Therefore, these hydrogels, holding ionic groups (such as carboxylic acid) can absorb large amount of water because of their improved hydrophilicity.

Hydrogels can be further classified based on their cross-linking chemistry. In chemically cross-linked hydrogel covalent bonds are present between the different polymer chains. This strong linkage is obtained by monomer polymerization in presence of a crosslinking agent, through several chemical strategies.

Physically cross-linked hydrogels, instead, are based on physical interaction between polymer chains (as polymer chain entanglement and/or non-covalent interactions). Sometimes physically cross-linked hydrogels are preferred because they avoid the use of crosslinking agents, which are usually toxic and can affect the integrity of the molecules entrapped into the hydrogel[13]. However, the attractive forces holding these networks together are typically based on hydrogen bonding, electrostatic or hydrophobic interactions and gels can be reversibly dissolved under certain conditions that would weaken these attractive forces, i.e. a change in pH[14].

Moreover, hydrogels can be grouped based on the interaction with the external environment[15]. In particular, hydrogels can change their size or shape in response to stimuli such as the temperature, pH[16,17], ionic strength[17], light[18] and electric field[19].

Finally, hydrogels can be classified based on their dimensions in microgels, microparticles and macrogels. Microgels have diameter included between 100 nm to 1μm and are usually definite as a colloidal stable system. Hydrogel microparticles have a diameter ranging from 10 to 100 μm, while increasing the diameter over 100 μm they are classified as macrogels.

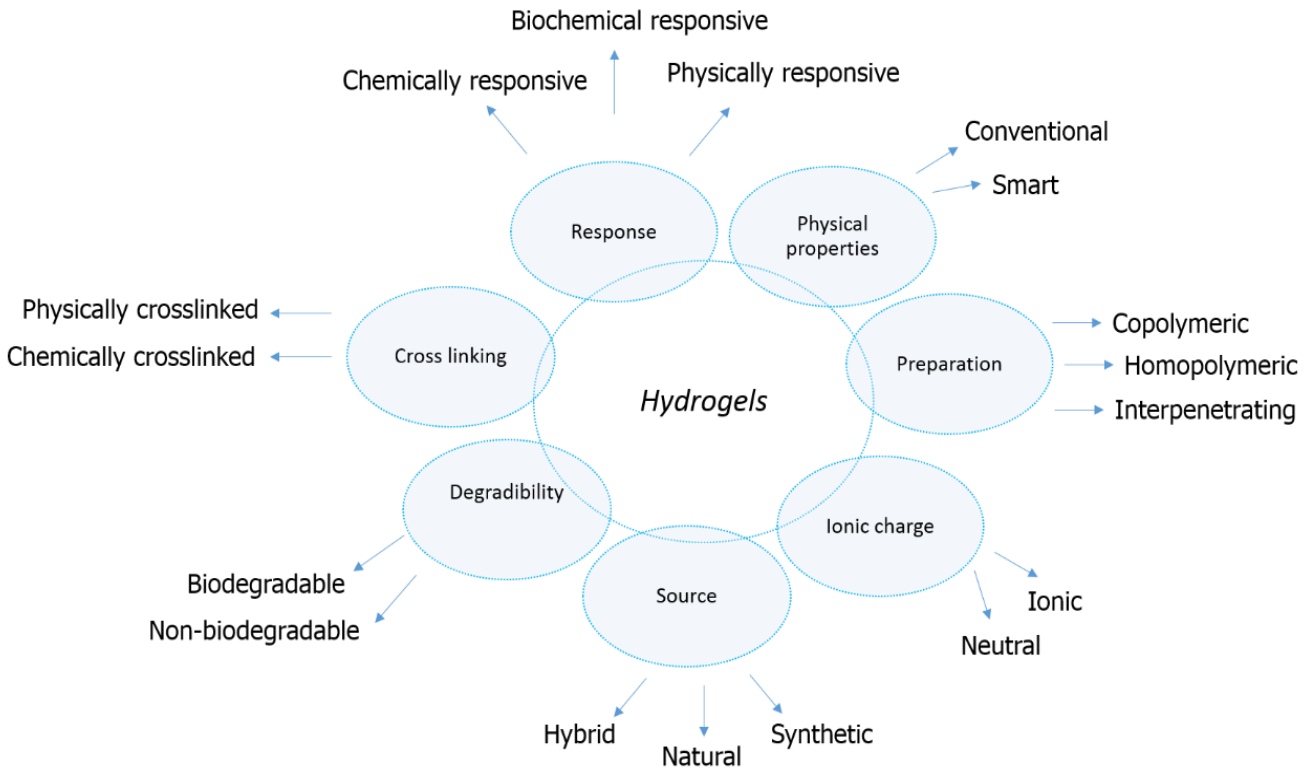

Figure 2 Classification of hydrogels

1.1.2. HYDROGEL MATERIALS

Many polymers are available to synthetize hydrogels as collagen, gelatin, chitosan, hyaluronic acid, alginate, poly(vinyl alcohol) (PVA), poly(propylene fumarate) (PPF), PNIPAAm[20], however, polyethylene glycols (PEGs) are the most used for diagnostic applications. The great popularity of PEG arises by the unique combination of physicochemical and biological properties of the polymer. These included the good solubility in water, the biocompatibility and the capacity to reject protein adsorption (antifouling)[21]. Moreover, PEGs are low-cost materials and they are available in several molecular weights and chemical modifications[22]. For all these appealing properties, PEGs are considered ideal materials to create hydrogels for biosensing applications.

To obtain PEG hydrogels, the polymerization reaction usually occurs by free-radical polymerization between (meth)acrylate or diacrylates PEG derivatives in presence of a UV-sensitive photoinitiator (hydroxyalkylphenone specie)[23]. In recent years, PEG hydrogels have been successfully obtained also by click chemistry. This chemistry comprises a variety of specific and controllable biorthogonal reactions. In particular, the recent development of copper-free click chemistry such as strain-promoted azide-alkyne

cycloaddition, radical mediated thiol-ene chemistry, DielseAlder reaction, tetrazole-alkene photo-click chemistry, and oxime reaction have allowed forming hydrogels using milder reaction conditions, with high reactivity and selectivity[24,25].

However, in order to customize hydrogels for a specific biosensing application is necessary to fine tune the hydrogel microstructure. Hydrogels must be accessible to target molecules maintaining their structural properties. To achieve this goal, the composition of monomers and the polymerization conditions must be tuned to optimize the porosity, the rigidity and the swelling behavior of the hydrogel. As an example, in UV polymerization, increasing the concentration of photoinitiator (1-10%) and the exposure time hydrogels with smaller pore and higher rigidity are obtained. Contrarily, the porosity is augmented increasing the molecular weight of PEG precursor and lowering its concentration. However, longer PEG chain or lower concentration of polymer reduce the cross-linking density with a consequent decrease of the hydrogels rigidity[26]. Porosity can also be modified adding an inactive porogen[27] to the precursor solution, that is washed away after the crosslinking. The diffusion of biomolecules is easily controlled in click chemistry, where the biophysical properties of the hydrogel are adjusted by altering the length of the PEG arms as well as the stoichiometric ratio of species involved in the biorthogonal reaction[28].

1.2. PROBE IMMOBILIZATION

Hydrogels for biosensing applications can be prepared by different synthesis processes, however, they must be functionalized with bio-recognition elements motifs such as peptides, enzyme or oligonucleotides to recognize the target. There are numerous immobilization strategies depending on the reactive groups on the substrate and biomolecule, the type of immobilization (covalent and non-covalent) and on the risk for biomolecule damage during the coupling (UV exposure, free radical temperature, strong solvents). The immobilization is carried out by physical adsorption of the bioprobes or by covalent coupling.

In physical adsorption, the immobilization of bioprobes does not require reactive chemical groups and is easily carried out incubating the bio-recognition elements with the substrates[29] or physically entrapping them into the polymer mesh during the crosslinking[30]. In both cases, low efficiency of immobilization or high non-specific adsorption is often achieved.

In covalent immobilization, bio-recognition elements are coupled on hydrogel through a covalent bond. In this way, a more robust control over the functionalization is obtained and leaching issues are avoided. Two strategies are mainly used in covalent immobilization. In the first, bioprobes are previously modified

with an opportune moiety and then immobilized during the polymerization process (*One-step immobilization*). In the second, bioprobes are immobilized after the polymerization step (*Two-step immobilization*). When PEG hydrogels are used as substrates, during the synthesis are usually added molecules with a reactive group (i.e. carboxyl group or biotin) and the bio-probes are immobilized using their own reactive groups or are modified with specific moieties (i.e. amino or streptavidin).

In DNA biosensors, bio-recognition elements as double strand and molecular beacon probes are widely used. They are immobilized on the substrate both during the polymerization process and after the synthesis of hydrogels.

1.2.1. DOUBLE STRAND PROBE

The double strand probe[31] is composed of two oligonucleotide sequences partially complementary that hybridize forming a stable duplex (figure 3A). Spontaneous dissociation of this double-stranded DNA probe is slow, but in presence of the target strand with higher stability, strand displacement occurs[32]. Strand displacement can be initiated at complementary single-stranded domains (referred to toeholds)[33,34] and advances through a branch migration process that is similar to a random walk (figure 3B). Indeed, in this process a domain displaces another of identical sequence by a series of reversible single nucleotide dissociation and hybridization steps[35]. The process of displacement is usually monitored by fluorescence emission fluctuation after tagging the strands with a fluorophore-quencher[31] or a fret pair[36].

By changing the toehold characteristics, the rate of strand-displacement reactions can be quantitatively controlled. In their studies Zhang and Winfee [37] demonstrated that tuning the length and sequence of the toehold domain the kinetics of strand displacement can be accurately modeled and predicted.

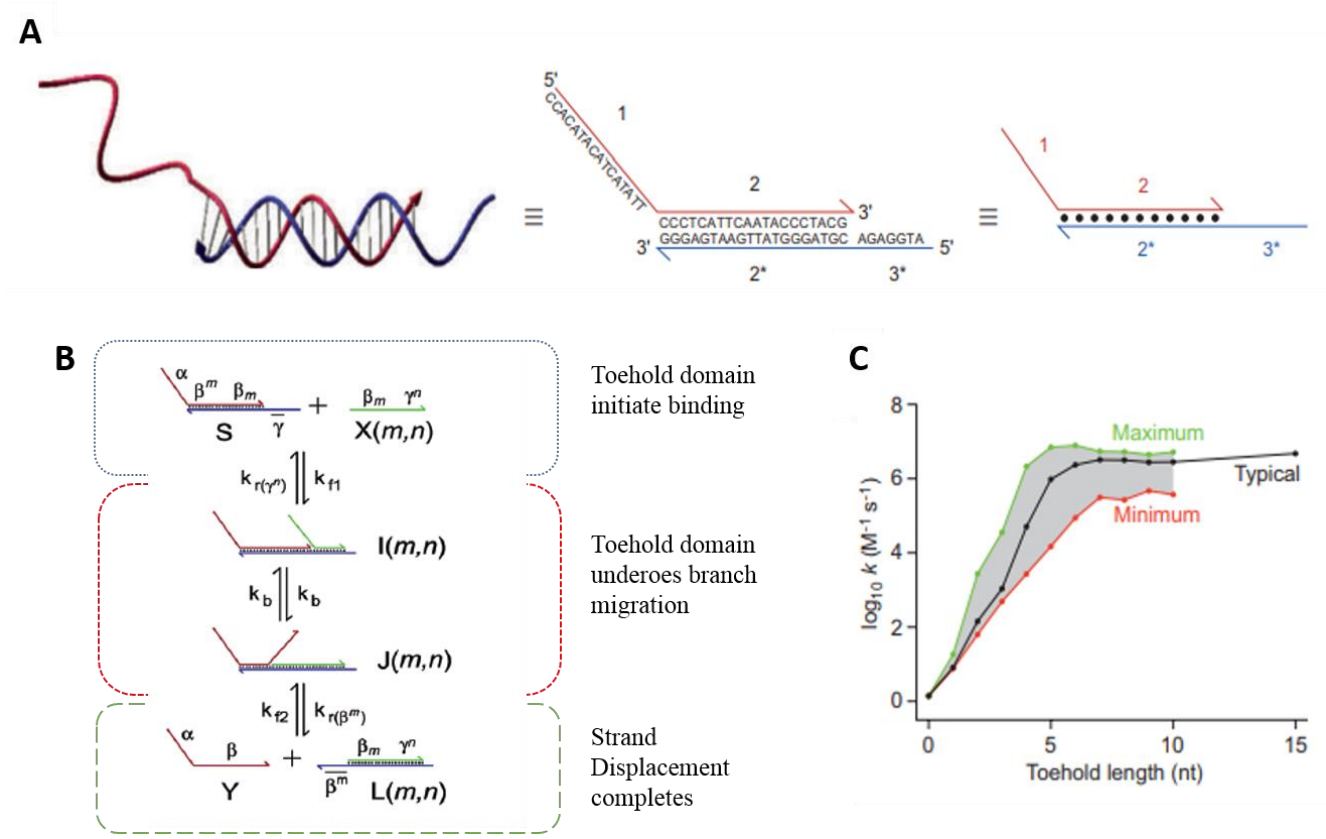

Figure 3 Double strand toehold mediated displacement assay. A) double strand probe structure. B) mechanism of displacement mediated by toehold domains; C) Strand displacement rate constant plotted against toehold length and composition (A/C Reprinted from Nat. Chem 2011 reference 38;-Reprinted from J. Am. Chem. Soc. 2009 ref 37;).

In particular, they have simplified the kinetics model of toehold strand displacement to a simple bimolecular reaction with second-order rate constants:

$$X\,(m,n) + \;S \underset{k_{(\gamma^n,\beta_m,\beta^m)}}{\overset{k_{(\beta^m,\beta_m,\gamma^n)}}{\rightleftharpoons}} Y + L\,(m,n)$$

The associated forward and reverse second-order rate constants $k_{(\beta^m,\,\beta_m,\,\gamma^n)}$ and $k_{(\gamma^n,\,\beta_m,\,\beta^m)}$ for this bimolecular reaction model (BM) of strand displacement are dependent on the sequences of the β^m,β_m, and γ^n domains (figure 3B), as well as the ambient temperature and salt concentrations[37].

In particular, they have shown that the rate constant of the strand displacement reaction can vary over a factor of 10^6, from 1 M^{-1} s^{-1} to 6×10^6 M^{-1} s^{-1} and that the GC composition of the toehold strand affects the kinetics rate of the displacement process. As shown in Figure **3**C, toehold composed of only G/C nucleotides (green line) has faster kinetics compared to toehold composed of roughly equal numbers of all four nucleotides, while toehold composed only of A/T nucleotides (red line) are the slowest. The grey region spanned by the green and red traces roughly shows the range of potential kinetics based on toehold

length. Based on this consideration is possible to fine engineering control over the kinetics of synthetic DNA devices[39].

The double strand probe can be also immobilized on solid surfaces. The hybridization between the probe and the target is converted by the transducer in an optical, electrochemical piezoelectric or thermal quantifiable signal.

In particular, microchips and microparticles have been functionalized with double strand probes for biosensing applications[40,41]. The density of immobilized capture probes and the equilibrium dissociation constants are calculated through a bimolecular, all-or-none model for hybridization of non-self-complementary sequences by Stevens et al,[42]. They have found that for an oligonucleotide of 22 mer, immobilized on paramagnetic particles (diameter 0.75 μm) the K_d value is in nM order and at higher temperatures hybridization on particles is more efficient than in solution.

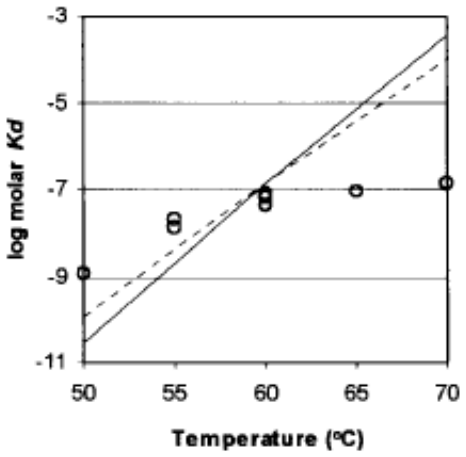

Figure 4 Constant dissociation K_d predicted from solution-phase thermodynamic parameters(lines) compared with those determined experimentally (empty circle) (Reprinted from Nucleic Acid Research, 1999, reference 42)

Oligonucleotide probes are also introduced during the polymerization reaction through a UV-polymerizable methacrylamide linker (Acrydite™). The incorporation of this group allows engineering various hydrogels reducing the time of synthesis. However, Pregibon et al[43] have proved that the efficiency of immobilization of these probes is affected by the amount of reactive species in precursor solutions (their efficiency of immobilization is estimated about ~5% to 25%). To improve the efficiency of immobilization, they have also suggested to use acrylate probes instead of methacrylate as is known that acrylates react faster than methacrylates[43].

Once the oligonucleotide-methacrylate probe is immobilized, it can hybridize with the partially complementary probe forming the double strand probe, otherwise, it can directly hybridize with the target sequence. In the latter, the hybridization is converted in an optical, electrochemical or piezoelectric or thermal quantifiable signal.

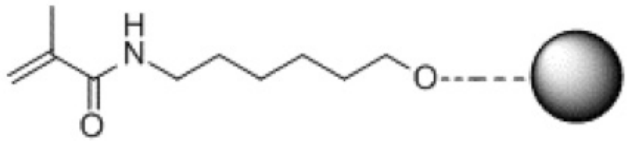

Figure 5 Acridyte™ group attached to oligonucleotide

1.2.2. MOLECULAR BEACON

Molecular beacons have been firstly introduced by Tyagi and Kramer more than 20 years ago[44]. Essentially, a molecular beacon is a single strand oligonucleotide sequence containing a fluorophore and a quencher in its opposite ends. It is composed by a target recognition sequence (loop) flanked by two self-complementary terminal arms (stem)[45,46]. Because of its sequence, in absence of target the two arms hybridize through a mono-molecular reaction forming a stem-loop structure. In such conformation the fluorophore and quencher are in close proximity with a consequent quenching of the fluorescence[47]. When the DNA or RNA target is present, hybridization between the target and the loop sequence of the molecular beacon takes place and the stronger intermolecular hybridization mechanically forces the weaker stem helix to open. Thus, the fluorophore and quencher are spatially separated and fluorescence is restored. Molecular beacons are widely used as oligonucleotide probes due to the higher thermodynamic stability of the hairpin structure, the efficient signal switching and the numerous reporter dyes available. These aspects allow reaching excellent sensitivity and selectivity, and real-time detection capability.

The design of this probe seems easy but is in reality quite sophisticated. Many studies have been focused on the practical rules to design molecular beacons[48–51]. Briefly, two are the main key factors which determine the characteristics and functionality of the molecular beacon: the probe structure and fluorescence signal switching. As regards the first, the specificity and sensitivity of molecular beacon for its target can be optimized by adjusting the probe length and the GC content. As general rules, the probe sequence has length comprised between 15-30 bases and is free from secondary structure. The stems are 5-7 base pair and have high GC content (75-100%). Shorter stem results faster hybridization, but suffers

from lower signal-to-background ratio[52,53]. Longer stems are particularly suitable for single mismatch detection, however, they have slower kinetics. The fluorescence signal switching is mainly based on dynamic or static fluorescence quenching. Many fluorophores and quenchers existing and they must be carefully selected[54].

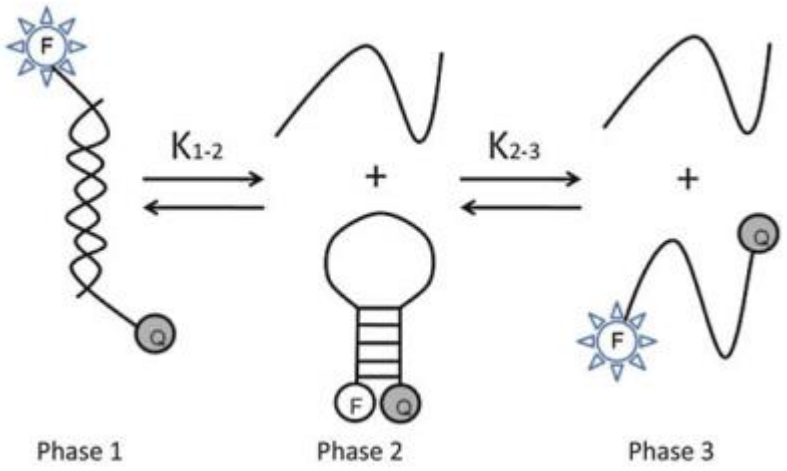

Figure 6 Phase transitions of molecular beacons with targets in solution. Phase 1: fluorescent molecular beacon–target duplex; phase 2: nonfluorescent stem–loop hairpin; and phase 3: fluorescent random coil (Reprinted from Springer. 2013, reference 51)

Molecular beacons can exist at least in three distinct states: molecular beacon–target duplex (phase 1), stem–loop hairpin (phase 2), and random coil (phase 3). The thermodynamic and the kinetics of these probes have been extensively studied by Bonnet[55] and Tsourkas[56]. In particular, they have studied the dissociation constants of the transition monitoring the melting curve of molecular beacons in presence and absence of the target. The dissociation constant K_{2-3} corresponding to the transition between stem–loop hairpin and random coil is given by:

$$K_{2-3}(\theta) = \left(\frac{F-\beta}{\gamma-F}\right)$$

where F is the fluorescence intensity at a given temperature θ, β is the fluorescence of molecular beacons in the hairpin form (obtained at low temperatures, such as 10°C), and γ is the fluorescence of molecular beacons in the random-coil form (obtained at high temperatures, such as 80°C) in the absence of targets.

The dissociation constant K_{1-2} describing the transition between molecular beacon–target duplex and the stem–loop hairpin can be calculated from the fluorescence data obtained by the melting measurements of molecular beacons in presence of the target:

$$K_{1-2}(T) = \frac{(\alpha - F)T_0}{(F - \beta) + (F - \gamma)K_{2-3}}$$

where α is the fluorescence intensity of molecular beacon–target duplex at low temperatures such as 10°C.

Their studies have demonstrated that the stem length of a molecular beacon has a greater effect on its equilibrium state than the loop length, and that a target with single-base mismatches exhibit a less favorable binding with molecular beacons. They have also demonstrated that a mismatch positioned in the center of the probe has a greater impact on equilibrium than a terminal mismatch. Furthermore, Chen et al[57] have proposed a three-step model to explain the molecular beacon kinetics in solution. They have proved that the first and second step (respectively the formation of few transient base pairs called *nucleus* and the opening of the stem with more base pairs between probe and target) are the rate-limiting steps, while the third step (complete hybridization between the probe and probe) is much faster.

Due to their excellent properties, molecular beacons have found many applications in biosensing for the detection of several molecules of interest[58–65] both in solution and immobilized on solid support. They are usually coupled by *two step* immobilization on a variety of supports as glass surfaces, on graphene, gold particles on optical fiber, however, despite all the efforts made, when molecular beacons are immobilized on solid surface the fluorescence background usually increases due to non-specific oligonucleotide-surface interaction and crowding effects[66] among the immobilized oligonucleotide probes. However, these issues are avoided immobilizing molecular beacons into materials with solution-like property. Recently, Dai et al and Ma et al[67] have proved that when molecular beacons (modified with a biotin) are used to functionalize surface-patterned poly(ethylene glycol) hydrogels (endowed with streptavidin), fluorescence background strongly decreased.

1.3. HYDROGEL CHARACTERISTICS FOR BIOSENSING

Many biosensors have been developed immobilizing oligonucleotide probes on solid surface, as in graphic-2D layered[-68], magnetic particles[69–71], particles[9,72–75], carbon nanomaterias[76] and microarrays[77,78]. These biosensors allow high-throughput analysis and parallel screening of several

molecules of interest[79], however, they suffer of some limitations[80], which affect the sensitivity, the specificity and the kinetics of detection. In particular, they are ascribable to the electrostatic repulsion between probe-probe[81,82], the steric hindrance between probe-target complex[83,84] and the non-specific adsorption[85] on solid substrates. Moreover, the design of the probes[86–89] and the different immobilization methods generate slower kinetics of hybridization and inhomogeneous signal distribution[90]. Hydrogels with their tridimensional polymer network can improve these issues, however, during the design of hydrogel-based assay a number of concerns must be taken into consideration. In particular, the swelling behavior of the hydrogel, the probe density and the molecules diffusion affect the sensitivity of the assay.

Firstly, the hydrogel structure at the molecular level must be optimized in order to enhance the hybridization between target molecules and immobilized probes, preserving the structural integrity of the hydrogel matrix. To achieve this goal, the monomer composition, the porosity, the rigidity and the swelling behavior of the hydrogel must be tuned. Concerning the porosity and the swelling behavior, it is possible to control these parameters by adjusting the starting material properties as the monomer concentration, the mass weight and the amount of cross-linker. For biosensing application, it is desirable that the diffusion and the target capture are not hindered by the biological fluids composition. For these reasons, hydrogels are opportunely engineered in order to preserve porosity, chemical background, and, therefore, the target diffusion.

The network structure of a hydrogel is characterized by the determination of the polymer fraction (v_2, s), the molecular weight of the polymer chain between two neighboring cross-linking points (Mc) and the correlation distance between them, also known as mesh size (ξ). The nature and the amount of polymer fraction define how a hydrogel is capable to imbibe and retain water, while the Mc and ξ are averaged parameters that define the accessibility and the transport of molecular species in the network[40]. However, all these parameters are described theoretically by the equilibrium swelling theory and the rubber elasticity, while a variety of techniques are available to experimentally measure and verify them[91].

The structural characterization of hydrogels is usually carried out on bulk, calculating the degree of hydration (swelling measurements) by weighting the amount of water up-taken by the polymer and converting it in the volumetric fraction according to the "equilibrium swelling theory" developed by Flory and Rehner[92] and then modified by Peppas and Merrill[93,94]. Swelling on hydrogel particles has been experimentally measured by few groups. Lee et al[95] have proved that the swelling on shape-encoded particles increases using PEGDA precursor with higher molecular weight, but the particle shape is isotropic. Recently, Battista et al[96] have demonstrated the direct determination of swelling on core/shell microgels responsive to pH, through atomic force microscopy (AFM) analysis.

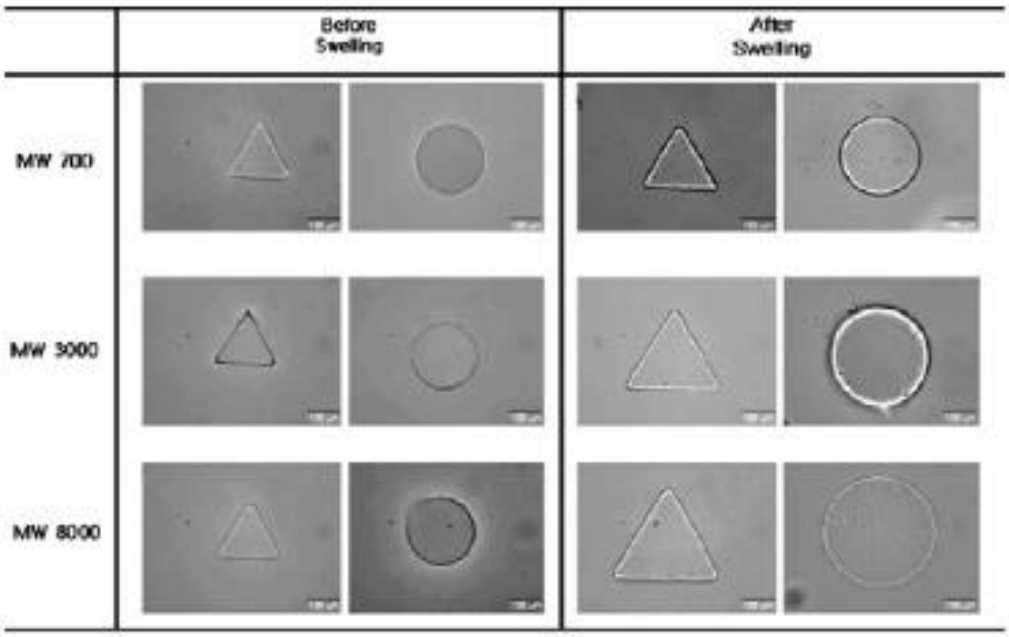

Figure 7 Swelling of hydrogel PEGDA microparticles synthetized with different molecular weight of starting monomer (Reprinted from Biomed. Microdevices, 2008, reference 95)

Another important parameter to take into account is the probe density. Differently from solid surfaces as microarray or polystyrene beads, hydrogels possess higher capacity of probe immobilization due to their tridimensional structure and increased surface area. As results, if first-order Langmuir kinetics is assumed, increasing the probes density more target/probe complex are formed at equilibrium with a consequently improved sensitivity. Comparing glass surfaces and hydrogel pads for microchips development, Srinivas et al[97] and Zubstov et al[98] have demonstrated that three-dimensional gel networks possess higher capacity for immobilization. They have proved that in surface-based systems the steric hindrance is a limitation with only $\sim 10^4$ molecules/μm^2 immobilized and increasing the amount of probe the immobilization efficiency is not improved. In contrast, hydrogel substrates allow immobilizing $\sim 10^5$ molecules/μm^2 (calculated on 10 μM of probe concentration and hydrogel height of 35 μm) achieving effective surface density at least 1 order of magnitude greater than glass surface. Furthermore, when solid surfaces are functionalized at maximum capability, the proximity between probes can decrease the target accessibility reducing the assay sensitivity. Otherwise, hydrogels allow immobilizing high amount of probes keeping enough distance between them, hence target is free to diffuse and hybridize with the probe[98].

Finally, the target diffusion within the polymer matrix must be considered. The structural parameters of hydrogels must be appropriately tuned to promote the diffusion of the target and improve the probe/target complex formation, thus the sensitivity of the detection. This because if the target is bigger than the mesh size of the polymer its diffusion is hindered or is very low. Contrary, if the polymer is too porous, fewer probes are immobilized during its functionalization, affecting the assay sensitivity.

In free solution and in absence of any interactions with other target biomolecules, the diffusion process is governed by Stokes-Einstein relation:

$$D_0 = \frac{k_B T}{(6\pi \eta R_h)}$$

where k_B is the Boltzmann constant, T is the temperature in kelvin, η is the solvent viscosity and R_h is the hydrodynamic radius of the target. In hydrogels, the diffusion is described by different models, based on the nature of the biomolecule target.

For oligonucleotide with Rg < a/2, where Rg is the gyration radius of the molecules and a is the mean gel pore size, the diffusion coefficient is calculated by the Zimm[99] model:

$$D_0 = \frac{0.196 k_B T}{(\eta R_h)} \approx N_0^{-1/2}$$

When Rg > a/2, the movement of an unattached chain by Brownian motion into the multi-chain system forming by the hydrogel is described by the reputation theory. The lateral movement of the chain is limited by gel fibers with a resulting loss of entropy that brings the chain to migrate inside a tube with length L = Na, where N is the number of pores occupied by the chain. In this condition:

$$D_0 = \frac{k_B T\, a^2}{(3\, N_k^2\, \zeta_k b^2)} \approx N_0^{-1/2}$$

a represents the pore size, N_K is the number of Kuhn segments ζK is the friction coefficient of a Kuhn segments, and b is the Kuhn length.

In this context, target diffusion and probe/target hybridization are widely studied and modeled in hydrogels. Sorokin et al[100] focused on the kinetics of oligonucleotides on microchips using hydrogel pads and have compared their performance with glass surfaces. They define the hybridization time as:

$$\tau_{diff}^{(H)} = \frac{R\tilde{m}K_a}{\beta\, D_{sol}(1 + K_a h_{sol})}$$

Where R is radius of microbeads, $\tilde{m}$ is the probe density for unit area, K_a is the association constant, β is a numerical factor and is equal to unity for hybridization on the microbeads, D*sol* is diffusion coefficient for target DNA in solution, h_{sol} is the homogenous concentration of target in solution.

They have demonstrated that although hydrogels show slower kinetics due to hinder diffusion of analytes within the mesh, the sensitivity at equilibrium and the capability to detect mismatch are increased compared to solid surfaces. This is explained as results of the better thermodynamic association constants within the hydrogel, that appears closer to the ideal solution because of the high water content and the sufficient space between probe molecules despite a higher effective probe density.

Diffusion studies have been carried out by Pregibon and Doyle[43] using a three-dimensional hydrogel array. They have considered a system where target oligonucleotides (T_s in solution and T within the particles) diffuse into the hydrogel and hybridize with probes P to form complexes TP. Considering that the rules governing this transport are complex, nonlinear and coupled, they have assumed that in a specific regime, which is relevant for most assays, the system can be simplified to a one-dimension problem. Scaling arguments can be made to reduce the complexity of this problem. In this way, they are able to calculate:

(1) the ratio of target to probe molecules γ:

$$\gamma = \frac{[T_s]_0 V_s}{([P]_0 N_p V_p)}$$

where $[T_s]_0$ and $[P]_0$ are respectively the concentration of target and probe at t = 0, Vs is the sample volume, Np is the number of particle and V_p is the volume of the particle;

(2) the rate of association versus diffusion which is given by the Damköhler number *Da*

$$Da = \frac{K_a [P]_0}{(D_{gel}/L^2)}$$

where k_a is the second-order association rate constants, D_{gel} is the target diffusivity and L is the characteristic length for the diffusion path, and

(3) the relative strength of hybridization κ:

$$\kappa = \frac{K_d}{[T_s]_0}$$

where K_d is the first-order dissociation constant.

In the study they have shown that for short oligonucleotide (20bp) k_a (10^6 $M^{-1}s^{-1}$) is much higher than D (10^{-11} m^2/s), therefore Da >> 1, if $[P]_0$ is about 10^{-6} M and L around 10^{-6} m; even at low amount (<10^{-18} mol) the probe can be considered in large excess, therefore $\gamma << 1$, while hybridization is very strong at initial target concentration ($\kappa << 1$) if considering K_d in the order of 10^{-13} M and $[T_s]_0$ around 10^{-11} M. In the case of larger oligonucleotide[101], k_a is around 10^3 $M^{-1}s^{-1}$, while assuming that D is the same of other biomolecules with the same Rg (10^{-8}–10^{-10} m^2/s), Da can be in the unity range if $[P]_0$ is about 10^{-6} M and L around 10^{-6} m; the probe can be considered in large excess even at low amount, therefore $\gamma <<1$. The study has also shown that the 3Dgel array is mass-transport limited since reaction occurs significantly faster than diffusion throughout the gel (Da>>1). These properties can reduce the target diffusion into the hydrogel with a consequent confinement of the signal at the outer edge of the hydrogel particles at low target concentrations.

To sum up, to design sensitive and specific assay based on functionalized hydrogel is very important to tune the polymer/probe composition in order to: avoid swelling effect in biological fluids; have high probe density but, at the same time, permit free diffusion of the target; and guarantee structural stability during the assay.

2. SYNTHESIS OF HYDROGELS

Hydrogels for sensing purpose must be synthetized with finely controlled size, shape and encoding in order to satisfy the bioassay necessity. One of the major advantages of use hydrogels is the multitude of chemical strategies available to synthesize them. These comprise one-step procedures like polymerization and parallel crosslinking of multifunctional monomers, as well as multiple step procedures, concerning synthesis of polymer molecules with reactive groups and their subsequent crosslinking

Microgels are synthetized starting from monofunctional monomers, from polymers or from macrogels. Their synthesis is essentially summarized in three categories based on the particle formation mechanism: homogeneous nucleation, emulsification and complexation.

In the first case, a solution of soluble monomer, including a cross-linking agent, is carried out and microgel particles form over the course of polymerization[102]. To obtain good control over the particle formation, the polymer obtained during the polymerization must be insoluble in solution or will form a macrogel. The homogeneous nucleation includes emulsion polymerization (EP), surfactant-free

emulsion polymerization (SEP), and microgel formation from a dilute polymer solution. In the first step of emulsion polymerization (EP), the monomer is present as a suspension mixed with a surfactant and a water-soluble free radical initiator, in the second step, the polymer is polymerized into a surfactant-stabilized microgel[103]. Emulsion polymerization is a robust method to obtain core-shell microgels. The core particles are firstly prepared by conventional emulsion polymerization and then are used as seeds for the second-stage shell polymerization[104]. This method gives core-shell particles monodisperse, as all oligomers formed in solution attached on pre-formed core particles, however, to avoid heteronucleation is important to control parameters such as the concentration of the core, initiator, surfactant and the shell monomer. In surfactant-free emulsion polymerization (SEP) starting from an unstable not colloidal precursor, particles aggregate to form new primary particles, then at the end of nucleation stage, all new precursor particles are captured by existing stable particles[105]. Moreover, microgels can be prepared by mixing two dilute water-soluble polymers that form complexes in water.

The second method is emulsification. In this case, an aqueous pregel solution (a monomer or a polymer) is suspended in an oil phase to give a water-in-oil emulsion. In the second gelation step, the emulsion droplets undergo a chemical reaction to gel each emulsion droplet[106].

The last method involves dilute solutions of oppositely charged polyelectrolytes to form colloidal dispersed, polyelectrolyte complexes[107].

However, these conventional techniques have some limitations due to the biomolecules incompatibility towards organic solvent or polymerization conditions. In addition, the low monodispersity and the need of codes for multiplex application have led to the development of new techniques to synthetize hydrogels.

Recently, microfluidics methods are arising in order to achieve major control on size and shape of microgels, to use milder chemistry and reduce time and cost of the synthesis. Among these, droplet generation based methods and flow lithography are the most used. The first method is competent for producing spherical or sphere-like particles, while the second is an ideal alternative for designing non-spherical particles, such as rods and flakes, which are more desirable in some particular applications.

Microfluidic assisted methods rely on the formation of a stable emulsion between two immiscible fluids as an oil phase (continuous phase) and a water phase (disperse phase). The synthesis occurs in a miniaturized device made of glass o polydimethylsiloxane (PDMS). The Disperse phase is usually composed by a water solution of monomer, biomolecules and cross-linker, while, for the continuous oil phase is used mineral oil, silicone oil, corn oil, hexadecane and fluorinated oil[108]. Additionally, a surfactant is added to prevent that droplets rapidly coalesce inside the devices[109]. The crosslinking of

polymeric monomers is achieved into the device (on-chip) or in separated vials (off-chip) and is induced by UV/Vis light[110], via thiol-Michael addition click reaction[111], or changing the temperature and ionic crosslinking[112]. As an example, PEG hydrogel microparticles have been widely synthetized by cross-linking of acrylate and methacrylate monomers in microfluidic[113]. The polymerization is carried out shining UV/Vis light on the solution in presence of specific photoinitiator based on hydroxyalkylphenone species (i.e., Darocur, Irgacure). The homolytic scission of C–C bonds generates a benzoyl free radical that allows the cross-links formation in the gel. Varying the parameters as the concentration of the photoinitiators, the intensity of light and the exposure time is possible to tune the mechanical rigidity and the pores of hydrogels.

Droplet generation is described as continuous on-chip production of water-in-oil emulsions based on the breakoff of droplets in two-phases at T-junction or in flow-focusing geometries. The formation of the droplet depends by several variabilities such as flow rates, viscosity of the fluid, dimensions of the geometry, capillary number (Ca) and the surface tension[114]. To obtain a stable emulsion and thus monodisperse droplets the optimal synthesis condition must be optimized. Moreover, in addition to the abovementioned other device geometries have been developed as micro-nozzle cross-flow system and co-axial capillaries[115]. Microfluidic droplet generation permits large production of monodisperse microparticles (10^5 per hours) spectrally or graphically encoded.

Doyle's group have introduced the Flow-lithography[116] in 2006. In this technique particles are synthetized in a PDMS microfluidic device, with high throughput (18,000 particles per second). The shape and size of the particles are controlled using a transparency mask, which shades the UV light beam used to photo-cure the co-flowing laminar streams in microfluidic channels. As results, they are able to obtain a high number codes combining graphical and spectral encoding, as well as differential chemistries are possible such as Janus particles[117].

Further improvements have been made developing the stop-flow lithography[118], where the pumping system is actuated so that the flow is stopped for few milliseconds allowing the polymerization through a mask. In such a way Doyle's group have obtained particles with graphical and spectral encoding as well as with multiple capture probes positioned in different regions.

Another great advantage of using hydrogel microparticle relies on the flexibility of manipulation. Assays based on hydrogel can be carried out in microtubes (50-500 μL), microplates for higher throughput (50-500 μL) or in microfluidic devices (<10 μL). Microparticles are washed and separated from the sample by centrifugation or, if magnetic microbeads are added during the polymerization, applying a magnetic field. The code reading and/or target quantification are usually measured by optical detection methods.

In particular, imaging methods as transmission, reflection and fluorescence microscopy or flow cytometry techniques are the most used.

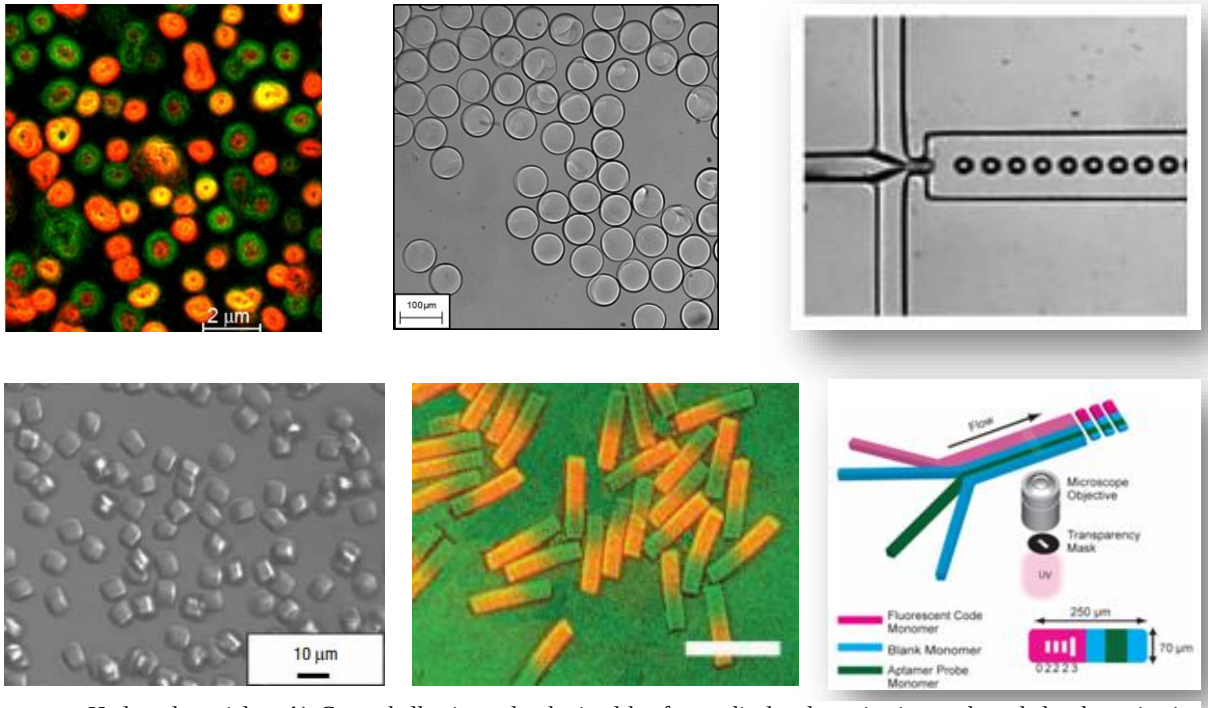

Figure 8 Hydrogel particles. A) Core–shell microgels obtained by free-radical polymerization and seeded polymerization (Reprinted by J. Am. Chem. Soc., 2015, reference 41; B) Hydrogel microparticles obtained by droplet generation; C) Flow-focusing microfluidic droplet generation device (Reprinted from Colloids Surf B Biointerfaces, 2016, reference 113); E) Microparticles synthetized by stop-flow lithography technique (Reprinted from Nat. Mater, 2006, 116); F) Janus particles by stop-flow lithography (Reprinted from Appl. Mater. Today, 2017, reference 117); F) Stop flow lithography mechanism (Reprinted from Nat. Mater, 2006, 116)

3. BIOMARKERS DESCRIPTION AND DETECTION BY HYDROGELS

A biomarker is a distinctive that can be objectively measured and evaluated as an indicator of a physiological as well as a pathological state[119]. Biomarkers include nucleic acids, proteins, metabolites, small molecules that can specifically and sensitively reflect a disease state. For this reason, they are suitable for diagnosis, prognosis as well as for disease monitoring during and following therapy.

Looking at figure 9 is clear the importance of biomarkers. They occupy a key role and are fundamental for personalized medicine development. Furthermore, the presence of these biomolecules free to circulate in biological fluid represents a non-invasive and specific way to diagnose diseases and tailor the therapy

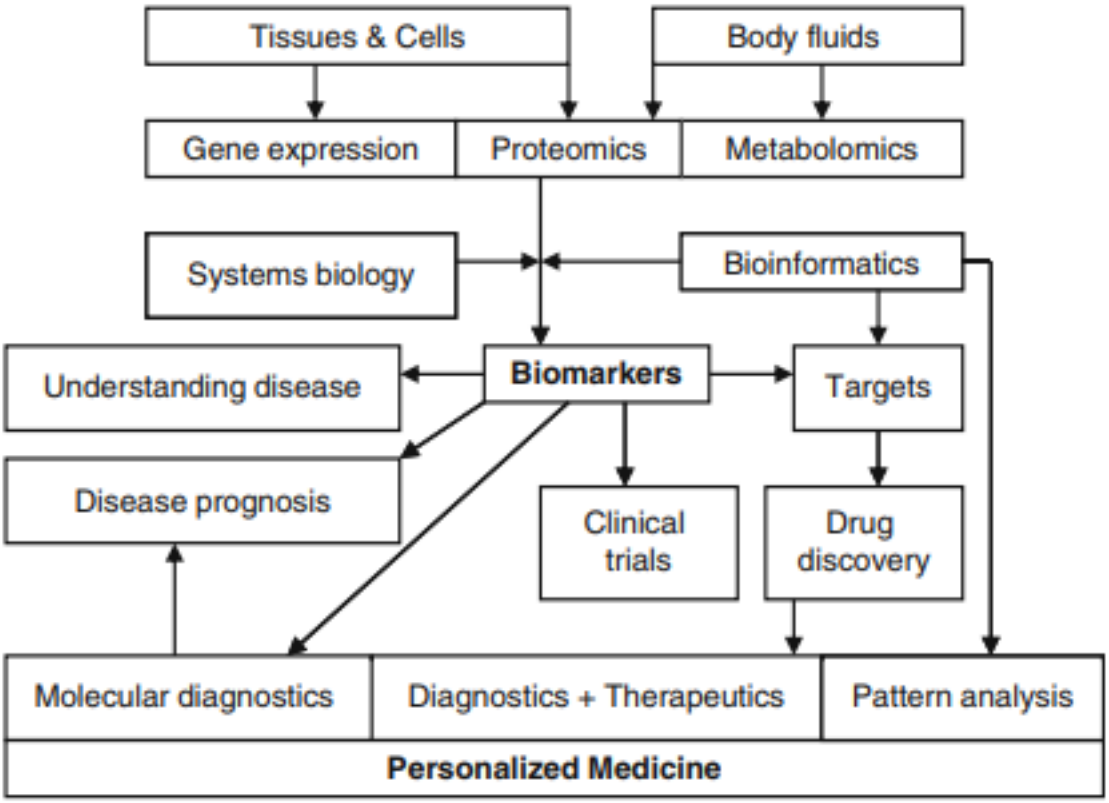

Figure 9 Relation of biomarkers to other technologies and health care (Reprinted from Springer, 2010, reference 120)

on the single individual, based on its predicted response. In this way inadequate and risky therapies are avoided improving the quality of life.

Moreover, current diagnostic techniques are often based on invasive, expensive and time-spending methods. In addition, these techniques are often affected by low specificity or can produce false results. Thus, circulating biomarker detection combined with sensitive biosensing technologies can promise more effective diagnostics, prognostics, and monitoring approaches for a wide range of clinical settings.

In particular, we focus on the development of hydrogel-based technologies to detect already validated circulating oligonucleotide biomarkers. Circulating nucleic acids have been described for the first time in 1948 by Mandel and Métas[121]. However, only at beginning of 90s their importance has been elucidated[122]. They can be separated based on their nature in circulating DNA and RNA biomarkers.

High levels of circulating DNA can be measured in physiological conditions or clinical states, such as exercise[123], infection[124] acute trauma[125], cerebral infarction[126] transplantation[127], and during pregnancy[128]. Furthermore, many studies have focused on the importance of circulating DNA in cancer

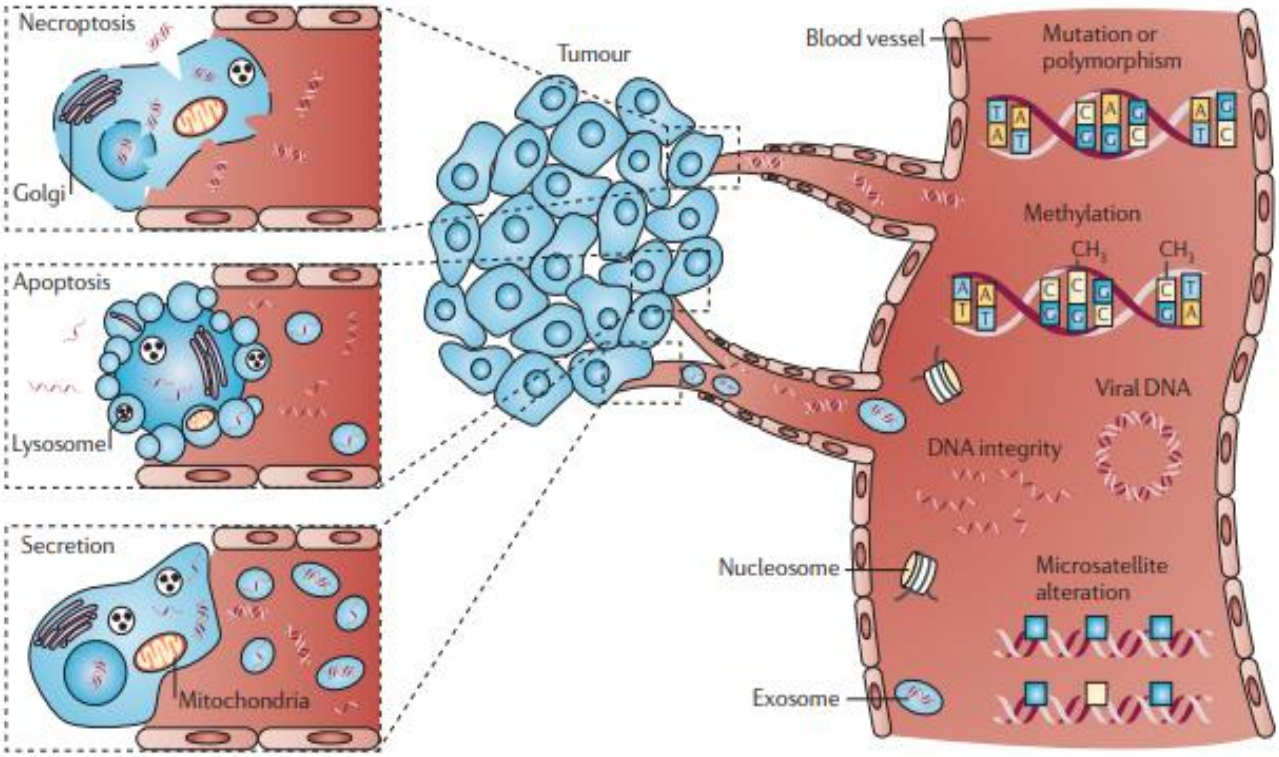

Figure 10 Circulating DNA is released in the serum of cancer patient by apoptosis, necrosis or secretion from the cancer cells. The DNAs circulating in human fluids have different size and is affected by mutation, methylation or alterations. Moreover, viral DNA is also detectable in some tumour caused by virus such as human papillomavirus (HPV), hepatitis B virus (HBV) and Epstein–Barr virus (EBV) (Reprinted from Nat Rev Cancer, 2011, [136]).

fields[129–132]. It has been hypothesized that circulating DNAs are produced via the release of nucleic acids during the apoptosis or necrosis of cancer cells or from tumour-derived exosomes[133].

Their size varies between small fragments of 70 to 200 base pairs and large fragments of about 21 kilobases[134]. Furthermore, in human fluids is possible to find both mitochondrial DNA (mtDNA)[135] and genomic DNA(gDNA). The latter includes coding and noncoding gDNA that can be used to examine microsatellite instability, loss of heterozygosity (LOH) [137], mutations[138], polymorphisms, methylation[139] and integrity[140] (size).

Circulating RNA are also detectable in human fluids. In particular, protein-coding messenger RNAs (mRNA), miRNAs, piRNAs, tRNAs and miscellaneous other non-coding RNA molecules are packed in extracellular vesicles and are released in fluids[141]. These RNAs are very stable and may serve as biomarkers since some of them have been associated with several diseases[142,143] The use of circulating RNAs in human fluids to detect and monitor diseases is rapidly growing. Therefore, the US National

Centre for Advancing Translational Sciences (NCATS) has recently launched the Extracellular RNA Communication Consortium to boost the use of circulating RNA in clinical applications tool[144].

MicroRNAs are small (20-25nt)[145], non-coding oligonucleotides that regulate gene expression acting at post-transcriptional levels [146-147]. They are involved in a wide range of biological processes[148–156] and due to their immense regulatory power, variation of microRNA levels can be utilized as potential biomarkers for the diagnosis and prognosis of a variety of diseases including viral infections, cancer and neurodegenerative diseases[157–164]. A comprehensive curated database of miRNA and other non-coding RNA biomarkers is available at http://mirandola.iit.cnr.it/. However, despite the encouraging results observed, little progress has been achieved in terms of producing effective biomarkers for the clinic application.

Protein-coding messenger RNAs (mRNA) have an essential role in numerous biological processes. Circulating fetal mRNAs in maternal plasma have been associated with prenatal defects[165,166]. Circulating mRNAs containing tumour-associated genetic alterations have been first validated in the 1990s in the plasma of patients with nasopharyngeal carcinoma[167]. Then the study has been extended to many other types of cancer and has been found that mRNAs can serve as a non-invasive biomarker in several cancers including breast, colorectal, lung and prostate cancer[168]. Moreover, circulating mRNAs have been associated with the progression[169] of the disease as well as to the therapies response[170].

Actually, the gold standard techniques to detect free circulating oligonucleotides rely on polymerase chain reaction PCR, qRT-PCR[171] and digital PCR[172,173], which offer enhanced sensitivity and specificity. but require complex, expensive, time-consuming and hard-working procedures. Recently, next-generation sequencing (NGS)[174,175] has emerged as an alternative option with greater dynamic range of detection, increased sensitivity and reproducibility. However, these techniques have critical limitations due to the pre-analytical steps, such as the collection of biofluids (e.g., blood, serum, plasma), the storage conditions, the extraction, purification, amplification and calibration steps often source of biases that can compromise the assay accuracy[176,177]. For these reasons, novel detection systems capable of direct and absolute quantification of oligonucleotides in body fluids are particularly required. In addition, these technologies must meet the requirements of sensibility and specificity needed in biosensing such as the improved LOD, single mutation specificity, low cost and rapid time of analysis.

In this context hydrogels are particularly successful. Kim et al[178] have recently developed a microfluidic platform that immobilizes hydrogel microparticles at defined locations and encapsulates particles in monodisperse droplets for the detection of a panel of microRNA with diagnostic value for prostate cancer

and triple negative breast cancer (let-7a, miR145, and miR221). They have achieved 0.1 amol sensitivity (employing an enzyme amplification method) in 4hr 30 min.

He et al,[179] have realized a switchable DNA hydrogel SERS (Surface enhancement Raman spectrum) platform for the detection of miR-155. They have used a Duplex-specific nuclease (DSN) as enzyme amplification strategy achieving 0.083 fM sensitivity, single nucleotide specificity and working directly in human serum.

Aliberti et al[40] have developed a multiplex specific oligonucleotide detection method to detect viral infections. They have used spectrally encoded microgels to detect viral cDNAs, reaching limit of detection in the rage of 0.1–0.9 nM and avoiding previous amplification steps.

Three different protein-coding messenger RNAs are detected by Choi et al,[27] by the means of hydrogel microparticles in multiplex. They have tuned the mesh of PEG polymer in order to permit the diffusion of mRNAs achieving amol limit of detection (employing an enzyme amplification method).

Ribosomal RNA sequences are detected by Ma et al,[180] coupling a NASBA amplification with a microgel-tethered molecular-beacon microarray. Their technology has allowed detecting 1 fM of amplicons in 75 minutes.

Additional hydrogel based bioassays recently developed to detect oligonucleotides are summarized in table 1.

Table 1 Hydrogel based bioassays for Nucleic acid detection

Target	Material	Probe	Detection	Sensitivity and multiplexing	Code	Reference
mRNA	PEGDA	Oligonucleotide (covalent)	capture extender, label extender, fluorescence readout	6 amol 3-plex	Graphical	27
microRNA oligonucleotide	PEGDA	Oligonucleotide (covalent)	Displacement assay	microRNA: fM oligonucleotide:pM 3-plex assay	Optical	40, 41
20–200 nt, microRNAs	PEGDA	Oligonucleotide (covalent)	Labeled targets or labeling with SAPE	20–200nt: subattomole miRNA: 1 amol	Graphical	43
microRNA	PEGDA	Oligonucleotide (covalent)	Universal labeling; Enzymatic amplification; fluorescence readout	0.1 amol 3-plex	Graphical	178

Target	Material	Probe	Detection	Sensitivity and multiplexing	Code	Reference
oligonucleotide	PEGDA	Oligonucleotide (covalent)	NASBA; Fluorescence readout	1 fM 3-plex	Spatial	180
21nt o	PEGDA + polyacrylamide	Oligonucleotide (covalent)	Complementary DNA	0.66 pM	Optical	181
microRNA	PEGDA	Oligonucleotide (covalent)	Universal labeling (T4 DNA ligase); rolling circle amplification; fluorescence readout	Amol 12-plex assay	Graphical	182
microRNA	PEGDA	Oligonucleotide (covalent)	Enzymatic amplification; Fluorescence readout	10 pg/µL 5-plex	Spatial	183
microRNA	Polyacrylamide	Oligonucleotide (covalent)	Complementary DNA	1 pM	-	184

4. AIM AND OUTLINE OF DISSERTATION

Since the first demonstration that hydrogels are innovative substrates to developing biosensors, many progress has been made in the field. This growing interest has driven us to develop biosensors based on hydrogel particles and, herein, some potential applications are described for the ultrasensitive detection of oligonucleotide biomarkers in human serum.

Although different devices have shown great potential and some of them are already available on the market, there is still the necessity of new platform, capable of detect biomarkers in human fluids with improved sensibility and specificity, avoiding amplification steps. In order to achieve this goal, we have been focusing on the research of appropriate materials, which combine biocompatibility and antifouling properties, and on the design of specific probes. Thus, PEG-hydrogel particles have been developed and in order to find the best condition for biosensing application both the structural properties of the hydrogel and the probes density have been tuned.

Our hydrogel-based biosensors allow overcoming the limitations of conventional techniques since manipulation of the sample is avoided. The detection is based on fluorescence optical readout and can be carried out in several common laboratory equipment.

In Chapter 2 microgels with core-shell structure are endowed with double strand probes to detect the presence of endogenous viral microRNA. The biosensing performances of these microgels are investigated highlighting their properties. In particular, the sensitivity scalable with the number of microgels, the versatility and the antifouling properties of microgels are elucidated. The assay developed represents an innovative way to detect Human Cytomegalovirus infection. Moreover, the assay allows overcoming the necessity of miRNA panels or threshold levels, whereas the endogenous hcmv-miR-US-4 is specifically synthetized and released in human serum by the virus.

In Chapter 3 microgels with core-shell structure are engineered with molecular beacon for microRNA detection. The reduce time of analysis, the specificity towards single nucleotide mutated target, as well as the enhanced sensitivity, scalable sensitivity and versatility represent a significant improvement of the biosensing technology based on microgels. In particular, a microgel-based biosensor for miR-21 detection in cancer application is described as case study.

In Chapter 4 a study to test the microgels assay performance in long similar oligonucleotides target detection is carried out. The assay is set-up using double strand and molecular beacon immobilized probes. This work has allowed defining the assay design guideline in order to develop high sensitive and specific microgels, also toward complex targets.

In Chapter 5, 3D-hydrogels microparticles by microfluidics are developed as biosensing element for miRNA detection. Firstly, the design of the double strand probe is arranged, then probe density and the composition of the hydrogel are established using bulk as scaffolds. Finally, this knowledge has been scaled down in microfluidics obtaining 3D-hydrogel biosensors for miRNA-143-3p detection, a miRNA involved in the early stage of Sclerosis lateral amyotrophic disease.

Finally, in Chapter 6 are synthetically presented conclusions and future perspectives.

REFERENCES

1. Huang, X., Liu, Y., Yung, B., Xiong, Y. & Chen, X. Nanotechnology-Enhanced No-Wash Biosensors for in Vitro Diagnostics of Cancer. *ACS Nano* **11,** 5238–5292 (2017).

2. Tadimety, A. *et al.* Advances in liquid biopsy on-chip for cancer management: Technologies, biomarkers, and clinical analysis. *Crit. Rev. Clin. Lab. Sci.* **55,** 140–162 (2018).

3. Peppas, N. A., Hilt, J. Z., Khademhosseini, A. & Langer, R. Hydrogels in Biology and Medicine: From Molecular Principles to Bionanotechnology. *Adv. Mater.* **18,** 1345–1360 (2006).

4. Caló, E. & Khutoryanskiy, V. V. Biomedical applications of hydrogels: A review of patents and commercial products. *Eur. Polym. J.* **65,** 252–267 (2015).

5. Li, J. & Mooney, D. J. Designing hydrogels for controlled drug delivery. *Nat. Rev. Mater.* **1,** 16071 (2016).

6. Van Vlierberghe, S., Dubruel, P. & Schacht, E. Biopolymer-Based Hydrogels As Scaffolds for Tissue Engineering Applications: A Review. *Biomacromolecules* **12,** 1387–1408 (2011).

7. Jagur-Grodzinski, J. Polymeric gels and hydrogels for biomedical and pharmaceutical applications. *Polym. Adv. Technol.* **21,** 27–47 (2010).

8. Shibayama, M. & Tanaka, T. in 1–62 (Springer, Berlin, Heidelberg, 1993). doi:10.1007/3-540-56791-7_1

9. Le Goff, G. C., Srinivas, R. L., Hill, W. A. & Doyle, P. S. Hydrogel microparticles for biosensing. *Eur. Polym. J.* **72,** 386–412 (2015).

10. Hoffman, A. S. & Ratner, B. D. *Synthetic Hydrogels for Biomedical Applications - a Review. American Chemical Society, Polymer Preprints, Division of Polymer Chemistry* **16,** (AMERICAN CHEMICAL SOCIETY, 1975).

11. Peppas, N. A., Bures, P., Leobandung, W. & Ichikawa, H. Hydrogels in pharmaceutical formulations. *Eur. J. Pharm. Biopharm.* **50,** 27–46 (2000).

12. Mann, B. A., Kremer, K. & Holm, C. The Swelling Behavior of Charged Hydrogels. *Macromol. Symp.* **237,** 90–107 (2006).

13. Hennink, W. . & van Nostrum, C. . Novel crosslinking methods to design hydrogels. *Adv. Drug Deliv. Rev.* **54,** 13–36 (2002).

14. Xiao, H. *et al.* A Multiple Shape Memory Hydrogel Induced by Reversible Physical Interactions at Ambient Condition. *Polymers (Basel).* **9,** 138 (2017).

15. Qiu, Y. & Park, K. Environment-sensitive hydrogels for drug delivery. *Adv. Drug Deliv. Rev.* **64,** 49–60 (2012).

16. Gupta, P., Vermani, K. & Garg, S. Hydrogels: From controlled release to pH-responsive drug delivery. *Drug Discov. Today* **7,** 569–579 (2002).

17. Zhang, K., Luo, Y. & Li, Z. Synthesis and characterization of a pH- and ionic strength-responsive hydrogel. *Soft Mater.* **5,** 183–195 (2007).

18. Zhao, Y. L. & Fraser Stoddart, J. Azobenzene-based light-responsive hydrogel system. *Langmuir*

25, 8442–8446 (2009).

19. Li, H. *et al.* Model development and numerical simulation of electric-stimulus-responsive hydrogels subject to an externally applied electric field. *Biosens. Bioelectron.* **19,** 1097–1107 (2004).

20. Ahmed, E. M. Hydrogel: Preparation, characterization, and applications: A review. *J. Adv. Res.* **6,** 105–121 (2015).

21. Zalipsky, S. & Harris, J. M. in 1–13 (1997). doi:10.1021/bk-1997-0680.ch001

22. Harris, J. M., Sedaghat-Herati, M. R., Sather, P. J., Brooks, D. E. & Fyles, T. M. in *Poly(Ethylene Glycol) Chemistry* 371–381 (Springer US, 1992). doi:10.1007/978-1-4899-0703-5_22

23. Nguyen, K. T. & West, J. L. Photopolymerizable hydrogels for tissue engineering applications. *Biomaterials* **23,** 4307–14 (2002).

24. Jiang, Y., Chen, J., Deng, C., Suuronen, E. J. & Zhong, Z. Click hydrogels, microgels and nanogels: Emerging platforms for drug delivery and tissue engineering. *Biomaterials* **35,** 4969–4985 (2014).

25. Barker, K. *et al.* Biodegradable DNA-enabled poly(ethylene glycol) hydrogels prepared by copper-free click chemistry. *J. Biomater. Sci. Polym. Ed.* **27,** 22–39 (2016).

26. Park, S. *et al.* Controlling uniformity of photopolymerized microscopic hydrogels. *Lab Chip* **14,** 1551–1563 (2014).

27. Choi, N. W. *et al.* Multiplexed detection of mRNA using porosity-tuned hydrogel microparticles. *Anal. Chem.* **84,** 9370–9378 (2012).

28. Deforest, C. A., Sims, E. A. & Anseth, K. S. Peptide-functionalized click hydrogels with independently tunable mechanics and chemical functionality for 3D cell culture. *Chem. Mater.* **22,** 4783–4790 (2010).

29. Nanduri, V. *et al.* Phage as a molecular recognition element in biosensors immobilized by physical adsorption. *Biosens. Bioelectron.* **22,** 986–992 (2007).

30. Russell, R. J., Pishko, M. V., Gefrides, C. C., McShane, M. J. & Cote, G. L. A fluorescence-based glucose biosensor using concanavalin A and dextran encapsulated in a poly(ethylene glycol) hydrogel. *Anal. Chem.* **71,** 3126–3132 (1999).

31. Li, Q., Luan, G., Guo, Q. & Liang, J. A new class of homogeneous nucleic acid probes based on specific displacement hybridization. *Nucleic Acids Res.* **30,** E5 (2002).

32. Yurke, B. & Mills, A. P. Using DNA to power nanostructures. *Genet. Program. Evolvable Mach.* **4,** 111–122 (2003).

33. Srinivas, N. *et al.* On the biophysics and kinetics of toehold-mediated DNA strand displacement. *Nucleic Acids Res.* **41,** 10641–10658 (2013).

34. Genot, A. J., Zhang, D. Y., Bath, J. & Turberfield, A. J. Remote toehold: A mechanism for flexible control of DNA hybridization kinetics. *J. Am. Chem. Soc.* **133,** 2177–2182 (2011).

35. Robinson, B. H. & Seeman, N. C. Simulation of double-stranded branch point migration. *Biophys.*

J. **51,** 611–626 (1987).

36. Massey, M. & Algar, W. R. Fluorescence resonance energy transfer (FRET) for DNA biosensors: FRET pairs and Förster distances for various dye–DNA conjugates. *Anal. Chim. Acta* **568,** 181–189 (2006).

37. Zhang, D. Y. & Winfree, E. Control of DNA strand displacement kinetics using toehold exchange. *J. Am. Chem. Soc.* **131,** 17303–17314 (2009).

38. Zhang, D. Y. & Seelig, G. Dynamic DNA nanotechnology using strand-displacement reactions. *Nat. Chem.* **3,** 103–113 (2011).

39. Zhang, D. Y. & Seelig, G. Dynamic DNA nanotechnology using strand-displacement reactions. *Nat. Chem.* **3,** 103–113 (2011).

40. Aliberti, A., Cusano, A. M., Battista, E., Causa, F. & Netti, P. A. High sensitive and direct fluorescence detection of single viral DNA sequences by integration of double strand probes onto microgels particles. *Analyst* **141,** 1250–1256 (2016).

41. Causa, F., Aliberti, A., Cusano, A. M., Battista, E. & Netti, P. A. Supramolecular spectrally encoded microgels with double strand probes for absolute and direct miRNA fluorescence detection at high sensitivity. *J. Am. Chem. Soc.* **137,** 1758–1761 (2015).

42. Stevens, P. W., Henry, M. R. & Kelso, D. M. DNA hybridization on microparticles : determining capture-probe density and equilibrium dissociation constants. **27,** 1719–1727 (1999).

43. Pregibon, D. C. & Doyle, P. S. Optimization of encoded hydrogel particles for nucleic acid quantification. *Anal. Chem.* **81,** 4873–4881 (2009).

44. Tyagi, S. & Kramer, F. R. Molecular Beacons: Probes that Fluoresce Upon Hybridization. *Nat. Biotechnol.* **14,** 303–308 (1996).

45. Goel, G., Kumar, A., Puniya, A. K., Chen, W. & Singh, K. Molecular beacon: a multitask probe. *J. Appl. Microbiol.* **99,** 435–442 (2005).

46. Wang, K. *et al.* Molecular Engineering of DNA: Molecular Beacons. *Angew. Chemie Int. Ed.* **48,** 856–870 (2009).

47. Lakowicz, J. R. in *Principles of Fluorescence Spectroscopy* 257–301 (Springer US, 1983). doi:10.1007/978-1-4615-7658-7_9

48. Zheng, J. *et al.* Rationally designed molecular beacons for bioanalytical and biomedical applications. *Chem. Soc. Rev.* **44,** 3036–3055 (2015).

49. Huang, K. & Martí, A. A. Recent trends in molecular beacon design and applications. *Anal. Bioanal. Chem.* **402,** 3091–3102 (2012).

50. Huang, J. *et al.* Design and bioanalytical applications of DNA hairpin-based fluorescent probes. *TrAC - Trends Anal. Chem.* **53,** 11–20 (2014).

51. Zhu, Z. in *Molecular Beacons* 1–17 (Springer Berlin Heidelberg, 2013). doi:10.1007/978-3-642-39109-5_1

52. Tsourkas, A., Behlke, M. A. & Bao, G. Structure-function relationships of shared-stem and

conventional molecular beacons. *Nucleic Acids Res.* **30,** 4208–15 (2002).

53. Yang, C. J., Lin, H. & Tan, W. Molecular assembly of superquenchers in signaling molecular interactions. *J. Am. Chem. Soc.* **127,** 12772–12773 (2005).

54. Marras, S. A. E. in *Fluorescent Energy Transfer Nucleic Acid Probes. Methods in Molecular Biology™, vol 335* 3–16 (Humana Press, 2006). doi:10.1385/1-59745-069-3:3

55. Bonnet, G., Tyagi, S., Libchaber, A. & Kramer, F. R. Thermodynamic basis of the enhanced specificity of structured DNA probes. *Proc. Natl. Acad. Sci.* **96,** 6171–6176 (1999).

56. Tsourkas, A., Behlke, M. A., Rose, S. D. & Bao, G. Hybridization kinetics and thermodynamics of molecular beacons. *Nucleic Acids Res.* **31,** 1319–1330 (2003).

57. Chen, C., Wang, W., Wang, Z., Wei, F. & Zhao, X. S. Influence of secondary structure on kinetics and reaction mechanism of DNA hybridization. *Nucleic Acids Res.* **35,** 2875–2884 (2007).

58. Marras, S. A., Kramer, F. R. & Tyagi, S. Multiplex detection of single-nucleotide variations using molecular beacons. *Genet. Anal.* **14,** 151–6 (1999).

59. Marras, S. A. E., Kramer, F. R. & Tyagi, S. *Genotyping SNPs With Molecular Beacons. Single Nucleotide Polymorphisms. Methods in Molecular Biology™* (Springer, Totowa, NJ, 2003). doi:10.1385/1-59259-327-5:111

60. Gui, Z. *et al.* Direct detection of circulating free DNA extracted from serum samples of breast cancer using locked nucleic acid molecular beacon. *Talanta* **154,** 520–525 (2016).

61. Giraldo-Vela, J. P. *et al.* Single-Cell Detection of mRNA Expression Using Nanofountain-Probe Electroporated Molecular Beacons. *Small* **11,** 2386–2391 (2015).

62. Kang, W. J. *et al.* Molecular beacon-based bioimaging of multiple microRNAs during myogenesis. *Biomaterials* **32,** 1915–1922 (2011).

63. Baker, M. B., Bao, G. & Searles, C. D. In vitro quantification of specific microRNA using molecular beacons. *Nucleic Acids Res.* **40,** (2012).

64. Li, J. J., Fang, X., Schuster, S. M. & Tan, W. Molecular beacons: A novel approach to detect protein - DNA interactions. *Angew. Chemie - Int. Ed.* **39,** 1049–1052 (2000).

65. Ma, C. *et al.* A novel kinase-based ATP assay using molecular beacon. *Anal. Biochem.* **372,** 131–133 (2008).

66. Nakano, S., Miyoshi, D. & Sugimoto, N. Effects of Molecular Crowding on the Structures, Interactions, and Functions of Nucleic Acids. *Chem. Rev.* **114,** 2733–2758 (2014).

67. Ma, Y. & Libera, M. Molecular crowding effects on microgel-tethered oligonucleotide probes. *Langmuir* **32,** 6551–6558 (2016).

68. Gong, Q., Wang, Y. & Yang, H. A sensitive impedimetric DNA biosensor for the determination of the HIV gene based on graphene-Nafion composite film. *Biosens. Bioelectron.* **89,** 565–569 (2017).

69. Kouassi, G. K. & Irudayaraj, J. Magnetic and Gold-Coated Magnetic Nanoparticles as a DNA Sensor. doi:10.1021/ac051621j

70. Ravalli, A. & Marrazza, G. Gold and Magnetic Nanoparticles-Based Electrochemical Biosensors for Cancer Biomarker Determination. *J. Nanosci. Nanotechnol.* **15,** 3307–3319 (2015).

71. Magnesphere, S., Particles, P. & Wi, M. Certificate of Analysis Instructions for use of this product can be found in the MagneSphere ® Magnetic Separation Products Technical Bulletin # TB246 , available online at : www.promega.com/tbs This lot passes the following Quality Control specifications. 5482 (2011).

72. Cao, Y. W. C., Jin, R. & Mirkin, C. A. Nanoparticles with Raman spectroscopic fingerprints for DNA and RNA detection. *Science (80-.).* **297,** 1536–1540 (2002).

73. Van Nguyen, K. & Minteer, S. D. DNA-functionalized Pt nanoparticles as catalysts for chemically powered micromotors: toward signal-on motion-based DNA biosensor. *Chem. Commun.* **51,** 4782–4784 (2015).

74. Sun, J. *et al.* DNA biosensor-based on fluorescence detection of E. coli O157:H7 by Au@Ag nanorods. *Biosens. Bioelectron.* **70,** 239–245 (2015).

75. Yola, M. L., Eren, T. & Atar, N. A novel and sensitive electrochemical DNA biosensor based on Fe@Au nanoparticles decorated graphene oxide. *Electrochim. Acta* **125,** 38–47 (2014).

76. Wang, J., Liu, G., Rasul Jan, M. & Zhu, Q. Electrochemical detection of DNA hybridization based on carbon-nanotubes loaded with CdS tags. *Electrochem. commun.* **5,** 1000–1004 (2003).

77. Hwang, B. H., Shin, H. H. & Cha, H. J. Optimization of DNA microarray biosensors enables rapid and sensitive detection. *Biotechnol. Bioprocess Eng.* **22,** 469–473 (2017).

78. Audrey Sassolas, Béatrice D. Leca-Bouvier, and & Blum*, L. J. DNA Biosensors and Microarrays. (2007). doi:10.1021/CR0684467

79. Klein, J. C. *et al.* Multiplex pairwise assembly of array-derived DNA oligonucleotides. *Nucleic Acids Res.* **44,** e43–e43 (2015).

80. Daniel, C., Roupioz, Y., Gasparutto, D., Livache, T. & Buhot, A. Solution-Phase vs Surface-Phase Aptamer-Protein Affinity from a Label-Free Kinetic Biosensor. *PLoS One* **8,** e75419 (2013).

81. Wong, I. Y. & Melosh, N. A. An electrostatic model for DNA surface hybridization. *Biophys. J.* **98,** 2954–63 (2010).

82. Traeger, J. C. & Schwartz, D. K. Surface-Mediated DNA Hybridization: Effects of DNA Conformation, Surface Chemistry, and Electrostatics. *Langmuir* **33,** 12651–12659 (2017).

83. Peterson, A. W., Heaton, R. J. & Georgiadis, R. M. The effect of surface probe density on DNA hybridization. *Nucleic Acids Res.* **29,** 5163–5168 (2001).

84. Macedo, L. J. A., Miller, E. N. & Opdahl, A. Effect of Probe–Probe Distance on the Stability of DNA Hybrids on Surfaces. *Anal. Chem.* **89,** 1757–1763 (2017).

85. Kimura-Suda, H., Petrovykh, D. Y., Tarlov, M. J. & Whitman, L. J. Base-Dependent Competitive Adsorption of Single-Stranded DNA on Gold. *J. Am. Chem. Soc.* **125,** 9014–9015 (2003).

86. Schmitt, T. J. & Knotts, T. A. Thermodynamics of DNA hybridization on surfaces. *J. Chem. Phys.* **134,** 205105 (2011).

87. Steel, A. B., Levicky, R. L., Herne, T. M. & Tarlov, M. J. Immobilization of Nucleic Acids at Solid Surfaces: Effect of Oligonucleotide Length on Layer Assembly. *Biophys. J.* **79,** 975–981 (2000).

88. Monserud, J. H. & Schwartz, D. K. Mechanisms of Surface-Mediated DNA Hybridization Mechanisms of Surface-Mediated DNA Hybridization. *ACS Nano* **8,** 4488–4499 (2014).

89. Irving, D., Gong, P. & Levicky, R. DNA Surface Hybridization: Comparison of Theory and Experiment. *J. Phys. Chem. B* **114,** 7631–7640 (2010).

90. Nimse, S. *et al.* Immobilization Techniques for Microarray: Challenges and Applications. *Sensors* **14,** 22208–22229 (2014).

91. Anseth, K. S., Bowman, C. N. & Brannon-Peppas, L. Mechanical properties of hydrogels and their experimental determination. *Biomaterials* **17,** 1647–57 (1996).

92. Flory, P. J. & Rehner, J. Statistical Mechanics of Cross-Linked Polymer Networks II. Swelling. *J. Chem. Phys.* **11,** 521–526 (1943).

93. Kofinas, P., Athanassiou, V. & Merrill, E. W. Hydrogels prepared by electron irradiation of poly(ethylene oxide) in water solution: unexpected dependence of cross-link density and protein diffusion coefficients on initial PEO molecular weight. *Biomaterials* **17,** 1547–1550 (1996).

94. Brannon-Peppas, L. & Peppas, N. A. Equilibrium swelling behavior of pH-sensitive hydrogels. *Chem. Eng. Sci.* **46,** 715–722 (1991).

95. Lee, W., Choi, D., Kim, J.-H. & Koh, W.-G. Suspension arrays of hydrogel microparticles prepared by photopatterning for multiplexed protein-based bioassays. *Biomed. Microdevices* **10,** 813–822 (2008).

96. Battista, E., Mazzarotta, A., Causa, F., Cusano, A. M. & Netti, P. A. Core-shell microgels with controlled structural properties. *Polym. Int.* **65,** 747–755 (2016).

97. Srinivas, R. L., Chapin, S. C. & Doyle, P. S. Aptamer-Functionalized Microgel Particles for Protein Detection. *Anal. Chem.* **83,** 9138–9145 (2011).

98. Zubtsov, D. A. *et al.* Effect of mixing on reaction–diffusion kinetics for protein hydrogel-based microchips. *J. Biotechnol.* **122,** 16–27 (2006).

99. Bloomfield, V. & Zimm, B. H. Viscosity, sedimentation, et cetera, of ring- and straight-chain polymers in dilute solution. *J. Chem. Phys.* **44,** 315–323 (1966).

100. Sorokin, N. V. *et al.* Kinetics of Hybridization on Surface Oligonucleotide Microchips: Theory, Experiment, and Comparison with Hybridization on Gel-Based Microchips. *J. Biomol. Struct. Dyn.* **24,** 57–66 (2006).

101. Walton, S. P., Stephanopoulos, G. N., Yarmush, M. L. & Roth, C. M. Thermodynamic and Kinetic Characterization of Antisense Oligodeoxynucleotide Binding to a Structured mRNA. *Biophys. J.* **82,** 366–377 (2002).

102. Heskins, M. & Guillet, J. E. Solution Properties of Poly(N-isopropylacrylamide). *J. Macromol. Sci. Part A - Chem.* **2,** 1441–1455 (1968).

103. Chern, C.-S. *Principles and applications of emulsion polymerization*. (Wiley, 2008).

doi:10.1002/9780470377949

104. Jones, C. D. & Lyon, L. A. Synthesis and characterization of multiresponsive core-shell microgels. *Macromolecules* **33,** 8301–8306 (2000).

105. Andersson, M. & Maunu, S. L. Structural studies of poly(N-isopropylacrylamide) microgels: Effect of SDS surfactant concentration in the microgel synthesis. *J. Polym. Sci. Part B Polym. Phys.* **44,** 3305–3314 (2006).

106. Robert G. Gilbert. *Emulsion polymerization: a mechanistic approach*. (Academic Press, 1995).

107. Feng, X., Pelton, R., Leduc, M. & Champ, S. Colloidal complexes from poly(vinyl amine) and carboxymethyl cellulose mixtures. *Langmuir* **23,** 2970–2976 (2007).

108. Luo, R.-C. & Chen, C.-H. Structured Microgels through Microfluidic Assembly and Their Biomedical Applications. *Soft* **01,** 1–23 (2012).

109. Baret, J. C. Surfactants in droplet-based microfluidics. *Lab Chip* **12,** 422–433 (2012).

110. Choi, C.-H., Jung, J.-H., Hwang, T.-S. & Lee, C.-S. In situ microfluidic synthesis of monodisperse PEG microspheres. *Macromol. Res.* **17,** 163–167 (2009).

111. Rossow, T. *et al.* Controlled synthesis of cell-laden microgels by radical-free gelation in droplet microfluidics. *J. Am. Chem. Soc.* **134,** 4983–4989 (2012).

112. Walther, B. *et al.* Drop deformation dynamics and gel kinetics in a co-flowing water-in-oil system. *J. Colloid Interface Sci.* **286,** 378–386 (2005).

113. Celetti, G., Natale, C. Di, Causa, F., Battista, E. & Netti, P. A. Functionalized poly(ethylene glycol) diacrylate microgels by microfluidics: In situ peptide encapsulation for in serum selective protein detection. *Colloids Surfaces B Biointerfaces* **145,** 21–29 (2016).

114. Wang, J.-T., Wang, J. & Han, J.-J. Fabrication of Advanced Particles and Particle-Based Materials Assisted by Droplet-Based Microfluidics. *Small* **7,** 1728–1754 (2011).

115. Kumacheva, E. *Microfluidic Reactors for Polymer Particles - Eugenia Kumacheva, Piotr Garstecki*. (Wiley, 2011).

116. Dendukuri, D., Pregibon, D. C., Collins, J., Hatton, T. A. & Doyle, P. S. Continuous-flow lithography for high-throughput microparticle synthesis. *Nat. Mater.* **5,** 365–369 (2006).

117. Yánez-Sedeño, P., Campuzano, S. & Pingarrón, J. M. Janus particles for (bio)sensing. *Appl. Mater. Today* **9,** 276–288 (2017).

118. Dendukuri, D., Gu, S. S., Pregibon, D. C., Hatton, T. A. & Doyle, P. S. Stop-flow lithography in a microfluidic device. *Lab Chip* **7,** 818 (2007).

119. Jain, K. K. in *The Handbook of Biomarkers* 147–175 (Springer New York, 2017). doi:10.1007/978-1-4939-7431-3_5

120. Jain, K. K. *The Handbook of Biomarkers*. (Humana Press, 2010). doi:10.1007/978-1-60761-685-6

121. MANDEL, P. & METAIS, P. Les acides nucléiques du plasma sanguin chez l'homme. *C. R. Seances Soc. Biol. Fil.* **142,** 241–3 (1948).

122. Schwarzenbach, H., Nishida, N., Calin, G. A. & Pantel, K. Clinical relevance of circulating cell-free microRNAs in cancer. *Nat. Rev. Clin. Oncol.* **11,** 145–156 (2014).

123. Breitbach, S., Sterzing, B., Magallanes, C., Tug, S. & Simon, P. Direct measurement of cell-free DNA from serially collected capillary plasma during incremental exercise. *J. Appl. Physiol.* **117,** 119–130 (2014).

124. De Vlaminck, I. *et al.* Noninvasive monitoring of infection and rejection after lung transplantation. *Proc. Natl. Acad. Sci.* **112,** 13336–13341 (2015).

125. Rodrigues Filho, E. M. *et al.* Elevated Cell-Free Plasma DNA Level as an Independent Predictor of Mortality in Patients with Severe Traumatic Brain Injury. *J. Neurotrauma* **31,** 1639–1646 (2014).

126. Tsai, N.-W. *et al.* The value of serial plasma nuclear and mitochondrial DNA levels in patients with acute ischemic stroke. *Clin. Chim. Acta* **412,** 476–479 (2011).

127. De Vlaminck, I. *et al.* Circulating Cell-Free DNA Enables Noninvasive Diagnosis of Heart Transplant Rejection. *Sci. Transl. Med.* **6,** 241ra77-241ra77 (2014).

128. Lo, Y. M. D. *et al.* Presence of fetal DNA in maternal plasma and serum. *Lancet* **350,** 485–487 (1997).

129. Diaz, L. A., Bardelli, A. & Bardelli, A. Liquid biopsies: genotyping circulating tumor DNA. *J. Clin. Oncol.* **32,** 579–86 (2014).

130. Cheng, F., Su, L. & Qian, C. *Circulating tumor DNA: a promising biomarker in the liquid biopsy of cancer*. **7,**

131. Wan, J. C. M. *et al.* Liquid biopsies come of age: towards implementation of circulating tumour DNA. *Nat. Rev. Cancer* **17,** 223–238 (2017).

132. Han, X., Wang, J. & Sun, Y. Circulating Tumor DNA as Biomarkers for Cancer Detection. *Genomics, Proteomics Bioinforma.* **15,** 59–72 (2017).

133. Stroun, M. *et al.* The origin and mechanism of circulating DNA. *Ann. N. Y. Acad. Sci.* **906,** 161–8 (2000).

134. Jahr, S. *et al.* DNA fragments in the blood plasma of cancer patients: Quantitations and evidence for their origin from apoptotic and necrotic cells. *Cancer Res.* **61,** 1659–1665 (2001).

135. Chiu, R. W. K. *et al.* Quantitative analysis of circulating mitochondrial DNA in plasma. *Clin. Chem.* **49,** 719–26 (2003).

136. Schwarzenbach, H., Hoon, D. S. B. & Pantel, K. Cell-free nucleic acids as biomarkers in cancer patients. *Nat. Rev. Cancer* **11,** 426–437 (2011).

137. Umetani, N. *et al.* Prediction of breast tumor progression by integrity of free circulating DNA in serum. *J. Clin. Oncol.* **24,** 4270–4276 (2006).

138. Castells, A. *et al.* K-ras mutations in DNA extracted from the plasma of patients with pancreatic carcinoma: Diagnostic utility and prognostic significance. *J. Clin. Oncol.* **17,** 578–584 (1999).

139. Ellinger, J. *et al.* CpG Island hypermethylation in cell-free serum DNA identifies patients with

localized prostate cancer. *Prostate* **68,** 42–49 (2008).

140. Umetani, N. *et al.* Increased Integrity of Free Circulating DNA in Sera of Patients with Colorectal or Periampullary Cancer: Direct Quantitative PCR for ALU Repeats. *Clin. Chem.* **52,** 1062–1069 (2006).

141. Gur Umu, S. U. *et al.* A comprehensive profile of circulating RNAs in human serum. *RNA Biol.* **15,** (2018).

142. Zaporozhchenko, I. A., Ponomaryova, A. A., Rykova, E. Y. & Laktionov, P. P. The potential of circulating cell-free RNA as a cancer biomarker: challenges and opportunities. *Expert Rev. Mol. Diagn.* **18,** 133–145 (2018).

143. Yuan, T. *et al.* Plasma extracellular RNA profiles in healthy and cancer patients. *Sci. Rep.* **6,** 19413 (2016).

144. Ainsztein, A. M. *et al.* The NIH Extracellular RNA Communication Consortium. *J. Extracell. Vesicles* **4,** 27493 (2015).

145. Ha, M. & Kim, V. N. Regulation of microRNA biogenesis. *Nat. Rev. Mol. Cell Biol.* **15,** 509–524 (2014).

146. Cullen, B. R. Transcription and processing of human microRNA precursors. *Mol. Cell* **16,** 861–865 (2004).

147. Hammond, S. M. An overview of microRNAs. *Adv. Drug Deliv. Rev.* **87,** 3–14 (2015).

148. Jovanovic, M. & Hengartner, M. O. miRNAs and apoptosis: RNAs to die for. *Oncogene* **25,** 6176–6187 (2006).

149. Mathieu, J. & Ruohola-Baker, H. Regulation of Stem Cell Populations by microRNAs. doi:10.1007/978-94-007-6621-1_18

150. Vasilatou, D., Papageorgiou, S., Pappa, V., Papageorgiou, E. & Dervenoulas, J. The role of microRNAs in normal and malignant hematopoiesis. *Eur. J. Haematol.* **84,** 1–16 (2010).

151. Kulshreshtha, R. *et al.* A MicroRNA Signature of Hypoxia. *Mol. Cell. Biol.* **27,** 1859–1867 (2007).

152. Chen, J.-F. *et al.* The role of microRNA-1 and microRNA-133 in skeletal muscle proliferation and differentiation. doi:10.1038/ng1725

153. Kawahara, H., Imai, T. & Okano, H. MicroRNAs in neural stem cells and neurogenesis. *Front. Neurosci.* 1–13 (2012). doi:10.3389/fnins.2012.00030

154. Kato, M., Castro, N. E. & Natarajan, R. MicroRNAs: Potential Mediators and Biomarkers of Diabetic Complications. doi:10.1016/j.freeradbiomed.2013.06.009

155. Najafi-Shoushtari, S. H. *et al.* MicroRNA-33 and the SREBP host genes cooperate to control cholesterol homeostasis. *Science (80-.).* **328,** 1566–1569 (2010).

156. Lindsay, M. A. microRNAs and the immune response Mark Lindsay.pdf. *Trends Imunol.* **29,** 343–351 (2008).

157. Lin, S. & Gregory, R. I. MicroRNA biogenesis pathways in cancer. *Nat. Rev. Cancer* **15,** 321–333 (2015).

158. Femminella, G. D., Ferrara, N. & Rengo, G. The emerging role of microRNAs in Alzheimer's disease. *Front. Physiol.* **6,** 1–5 (2015).

159. Hitachi, K. & Tsuchida, K. Role of microRNAs in skeletal muscle hypertrophy. *Front. Physiol.* **4 JAN,** 1–7 (2014).

160. Condorelli, G., Latronico, M. V. G. & Cavarretta, E. microRNAs in cardiovascular diseases: current knowledge and the road ahead. *J. Am. Coll. Cardiol.* **63,** 2177–87 (2014).

161. Nielsen, L. B. *et al.* Circulating levels of MicroRNA from children with newly diagnosed type 1 diabetes and healthy controls: Evidence that miR-25 associates to residual beta-cell function and glycaemic control during disease progression. *Exp. Diabetes Res.* **2012,** (2012).

162. Rottiers, V. & Näär, A. M. MicroRNAs in metabolism and metabolic disorders. *Nature Reviews Molecular Cell Biology* **13,** 239–251 (2012).

163. Wang, J., Chen, J. & Sen, S. MicroRNA as Biomarkers and Diagnostics. *J. Cell. Physiol.* **231,** 25–30 (2016).

164. Cullen, B. R. Viral and cellular messenger RNA targets of viral microRNAs. *Nature* **457,** 421–425

165. Zhou, J. *et al.* Maternal plasma levels of cell-free β-HCG mRNA as a prenatal diagnostic indicator of placenta accrete. *Placenta* **35,** 691–5 (2014).

166. Farina, A. The Role of RNAs and microRNAs in Non-Invasive Prenatal Diagnosis. *J. Clin. Med.* **3,** 440–452 (2014).

167. Lo, K. W. *et al.* Analysis of cell-free Epstein-Barr virus associated RNA in the plasma of patients with nasopharyngeal carcinoma. *Clin. Chem.* **45,** 1292–4 (1999).

168. Miura, N., Hasegawa, J. & Shiota, G. *Serum Messenger RNA as a Biomarker and its Clinical Usefulness in Malignancies Background of Circulating Nucleic Acids*. *Clinical Medicine: Oncology* **2,** (2008).

169. March-Villalba, J. A. *et al.* Cell-free circulating plasma hTERT mRNA is a useful marker for prostate cancer diagnosis and is associated with poor prognosis tumor characteristics. *PLoS One* **7,** e43470 (2012).

170. Rapisuwon, S., Vietsch, E. E. & Wellstein, A. Circulating biomarkers to monitor cancer progression and treatment. (2016). doi:10.1016/j.csbj.2016.05.004

171. Navarro, E., Serrano-Heras, G., Castaño, M. J. & Solera, J. Real-time PCR detection chemistry. *Clin. Chim. Acta* **439,** 231–250 (2015).

172. Gao, F. *et al.* Microdroplet Digital PCR: Detection and Quantitation of Biomarkers in Archived Tissue and Serial Plasma Samples in Patients with Lung Cancer. *J. Thorac. Oncol.* **10,** 212–217 (2015).

173. Vogelstein, B. & Kinzler, K. W. Digital PCR. *Proc. Natl. Acad. Sci. U. S. A.* **96,** 9236–41 (1999).

174. Ma, M. *et al.* 'Liquid biopsy'-ctDNA detection with great potential and challenges. *Ann. Transl. Med.* **3,** 235 (2015).

175. Shendure, J. & Ji, H. Next-generation DNA sequencing. *Nat. Biotechnol.* **26,** 1135–1145 (2008).

176. Keller, A. *et al.* Sources to variability in circulating human miRNA signatures. *RNA Biol.* **14,** 1791–1798 (2017).

177. Perakis, S. & Speicher, M. R. Emerging concepts in liquid biopsies. *BMC Med.* **15,** (2017).

178. Kim, J. J., Chen, L. & Doyle, P. S. Microparticle parking and isolation for highly sensitive microRNA detection. *Lab Chip* **17,** 3120–3128 (2017).

179. He, Y., Yang, X., Yuan, R. & Chai, Y. Switchable Target-Responsive 3D DNA Hydrogels As a Signal Amplification Strategy Combining with SERS Technique for Ultrasensitive Detection of miRNA 155. *Anal. Chem.* **89,** 8538–8544 (2017).

180. Ma, Y., Dai, X., Hong, T., Munk, G. B. & Libera, M. A NASBA on microgel-tethered molecular-beacon microarray for real-time microbial molecular diagnostics. *Analyst* **142,** 147–155 (2017).

181. Zhao, Y., Zhao, X., Tang, B., Xu, W. & Gu, Z. Rapid and Sensitive Biomolecular Screening with Encoded Macroporous Hydrogel Photonic Beads. *Langmuir* **26,** 6111–6114 (2010).

182. Chapin, S. C., Appleyard, D. C., Pregibon, D. C. & Doyle, P. S. Rapid microRNA profiling on encoded gel microparticles. *Angew. Chemie - Int. Ed.* **50,** 2289–2293 (2011).

183. Choi, W. *et al.* Hydrogel micropost-based qPCR for multiplex detection of miRNAs associated with Alzheimer's disease. *Biosens. Bioelectron.* **101,** 235–244 (2018).

184. Garcia-Schwarz, G. & Santiago, J. G. Integration of On-Chip Isotachophoresis and Functionalized Hydrogels for Enhanced-Sensitivity Nucleic Acid Detection. *Anal. Chem.* **84,** 6366–6369 (2012).

CHAPTER 2

"Toehold-mediated strand displacement Microgels: bioassay for Cytomegalovirus infection diagnosis"

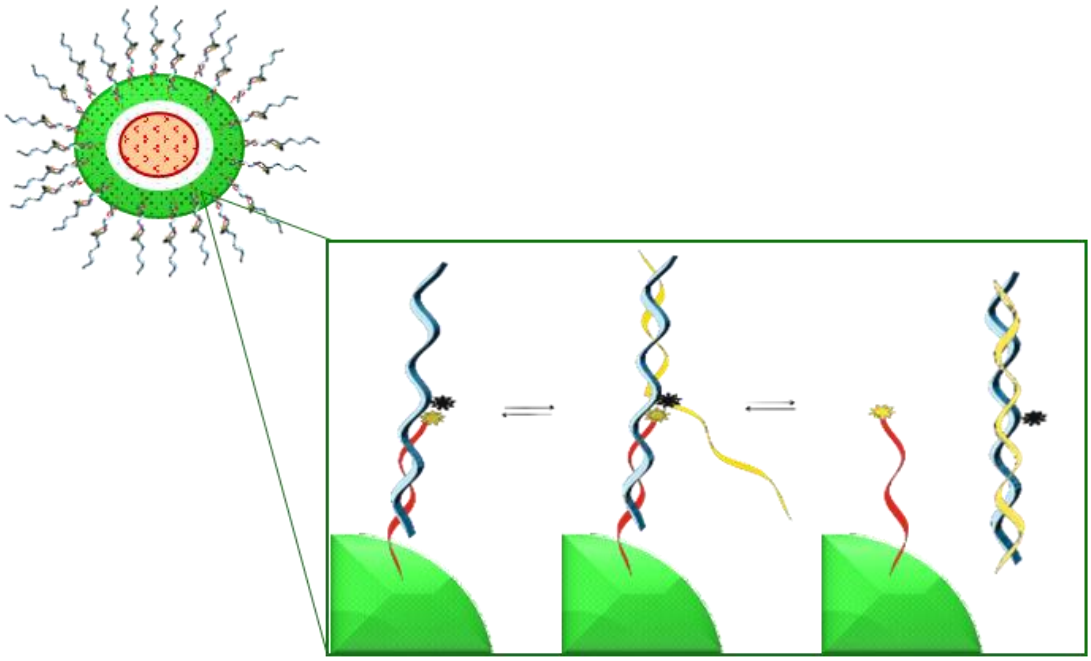

The work described in this chapter is part of a manuscript published:

Tania Mariastella Caputo, Annunziata Cummaro, Vincenzo Lettera, Alessia Mazzarotta, Edmondo Battista, Paola Antonio Netti e Filippo Causa***. "One-step scalable fluorescent microgel bioassay for endogenous viral miR-US4-5p ultrasensitive detection"*** Analyst, 2018, http://dx.doi.org/10.1039/C8AN02166J

1. INTRODUCTION

Human Cytomegalovirus (hcmv) is a member of Herpesviridae family, Betaherpesviridae subfamily, genus Cytomegalovirus and represents a significant cause of morbidity and mortality in compromised population. The virus has a worldwide distribution (affecting around 60% of adults in industrialized countries and 100% in poorer countries)[1], higher host specificity, low replication cycle and long latency period. Cytomegalovirus infection is often asymptomatic in immunocompetent people. However, the infection can induce serious clinical complications or death in new-borns and immunosuppressed people[2,3].

Actually, the conventional method to univocally detect the human cytomegalovirus infection is based on the isolation of virus from cells, by viral culture. The assay requires long time of analysis (about 4 weeks) and is affected by low sensitivity. These conditions have led to the development of several new diagnostic techniques[4–6]. However, despite all the efforts made, a specific diagnostic test able to work in low-sample-volume of human fluids, avoiding preliminary steps of purification and amplification is still lacking.

MicroRNAs have attracted great attention in clinical application. They are involved in a wide range of biological processes[7–15]and are used as potential biomarkers for the diagnosis and prognosis of a variety of diseases, including viral infections[16–22]. Recent works prove that viruses are not only able to modify human microRNA expression, but some of them[23], including Beta-Herpes viruses, are also competent to encode for their own sets of endogenous viral microRNAs[24–26]. Viral microRNAs are differentially expressed during the viral lifecycle and they affect both viral and cellular transcript. In particular, endogenous hcmv microRNAs have an active role in the complex regulation of host cell metabolism and in establishing latency and immune evasion[27,28].

For these reasons, use an endogenous viral microRNA as a biomarker is a promising method to overcome some limitations associated to conventional oligonucleotide biomarkers and improve hcmv diagnosis. In clinical routine, indeed, in order to use human microRNAs as biomarkers, it is necessary to establish a physiological threshold level to distinguish healthy from infected people. Additionally, microRNAs are often affected by inter- and intra-individual variability[29,30], which makes the threshold level complex to quantify[31]. Contrariwise, since endogenous viral microRNAs are absent in healthy people, their presence is indicative of infection and does not require to set a threshold level, avoiding misdiagnoses. Along this line, a circulating endogenous viral microRNA (hcmv-miR-UL22A-5p) has been used as a specific biomarker of cytomegalovirus infection after solid organ transplantation[32].

Furthermore, it is proved that the hcmv-miR-US4-5p has a primary role in cytomegalovirus infection. The miR is released by the virus during the active stage of infection[33] and has an effective role on the immune response[34]. Due to its recognized role, it has been validated as circulating biomarker for the follow-up of pharmacological therapy [35]. Therefore, the circulating hcmv-miR-US4-5p might be used as biomarker since its presence is a clear indication of cytomegalovirus active infection. Hence, its detection represents an innovative approach for the accurate diagnosis of infection.

Through the years, beads-based assays have been renowned in the analytical field for their efficiency in biomarker detection, including nucleic acids[36]. However, beads suffer of some limitations, such as the non-specific interactions and low kinetics of reaction. Hydrogel microparticles (e.g. microgels), differently, due to their solution-like environment, chemical tunability and non-fouling nature in human fluids proved promising in the detection of various biomolecules[37–39] overcoming limitations observed in conventional bead based assays. In particular, microgels are easily synthesized by several strategies[40], encoded with optical or morphological barcodes[41–43] and functionalized with probes for capture and detection of clinically relevant biomarkers such as proteins, DNA, mRNA, and microRNA (miRNA)[44–46].

Based on these considerations, in this chapter we have described an innovative diagnostic microgel assay for active cytomegalovirus infection disease, based on endogenous hcmv-miR-US4-5p detection. The combination of antifouling and biocompatible properties of PEG microgels with the integration of probe sequences allow to obtain a direct, amplification-free bioassay for specific hcmv-miR-US4-5p quantification. In particular, we have achieved a tuneable optical detection, based on the number of microgels used for assay, reaching attomolar sensitivity.

2. EXPERIMENTAL SECTION

2.1. Materials

Poly(ethylene glycol) dimethacrylate average Mn 550 (PEGDMA), Acrylic acid (AAc), Potassium persulfate (KPS), Fluoresceine O-methacrylate, 1-ethyl-3-(3-dimethylaminopropyl) carbodiimide (EDC) and Polyvinyl alcohol 40-88 (PVA), Dimethyl Sulfoxide (DMSO), Sodium Hydroxide, and 4-Morpholineethanesulfonic acid sodium salt (MES) were all purchased from Sigma-Aldrich and used as received. The dye Methacryloxyethylthiocarbonylrhodamine B was obtained from Polyscience Inc. Tris buffer 1M, pH 8 was supplied by Applichem GmbH. DNA and RNA oligonucleotides were purchased from Metabion International AG GmbH with HPLC purification. Human serum was supplied by Lonza.

2.2. Probe design

The oligonucleotide probes were designed as DNA double strand (ds) sequences appropriately tailored on the target sequence hcmv-miR-US4-5p, according to specific requirements. In particular, thermodynamic parameters, sequence alignment and folding were considered to improve the ds-probe stability, avoid alignment with non-specific sequences and minimize secondary structure. The target sequence was synthesized according to mirbase.org[47] and thermodynamic parameters (melting temperature, stability, and folded fraction at assay condition) were predicted using appropriate tools (OligoAnalyzer 3.1 (IDT-Integrated, D. N. A. 2014) and Oligocalc[48]). Then, the ds probe length was carefully evaluated to allow a stable hybridization between the oligonucleotide strands at physiological ionic strength and predict the free energy of displacement (ΔGdisplacement). The alignment scores were predicted by mirbase.org and NCBI blast[49], while folding was simulated through UNAFold web server[50]. The target recognition is based on toehold mediated strand displacement mechanism. For this purpose, an oligonucleotide quencher strand (Q) fully complementary to the target, is designed with an internal Black Hole Quencher (dT-BHQ2). This strand is partially complementary to a shorter tail (F), labelled with a fluorophore (ATTO647N) at the 5'terminus and a C6-spacer with amine linker on the 3' terminus. Quenching efficiency and kinetics of displacements for the selected ds-probe were measured by spectrofluorometer. Displacement efficiency was measured mixing 5nM of pre-hybridized ds tail-quencher with 1:1 and 1:10 target solution, in 500 µL of 100 mM TRIS buffer pH 8 enriched with 200 mM NaCl (hybridization buffer). Moreover, ds-probe specificity was tested spiking 50 nM of non-matching microRNA (table 1) (10-fold excess) in hybridization buffer alone and in presence of equimolar target viral microRNA. The emission intensity was monitored over 24 hours. Assay performance in complex matrixes was carried out adding 50 nM of synthetic target hcmv-miR-US4-5p in human serum sample (200 µL of human serum and 300 µL of hybridization buffer) in presence of 5 nM of free ds-probe and kinetics of recovery was monitored for 24 hours by spectrofluorometer. Quenched samples were used as reference in order to evaluate the displacement efficiency.

Table 1 Oligonucleotide sequences used and their thermodynamic parameters (predictions calculated setting: 5nM of DNA, 200mM of Na+, pH 7-8, 5°C).

	SEQUENCE (5'-3')	Tm (°C)	ΔG (kcal/mol)
Tail strand(F)	GGGGGATGTCTG	41.2	QFhyb=-23.75
Quencher strand (Q)	CAGACATCCCCCTGCACGTCCA	67.2	QThyb=-45.29
hcmv-miR-US4-5p (T)	UGGACGUGCAGGGGGAUGUCUG		
			ΔGdisplacement= -21.54
Non-matching miRNA	UGAGAUGAAGCACUGUAGCUC		

2.3. Microgel synthesis and functionalization

Core-shell microgels were obtained through a multistep synthesis. Firstly, core nanoparticles, composed of 1% (w/v) PEGDMA and 0.1mM rhodamine B acrylate monomer, were synthetized by free-radical precipitation polymerization. The reaction was carried out in aqueous solution of 1% (w/v) PVA using 2.2 mM of KPS as thermal initiator. The solution was heated to 65°C stirring vigorously for 7 hours while purged with N_2 gas. Once dialyzed, the rhodamine-labelled core was used as a seed for the subsequent two shells polymerization. The first shell was obtained adding to the aqueous solution of core microgel PEGDMA 0.5% (w/v), PVA 0.5% (w/v) and KPS (1.1 mM). The solution was heated to 65 ºC for 6 hours in N_2 atmosphere. The second shell was obtained adding to the aqueous suspension of core/1°shell microgels PEGDMA 0.5% (w/v), Acrylic acid 0.25% (w/v), Fluoresceine O-methacrylate (0.1 mM), KPS (1.1 mM) and carried out the reaction at 65 ºC for 6 hours in N_2 atmosphere. The core-shell microgels size and electrophoretic mobility were characterized by Dynamic light scattering (Malvern Zetasizer Nano ZS instrument, 633 nm laser, 173° scattering angle). Carboxyl groups content was quantified by titration before further conjugation of the probe.

Bioconjugation optimization was performed by changing the amount of coupling agent (EDC) and the amino-fluorescent tail strand. First, several EDC concentrations (20, 200, 500, 1000, 2000 mM) were tested by reacting 1 mg of microgels and 1 nmol of fluorescent tail strand in a final volume 500 µL of coupling buffer (0.1 M MES pH 4.8), overnight at room temperature. Afterwards, 1 mg of microgels was coupled with 300, 600,1000 and 1500 pmol of fluorescent tail strand by using the optimized EDC concentration. The functionalized microgels were washed three times and resuspended in 500 µL of hybridization buffer. The amount of the tail bound to the microgel surface was calculated from the difference between the initial and the supernatant labelled tail concentration. The quenching step was performed adding 10-fold excess of quencher strand (3, 6, 10, 15 nmol) to the functionalized microgels and incubating overnight at room temperature. The quenched microgels were washed three times and resuspended in 500 µL of hybridization buffer.

2.4. Fluorescence measurement

Quenching efficiency and recovery of fluorescence after the toehold mediated strand displacement assay were recorded by spectrofluorometer and by confocal microscopy. Double strand functionalized microgel solutions were prepared after mixing 25 µg, 12.5 µg and 2.5 µg of microparticles to 500 µL of hybridization buffer containing target sequences from 10^{-9} to 10^{-18}M. The assay was run with final microgel concentration of 50 µg/mL, 25 µg/mL and 0.5 µg/mL (respectively

corresponding to $1.45 \cdot 10^9$, $7.25 \cdot 10^8$ and $1.45 \cdot 10^7$ microgels) and incubated at room temperature overnight. For the spectrofluorometer measurements the samples were analysed unprocessed, while were diluted to 0.5 µg/mL for the confocal microscopy analysis. Assay performance in complex matrixes was carried out spiking 50 nM of synthetic target hcmv-miR-US4-5p in human serum sample (200 µL of human serum and 300 µL of hybridization buffer) in presence of 50 µg/mL of microgels. The kinetics of recovery was measured for 24 hours by spectrofluorometer. Moreover, functionalized and quenched microgels were stored at 4°C in hybridization buffer and stability was monitored over one year. Recurrently, 50 µg/mL of microgels were resuspended from the stock and fluorescence measured by spectrofluorometer. Fluorescence spectra were collected in a 1 cm path length cuvette with a Horiba JobinYvon model FluoroMax-4 spectrofluorometer equipped with a Peltier temperature controller. The probe sequences were excited at 647nm (slit width of 5 nm) and emission spectra were collected from 667 to 750 nm (slit width of 5 nm). In addition, in order to quantify the rhodamine copolymerized into the core, microgels were excited at 548 nm and emission was collected from 568 to 650 nm (slit width of 5 nm). Fluorescence kinetics curves were obtained by plotting the wavelength emission maximum as a function of the time and fitted by one phase association equation to calculate the specific rate constants.

Confocal microscopy fluorescence measurements were performed by means of a Confocal laser scanning microscope Leica SP5 with an objective HCX PL APO CS 63x1.40 oil (Zeiss). Helium neon laser 543nm and 633nm were used for ATTO647N and rhodamine excitation. Power lasers and detector gains were kept always constant with a section thickness 3.04 airy unit, scan speed 8000 Hz and an image size of 144.7x144.7 μm^2 (resolution 1024x1024). For each target concentration, the sample was loaded onto µ-slide VI 0.4 ibidi (Ibidi, Martinsried, DE), and the images were collected. More than 200 microgels were analysed using a custom image-processing software (ParticleINTcalc_Dannhauser 2016V2.5).

In addition, fluorescent measurements were acquired and analysed by a BD FACSCanto II flow-cytometer and DIVA software (Becton Dickinson, Fullerton, CA). Measurements were carried out adding 10^6 microgels in 1mL of buffer and analysing the forward and side scattering setting the population in the middle of the plot. Gated the position, the particles with positive value were selected and for those selected was analysed the intensity of Fluoresceine, Rhodamine(PE) and Atto647N (APC).

2.5. Statistical analysis

All experiments were performed at least three times, reported as mean ± standard deviation and analysed statistically by paired Student's test. Significant difference was determined at P values smaller than 0.05.

3. RESULTS AND DISCUSSION

3.1. Probe design

In order to develop an assay for microRNA detection we select a specific biomarker and, based on that, a DNA double strand probe is designed (Figure 1A). Such probe is then mounted on the surface of a microgel and it is capable to recognize single strand target by increasing its fluorescence emission (Figure 1B). Microgel assay is, indeed, based on a fluorescence increase upon the target addition and it is characterized by a scalable sensitivity with a limit of detection correlated to the number of microgels used in the assay (Figure 1C-D). The DNA double strand probe consists of a quencher strand (25nt) fully complementary to the target, internally modified with a Black Hole Quencher2 (BHQ2), and a shorter (12nt) fluorescent tail strand. When the

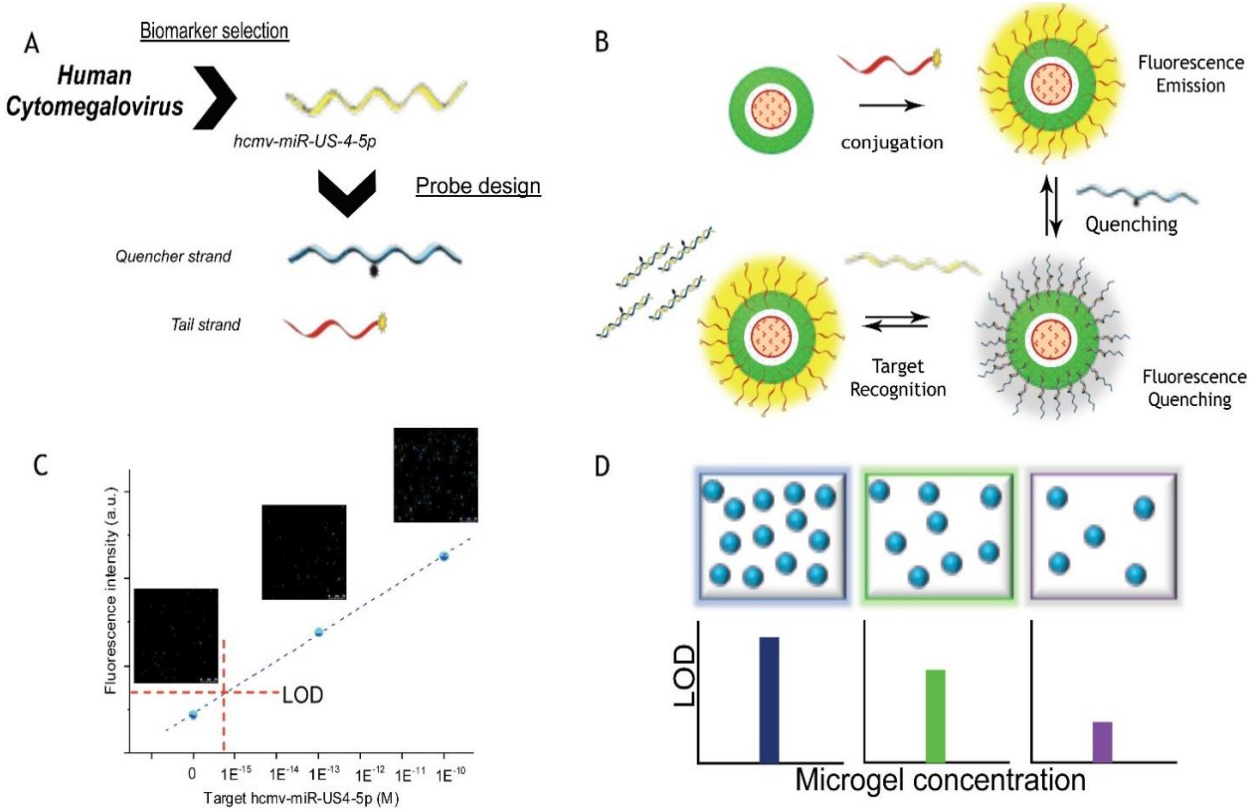

Figure 1 Overview of the assay: A) Double strand probe is designed based on specific biomarker selection. B) Microgel functionalization and fluorescence recovery mechanism involved in target detection. C) Microgels assay working range (nM-aM) and D) LOD tunability is based on the number of microgels used for assay.

quencher and the fluorescent tail strands hybridize, the fluorophore and quencher come in close proximity and fluorescence quenching occurs. In presence of the target, the toehold displacement is initiated by its binding to the quencher strand[51]. The target replaces the fluorescent strand by a mechanism defined as "branch migration". The branch point of quencher-target pair moves random walking over the domain of quencher-fluorescent tail strand. If the branch point advances sufficiently far the quencher strand is fully displaced and the strand exchange is complete[52,53].

To achieve high sensitivity and specificity in hcmv-miR-US4-5p identification, the DNA double strand probe sequences have been opportunely designed according to alignment studies and thermodynamic parameters simulation.

The oligonucleotide alignment is defined by the raw score (*S*) and E-value. *S* corresponds to the local alignment of similar segments to our specific sequences, while E-value is the expected amount of random sequences that have equivalent alignment. Higher raw score and smaller e-

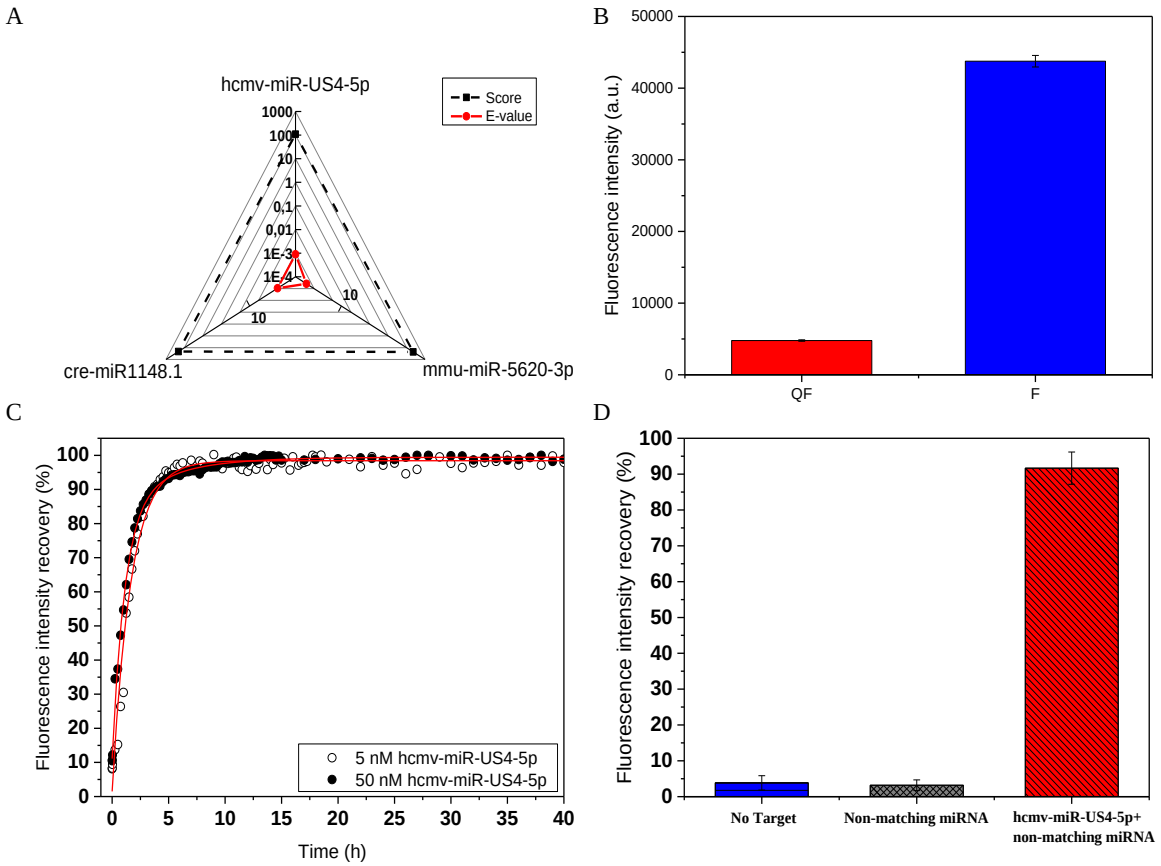

Figure 2 A) Representation of alignment results for hcmv-miRUS4-5p calculated by mirbase.org B)Fluorescence emission intensity of the tail labelled strand(F, 5nM) and duplex tail-quencher strand (QF, 5nM 1:1 ratio). C) Fluorescence recovery as a function of time in toehold-mediated strand displacement assay after addition 5nM (empty circle) and 50 nM (full circle) of hcmv-miR-US4-5p target, in homogeneous condition; D) Fluorescence recovery in presence of 10-fold excess of non-matching miRNA alone (black column) and mixed with the target (red column).

value (10^{-4} order) are indicative of a significant match. From the alignment studies resulted that no human microRNA or circulating DNA sequences are associated to the hcmv-miR-US4-5p sequence. As shown, only two microRNAs align with the hcmv-miR-US4-5p sequence and they are ascribable to viral microRNA synthetized during the cytomegalovirus infection in other species (Figure 2A). In particular, miR-5620-3p has a total S of 66, E-value of 2.9 and is expressed by *mus musculus* (house mouse), while the miR1148.1 has S of 65, E-value of 3.5 and is expressed by *Chlamydomonas reinhardtii* (green alga). Alignment data suggest very high specificity for the selected target and consequently for the assay.

Oligonucleotide probes must be designed considering thermodynamic and folding parameters. Thermodynamic parameters are accurately predicted during the design of the oligonucleotide double strand probes. In particular, the length of the strands is optimized to guarantee both higher probe hybridization in absence of target (Tm>37°C) and appropriate free energy (ΔG) of displacement in presence of the target (Table 1). The ΔG of displacement is calculated as the difference between the free energy of hybridization predicted for the target/quencher pair and that expected for quencher/tail pair (Table 1). As the ΔG of displacement is the driven force of this process, the probes are designed in order to gain about -20 kcal/mol from the displacement. In our specific case, the predicted ΔG of displacement is -21.54 kcal/mole (Table 1).

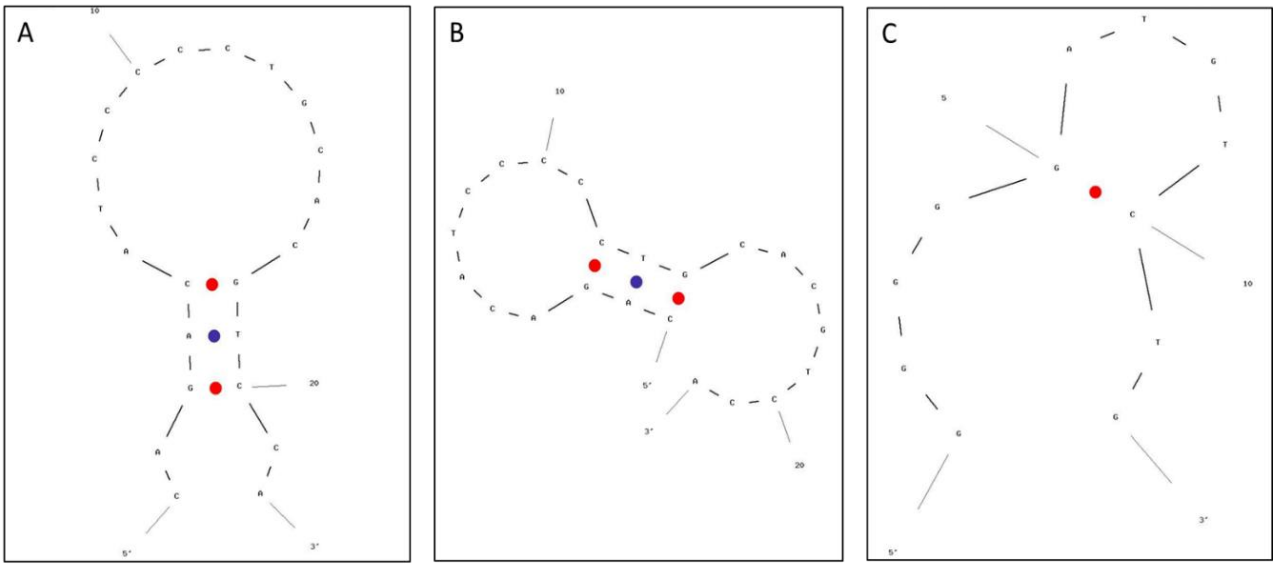

Figure 3 A-B) Quencher strand (Q) and C) Tail strand (T) folding simulations and their relative free energy

Complex oligonucleotide folding or stable secondary structures could decrease the probes hybridization or hindered the displacement. Based on the folding simulations, stable secondary structures are not expected for the ds-probes presented in this work (Figure 3).

Once optimized the design, ds-probe are synthetized and tested in solution. For our specific labelled tail-quencher duplex, the quenching efficiency is about 90% in hybridization buffer (homogeneous conditions) (Figure 2B). In the Figure 2C the fluorescence emission of ds-probe in presence of different amounts of hcmv-miR-US4-5p target is shown as a function of time. When the viral RNA target sequence is added to the hybridization buffer containing 5nM of ds-probe in homogenous, a quick recovery of fluorescence is recorded. No relevant difference is observed adding 5nM and 50 nM of target (corresponding to equimolar concentration and 10-fold excess) and in both cases, complete target displacement and subsequent recovery of the signal is achieved in about 5 hours, as indicated by the "plateau" region of the kinetics profile (Figure 2C). The time constants, calculated by the non-linear fitting of the kinetics experiment, resulted 1.57 hours and 1.7 hours respectively for 5nM and 50nM of miRNA target.

Moreover, we have tested the ds-probe specificity using a not matching sequence. As showed in Figure 2D, no recovery of fluorescence is recorded after 24 hours when 10-fold excess of the target is mixed with the ds-probes.

3.2. Microgel synthesis and functionalization

Multifunctional microgels with core-shell architecture are obtained combining free radical polymerization and seeded polymerization reaction[43,44]. Microgels result monodispersed with a core, first and second shell size average of 416.2 ± 0.9, 889.4 ± 18.05 and 1002.0 ± 16.3 nm respectively (Table 2). The outmost layer presents a net charge of -15 mV due to the copolymerization of acrylic acid that confers the colloidal stability and provides the carboxyl groups for the conjugation of DNA probes (Figure 4A).

Several bioconjugations have been tested. From our studies result that the best assay performances are achieved using 500 mM of EDC (Figure 4B inset) and 1000 pmol of fluorescent tails (corresponding to probe density of $1.0^2 \times 10^4$ DNA tail probes/microgels). In such condition, after the addition of the quencher strands, we have reached a quenching efficiency of 76.46%. Both decreasing and increasing the amount of immobilized fluorescent tail, we have observed a decrease of the quenching efficiency. In particular, a quenching efficiency of 42.6%, 56.4% and 58.4% is measured at 300, 600, 1500 pmol respectively (Figure 4C).

Table 2 Hydrodynamic diameter (Dh) and ζ potential measurement of microgels

	Z average ($D_{H,}$ nm)	PDI	Zeta potential (mV)
Core	416.2±0.9	0.006	-3.67±0.287
First shell	889.4±18.05	0.078	-6.52±0.0557
Second shell	1002.0±16.3	0.28	-15.1±0.379

These data are explained considering that probes are conjugates on the outmost layer of a microgel. Differently from the 2D surface, the oligonucleotide strands are immobilized within a three-dimensional polymer network of approximate radius of 200 nm and not only on a surface. Furthermore, the microgel shells are interpenetrated[54], this means that along the thickness of the functionalizable layer, the innermost section could hinder the hybridization due to the reduction of the polymer network mesh size and the increase electrostatic repulsions. As consequence, the hybridization between the immobilized fluorescent tail and the quencher strand is hindered in the innermost zone of the gel and fluorescence background is generated. At low coupling concentrations (300 pmol), the fluorescent background due to innermost un-quenched probes has a greater effect on the background as confirmed by the Signal/Noise ratio (S/N=1.74). Increasing the functionalization to 600 and then 1000 pmol, S/N ratio increases from 2.29 to 4.25. This because increasing the total amount of tails hybridized, the deepest un-quenched tails have less influence on the background and thus the efficiency of quenching is improved. Increasing the probe density to 1500 pmol, the efficiency of quenching decreases due to the crowding effect.

In order to compare the homogenous and heterogeneous kinetics of displacement, we have used 50 µg/mL of functionalized beads, corresponding to 5 nM of fluorescent probes attached on the microgel surface. As expected, kinetics of displacement on the microgels are correlated to the concentration of the added target (Figure 4D). The time constant, calculated by the non-linear fitting, is 3.36 hours when 10-fold excess of target are mixed with microgels and 7.6 hours at equimolar amount. Therefore, in heterogeneous condition, a slightly lower recovery of fluorescence intensity at equilibrium is observed, even though more evident is the depletion of the characteristic time of the kinetic processes. Both phenomena can be ascribable to the limited molecular mobility of the oligonucleotide double strand probes at polymer interface along with a reduced accessibility of the target within the outer microgel layer.

A rigorous control over the microgels used in each reaction run is maintained through simultaneously fluorescence measurements of the reporter (ATTO647N) and internal reference (Rhodamine). This is essential to avoid false results due to a different number of analysed microparticles.

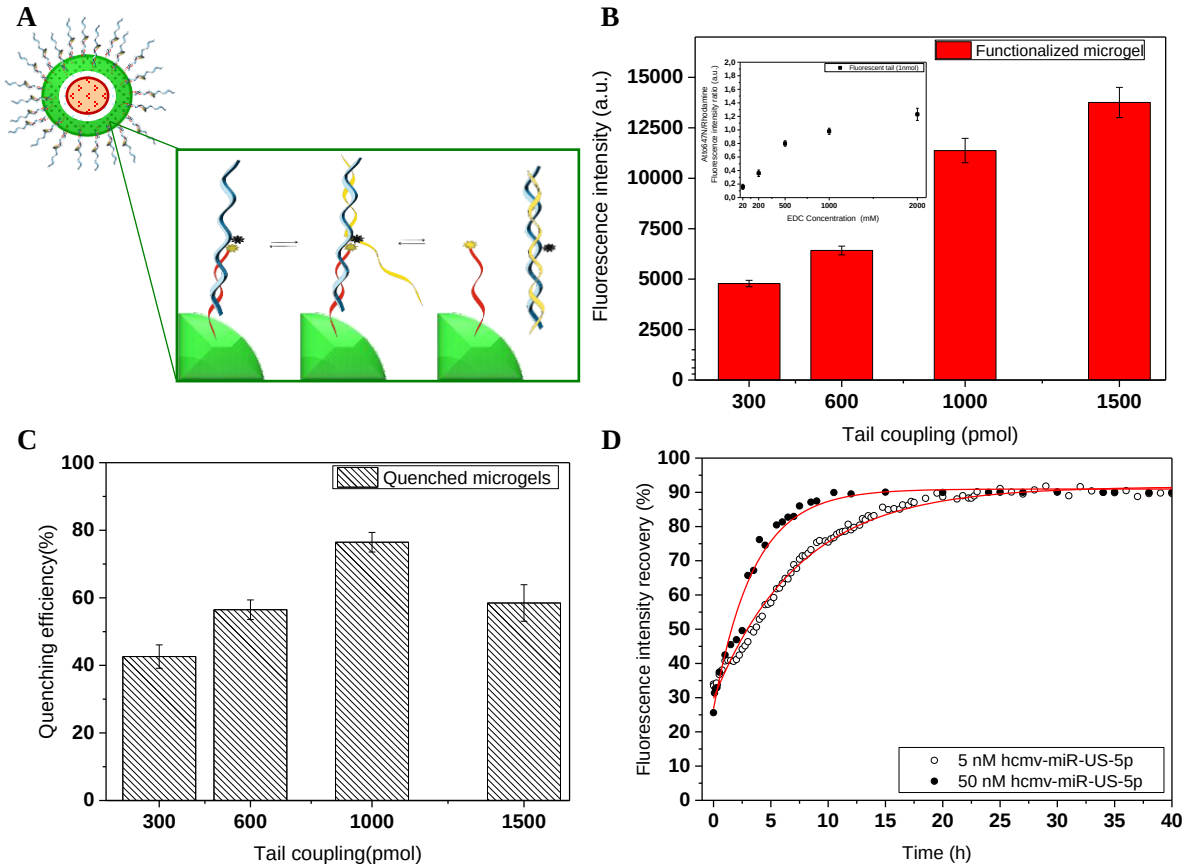

Figure 4 A) Schematic representation of the toehold mediated strand displacement assay on microgel beads; B) Fluorescence intensity measured for 50µg/mL of microgels with different functionalization grade before the quenching step. In the inset, coupling efficiency obtained for a fixed fluorescent tail and microgels amount increasing the EDC concentrations. Data are presented as fluorescence ratio between the reporter (Atto647N) and the reference dye(Rhodamine); C) Quenching efficiency of the above-mentioned functionalised microgels; D) Fluorescence recovery as a function of time in toehold mediated strand displacement assay after addition 5nM (empty circle) and 50 nM (full circle) of hcmv-miR-US4-5p target.

3.3. Assay set-up

Microgel beads are tested toward several assay conditions and fluorescence is measured by confocal laser scanning microscope (CLSM) and spectrofluorometer. CLSM is an image-based approach where the fluorescence emission of single particle is measured and related to the amount of target added.

The pictures collected during the assay clearly show the microgel core/shell architecture. The core, made of the PEGDMA-Rhodamine copolymer (coloured in red), is surrounded by fluorescent tail strands emitting in the not-overlapping channel of ATTO647N (coloured in blue) (Figure 5A). For each sample,

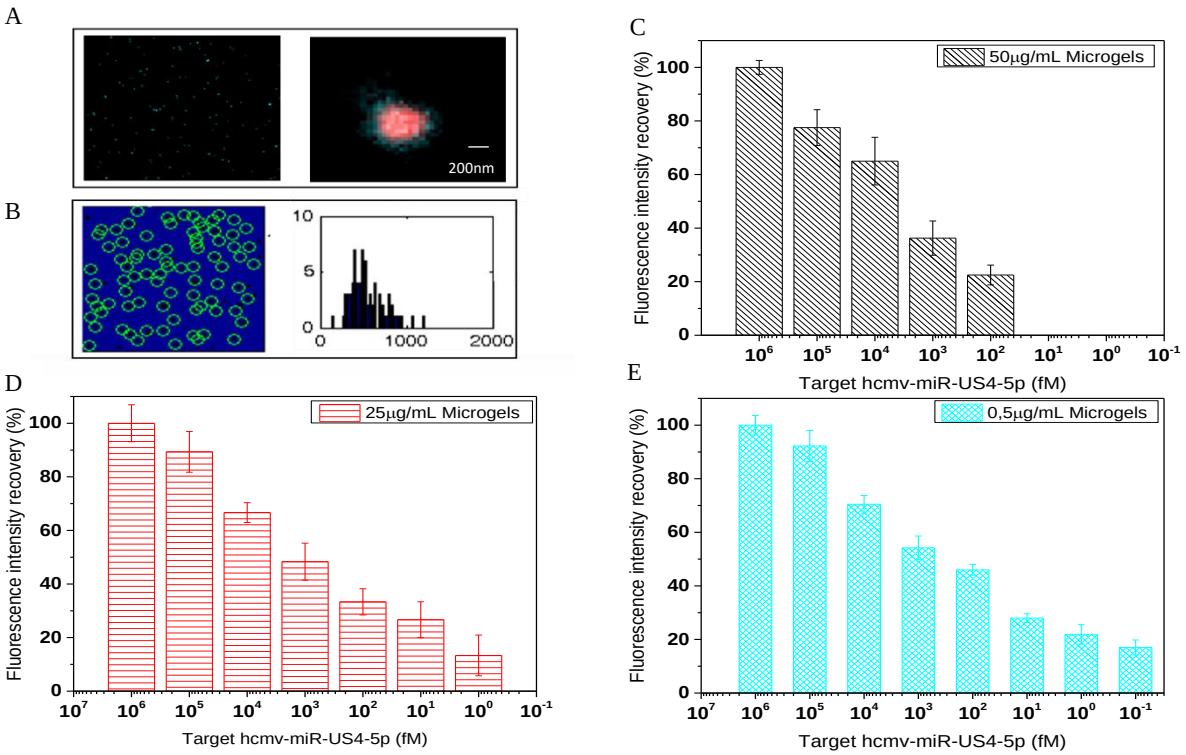

Figure 5A) Images collected by CLSM and B) analysed with the software dedicate; Fluorescence intensity recovery, in presence of hcmv-miR-US4-5p (106-10-1 fM) obtained using with 50µg/mL (C), 25µg/mL (D) and 0.5µg/mL(E) of microgels

more than 100 fluorescent microparticles per image are taken and data are processed by an "in house" developed image analyser (Figure 5B), routinely setting many parameters. In particular, we initially set the threshold intensity, then we select the ROI around microgel and we measure the intensity and the signal-to-noise ratio.

In order to validate the working range, the sensitivity and the limit of detection, a wide range of viral microRNA target concentrations is explored and the number of microgels are tuned for each assay (50 µg/mL, 25 µg/mL and 0.5 µg/mL). We have proved that the fluorescence recovery on a single microgel allows the detection of the target in a dynamic working range of 10^{-9}–10^{-18} M. We have not explored higher target concentrations since circulating microRNAs are mainly expressed in nM-fM range[55]. The minimum target presence distinguishable from the background noise has a concentration comprised between femtomolar to attomolar. Furthermore, as reported in Figure 5C, D and E, the recovery of fluorescence increases exponentially with the hcmv-mir-US4-5p concentration, while the limit of detection (LOD) value decreases substantially reducing the number of microgels for assay (Table 3). LODs in the order of 39.1 fM, 11.7 fM, 156 aM are achieved when 50 µg/mL, 25 µg/mL and 0.5 µg/mL

of microgels are used respectively. Thus, this microgel based assay shows a scalable sensitivity, being tuneable over a wide range of target concentrations. Such enhanced results are difficult to achieve with standard amplification free methods.

In fact, acting as target concentrator, microgels improve the sensitivity of toehold-mediated strand displacement assay, increasing both the range of target detectable and the sensitivity, avoiding target amplification[44,45,56].

Furthermore, as shown in Figure 6A microgel assay is particularly suited for common laboratory equipment (e.g. spectrofluorometer and flow cytometer). We set assay conditions by using 50 µg/mL and 25 µg/mL of microgels. Indeed, increasing the microgel concentration, scattering events dramatically risen, while below 25 µg/mL it is not possible to isolate the fluorescence signal from background noise. For both microgel concentration tested the working range of the assay is comprised between nM to fM (Figure 6A). LOD of 354 fM is achieved testing 50 µg/mL of microgels. Decreasing the microgel concentration to 25 µg/mL, the LOD increases reaching 283 fM. Thus, we have proved that

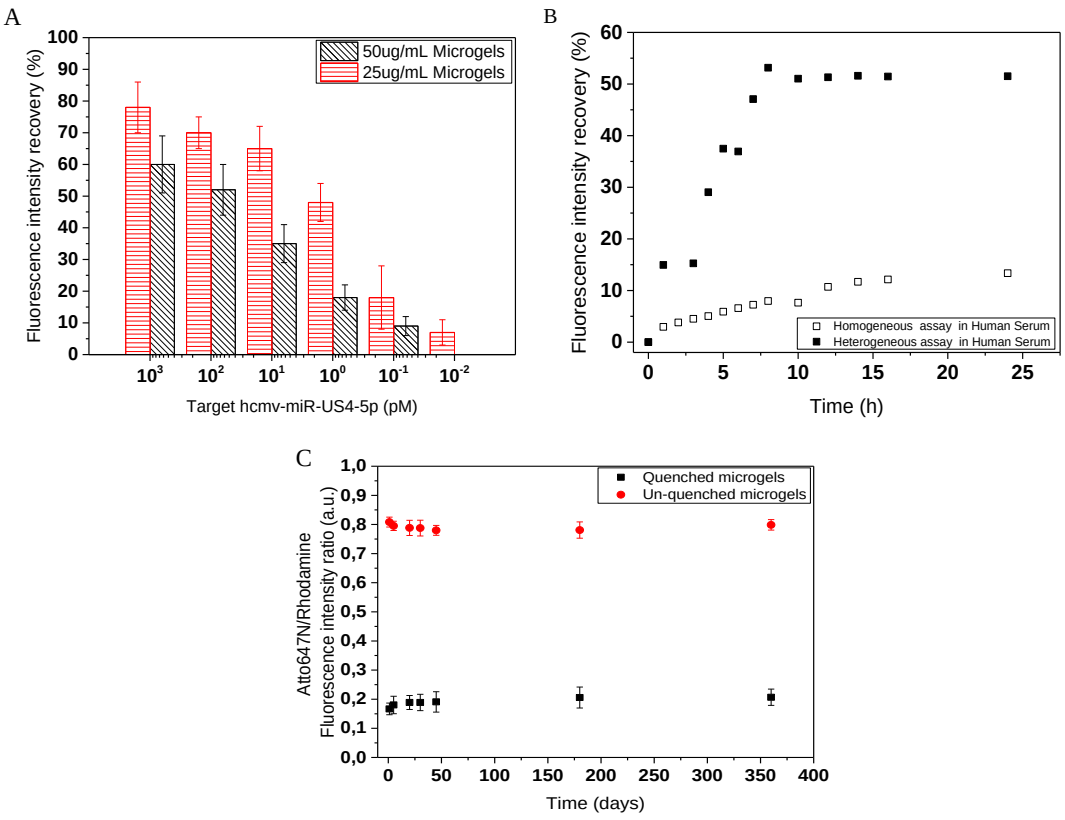

Figure 6 A) Microgels fluorescence recovery measured by spectrofluorometer: using 50 and 25 µg/mL of microgels. B) Comparison between homogenous (5nM of free double strand probe, empty square) and heterogeneous (50µg/mL of functionalised microgels, full black square) assay in human serum in presence of excess of target (50nM); C) Microgel stability measured over a range of 1 years. Black square corresponding to quenched microgels, while red dots to un-quenched microgels. Data are presented as fluorescence intensity ratio between the reporter (Atto647N) and the reference dye(Rhodamine).

spectrofluorometer readout significantly reduces the analysis time and processing steps keeping the sensitivity required for the microRNA detection.

Table 3 Non-linear regression data analysis for ds displacement assay and microgel-based assay performed in presence of hcmv-miR-US4-5p target.by confocal laser scanner microscopy.

Microgel concentration (µg/mL)	slope	Standard error (slope)	Intercept	Standard Error (intercept)	LOD (fM)	R-Sq
50	88.796	16.721	-206.65	76.053	37.12	0.93
25	29.788	7.4 96	18.049	20.564	11.7	0.88
0.5	27.505	1.726	86.419	1.774	0.156	0.99

Table 4 Non-linear regression data analysis for ds displacement assay and microgel-based assay performed in presence of hcmv-miR-US4-5p target by Fluorimeter

Microgel concentration (µg/mL)	slope	Standard error (slope)	Intercept	Standard Error (intercept)	LOD (fM)	R-Sq
50	8.339	2.201	12.009	2.37	354	0.924
25	26.407	3.03	20.079	3.19	283	0.95

Finally, microgels performance are tested in complex fluids, spiking the microRNA target into the human serum solution. As shown in Figure 6B, ds-probes conjugated on microgels (heterogeneous condition) are more efficient in target recognition compared to free probes in solution (homogenous condition). This is mainly due to the hydrophilic polymeric background of PEG that provides antifouling and solution-like properties to the microgel. Therefore, serum proteins are rejected from the microgel surface, while probes are protected within the hydrogel environment.

Moreover, as shown in Figure 6C, microgels stability is monitored for 12 months without any substantial loss of fluorescence intensity, suggesting a long shelf life and assay stability.

Microgels are also examined by a flow cytometer. Analysis have shown that is possible to discriminate the fluorescence emission of the particle architecture, measuring the core (Rhodamine), the second shell (Fluorescein) fluorescence emission (Figure 7A) and the probe contribution (ATTO647N) before and after the quenching (respectively unquenched and quenched condition Figure 7 B-C). As shown, the fluorescence ratio between the copolymerized dyes into the microgels (FITC/Rho reported as PE) is

stable for all samples measured. In addition, the signal to noise for the conjugation analysed is comparable with that observed by confocal microscopy (S/N= 2.53).

A

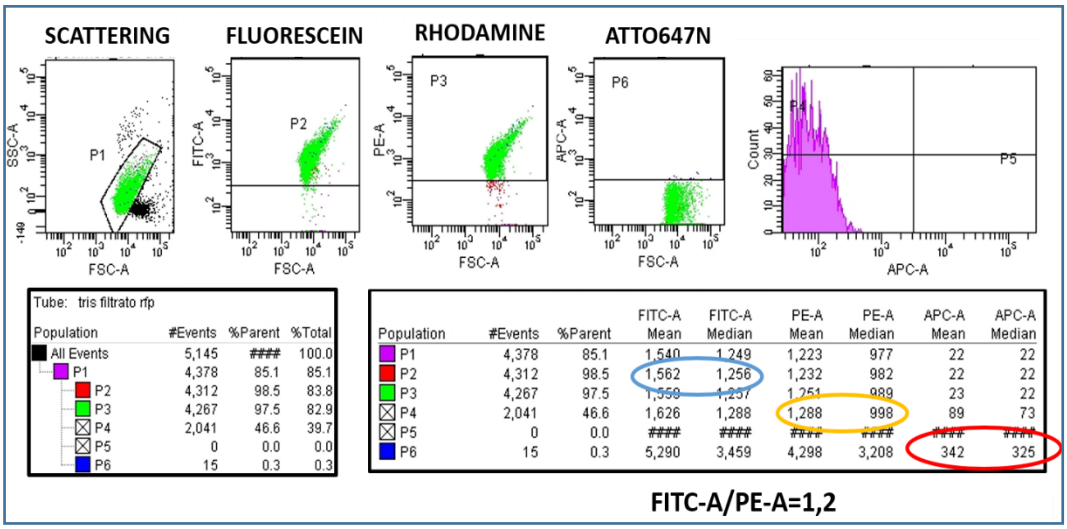

B

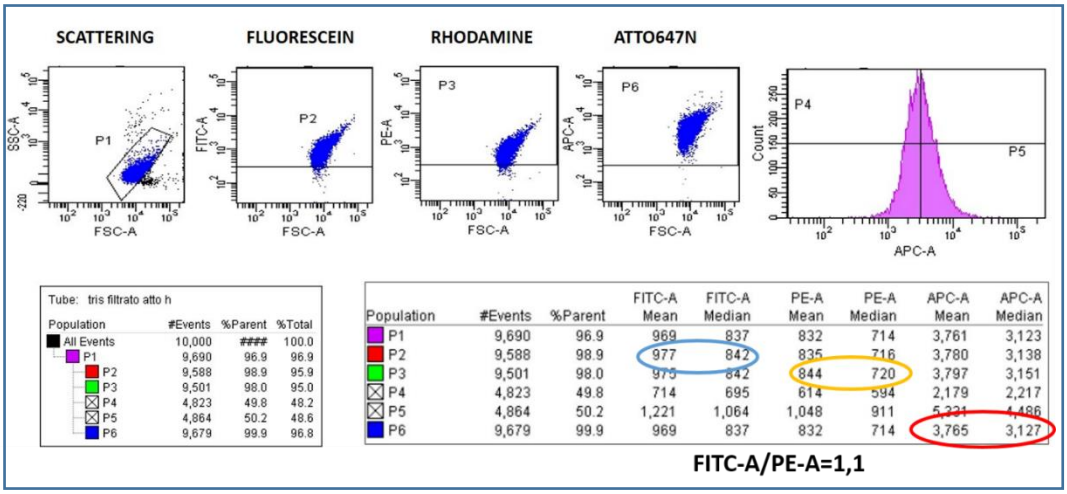

C

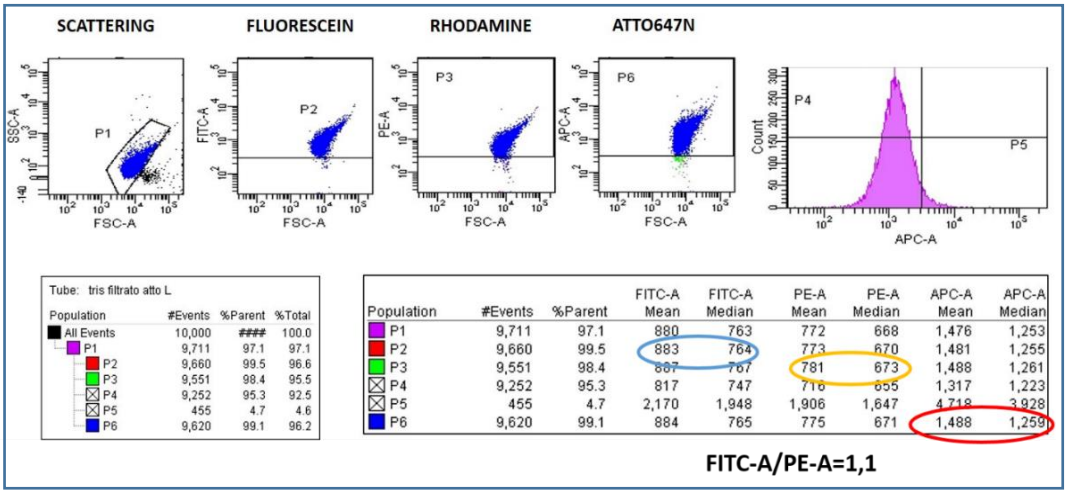

Figure 7 FACS measurements: A) Microgel without functionalization; B) Unquenched microgel; C) Quenched microgel

4. CONCLUSION

Current diagnostic techniques for hcmv detection are time spending and expensive. We have proposed a ultrasensitive, specific and versatile microgel assay able to detect viral endogenous circulating microRNAs in body fluids, overtaking the clinical requirements of panels and threshold level settings.

In this chapter we have designed a heterogeneous assay by using PEG microgels armed with short fluorescent DNA double strand probes for the specific detection of viral microRNA biomarker by toehold-mediated strand displacement assay.

The combination of the antifouling and solution-like microgels properties with the fluorescent signal confinement of specific probe into small volume allows to perform direct target detection in complex fluids.

Further, simply tweaking the assay microgel set-up, hcmv-miR-US4-5p has been detected with scalable sensitivity (down to about 150 aM) and over a wide dynamic range (from nM to aM). The proposed microgels can be also integrated in microfluidic device for in flow real time detection[57].

Therefore, the microgel assay might represent a smart platform able to diagnose cytomegalovirus active infections. These technologies can comply with several biomarkers, leading the way towards simpler and portable analytical devices.

From the clinical point of view further investigations are still ongoing and studies on real samples and PCR-based diagnostic tests are planned to measure the accuracy of our technology.

References

1. Griffiths, P., Baraniak, I. & Reeves, M. The pathogenesis of human cytomegalovirus. *J. Pathol.* **235,** 288–297 (2015).
2. Goderis, J. *et al.* Hearing loss and congenital CMV infection: a systematic review. *Pediatrics* **134,** 972–82 (2014).
3. Schottstedt, V. *et al.* Human Cytomegalovirus (HCMV) - Revised. *Transfus. Med. Hemother.* **37,** 365–375 (2010).
4. Ross, S. A., Novak, Z., Pati, S. & Boppana, S. B. Overview of the diagnosis of cytomegalovirus infection. *Infect. Disord. Drug Targets* **11,** 466–74 (2011).
5. Hodinka, R. in *Manual of Clinical Microbiology* 1718–37 (American Society of Microbiology, 2015). doi:10.1128/9781555817381.ch100
6. Al-Omari, A., Aljamaan, F., Alhazzani, W., Salih, S. & Arabi, Y. Cytomegalovirus infection in immunocompetent critically ill adults: literature review. *Annals of Intensive Care* **6,** 110 (2016).
7. Lindsay, M. A. microRNAs and the immune response Mark Lindsay.pdf. *Trends Imunol.* **29,** 343–351 (2008).
8. Bueno, M. J. & Malumbres, M. MicroRNAs and the cell cycle. *Biochim. Biophys. Acta - Mol. Basis Dis.* **1812,** 592–601 (2011).
9. De Guire, V. *et al.* Circulating miRNAs as sensitive and specific biomarkers for the diagnosis and monitoring of human diseases: Promises and challenges. *Clin. Biochem.* **46,** 846–860 (2013).
10. Najafi-Shoushtari, S. H. *et al.* MicroRNA-33 and the SREBP host genes cooperate to control cholesterol homeostasis. *Science (80-.).* **328,** 1566–1569 (2010).
11. Jovanovic, M. & Hengartner, M. O. miRNAs and apoptosis: RNAs to die for. *Oncogene* **25,** 6176–6187 (2006).
12. Kawahara, H., Imai, T. & Okano, H. MicroRNAs in neural stem cells and neurogenesis. *Front. Neurosci.* 1–13 (2012). doi:10.3389/fnins.2012.00030
13. Kulshreshtha, R. *et al.* A MicroRNA Signature of Hypoxia. *Mol. Cell. Biol.* **27,** 1859–1867 (2007).
14. Vasilatou, D., Papageorgiou, S., Pappa, V., Papageorgiou, E. & Dervenoulas, J. The role of microRNAs in normal and malignant hematopoiesis. *Eur. J. Haematol.* **84,** 1–16 (2010).
15. Wang, J., Chen, J. & Sen, S. MicroRNA as Biomarkers and Diagnostics. *J. Cell. Physiol.* **231,** 25–30 (2016).
16. Hébert, S. S. & De Strooper, B. Alterations of the microRNA network cause neurodegenerative disease. *Trends in Neurosciences* **32,** 199–206 (2009).

17. Condorelli, G., Latronico, M. V. G. & Cavarretta, E. microRNAs in cardiovascular diseases: current knowledge and the road ahead. *J. Am. Coll. Cardiol.* **63,** 2177–87 (2014).
18. Nielsen, L. B. *et al.* Circulating levels of MicroRNA from children with newly diagnosed type 1 diabetes and healthy controls: Evidence that miR-25 associates to residual beta-cell function and glycaemic control during disease progression. *Exp. Diabetes Res.* **2012,** (2012).
19. Femminella, G. D., Ferrara, N. & Rengo, G. The emerging role of microRNAs in Alzheimer's disease. *Front. Physiol.* **6,** 1–5 (2015).
20. Lin, S. & Gregory, R. I. MicroRNA biogenesis pathways in cancer. *Nat. Rev. Cancer* **15,** 321–333 (2015).
21. Rottiers, V. & Näär, A. M. MicroRNAs in metabolism and metabolic disorders. *Nature Reviews Molecular Cell Biology* **13,** 239–251 (2012).
22. Hitachi, K. & Tsuchida, K. Role of microRNAs in skeletal muscle hypertrophy. *Front. Physiol.* **4 JAN,** 1–7 (2014).
23. Louten, J., Beach, M., Palermino, K., Weeks, M. & Holenstein, G. MicroRNAs expressed during viral infection: Biomarker potential and therapeutic considerations. *Biomarker Insights* **10,** 25–52 (2016).
24. K. Meshesha, M. The microRNA Transcriptome of Human Cytomegalovirus (HCMV). *Open Virol. J.* **6,** 38–48 (2012).
25. Pfeffer, S. *et al.* Identification of microRNAs of the herpesvirus family. *Nat. Methods* **2,** 269–276 (2005).
26. Grey, F. *et al.* Identification and Characterization of Human Cytomegalovirus-Encoded MicroRNAs. *J. Virol.* **79,** 12095–12099 (2005).
27. Cullen, B. R. Viral and cellular messenger RNA targets of viral microRNAs. *Nature* **457,** 421–425
28. Meshesha, M. K., Bentwich, Z., Solomon, S. A. & Avni, Y. S. In vivo expression of human cytomegalovirus (HCMV) microRNAs during latency. *Gene* **575,** 101–107 (2016).
29. Keller, A. *et al.* Sources to variability in circulating human miRNA signatures. *RNA Biol.* **14,** 1791–1798 (2017).
30. Yoon, H., Belmonte, K. C., Kasten, T., Bateman, R. & Kim, J. Intra-and Inter-individual Variability of microRNA Levels in Human Cerebrospinal Fluid: Critical Implications for Biomarker Discovery. *Sci. Rep.* **7,** 1–13 (2017).
31. McDonald, J. S., Milosevic, D., Reddi, H. V., Grebe, S. K. & Algeciras-Schimnich, A. Analysis

of circulating microRNA: Preanalytical and analytical challenges. *Clin. Chem.* **57,** 833–840 (2011).

32. Lisboa, L. F. *et al.* Hcmv-miR-UL22A-5p: A biomarker in transplantation with broad impact on host gene expression and potential immunological implications. *Am. J. Transplant.* **15,** 1893–1902 (2015).
33. Stark, T. J., Arnold, J. D., Spector, D. H. & Yeo, G. W. High-Resolution Profiling and Analysis of Viral and Host Small RNAs during Human Cytomegalovirus Infection. *J. Virol.* **86,** 226–235 (2012).
34. Kim, S. *et al.* Human cytomegalovirus microRNA miR-US4-1 inhibits CD8(+) T cell responses by targeting the aminopeptidase ERAP1. *Nat. Immunol.* **12,** 984–91 (2011).
35. Pan, Y. *et al.* Circulating human cytomegalovirus-encoded HCMV-miR-US4-1 as an indicator for predicting the efficacy of IFNα treatment in chronic hepatitis B patients. *Sci. Rep.* **6,** 23007 (2016).
36. Rödiger, S. *et al.* Nucleic acid detection based on the use of microbeads: A review. *Microchim. Acta* **181,** 1151–1168 (2014).
37. Le Goff, G. C., Srinivas, R. L., Hill, W. A. & Doyle, P. S. Hydrogel microparticles for biosensing. *Eur. Polym. J.* **72,** 386–412 (2015).
38. Battista, E., Causa, F. & Netti, P. Bioengineering Microgels and Hydrogel Microparticles for Sensing Biomolecular Targets. *Gels* **3,** 20 (2017).
39. Celetti, G., Natale, C. Di, Causa, F., Battista, E. & Netti, P. A. Functionalized poly(ethylene glycol) diacrylate microgels by microfluidics: In situ peptide encapsulation for in serum selective protein detection. *Colloids Surfaces B Biointerfaces* **145,** 21–29 (2016).
40. Ahmed, E. M. Hydrogel: Preparation, characterization, and applications: A review. *J. Adv. Res.* **6,** 105–121 (2015).
41. Choi, N. W. *et al.* Multiplexed detection of mRNA using porosity-tuned hydrogel microparticles. *Anal. Chem.* **84,** 9370–9378 (2012).
42. Chapin, S. C., Appleyard, D. C., Pregibon, D. C. & Doyle, P. S. Rapid microRNA profiling on encoded gel microparticles. *Angew. Chemie - Int. Ed.* **50,** 2289–2293 (2011).
43. Pregibon, D. C., Toner, M. & Doyle, P. S. Multifunctional encoded particles for high-throughput biomolecule analysis. *Science (80-.).* **315,** 1393–1396 (2007).
44. Causa, F., Aliberti, A., Cusano, A. M., Battista, E. & Netti, P. A. Supramolecular spectrally encoded microgels with double strand probes for absolute and direct miRNA fluorescence detection at high sensitivity. *J. Am. Chem. Soc.* **137,** 1758–1761 (2015).

45. Aliberti, A., Cusano, A. M., Battista, E., Causa, F. & Netti, P. A. High sensitive and direct fluorescence detection of single viral DNA sequences by integration of double strand probes onto microgels particles. *Analyst* **141,** 1250–1256 (2016).
46. Appleyard, D. C., Chapin, S. C., Srinivas, R. L. & Doyle, P. S. Bar-coded hydrogel microparticles for protein detection: Synthesis, assay and scanning. *Nat. Protoc.* **6,** 1761–1774 (2011).
47. Kozomara, A. & Griffiths-Jones, S. MiRBase: Annotating high confidence microRNAs using deep sequencing data. *Nucleic Acids Res.* **42,** D68–D73 (2014).
48. Kibbe, W. A. OligoCalc: An online oligonucleotide properties calculator. *Nucleic Acids Res.* **35,** W43-6 (2007).
49. Altschul, S. F., Gish, W., Miller, W., Myers, E. W. & Lipman, D. J. Basic local alignment search tool. *J. Mol. Biol.* **215,** 403–410 (1990).
50. Markham, N. R. & Zuker, M. in *Methods in Molecular Biology* **453,** 3–31 (Humana Press, 2008).
51. Genot, A. J., Zhang, D. Y., Bath, J. & Turberfield, A. J. Remote toehold: A mechanism for flexible control of DNA hybridization kinetics. *J. Am. Chem. Soc.* **133,** 2177–2182 (2011).
52. Zhang, D. Y. & Seelig, G. Dynamic DNA nanotechnology using strand-displacement reactions. *Nat. Chem.* **3,** 103–113 (2011).
53. Zhang, D. Y. & Winfree, E. Control of DNA strand displacement kinetics using toehold exchange. *J. Am. Chem. Soc.* **131,** 17303–17314 (2009).
54. Battista, E., Mazzarotta, A., Causa, F., Cusano, A. M. & Netti, P. A. Core-shell microgels with controlled structural properties. *Polym. Int.* **65,** 747–755 (2016).
55. Grasedieck, S. *et al.* Impact of serum storage conditions on microRNA stability. *Leukemia* **26,** 2414–2416 (2012).
56. Riahi, R., MacH, K. E., Mohan, R., Liao, J. C. & Wong, P. K. Molecular detection of bacterial pathogens using microparticle enhanced double-stranded DNA probes. *Anal. Chem.* **83,** 6349–6354 (2011).
57. Dannhauser, D. *et al.* In-flow real-time detection of spectrally encoded microgels for miRNA absolute quantification. *Biomicrofluidics* **10,** 064114 (2016).

CHAPTER 3

"Molecular Beacons bioconjugated Microgels: bioassay for miRNA biomarker detection in Cancer"

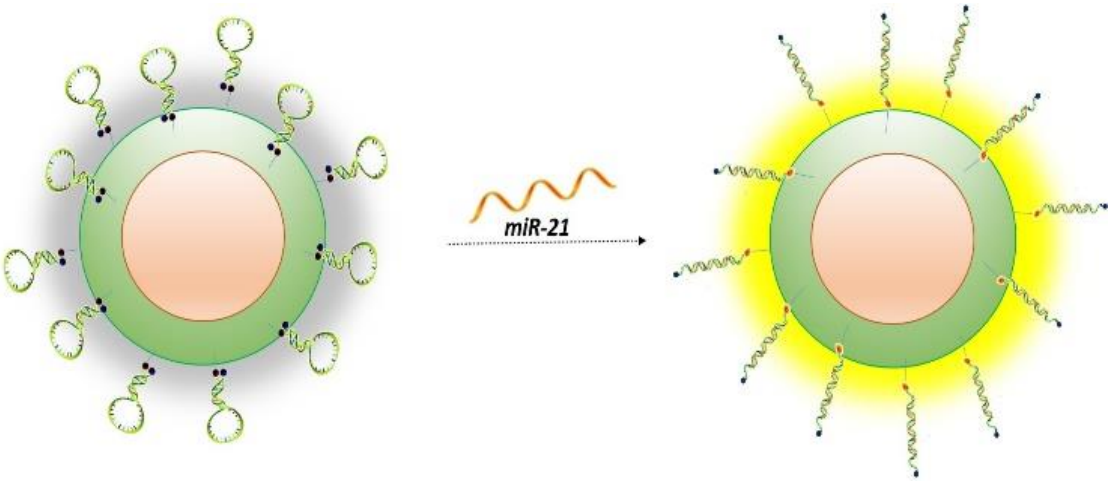

1. INTRODUCTION

The World Health Organization has estimated that Cancer is the second leading cause of death globally, with 9.6 million of deaths only in 2018[1]. Moreover, mortality can be reduced if cancer is detected and treated early. Therefore, it is imperative to identify novel, more sensitive, and easy-to-perform assay for specific early biomarkers detection, which can be used in diagnosis and prognosis of cancers.

MicroRNA (or miRNA) are non-coding RNA sequence of about 22-25nt. They are involved in the regulation of the gene expression at post-transcriptional level inducing translational inhibition or transcript degradation[2]. Because of this pivotal role, circulating microRNAs (miRNAs) have emerged as a new type of biomarkers for the early diagnosis, prognosis and follow up of several pathological conditions[3], included cancer[4]. The miR-21 has been the most studied miRNA (along with let-7) due to its ubiquitous role in various biological processes[5]. It is involved in several positive and negative feedback loops and is probably one of the most dynamic miRNAs responsive to various stimuli[6]. It is proved that miR-21 expression levels are usually up-regulated in cancer[7] and it functions as an oncogene[8,9]. Therefore, since dysregulation of miR-21 represents a common feature of a cancer process, it is often considered as an early biomarker.

Traditional methods for detect miRNA are mainly based on amplification methods and in situ hybridization[10,11]. However, despite all the techniques developed, miRNA detection is still challenging because of the small size, the sequence similarity, the low abundance and intra- and inter-variability[12]. For this reason, although miRNAs have widely proved to be suitable biomarkers, their application in clinical practice is still limited, and the developing of innovative methods of detection is required.

In this context, the use of molecular beacon for microRNA detection is particularly interesting. Essentially, a molecular beacon[13] is a single strand oligonucleotide sequence containing a fluorophore and a quencher in its opposite ends. It comprises a central portion (loop) complementary to the target and two self-complementary terminal arms (stem)[14,15]. Because of its design, in absence of target it is conformed in stem-loop hairpin structure and the fluorophore and quencher are in close proximity with a consequent quenching of the fluorescence[16]. When the target hybridizes with the loop a stable duplex is formed and the stem is mechanically forced to open. Hence, the fluorophore and quencher are spatially separated and fluorescence is restored. Many studies have been focused on the practical rules to design molecular beacons[17,18] and on their enhanced properties[19]. In particular, due to their unique structural and thermodynamic properties, molecular beacons are capable to differentiate between two target sequences that differ by as little as a single nucleotide[20,21].

From their discovery, many advances in bioanalytical methods development have been carried out also because of the advantages offered by the molecular beacons. As proof of this, they have been integrated with several technologies[22–30] for bioanalytes detection[31–36]. Moreover, molecular beacons have been integrated on solid surfaces and used as biosensors[37–43]. However, when molecular beacons are immobilized on solid surfaces the fluorescence background usually increases due to non-specific oligonucleotide-surface interaction and crowding effects[44] among the immobilized oligonucleotide probes. As results, both the hybridization ratio and the assay sensitivity are affected. To increase signal-to-background ratio substrate as graphene[45] or gold[46] or long spacer as poly(thymidine/adenosine) (poly(T/A)) and poly(ethylene glycol) (PEG)[42] have been used. Alternatively, surface polymer coating [47] and nucleic acid analogues[48] have been used to increase the molecular beacon stability. Such modifications decrease the surface effect and slightly improve the mb performance. Gold surfaces represent a valid substrate to immobilize quencher-free molecular beacons by standard gold-thiol chemistry. These functionalized substrates achieve nanomolar sensitivity and high specificity[49]. Nevertheless, non-specific adhesion and non-uniform distribution of mb on the gold surface can reduce the biosensing performance. Molecular beacons have been also immobilized on substrates as graphene[45,50,51], that works as a super-quencher with a long-range nanoscale energy transfer property. As results, when molecular beacons are immobilized on graphene oxide substrates, the fluorescence background strongly decreases and the signal-to-noise (hence the sensitivity) increases. These biosensors show single nucleotide polymorphism selectivity and low sensitivity (comprises in nanomolar to picomolar order), indeed, they usually require the combination with amplification methods[52]. However, for each substrate non-specific adsorption occurring in biological fluids largely impairs direct and easy detection of target oligonucleotides, while kinetics is depressed after immobilization on solid surface[53]. Even though the performance of surface-immobilized MBs has been significantly improved by using the newly developed immobilization techniques and surface treatment approaches, sensitivity was still low.

Recent studies have proved that when molecular beacons are bio-conjugated into materials with solution-like property, as poly(ethylene glycol) hydrogels, fluorescence background strongly decreases[54]. In this specific case, indeed, molecular beacon hybridization is comparable to that obtained in solution.

Based on these considerations, in this chapter is described the development of a molecular beacons-bioconjugated microgel assay for miR-21 detection for cancer application. Core-shell microgels endowed with carboxylic moieties are synthetized and the molecular beacon design is optimized for the purpose. Then, the density of the conjugated in the outermost shell is tuned and the assay set-up. The results have demonstrated that such molecular beacon-conjugated microgels are capable of fM sensitivity without

preliminary amplification steps, single nucleotide polymorphism discrimination and reduced time of analysis.

2. EXPERIMENTAL SECTION

2.1. Materials

Poly(ethylene glycol) dimethacrylate average Mn 550 (PEGDMA), Acrylic acid (AAc), Potassium persulfate (KPS), Fluoresceine O-methacrylate, 1-ethyl-3-(3-dimethylaminopropyl) carbodiimide (EDC) and Polyvinyl alcohol 40-88 (PVA), Dimethyl Sulfoxide (DMSO), Sodium Hydroxide, 4-Morpholineethanesulfonic acid sodium salt (MES) and water biological grade were all purchased from Sigma-Aldrich and used as received. The dye Methacryloxyethylthiocarbonyl-rhodamine B was obtained from Polyscience Inc. Phosphate buffered saline tablets were supplied by MP biomedicals. DNA and RNA oligonucleotides were purchased from Metabion International with HPLC purification.

2.2. Molecular beacon design

Two molecular beacons complementary to the miR-21 were designed. The molecular beacons contained a fixed loop complementary to the target made of 22 bases and a stem of 5 or 6 bases (MBS5 or MBS6). The 5' terminus was modified with an ATTO647N fluorophore and a 12-carbon amino spacer while a BlackBerry Quencher 650 (BBQ-650) was added on the 3' terminus. Both molecular beacons were suspended in nuclease-free water to a concentration of 100μM and stored at -20°C. To assess the specificity of molecular beacons, non-matching sequence (miR-143) and three mutants of the wild-type miR-21 were also tested in the hybridization assays. Specifically, for the miR-21 mutants, 1, 2, or 3 nucleotides of the sequence were modified: miR-21-1a had one nucleotide mutated at the end of the loop near the stem; miR-21-1b had one mutated nucleotide in the centre of the loop; miR-21-2 had both mutated nucleotides in the centre and at the end of the loop; miR-21-3 had three mutated nucleotides.
The kinetics of hybridization in presence of the wild-type miR21, the mutated miR-21 sequences and a non-matching miR were measured mixing 500nM of the sequences to 50nM of molecular beacon in 500μL of PBS buffer. The fluorescence recovery as function of the time was recorded by spectrofluorometer.

Table 1 Molecular beacons and target sequences tested

	Sequence (5'-3')	Length (nt)
MBS5	**<u>CGCGC</u>***TCAACATCAGTCTGATAAGCTA***<u>GCGCG</u>**	32
MBS6	**<u>CGCGCG</u>**TCAACATCAGTCTGATAAGCTA**<u>CGCGCG</u>**	34
miR-21	UAGCUUAUCAGACUGAUGUUGA	22
miR-21-1a	UA**U**CUUAUCAGACUGAUGUUGA	22
miR-21-1b	UAGCUUAUCA**A**ACUGAUGUUGA	22
miR-21-2	UA**U**CUUAUCA**A**ACUGAUGUUGA	22
miR-21-3	UA**U**CUUAUCA**A**ACUGAUGUU**A**A	22
Non-matching (miR-143-3p)	UGAGAUGAAGCACUGUAGCUC	21

The nucleotides of the loop are in italics, while those of the stem in bold underline. The mutations introduced in the sequences are in bold.

Fluorescence spectra were collected in a 1 cm path length cuvette with a Horiba JobinYvon model FluoroMax-4 spectrofluorometer equipped with a Peltier temperature controller. The sample was excited at 647nm with a slit width of 5nm, and emission spectra were collected from 667 to 750nm with a slit width of 5nm.

Melting curves for both molecular beacons alone and in presence of the miRNA sequences were recorded to calculate their melting temperatures. Melting curves were obtained monitoring the fluorescence intensity as function of the temperature. In particular, 500µL of PBS buffer solution containing 50nM of molecular beacon alone or mixed with 500nM of miRNA was initially denatured (3 min 95°C), then the temperature was decreased from 95°C to 20°C, with scan rate of 1°C/2min. Fluorescence spectra were measured as described above, exciting the sample at 647nm and collecting the emission intensity from 667 to 750nm.

2.3. Microgel synthesis

Microgels with multi-shell architecture were synthetized through a multistep synthesis as previously described. Briefly, core nanoparticles made of PEGDMA 1% (w/v) and rhodamine B acrylate monomer (0.1mM) were synthetized via free-radical precipitation polymerization. As

initiator was used KPS (2.2 mM) in PVA 1% (w/v), heating to 65ºC for 7 hours in N_2 atmosphere. Nanoparticles were dialyzed and worked as a seed for the subsequent two shells polymerization. The first shell was obtained adding to the aqueous suspension of core microgels PEGDMA 0.5% (w/v), PVA 0.5% (w/v) and KPS (1,1 mM), heating to 65 ºC for 6 hours in N_2 atmosphere. The second shell was obtained adding to the aqueous suspension of core/1°shell microgels PEGDMA 0.5% (w/v), Acrylic acid 0.25% (w/v), Fluoresceine O-methacrylate (0.1 mM) and KPS (1,1 mM). The microgels size and electrophoretic mobility were characterized by Dynamic light scattering (Malvern Zetasizer Nano ZS instrument, 633 nm laser, 173° scattering angle). Carboxyl groups content was quantified by titration before further conjugation of the molecular beacon.

2.4. Molecular beacons conjugation.

Bioconjugation was optimized coupling 1, 0.5 and 0.1 nmol of molecular beacons. Before the reaction 1mg of microgel was incubated in 450µL MES pH 6, while molecular beacons were incubated in 50µL MES pH 6 enriched with 200mM of NaCl, both for at least 5 hours. After, the carboxylic groups on microgel were activated using 500mM of the coupling agent EDC stirring vigorously for 30 min at 5°C. Subsequently, the pre-hybridized molecular beacon solution was added to the microgels incubating overnight at room temperature. Molecular beacons-bioconjugated microgels (mb-microgels) were washed 3 times to remove the unreacted molecular beacons and resuspended in PBS buffer. For each microgel functionalization, the kinetics of hybridization with the miR-21 target was measured through a spectrofluorometer. For this purpose, 20nM of wild-type miR-21 solution was mixed with 25 µg/mL of mb-microgels in 500µL of hybridization buffer.

2.5. Specificity

The assay specificity was tested adding 5 µg/mL of mb-microgels (with 0.1 nmol functionalization) to 20 µL of buffer solution containing 50 pM of each mutated miR-21 sequences, 50 pM of non-matching miR (miR-143) and 50 pM of 1:1 miR21-1a/miR-143(table 1). Moreover, mb-microgels were mixed with 50 pM of wild-type miR-21 containing 50 pM or 5 nM of mir21-1a and 50 pM or 5 nM of 1:1 of miR21-1a/miR-143. The solution was incubated overnight at room temperature, images were collected and analysed.

2.6. Microgel assay

The assay was easily performed mixing the microgels to the sample solution containing the target sequences, without preliminary steps of amplification. The solution was incubated at room temperature and then fluorescence recovery was measured. In particular, mb-microgels limit of detection (LOD) and limit of quantification (LOQ), scalable sensitivity, kinetics of hybridization, and specificity were measured by confocal laser scanning microscopy (CLSM).

To estimate the LOD and LOQ 5 µg/mL of each mb-microgels were mixed with 20 µL of samples at different target concentrations, ranging from nM to aM, loaded into µ-slide 18 well-flat (Ibidi, Martinsried, DE) and incubated at room temperature overnight. In the same way, the concentration of mb-microgels with 0.1 nmol functionalization was decreased to 0.5 µg/mL and tested towards 20 µL of samples at different target concentrations.

Kinetics of hybridizations were measured mixing 100 nM and 100 pM of wild-type miR-21 with 5 µg/mL of mb-microgels in a final volume of 20 µL. Fluorescence intensity was collected after 1, 3, 5 and 24 hours. The samples were analysed by CLSM-SP5 with an objective HCX PL APO CS 63x1.40 oil (Zeiss), by using Helium neon laser 543 nm and 633 nm. Power lasers and detector gains were kept always constant with a section thickness 3.04 airy unit, scan speed 8000 Hz and an image size of 144.7x144.7 μm^2 (resolution 512x512). For each target concentration, 3 or more images were collected and more than 500 microgels were analysed. The images were thresholded by Otsu algorithm and then processed with the Image J Analyze Particles function to computationally determine the number of single fluorescent particles sizing in the range of 1µm. Furthermore, mb-microgels fluorescence intensity was measured by the means of a flow cytometer (BD FACS Canto II flow-cytometer and DIVA software (Becton Dickinson, Fullerton, CA)). Measurements were carried out adding 10^6 microgels in 1mL of buffer and analysing the forward and side scattering setting the population in the middle of the plot. Gated the position, the particles with positive value were selected and for those selected was analysed the intensity of Fluoresceine, Rhodamine(PE) and Atto647N (APC).

2.7. Human serum analysis

To prove the enhanced detection ability of microgels in complex fluid, the assay was also performed in human serum mixing 5µg/mL of mb-microgels and 20uL of human serum in which

was spiked 100nM of miR-21. The sample were loaded into the μwell and incubated at room temperature. Then, images were collected by CLSM as previously described and analysed.

2.8. Statistical analysis

All experiments were performed at least three times, reported as mean ± standard deviation and analysed statistically by paired Student's test. Significant difference was determined at P values smaller than 0.05.

To estimate the Limit of detection and the Limit of quantification the values, subtracted of the background and reported as mean ± standard deviation, are fitted applying a linear regression The LOD values is calculated as three standard error (SE) above the slope, while the LOQ corresponds to ten standard deviation (SD) above the slope.

3. RESULTS AND DISCUSSION

3.1. Molecular beacon design.

The design of molecular beacon affects both the sensitivity and the specificity of the hybridization with the target. The main parameters considered during the molecular beacon design are the length, the sequence of the loop and the stem, as they participate in the three different conformational states: bound-to-target, stem-loop and random-coil. Many reviews focused on this field, however, nobody has already developed an assay based on PEG microgels functionalized with molecular beacons for miRNA detection. For this reason, to further obtain a performant assay, two molecular beacons, MBS5 and MBS6(table1), are properly designed and tested. The molecular beacons share a common loop (22nt) complementary to the miR-21 and a stem of 5 (MBS5) or 6 (MBS6) bases. For their design, several specific software are used to predict the structure and thermodynamic properties. Based on the folding predictions, secondary structures (Figure 1) are absent in the loop, in both sequences. Moreover, due to the high GC content, the stem guarantees high stability ($\Delta G<0$) in assay conditions.

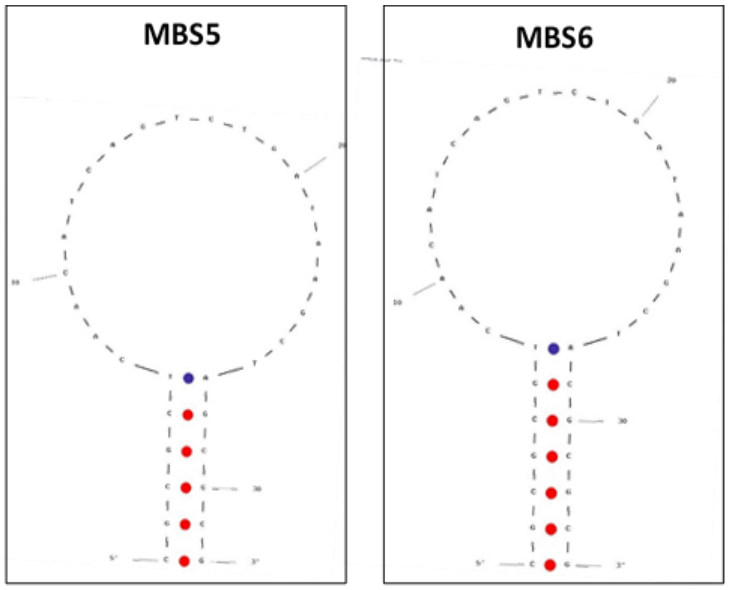

	ΔG (kcal.mole^{-1})	Tm (°C)	ΔH (kcal.mole^{-1})	Δs (cal.K^{-1} mol^{-1})
MBS5	-6.23	66.2	-51.3	-151.16
MBS6	-8.7	73.2	-62.5	-180.45

Figure 1 Folding simulation prediction of MBS5 and MBS6 and predicted thermodynamic parameters

Molecular beacons are previously tested in solution. As expected, molecular beacon with a shorter stem (MBS5) results faster in target hybridization compared to the molecular beacon with a longer stem (MBS6). In particular, as shown in Figure 2A, MB5 needs 30 minutes to reach the complete target hybridization, while MBS6 requires about 150 minutes in the same experimental condition (Figure 2B). Moreover, the temperature of melting increases with the length of the stem varying from 72.5 °C for MBS5 to 82.5 °C for MBS6 (Figure 3).

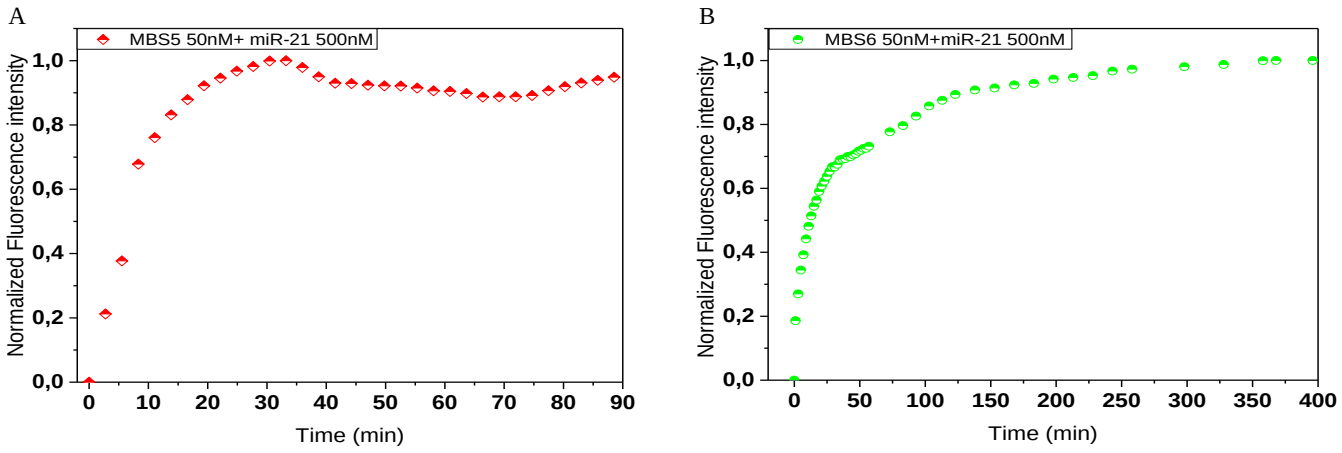

Figure 2 Hybridization kinetics of molecular beacon MBS5 (A) and MBS6(B) in the presence of wild-type target miR-21 in hybridization buffer at rt.

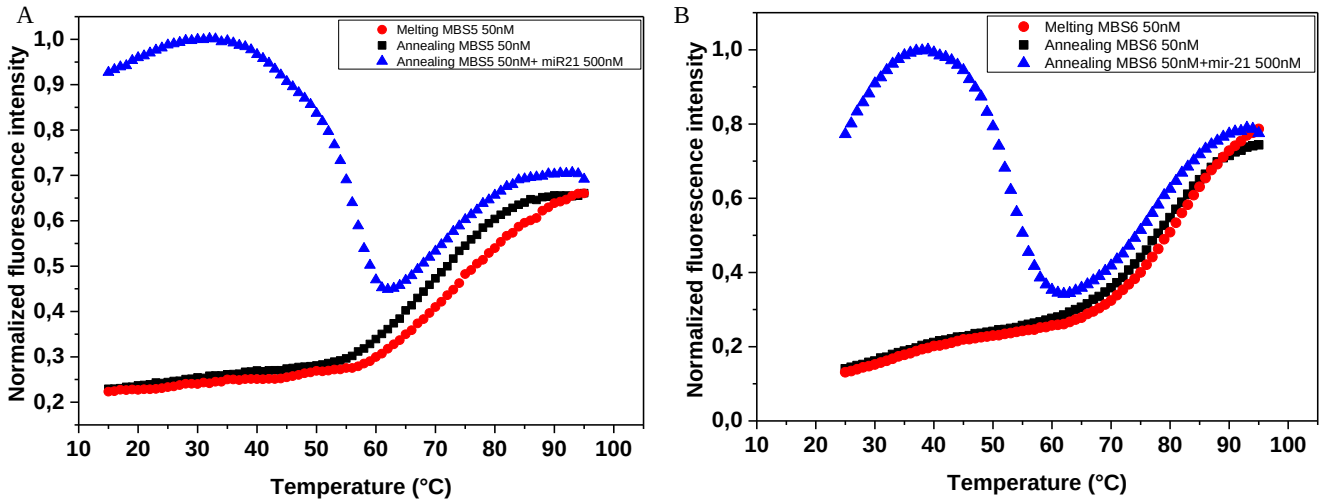

Figure 3 Melting and annealing profiles of MBS5(A) and MBS6 (B). Molecular beacons were melted from 20 to 95°C (red circle) and annealed (black square) in hybridization buffer. Moreover, MBS5 and MBS6 were priory melted to 95°C and then annealed until 20°C in presence of 500nM (10fold excess respect to MB) of miR-21 wild type (blue triangle).

Both molecular beacons prove an enhanced specificity in target recognition in solution. In particular, the hybridization kinetics and melting curve of MBS5 and MBS6 with miR-21 containing one two or three modifications are analysed.

As shown in Figure 4A and B, the fluorescence increment, due to the hybridization with the mutated miR, is negligible compared to the wild-type miR-21.

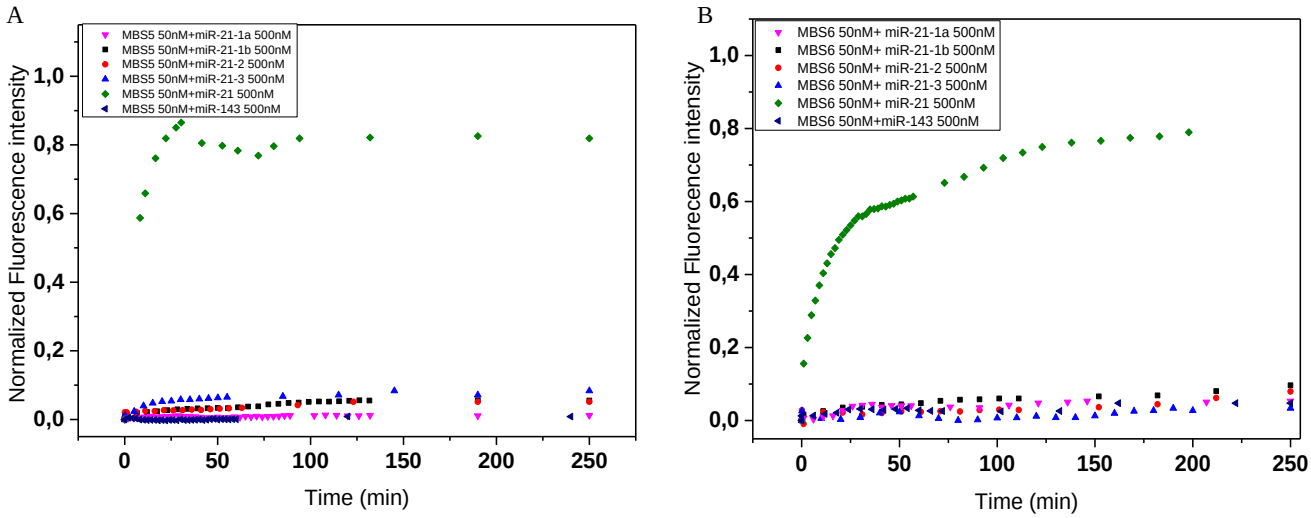

Figure 4 Hybridization kinetics of molecular beacon MBS5 (A) and MBS6 (B) in the presence of wild-type and mutants miR-21.

The melting curves confirm that with proper design, molecular beacons have the potential to distinguish single-base variations in target miRNA. Indeed, the melting temperature of the miR-MB duplex decreases as the number of point mutations increase (Figure 5-**Table 2**).

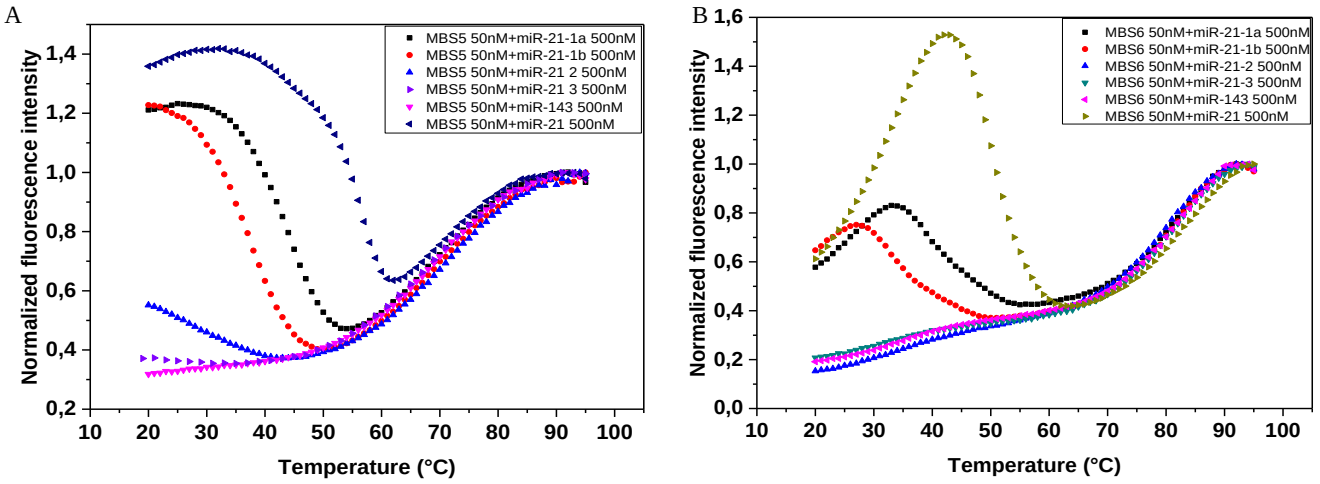

Figure 5 Melting and annealing profiles of MBS5 (A) and MBS6 (B). Molecular beacons were melted from 20 to 95°C and then annealed until 20°C in presence of 500nM (10fold excess respect to MB) of miR-21 wild type, mutated miR-21 (-1-a, -1-b, -2, -3) and non-matching miR-143.

Table 2 Melting temperature (Tm) predicted and calculated of MBS5 and MBS6. The temperatures refer to 50mM of molecular beacons in PBS buffer without the addition of miR or mixed with 500nM miR.

	Tm (°C) Predicted		Tm (°C) Calculated	
	MBS5	MBS6	MBS5	MBS6
Without Target	66.2	73.2	72.5	82.5
MBS+miR21	57		57.5	53.5
MBS+miR21-1a	48.9		44.5	38.5
MBS+miR21-1b	50.13		37.5	32.5
MBS+miR21-2	40.05		28.5	-
MBS+miR21-3	26.6		24	-
MBS+miR-143	-		-	-

3.2. Microgel synthesis and bioconjugation.

Microgels, synthetized combining free-radical and seeded polymerization reaction, have a final diameter of 1 μm and 1.71 μmoli/mg of carboxylic moieties for further functionalization, as described in Chapter 2. They have presented colloidal properties and enhanced stability in the time. In order to set the optimal density of molecular beacon, several bioconjugations have been carried out. Before the carbodiimide coupling, molecular beacons are pre-hybridized in MES buffer with higher ionic strength to help maintain the MB stem-loop structure. Such step is introduced to prevent that not annealed molecular beacons diffuse into the innermost layer of the microgel shell, where they can be hindered to conform in their darker hairpin structure, thus, increasing the background fluorescence.

From the bioconjugation analysis has been observed that both the signal-to-noise and the assay sensitivity are affected increasing the number of molecular beacons coupled to the microgel (Figure 6). In particular, the signal-to-noise ratio increases about twice reducing the functionalization from 1 nmol to 0.1 nmol for both molecular beacons (1.78- and 1.6-fold for MBS5 and MBS6 respectively).

These results are consistent with other studies and are especially associated with the crowding effect between molecular beacons. At higher density of functionalization, the hybridization with the target is reduced due to conformational limitations imposed by the proximity of stem-loop molecular beacons or by miR-MB duplexes. Therefore, decreasing the molecular beacon density such constraints are reduced and the signal-to-noise increases.

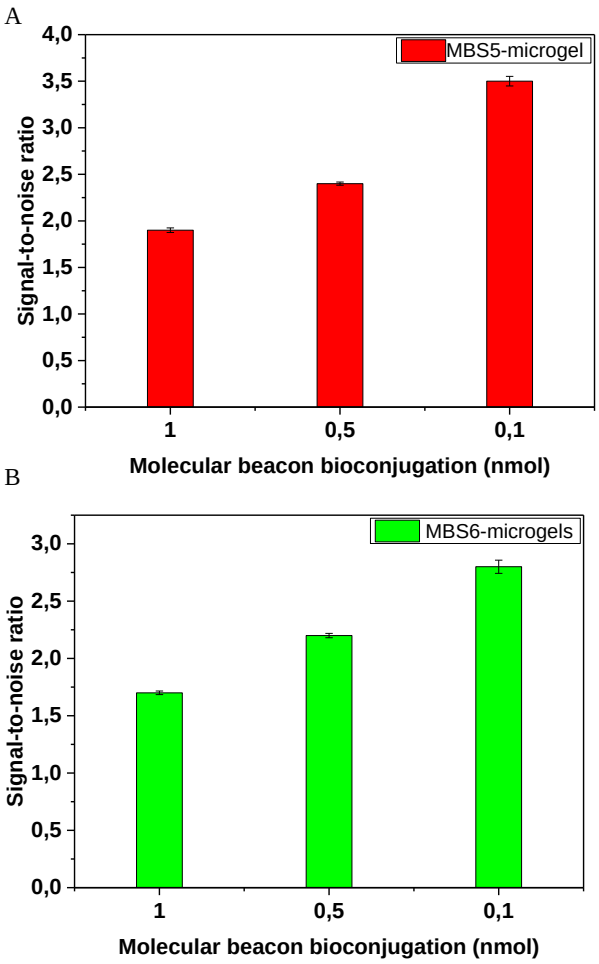

Figure 6 Signal-to-noise ratio of MBS5 (A) and MBS6(B) at different functionalization degree.

3.3. Assay sensitivity and kinetics

The mb-microgels are analysed to define their sensitivity and kinetic of hybridizations. The results obtained (Figure 7) testing a wide range of target miR-21 (from nM to aM) clearly show that the limit of detection (LOD) and limit of quantification (LOQ) increase decreasing both the length of the molecular beacon stem and the functionalization ratio. In particular, microgels functionalized with MBS5 reach 71.2 pM, 3.41 pM and 105.77 fM of LOD and 215 pM, 10.32 pM and 320.5 fM of LOQ, coupling respectively 1, 0.5 and 0.1 nmol of molecular beacons. Microgels functionalized with MBS6, instead, achieve 443.85 pM, 238.5 pM and 324.8 fM of

LOD and 1.34 nM, 465.8 pM and 984 fM of LOQ, conjugating respectively 1, 0.5 and 0.1 nmol of molecular beacons (**Table 3**).

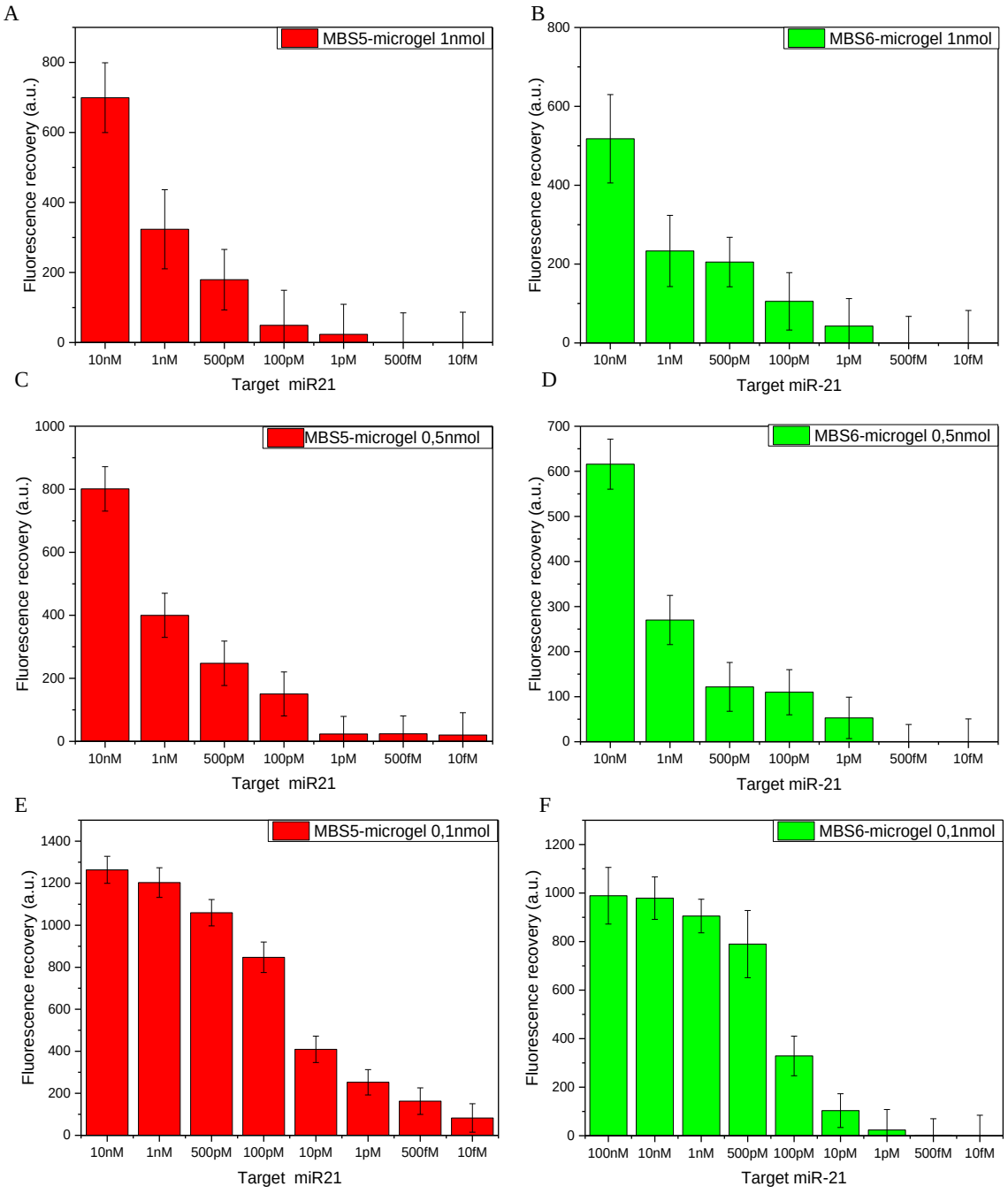

Figure 7 MBS5-microgels (red) and MB6-microgels (green) assay performances. A -B) microgels coupled with 1nmol, C-D) 0.5nmol and E-F) 0.1nmol of molecular beacons.

Table 3 Data analysis for mb-microgels assay

Mb-microgel (5µg/mL)	**SE**	**SD**	**R- sq**	**Slope**	**LOD (pM)**	**LOQ (pM)**
MBS5-m 1nmol	3.942419	6.828468	0.9989	0.3164	71.21	215.817
MBS5-m 0.5nmol	0.761043	1.318165	0.999	1.2763	3.4082	10.3280
MBS5-m 0.1nmol	3.237186	5.503217	0.993	0.1717	0.1057	0.32051
MBS6-m1nmol	23.57572	40.83433	0.958	0.3036	443.85	1345.00
MBS6-m0.5nmol	34.325	59.45262	0.7918	0.8224	238.56	465.820
MBS6-m 0.1nmol	6.155026	10.46354	0.989	0.163	0.3248	0.98434

Furthermore, mb-microgels assay shows a scalable sensitivity (Figure 8), indeed, decreasing the concentration of microgels to 0.5µg/mL per assay the LOD further decreases. Specifically, MBS5-microgels reach a LOD of 12.1 fM and LOQ of 36.7 fM, while MBS6-microgels reach 13.7 fM of LOD and 41.6 fM of LOQ (**Table 4**).

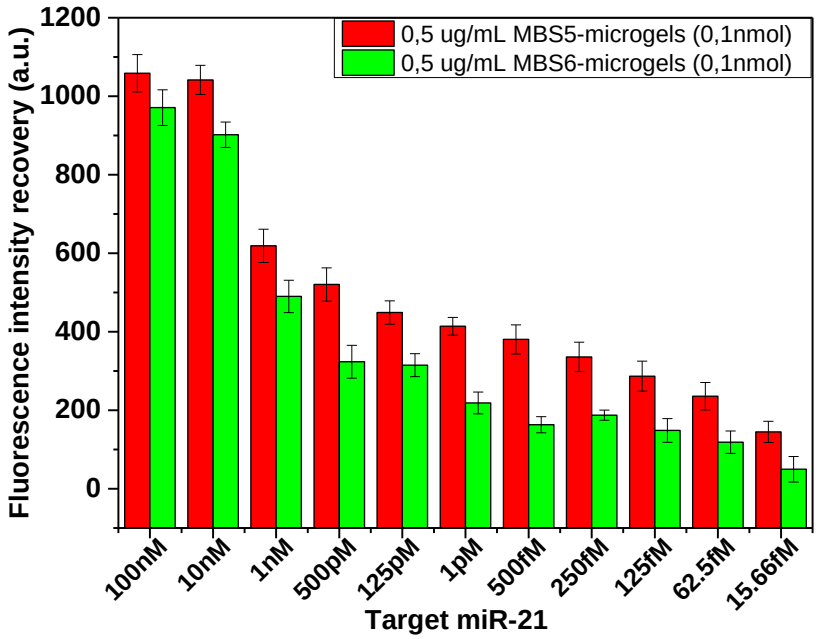

Figure 8 Target detection performances of mb-microgels with concentration scaled to 0.5ug/mL.

Table 4 Data analysis for mb-microgels assay

Mb-microgel (0.5µg/mL)	**SE**	**SD**	**R-sq**	**Slope**	**LOD (fM)**	**LOQ (fM)**
MBS5-m 0.1nmol	3.454826	5.873204	0.9976	0.0016	12.11	36.7
MBS6-m 0.1nmol	3.915771	6.65681	0.9969	0.0016	13.72	41.6

Established that the lowest functionalization is the most performing in terms of sensitivity, we have explored the kinetic of hybridizations characteristic of each coupling by spectrofluorometer and confocal microscope. The kinetics of hybridizations obtained by spectrofluorometer confirm that decreasing the functionalization the hybridization time decreases too. In particular, MBS5 and MBS6-microgels are able to recognize the target in less than 1 hour when the 0.1 nmol functionalized microgels are measured (Figure 9A-B). Increasing the functionalization degree, the kinetics of hybridizations slow down, however, all microgel types (0.5 nmol and 1 nmol) tested reach the plateau region in about 5 hours.

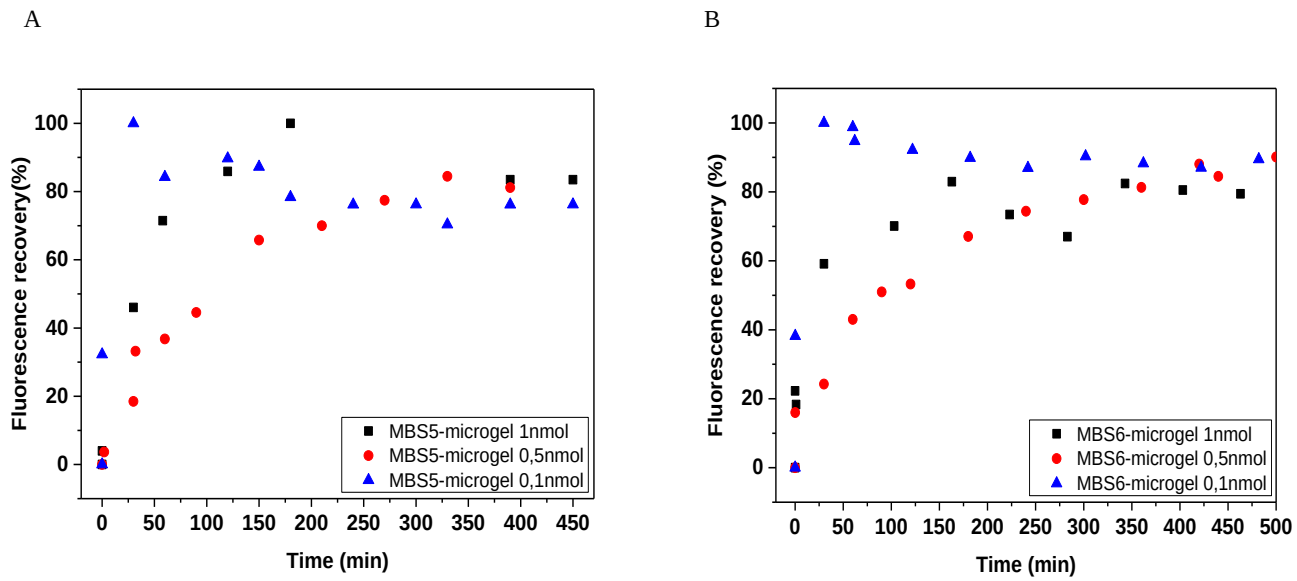

Figure 9 MBS5-(A) and MBS6-(B) microgels kinetic of hybridizations measured by spectrofluorometer

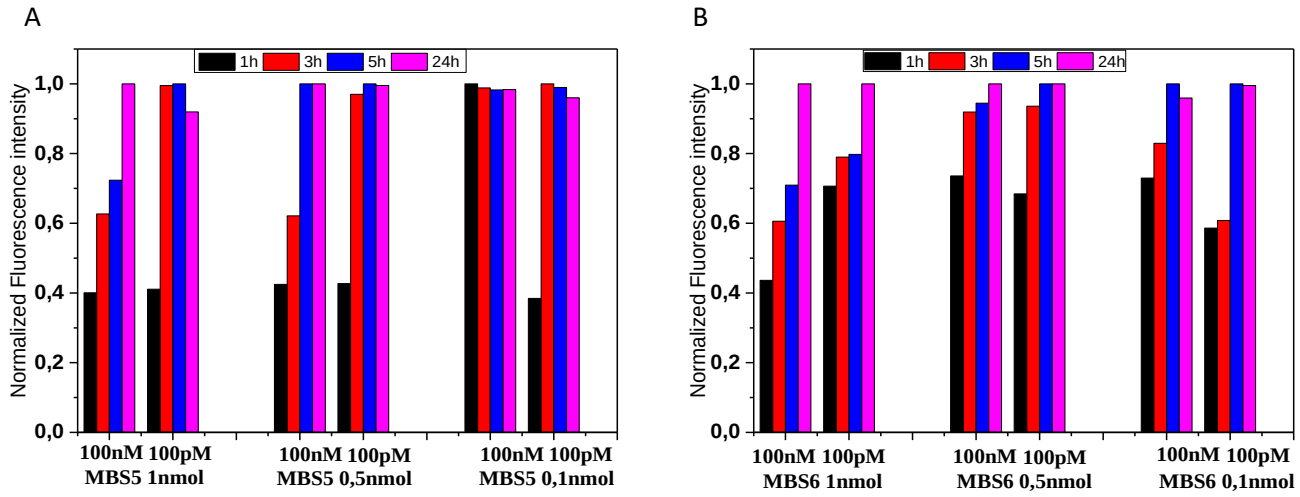

Figure 10 MBS5(A) and MBS6(B) kinetic of hybridizations measured by confocal microscope.

The kinetics of hybridizations have been calculated also by confocal microscopy, decreasing the microgel concentration to 5 µg/mL for assay. The measurements carry out on microgels show that MBS5-microgels with higher functionalization need more than 5 hours to completely hybridize with the target miR-21 (Figure 10A). Decreasing the functionalization to 0.5 nmol the process is completed in 5 hours. However, the most interesting performances are obtained by the microgels with lower functionalization degree. Indeed, these mb-microgels reach a complete hybridization in 1-3 hours even at low target concentration (Figure 10A). Microgels conjugated to MBS6, compared to those functionalized with MBS5, show slower kinetics of hybridization as observed also in solution. However, the microgels with lower functionalization (0.5 nmol and 0.1 nmol) reach the completely target hybridization in a maximum of 5 hours (Figure 10 B).

The performance of molecular beacon probes free in solution has usually been considered to be much higher than that of molecular beacons coupled to a variety of solid substrates such as microarray or microparticles. For this reason, molecular beacon functionalized surfaces have not found many applications in biomedical field compared to the free molecular beacon in solution. Thus, the enhanced performance demonstrated in this study are mostly ascribable to PEG microgel properties. Indeed, they are capable to swell and retain large volume of water generating a solution-like environment. This environment is approximate to a solution for the molecular beacon. Furthermore, molecular beacons are endowed with a long 12 carbon spacer to reduce the steric interactions between the surface of the polymer and itself, that can decrease the signal-to-noise ratio.

3.4. Assay specificity

The capacity to discriminate between oligonucleotide sequences with a single or multiple mutation is a fundamental requirement involved in the developing an analytical assay. Microgels specificity has been tested in presence of non-matching sequence (miR-143-3p) and miR-21 mutants. As shown in the Figure 11, MBS5-microgels are very stable towards non-matching sequence. A considerable fluorescence increment is measured only after the hybridization with the wild-type target. MBS5-microgels show a slight increase of fluorescence only in presence of mir-21-1a and mir-21-1b. Such increase corresponded to the 13.1% and 14.3% of the maximum fluorescence measured after the hybridization with the wild-type miR-21 at equivalent concentration (Figure 11).

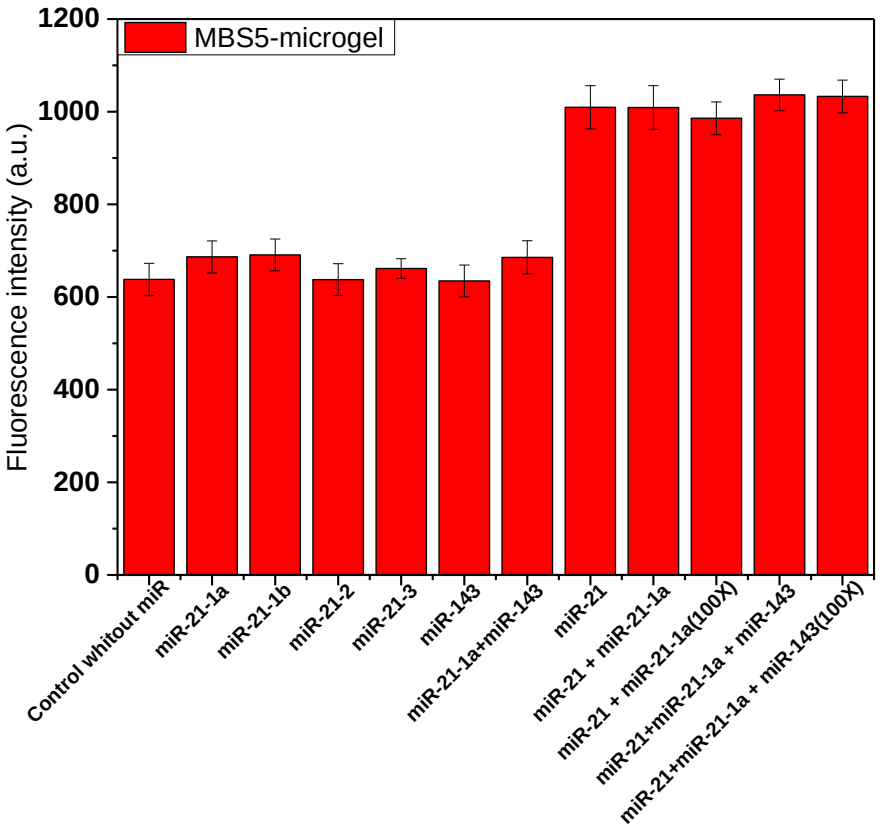

Figure 11 MBS5-microgels specificity tested towards wild-type miR-21, four mutated miR-21 sequences and a non-matching sequence (miR-143).

MBS6-microgels, instead, show higher specificity and any fluorescence increment is measured also when they are mixed with mir-21-1a and mir-21-1b (Figure 12). Both mb-microgels are

stable in presence of mixture of miRNAs, as miR-21-1a and miR-143. Moreover, when these sequences are added to the wild-type target, they do not interfere or contribute with its recognition. As results, the same increase in fluorescence intensity is measured both when miR-21-1a is alone and when it is combined with miR-143 added 1:1(50 pM) or 1:100(5 nM) to the wild-type miR-21.

These results confirm that mb-microgels due to the superior properties of molecular beacon in target recognition can be usefully applied in case of single nucleotide polymorphism (SNP) or in presence of homologous sequences.

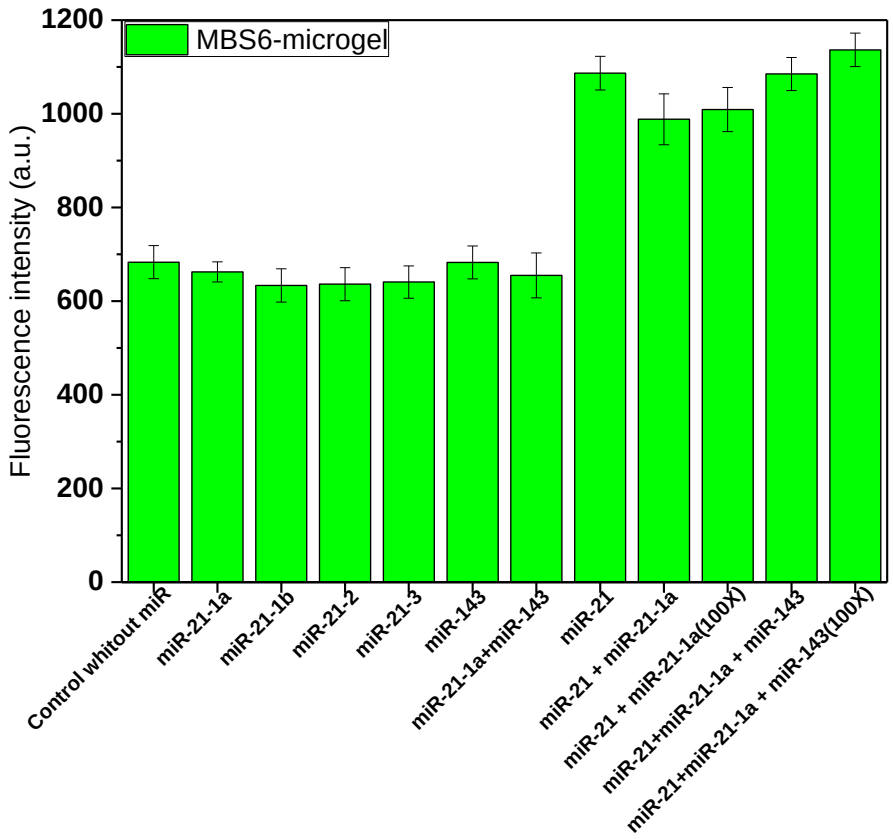

Figure 12 MBS6-microgels specificity tested towards wild-type miR-21, four mutated miR-21 sequences and a non-matching sequence (miR-143).

3.5. Human serum assay

MBS5-microgels and MBS6-microgels are added to a small volume of human serum and tested without prior manipulation of the sample. As expected both MB-microgels are capable to detect the wild-type target in human serum with results analogous to those obtained in hybridization buffer (Figure 13). Indeed, due to the anti-fouling nature of PEG, interfering proteins circulating in body fluids (in this case in human serum) are rejected from the surface of microgels. Thus, microgels permit to minimize non-specific interaction allowing the diffusion of oligonucleotides or small molecules within the polymer network. This result highlights the enhanced efficiency of functionalized microgels as mix-read biosensors, which represents an innovative and interesting field in biosensing.

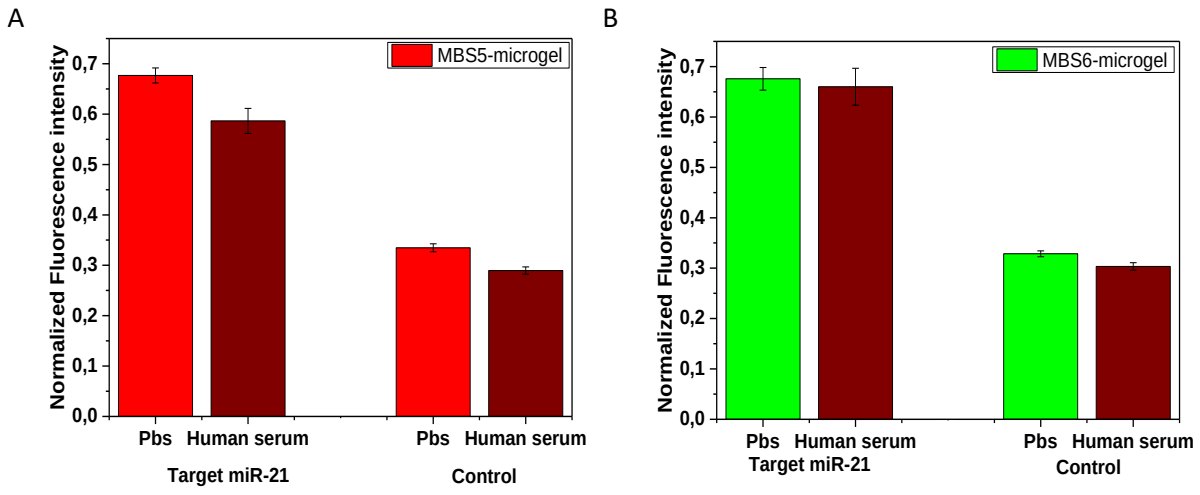

Figure 13 Mb-microgels assay in human serum. Fluorescence ATTO 647N intensity value is normalized to the rhodamine intensity.

Microgels are also analysed by flow cytometer. As clearly showed in the Appendix, the emission intensity of Fluorescein and Rhodamine is stable for all the sample analysed, while a broad curve in Atto647N (APC) is observed due to the presence of molecular beacon in stem-loop or hybridized conformation. From the data analysis results that microgels achieved sensitivity

comparable to static measurement, with signal distinguishable from the background down to 100 fM target concentration (Table 5).

Moreover, the signal-to-background ratio of the mb-microgels analysed by CLSM in PBS/serum and by FACS are similar, confirming the high stability and versatility of these microgels (Figure 14).

Table 5 FACS analysis results

	Fitc	**Rho**	**Atto 647N**	**Atto/Rho**
MBS5-microgel 0,1nmol	602	719	363	0,504
Target 100nM	583	693	674	0,972
Target 1nM	585	697	408	0,585
Target 500pM	595	707	402	0,568
Target 1pM	588	700	366	0,522
Target 100fM	564	674	345	0,511

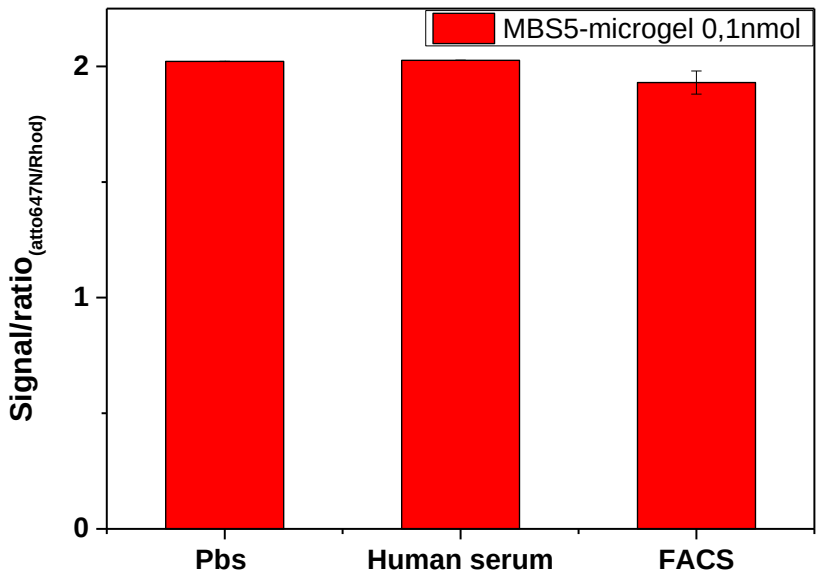

Figure 14 Signal-to-ratio of MBS5-microgels calculated by CLSM in PBS and in serum and by FACS

4. CONCLUSION

Many efforts have been made in detection methods, however, diagnostic tests for miRNA still suffer of important limitations such as the cost, the time of analysis, the complexity in specific probes design and the technical difficulties in results interpretation.

We have synthetized PEG-microgels functionalized with molecular beacons for the detection of miR-21. Such miRNA is highly expressed in cancer cells and is free to circulate in human fluids in many pathological states associated with cancer. Indeed, the miR-21 is usually used as biomarker in for the early diagnosis, in the prognosis and the follow-up of several types of cancers.

We have tuned the probe density of the molecular beacons and the concentration of microgels achieving fM sensitivity. We have proved that mb-microgels are characterized by enhanced specificity as they can distinguish the wild-type target from a mutant, even for a single nucleotide. Furthermore, microgels are stable in the presence of higher amount of interfering oligonucleotides and in complex fluids, as human serum.

Combining an optimized probe design with the solution-like and antifouling properties of the microgels, the fluorescent signal is efficiently concentrated into a small volume allowing to specifically detect the miR-21 in low fM order, without amplification steps in 3 hours, using only 20 µL of sample. In this study the hydrogel technology has been specifically developed for miR-21 detection, however, it can be tuned for several miRNAs but also for mRNA and other single strand oligonucleotides leading the way towards non-invasive, sensitive and portable analytical devices.

In conclusion, the aim of this work was to develop a sensitive and specific technology to detect circulating biomarkers. The system has proved to be suitable for the purpose, the diagnostic application on real sample are still preliminary and require additional tests to be clinically validated.

REFERENCES

1. World Health Organization. *PRESS RELEASE N° 263*. (2018).
2. Bartel, D. P. MicroRNAs: Genomics, Biogenesis, Mechanism, and Function. *Cell* **116,** 281–297 (2004).
3. De Guire, V. *et al.* Circulating miRNAs as sensitive and specific biomarkers for the diagnosis and monitoring of human diseases: Promises and challenges. *Clin. Biochem.* **46,** 846–860 (2013).
4. Schwarzenbach, H., Nishida, N., Calin, G. A. & Pantel, K. Clinical relevance of circulating cell-free microRNAs in cancer. *Nat. Rev. Clin. Oncol.* **11,** 145–156 (2014).
5. Kumarswamy, R., Volkmann, I. & Thum, T. Regulation and function of miRNA-21 in health and disease. *RNA Biol.* **8,** 706–13 (2011).
6. Krichevsky, A. M. & Gabriely, G. miR-21: A small multi-faceted RNA. *J. Cell. Mol. Med.* **13,** 39–53 (2009).
7. Volinia, S. *et al.* A microRNA expression signature of human solid tumors defines cancer gene targets. *Proc. Natl. Acad. Sci.* **103,** 2257–2261 (2006).
8. Pfeffer, S. R., Yang, C. H. & Pfeffer, L. M. The Role of miR-21 in Cancer. *Drug Dev. Res.* **76,** 270–277 (2015).
9. Feng, Y.-H. & Tsao, C.-J. Emerging role of microRNA-21 in cancer. *Biomed. Reports* **5,** 395–402 (2016).
10. Hunt, E. A., Broyles, D., Head, T. & Deo, S. K. MicroRNA Detection: Current Technology and Research Strategies. *Annu. Rev. Anal. Chem.* **8,** 217–237 (2015).
11. Tian, T., Wang, J. & Zhou, X. A review: microRNA detection methods. *Org. Biomol. Chem.* **13,** 2226–2238 (2015).
12. De Planell-Saguer, M. & Rodicio, M. C. Detection methods for microRNAs in clinic practice. *Clin. Biochem.* **46,** 869–878 (2013).
13. Tyagi, S. & Kramer, F. R. Molecular Beacons: Probes that Fluoresce Upon Hybridization. *Nat. Biotechnol.* **14,** 303–308 (1996).
14. Goel, G., Kumar, A., Puniya, A. K., Chen, W. & Singh, K. Molecular beacon: a multitask probe. *J. Appl. Microbiol.* **99,** 435–442 (2005).
15. Wang, K. *et al.* Molecular Engineering of DNA: Molecular Beacons. *Angew. Chemie Int. Ed.* **48,** 856–870 (2009).

16. Lakowicz, J. R. in *Principles of Fluorescence Spectroscopy* 257–301 (Springer US, 1983). doi:10.1007/978-1-4615-7658-7_9
17. Zheng, J. *et al.* Rationally designed molecular beacons for bioanalytical and biomedical applications. *Chem. Soc. Rev.* **44,** 3036–3055 (2015).
18. Marras, S. A. E. in *Fluorescent Energy Transfer Nucleic Acid Probes. Methods in Molecular Biology™, vol 335* 3–16 (Humana Press, 2006). doi:10.1385/1-59745-069-3:3
19. Tsourkas, A., Behlke, M. A., Rose, S. D. & Bao, G. Hybridization kinetics and thermodynamics of molecular beacons. *Nucleic Acids Res.* **31,** 1319–1330 (2003).
20. Marras, S. A., Kramer, F. R. & Tyagi, S. Multiplex detection of single-nucleotide variations using molecular beacons. *Genet. Anal.* **14,** 151–6 (1999).
21. Marras, S. A. E., Kramer, F. R. & Tyagi, S. *Genotyping SNPs With Molecular Beacons*. *Single Nucleotide Polymorphisms. Methods in Molecular Biology™* (Springer, Totowa, NJ, 2003). doi:10.1385/1-59259-327-5:111
22. Sonkar, S. C. *et al.* A molecular-beacon-based asymmetric PCR assay for easy visualization of amplicons in the diagnosis of trichomoniasis. *Biosens. Bioelectron.* **86,** 41–47 (2016).
23. Sum, S. S. *et al.* Real-time PCR assay using molecular beacon for quantitation of hepatitis B virus DNA. *J Clin Microbiol* **42,** 3438–3440 (2004).
24. Marras, S. A. E., Russell Kramer, F. & Tyagi, S. Multiplex detection of single-nucleotide variations using molecular beacons. *Genet. Anal. Biomol. Eng.* **14,** 151–156 (1999).
25. Gubala, A. J. & Proll, D. F. Molecular-beacon multiplex real-time PCR assay for detection of Vibrio cholerae. *Appl. Environ. Microbiol.* **72,** 6424–8 (2006).
26. Nadal, A., Coll, A., Cook, N. & Pla, M. A molecular beacon-based real time NASBA assay for detection of Listeria monocytogenes in food products: Role of target mRNA secondary structure on NASBA design. *J. Microbiol. Methods* **68,** 623–632 (2007).
27. Dimov, I. K. *et al.* Integrated microfluidic tmRNA purification and real-time NASBA device for molecular diagnostics. *Lab Chip* **8,** 2071–2078 (2008).
28. Zhao, Y. *et al.* Rapid real-time nucleic acid sequence-based amplification-molecular beacon platform to detect fungal and bacterial bloodstream infections. *J. Clin. Microbiol.* **47,** 2067–2078 (2009).
29. Bakthavathsalam, P., Longatte, G., Jensen, S. O., Manefield, M. & Gooding, J. J. Locked nucleic acid molecular beacon for multiplex detection of loop mediated isothermal amplification. *Sensors Actuators, B Chem.* **268,** 255–263 (2018).

30. Vargas, D. Y., Kramer, F. R., Tyagi, S. & Marras, S. A. E. Multiplex Real-Time PCR Assays that Measure the Abundance of Extremely Rare Mutations Associated with Cancer. *PLoS One* **11,** e0156546 (2016).
31. Gui, Z. *et al.* Direct detection of circulating free DNA extracted from serum samples of breast cancer using locked nucleic acid molecular beacon. *Talanta* **154,** 520–525 (2016).
32. Giraldo-Vela, J. P. *et al.* Single-Cell Detection of mRNA Expression Using Nanofountain-Probe Electroporated Molecular Beacons. *Small* **11,** 2386–2391 (2015).
33. Kang, W. J. *et al.* Molecular beacon-based bioimaging of multiple microRNAs during myogenesis. *Biomaterials* **32,** 1915–1922 (2011).
34. Baker, M. B., Bao, G. & Searles, C. D. In vitro quantification of specific microRNA using molecular beacons. *Nucleic Acids Res.* **40,** (2012).
35. Li, J. J., Fang, X., Schuster, S. M. & Tan, W. Molecular beacons: A novel approach to detect protein - DNA interactions. *Angew. Chemie - Int. Ed.* **39,** 1049–1052 (2000).
36. Ma, C. *et al.* A novel kinase-based ATP assay using molecular beacon. *Anal. Biochem.* **372,** 131–133 (2008).
37. Choi, N. W. *et al.* Multiplexed detection of mRNA using porosity-tuned hydrogel microparticles. *Anal. Chem.* **84,** 9370–9378 (2012).
38. Wang, H.-N. & Vo-Dinh, T. Multiplex detection of breast cancer biomarkers using plasmonic molecular sentinel nanoprobes. *Nanotechnology* **20,** 065101 (2009).
39. Wang, C. *et al.* Elaborately designed diblock nanoprobes for simultaneous multicolor detection of microRNAs. *Nanoscale* **7,** 15822–15829 (2015).
40. Guo, Q., Bai, Z., Liu, Y. & Sun, Q. A molecular beacon microarray based on a quantum dot label for detecting single nucleotide polymorphisms. *Biosens. Bioelectron.* **77,** 107–110 (2016).
41. Horejsh, D. *et al.* A molecular beacon, bead-based assay for the detection of nucleic acids by flow cytometry. doi:10.1093/nar/gni015
42. Yao, G. & Tan, W. Molecular-beacon-based array for sensitive DNA analysis. *Anal. Biochem.* **331,** 216–223 (2004).
43. Du, H., Disney, M. D., Miller, B. L. & Krauss, T. D. Hybridization-Based Unquenching of DNA Hairpins on Au Surfaces: Prototypical "Molecular Beacon" Biosensors. *J. Am. Chem. Soc.* **125,** 4012–4013 (2003).
44. Nakano, S., Miyoshi, D. & Sugimoto, N. Effects of Molecular Crowding on the Structures, Interactions, and Functions of Nucleic Acids. *Chem. Rev.* **114,** 2733–2758 (2014).

45. Darbandi, A. *et al.* Molecular beacon anchored onto a graphene oxide substrate. *Nanotechnology* **28,** 375501 (2017).
46. Dubertret, B., Calame, M. & Libchaber, A. J. Single-mismatch detection using gold-quenched fluorescent oligonucleotides. *Nat. Biotechnol.* **19,** 365–370 (2001).
47. Wang, H. *et al.* Label-free hybridization detection of a single nucleotide mismatch by immobilization of molecular beacons on an agarose film. *Nucleic Acids Res.* **30,** e61 (2002).
48. Wang, L., Yang, C. J., Medley, C. D., Benner, S. A. & Tan, W. Locked Nucleic Acid Molecular Beacons. *J. Am. Chem. Soc.* **127,** 15664–15665 (2005).
49. Xu, Q. *et al.* Rapid, Surfactant-Free, and Quantitative Functionalization of Gold Nanoparticles with Thiolated DNA under Physiological pH and Its Application in Molecular Beacon-Based Biosensor. *ACS Appl. Mater. Interfaces* **8,** 27298–27304 (2016).
50. Yin, H., Zhou, Y., Zhang, H., Meng, X. & Ai, S. Electrochemical determination of microRNA-21 based on graphene, LNA integrated molecular beacon, AuNPs and biotin multifunctional bio bar codes and enzymatic assay system. *Biosens. Bioelectron.* **33,** 247–253 (2012).
51. Li, F. *et al.* A graphene-enhanced molecular beacon for homogeneous DNA detection. *Nanoscale* **2,** 1021–1026 (2010).
52. Cui, L. *et al.* Graphene oxide-protected DNA probes for multiplex microRNA analysis in complex biological samples based on a cyclic enzymatic amplification method. *Chem. Commun.* **48,** 194–196 (2012).
53. Chan, V., Graves, D. J. & McKenzie, S. E. The biophysics of DNA hybridization with immobilized oligonucleotide probes. *Biophys. J.* **69,** 2243–2255 (1995).
54. Dai, X., Yang, W., Firlar, E., Marras, S. A. E. & Libera, M. Surface-patterned microgel-tethered molecular beacons. *Soft Matter* **8,** 3067 (2012).

APPENDIX

FACS measurements

Dot plot of MBS5-microgels in hybridization buffer

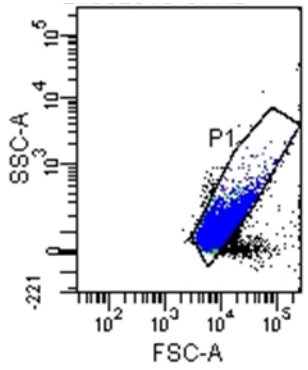

Population	#Events	%Parent	FITC-A Mean	FITC-A Median	PE-A Mean	PE-A Median	APC-A Mean	APC-A Median	APC-A %CV
P1	20,000	96.8	602	513	719	601	363	218	214.2
P2	17,425	87.1	658	551	762	639	379	229	210.9
P3	19,241	96.2	614	523	738	613	370	223	213.4
P4	17,247	86.2	615	527	734	617	376	255	102.9
P5	141	0.7	1,686	993	2,024	1,132	5,987	4,281	96.5
P6	7,602	38.0	757	616	901	721	764	517	150.3

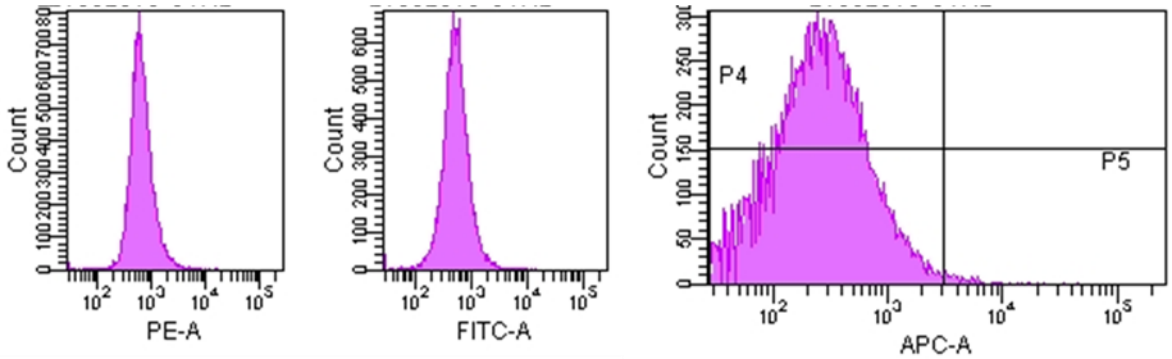

Dot plot of MBS5-microgels mixed with target miR-21 100nM in hybridization buffer

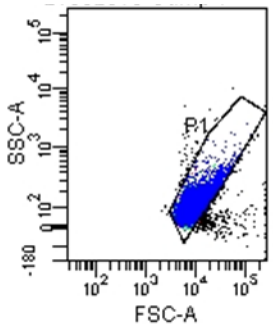

Population	#Events	%Parent	FITC-A Mean	FITC-A Median	PE-A Mean	PE-A Median	APC-A Mean	APC-A Median	APC-A %CV
P1	20,000	97.3	583	504	693	591	674	448	147.6
P2	17,384	86.9	637	544	733	627	709	476	145.5
P3	19,219	96.1	594	514	712	603	683	456	146.1
P4	18,762	93.8	577	508	686	594	615	462	84.5
P5	351	1.8	1,324	961	1,592	1,198	5,584	4,320	72.7
P6	13,319	66.6	649	555	770	649	937	657	120.6

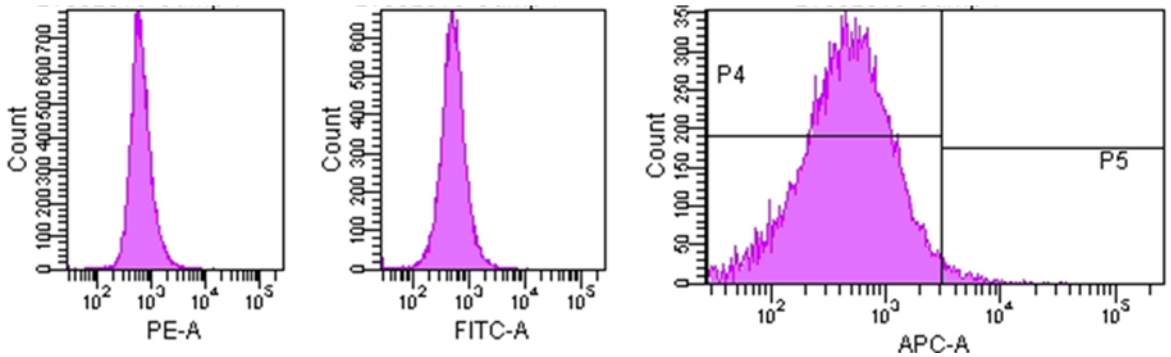

Dot plot of MBS5-microgels mixed with target miR-21 1nM in hybridization buffer

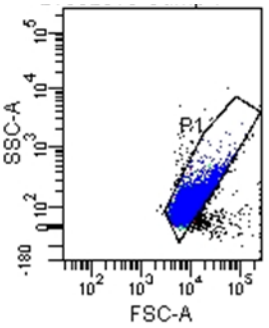

Population	#Events	%Parent	FITC-A Mean	FITC-A Median	PE-A Mean	PE-A Median	APC-A Mean	APC-A Median	APC-A %CV
P1	20,000	98.3	585	507	697	593	408	253	185.6
P2	17,424	87.1	638	542	737	630	430	267	183.2
P3	19,294	96.5	595	516	714	603	414	257	184.1
P4	17,727	88.6	592	518	705	605	406	286	99.1
P5	167	0.8	1,595	1,013	1,909	1,325	6,067	4,609	68.2
P6	8,615	43.1	705	587	838	692	781	534	132.7

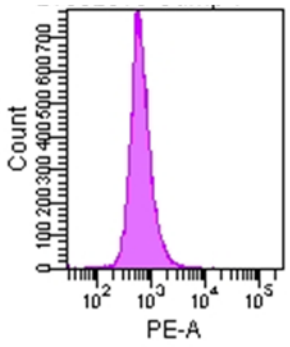

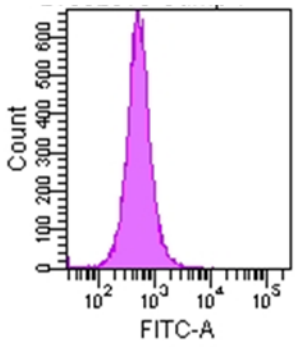

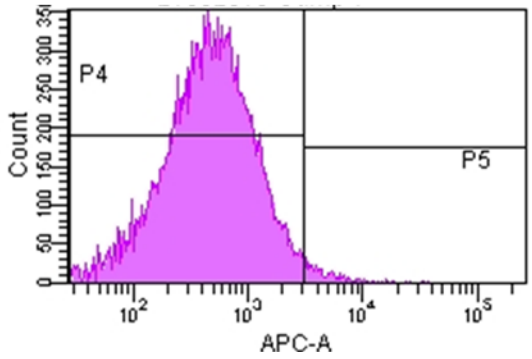

Dot plot of MBS5-microgels mixed with target miR-21 500pM in hybridization buffer

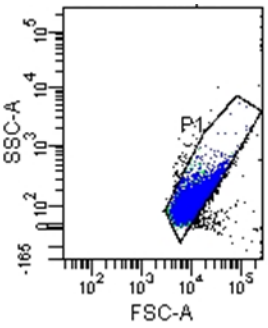

Population	#Events	%Parent	FITC-A Mean	FITC-A Median	PE-A Mean	PE-A Median	APC-A Mean	APC-A Median	APC-A %CV
P1	20,000	98.3	595	512	707	598	402	247	224.3
P2	17,515	87.6	648	550	747	634	423	260	224.9
P3	19,295	96.5	606	522	724	610	408	252	223.5
P4	17,627	88.1	604	526	717	612	403	281	99.8
P5	156	0.8	1,648	1,023	1,952	1,262	6,404	4,355	107.8
P6	8,486	42.4	725	606	860	706	780	526	164.9

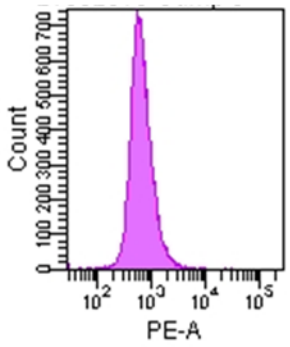

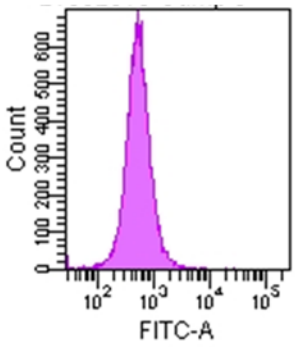

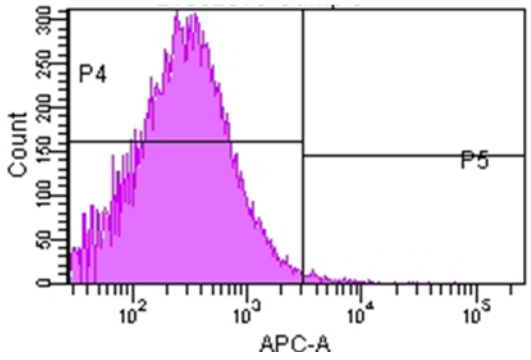

Dot plot of MBS5-microgels mixed with target miR-21 1pM in hybridization buffer

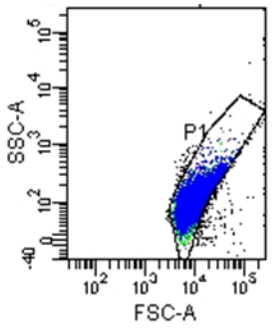

Population	#Events	%Parent	FITC-A Mean	FITC-A Median	PE-A Mean	PE-A Median	APC-A Mean	APC-A Median	APC-A %CV
P1	20,000	98.5	588	507	700	592	366	211	304.4
P2	17,436	87.2	641	545	740	629	385	223	300.5
P3	19,270	96.4	599	516	718	603	370	214	299.4
P4	17,137	85.7	600	519	714	608	366	249	105.2
P5	154	0.8	1,402	881	1,673	1,109	7,318	4,585	132.7
P6	7,299	36.5	731	602	867	709	801	513	219.4

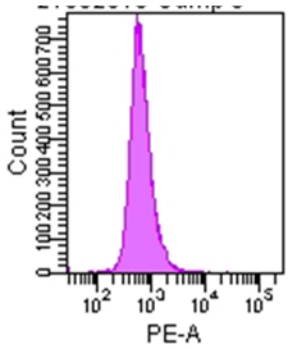

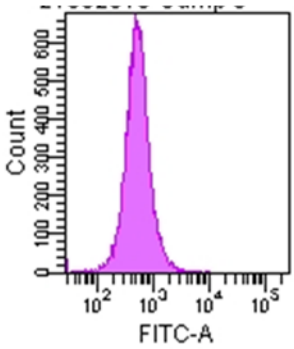

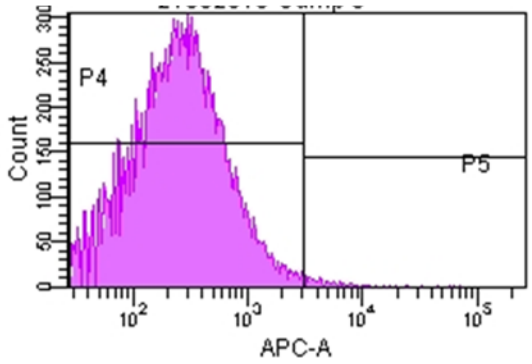

Dot plot of MBS5-microgels mixed with target miR-21 100fM in hybridization buffer

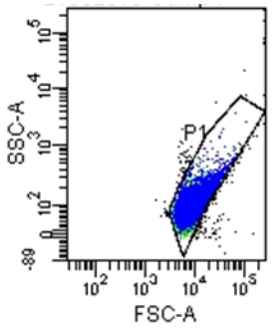

Population	#Events	%Parent	FITC-A Mean	FITC-A Median	PE-A Mean	PE-A Median	APC-A Mean	APC-A Median	APC-A %CV
P1	20,000	98.8	564	491	674	577	345	213	211.2
P2	17,082	85.4	622	531	716	612	360	226	174.0
P3	19,237	96.2	575	500	692	587	349	217	208.2
P4	17,185	85.9	576	503	688	588	364	252	102.2
P5	118	0.6	1,502	876	1,786	985	6,130	4,392	94.6
P6	7,401	37.0	689	568	822	664	736	513	147.4

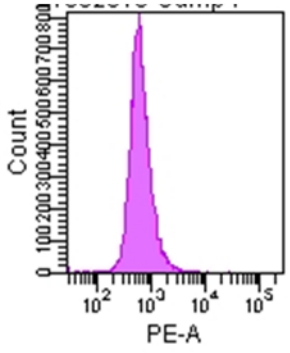

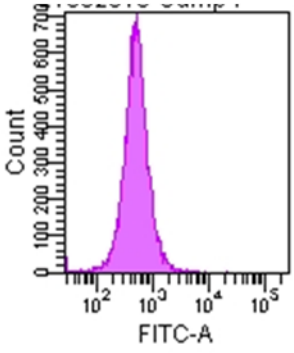

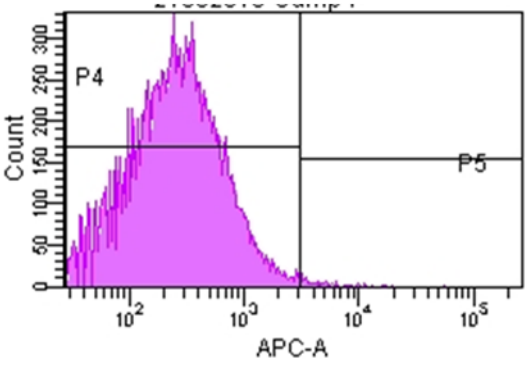

CHAPTER 4

"Microgels for long oligonucleotide sequence detection"

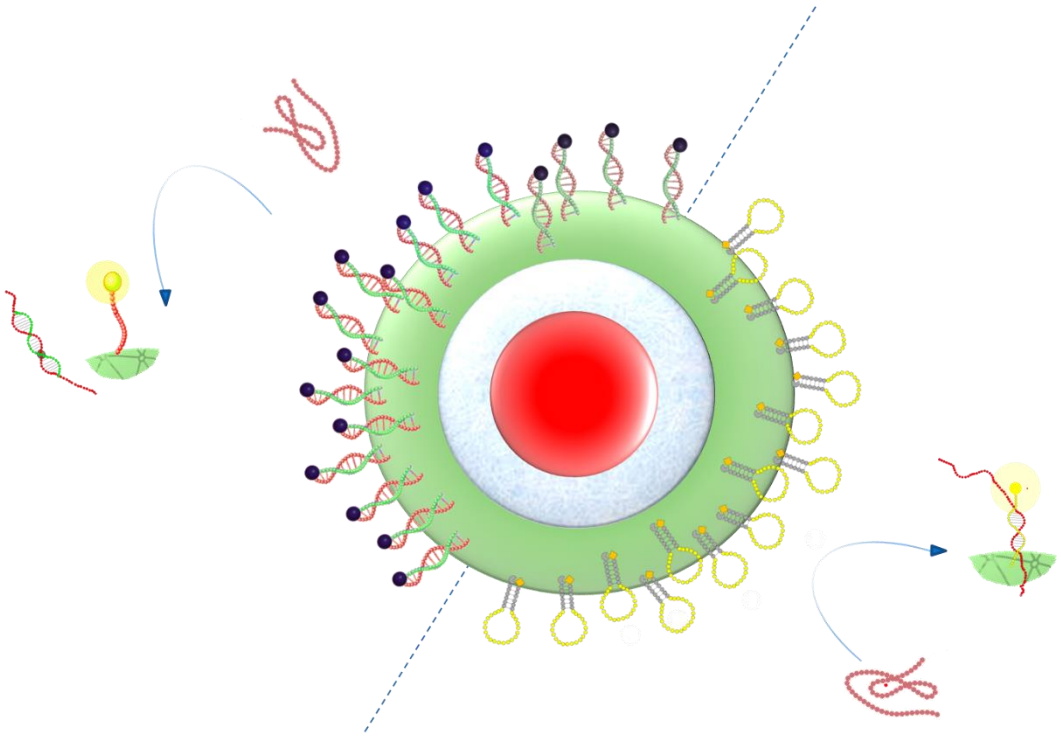

1. INTRODUCTION

Sensitive and specific detection of oligonucleotides is extremely important in clinical application. It is proved that higher levels of nucleic acids are free to circulate in body fluids during many clinical disorders. As consequence, free oligonucleotides in human fluids may serve as minimally invasive biomarkers[1,2].

The '*liquid biopsy*'[3] technology aims to detect these circulating oligonucleotides in human fluids to diagnostic several diseases avoiding invasive procedures as biopsies. Circulating RNA molecules[4] such as protein-coding messenger RNAs (mRNA), are correlated to cancer[5,6] or prenatal disorders[7]. Cell-free long coding RNAs (lncRNA) have been proposed as biomarkers for diagnosis and prognosis of many pathologies as non-small cell lung cancer[8], acute myocardial infarction[9], bladder cancer[10] hepatocellular carcinoma[11]. DNA molecules are also free to circulate in human fluids and they are involved in many processes as immunity[12], aging[13] or are used as biomarker in prenatal screening[14], stroke[15], infarction[16], trauma[17], infection[18]. However, one of the most studied clinical application is the detection of circulating tumour DNA (ctDNA) as non-invasive assessment of cancer[19–21].

To support such applications many analytical methods have been developed and validated. In particular, since the polymerase chain reaction (PCR) was introduced in 1985, PCR has become the most applied technology especially in medical communities[22]. PCR, qRT-PCR[23] and digital PCR[24,25] techniques are routinely used since they offer enhanced sensitivity and specificity. However, these techniques require complex, expensive, time-consuming and hard-working procedures that have induced scientists to developed alternative analytical methods. Therefore, many new technologies for oligonucleotide sequencing and quantification have been made[26]. PCR-free biosensing methods have been developed and many of the most innovative technologies relay on optical[27] or electrochemical[28] sensors combined with DNA hybridization. These biosensors are often combined with enzyme-based signal amplification to achieve better sensitivity[29] or modified with oligonucleotide analogues[30] to increase the specificity.

In this chapter the performances of microgels in long oligonucleotide sequence detection were investigated. As proof-of-concept experiment reported herein, two long single strand oligonucleotide with high sequence similarity were chosen as initial targets. For each target, double strand probe- and molecular beacon-microgels are designed and tested. Firstly, the practical rules to design probes for long oligonucleotide target detection were set. Then microgels performance in long target detection were evaluated and compared to those observed with short oligonucleotides in chapter 2 and 3.

The aim is to lead the way forward further application of functionalized microgels for the detection of long oligonucleotide biomarkers as mRNA, lncRNA, cDNA and with the appropriate modifications to double strand DNA. This because there is an increasing demand for sensitive and specific assays able to detect the mentioned oligonucleotides in complex fluids, especially for *liquid biopsy* application.

2. EXPERIMENTAL SECTION

2.1. Materials

Poly(ethylene glycol) dimethacrylate average Mn 550 (PEGDMA), Acrylic acid (AAc), Potassium persulfate (KPS), Fluoresceine O-methacrylate, 1-ethyl-3-(3-dimethylaminopropyl) carbodiimide (EDC) and Polyvinyl alcohol 40-88 (PVA), Dimethyl Sulfoxide (DMSO), Sodium Hydroxide, 4-Morpholineethanesulfonic acid sodium salt (MES) were purchased from Sigma Aldrich. The dye Methacryloxyethylthiocarbonyl-rhodamine B was obtained from Polyscience Inc. Phosphate buffered saline tablets were supplied by MP biomedicals. DNA and RNA oligonucleotides were purchased from Metabion International with HPLC purification.

2.2. Probe design

To detect long oligonucleotide sequences, probe design approaches described in chapter 2 and 3 were compared. For this purpose, double strand and molecular beacon probes were designed and tested.

DNA double strand (ds) probes were designed based on the target sequences P1 and P2 (Table 1). The target sequences have length of 111 nucleotides and 70% of sequence similarity. The sequence alignment, folding considering and thermodynamic parameters were considered to improve the specificity and enhance the sensitivity of the target detection. The alignment scores were estimated by NCBI blast, while folding was predicted through UNAFold web server. Thermodynamic parameters (melting temperature, ΔG ΔH ΔS) were predicted using appropriate tools (OligoAnalyzer 3.1 (IDT-Integrated, D. N. A. 2014) and Oligocalc). The target recognition was based on a displacement assay mediated by a toehold strand mechanism as already discussed in chapter 1-2. The oligonucleotide quencher strand (Q) fully complementary to the target, was designed with an internal Black Hole Quencher (dT-BHQ2). This strand is partially complementary to a shorter tail (F), labelled with a fluorophore (ATTO647N) at the 5'terminus and a C6-spacer with amine linker on the 3' terminus (Table 1). Quenching efficiency and kinetics of displacements for the selected ds probe were measured by a spectrofluorometer. Displacement efficiency was calculated mixing 5nM of pre-hybridized ds probe with

50, 5 and 0.5 nM of target solution, in 500 µL of 100 mM TRIS buffer pH 8 enriched with 200mM NaCl (hybridization buffer). Moreover, ds-probe cross-reactivity was tested spiking 500 nM of homologous Target P2 (Table 1) (10-fold excess) in 500 µL of hybridization buffer containing 50 nM of ds-P1and monitoring the emission intensity over 24 hours. Subsequently, 500 nM of the specific target P1 was added and recovery of fluorescence monitored for 24 hours. In the same way, cross-reactivity was measured for 50 nM of ds-P2, spiking 500 nM of homologous P1 and following the fluorescence emission for 24 hours, then target P2 was added and recovery of fluorescence recorder for further 24 hours.

Two molecular beacons (MBP1-MBP2) were designed based on the folding of the specific target P1 and P2. The molecular beacons contained a stem of 6 bases and a loop complementary to the target site made of 24 (P1) or 23 (P2) bases. The 5'terminus was modified with an ATTO647N fluorophore and a 12-carbon amino spacer while a BlackBerry Quencher 650 (BBQ-650) was added on the 3' terminus. Both molecular beacons were suspended in nuclease-free water (100 µM final concentration) and stored at -20°C. The sequence alignment, the folding considering and thermodynamic parameters were predicted using the software aforementioned. To assess the specificity of both molecular beacons cross-reactivity experiments were carried out as already described for the ds-probes. The kinetics of hybridizations in presence of the specific target was measured mixing 500 nM of the sequences with 50 nM of molecular beacon in 500 µL of hybridization buffer. Melting curves for both molecular beacons were made to identify their melting temperatures. Melting curves were obtained monitoring the fluorescence intensity as function of the temperature. In particular, 500 µL of hybridization buffer solution containing 50 nM of molecular beacon alone or mixed with 500 nM of target was initial denatured (3 min 95°C), then the temperature was decreased from 95°C to 20°C, with a scan rate of 1°C/2min. Moreover, kinetics of hybridizations and melting curves were performed in presence of a shorter target, containing only the sequence complementary to the loop, in the same experimental condition. The binding of P1 and P2 target (111) was investigated by means of fluorescence titration experiments. Titration experiments were carried out at 25 °C in 500 µL of hybridization buffer, by stepwise addition (2 or 4 µL) of target P1/P2 solutions (2.5 µM) to a cell containing a fixed concentration (50 nM) of MBP1/MBP2 solution. After each addition of target, the solution was allowed to equilibrate and then fluorescence spectra were collected. Titration curves were obtained by plotting the recovery of fluorescence measured versus the target concentration. The dissociation constant Kd, was estimated from this plot by fitting the resulting curve by non-linear curve fit (dose-response function).

Fluorescence spectra were collected in a 1 cm path length cuvette with a Horiba JobinYvon model FluoroMax-4 spectrofluorometer equipped with a Peltier temperature controller. The sample was excited at 647 nm with a slit width of 5 nm, and emission spectra was collected from 667 to 750 nm with a slit width of 5 nm.

2.3. Microgel synthesis and bioconjugation

Microgels with multi-shell architecture were synthetized through a multistep synthesis as described in chapter 2 and 3 and functionalized with double strand and molecular beacon probes. In the first case, bioconjugation was carried out coupling 1.5, 1 and 0.5 nmol of pre-hybridized ds-probe P1 and P2. Molecular beacons were conjugate on microgels using 0.5, 0.25 and 0.1 nmol of probes MBP1 and MBP2. Before the coupling reaction, 1 mg of microgel was incubated in 450 µL MES pH 6, while ds-probe and molecular beacon probes were incubated in 50 µL MES pH 6 enriched with 200 mM of NaCl, both for 5 hours. After, the carboxylic groups on microgels were activated using 500 mM of the coupling agent EDC stirring vigorously for 30 min at 5°C. Subsequently, the solution containing the probes was added to the microgels and the reaction was carried out overnight at room temperature. Functionalized microgels were washed 3 times to remove the unreacted probes and resuspended in hybridization buffer.

Kinetics of hybridizations on microgels were measured through a spectrofluorometer. 50 µg/mL of ds-P1 microgels (0.5 nmol) were mixed with 500 nM of Target P1 (111nt) in a final volume of 500 µL. Moreover, 50 µg/mL of MBP1- and MBP2-microgels (Low, Medium and High concentration) were mixed with 500 µL of hybridization solution containing 500 nM of target P1 and P2 both as long or short sequence.

2.4. Microgel assay

The assay was carried out mixing the functionalized microgels to the sample solution containing the target sequences, without preliminary steps of amplification. The solution was incubated o/v at room temperature and fluorescence emission analysed by confocal laser scanning microscopy (CLSM).

To estimate the working range, the limit of detection (LOD) and quantification (LOQ), 5 µg/mL of each microgel batch was mixed with 20µL of samples at different P1/P2 target concentrations, ranging from nM to fM. The solution was loaded into µ-slide 18 well-flat (Ibidi, Martinsried, DE) and incubated at room temperature overnight. Fluorescence intensity was measured by CLSM-SP5 with an objective HCX PL APO CS 63x1.40 oil (Zeiss), by using Helium neon laser 543 nm and 633 nm. Power lasers and detector gains were kept always constant with a section thickness 3.04 airy unit, scan speed 8000 Hz and

an image size of 144.7x144.7 μm^2 (resolution 512x512). For each target concentration, 3 or more images were collected and more than 500 microgels were analysed. The images were thresholded by Otsu algorithm and then processed with the Image J Analyze Particles function to computationally determine the number of single fluorescent particles sizing in the range of 1µm.

2.5. Statistical analysis

All experiments were performed at least three times, reported as mean ± standard deviation and analysed statistically by paired Student's test. Significant difference was determined at P values smaller than 0.05.

To estimate the Limit of detection (LOD) and the Limit of quantification(LOQ), the values, subtracted of the background and reported as mean ± standard deviation, were fitted applying a linear regression. LOD values were calculated as three standard error (SE) above the slope, while the LOQ corresponded to ten standard deviation (SD) above the slope.

Table 1 Sequence, length, modifications and thermodynamic parameters of the DNA probes and targets used in microgel assay. All parameters are calculated by IDT-Integrated, D. N. A. "Technologies. OligoAnalyzer 3.1. Web setting respectively 50nM and 200mM as oligonucleotide and Na^+concentration.

	SEQUENCE (5'-3')	LENGTH (nt)	Tm (°C)	ΔG (Kcal/mol)	ΔH (kcal/mol)	ΔS cal/(K·mol)
Tail P1	*Atto647N*-A GAG CGG TCT GAT-*C6-NH₂*	13	50.121	-14.25	-95.9	-263.27
Quencher-P1	ATC AGA CCG CTC (dT-*BHQ2*)CA ATG CCA AAC TCT TCA	30	72.49	-34.5 ΔG_d=-17.3	-235.1	-646.8
Tail P2	*ATTO647N*-ATGGCCAAAGCC-C6-*NH₂*	12	49.27	-13.75	-89	-242.64
Quencher-P2	GGC TTT GGC CA(dT-*BHQ2*) CGG CGC AAG ACA GTT AGT	30	77.49	-38.4 ΔG_d=-21.78	-242.8	-659.05
MBP1	*NH₂ -C12-* (*ATTO647N*)**GGCGCG**-GACCGC TCTCAATGCC AAACTCTT-**CGCGCC** (*BBQ650*)	36	69.2	Stem=-6.78	-52.5	-153.34
MBP2	*NH₂ -C12-* (ATTO647N)**GGCGCG**-TCATCGTGCC GACTTCTATGCCC-**CGCGCC** (BBQ650)	35	70.6	Stem=-6.23	-51.3	-149.15
P1 SHORT	AAG AGT TTG GCA TTG AGA GCG GTC	24	68.51	-27.78	-188.9	-514.49
P2 SHORT	GGG CAT AGA AGT CGG CAC GAT GA	23	70.13	-27.98	-182.6	-498.53
P1 (NC000964.3)	CATTATTTCA AATGCGTCAT GCACGACAAA TTGCCTTGCG CCTGTTGTAA AAGTGCTGGA TGAAGAGTTT GGCATTGAGA GCGGTCTGAT GACTACAGTT CATGCGTATA C	111	85.1	-132.76	-911.6	-2511.16
P2 (CP017631.1)	CATTGTTTCC GTGGCGTCAT GCACC ACTAA CTGTCTTGCG CCGATGGCCA AAGCCTTGCA TGACAGTTTC GGGATAGAAG TCGGCACGAT GACGACCATT CATGCCTATA C	111	89.23	-143.19	-921.6	-2509.78

Modifications are reported in Italics, while the molecular beacon stem in bold underline. ΔG_d is the free energy of displacement.

3. RESULTS AND DISCUSSION

In this chapter the microgels biosensing capability of detect long oligonucleotide sequences is investigated. To do this we have compared the analytical sensitivity of hydrogels engineered with two different probes: double strand and molecular beacons. Furthermore, to demonstrate the efficiency of our hydrogel assay, two DNA sequences (P1 and P2 table 1) with a high degree of homology (about 70%) are selected as Target molecules.

3.1. Double strand-microgel assay

Double strand probes are properly designed based on P1-P2 Target sequences. The ds probe results from the hybridization between a short-labelled tail (F) and a longer strand internally modified with a quencher (Q). The mechanism of detection consists of a double strand displacement assay as already discussed in chapter 2. Briefly, when the tail-F and the quencher-Q strands hybridize a consequent quenching of fluorescence is measured. In presence of the target complementary to the Q strand, an energetically favourable displacement process starts (ΔG displacement about -20 kcal/mol) and stable Target-Quencher duplex is formed. This event causes a recovery of fluorescence directly correlated to the amount of target detected. However, in this case, the recognition between the quencher and the target is localized on a small portion (<30nt) of the target sequence (>100). For that reason, the specific target site has been opportunely selected in order to have the higher sequence variability, favourable ΔG displacement and less hindered folding. To achieve enhanced sensitivity, the length of the ds-probe P1 and P2 are tuned and their folding is simulated. Adjusting the length of the probe thermodynamic parameters are optimized and ΔG of displacement of -17.3 and -21.7 kcal/mol are respectively predicted for the P1 and P2 (Table 1). Stable secondary structures that could decrease the hybridization ratio are not predicted from the folding simulations (Figure 1 A- B). Once synthetized, ds-probes are previously tested in solution and then mounted on microgels.

After the addition of the quencher a strong fluorescence decrease has been measured in solution for both P1 and P2 probes, with quenching efficiency assess to 95% and 89% for QF-P1 and QF-P2 respectively (Figure 1C-D). Regarding the kinetics of displacement in solution, when QF-P1 is tested the displacement process is completed in about 3 hours using 10-fold excess of target ss P1 (Figure 1E). However, decreasing the target concentration the kinetics of hybridization are slower and less efficient. A maximum displacement of 25% is recorded in 5 hours adding 500pM of target. The ds-P2 results less efficient in target recovery compared to ds-P1 in the same experimental condition. Indeed, after 6 hours

displacement efficiency of 60%, 25% and 12% is achieved using 50nM, 5nM and 500pM of Target ss P2 (Figure 1F).

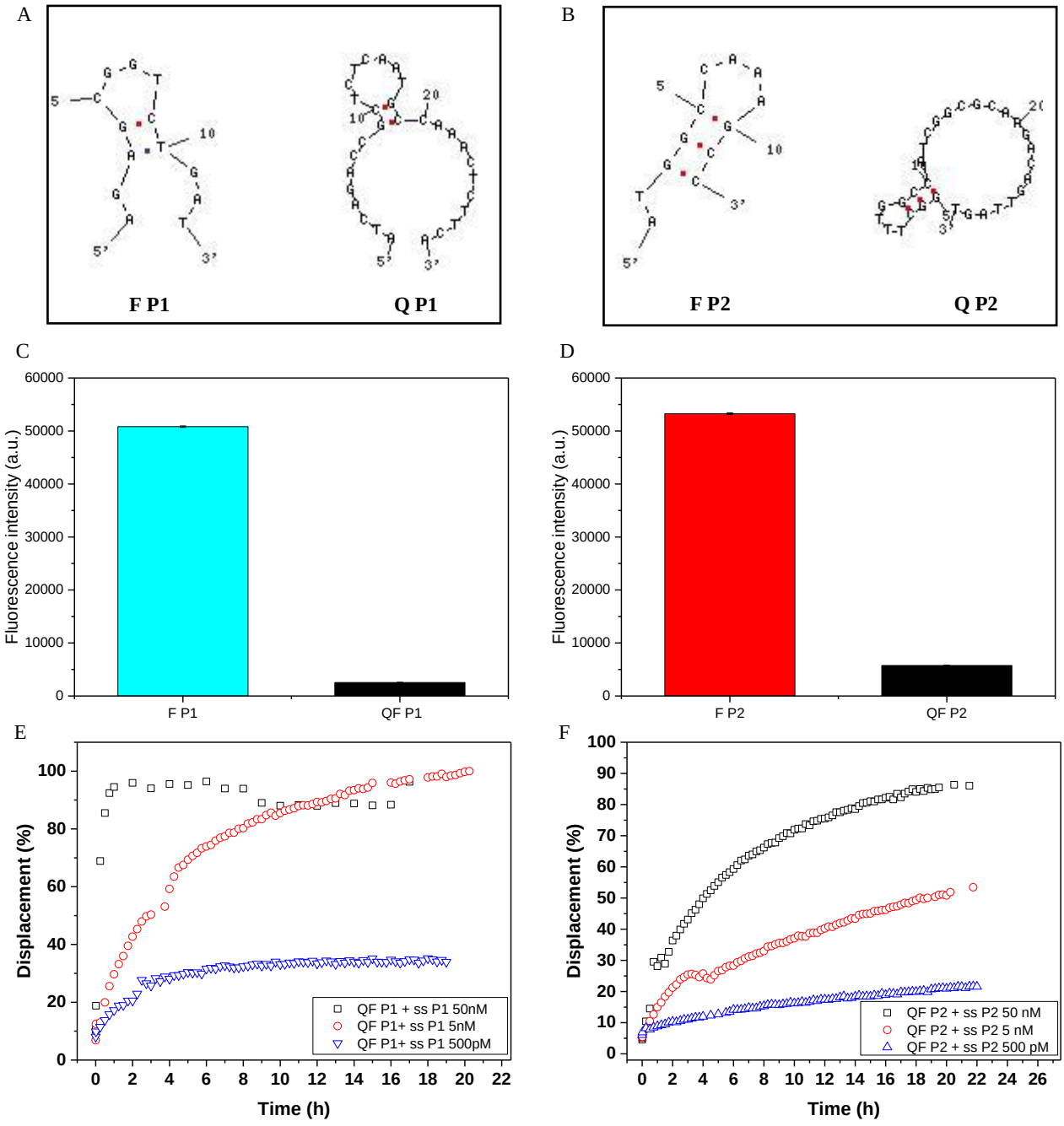

Figure 1 Ds-Probe study: folding simulation (P1-A, P2-B), fluorescence analysis (P1-C, P2-D) and kinetics of hybridizations (P1-E, P2-F)

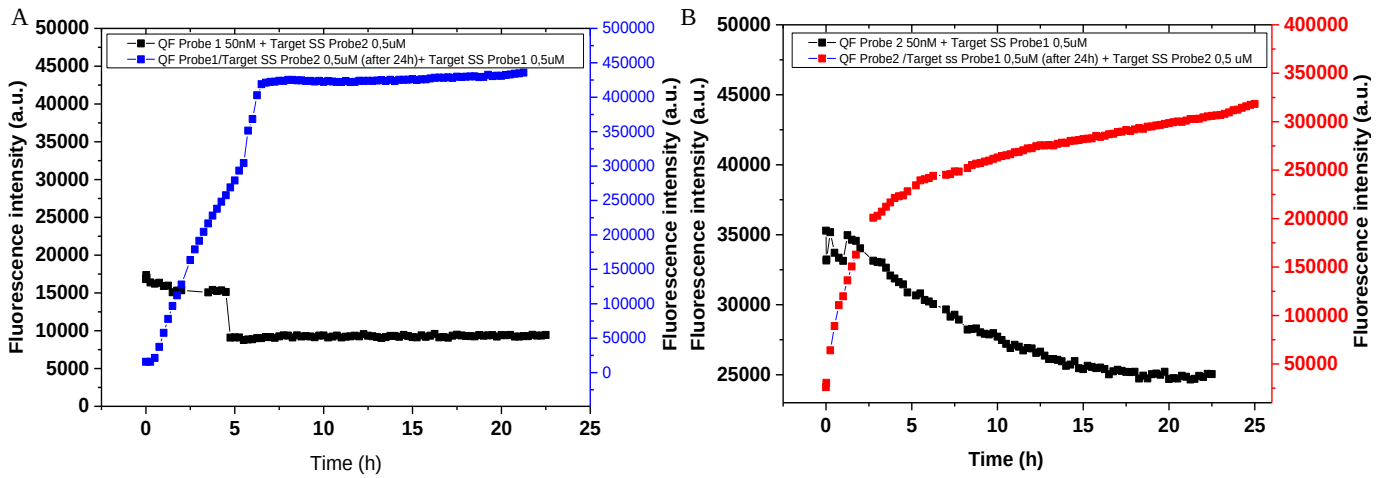

Figure 2 Cross-reactivity experiments: ds-P1 (A) and ds-P2 (B) probes were monitored in presence of the correspondent homologous Target ss P2 and P1(black square). After that, the specific target P1(blue square) and P2 (red square) is added and fluorescence emission collected for the following 24hours.

Cross-reactivity experiments have been carried out to prove the specificity of the probes. As clearly shown in Figure 2, in presence of high concentration of homologous sequence, both ds-probe QF-P1 and QF-P2 are very stable and fluorescence increment is not recorded for 24 hours. Then, the specific target is spiked into the solution and a significant recovery of fluorescence is measured. Such results confirm that our optimized ds-probes have improved specificity toward target with high sequence similarity, an essential requirement in oligonucleotide detection.

Double strand probes have been bioconjugated on the microgels, by carbodiimide chemistry. Several concentrations are tested, and the best results are obtained conjugating 0.5nmol of pre-hybridized ds strand probes. After the functionalization, microgels are analysed by CLSM. Quenching efficiency of 76.96% and 51.8% is measured for dsP1-microgels and dsP2-microgels (Figure 2A-B).

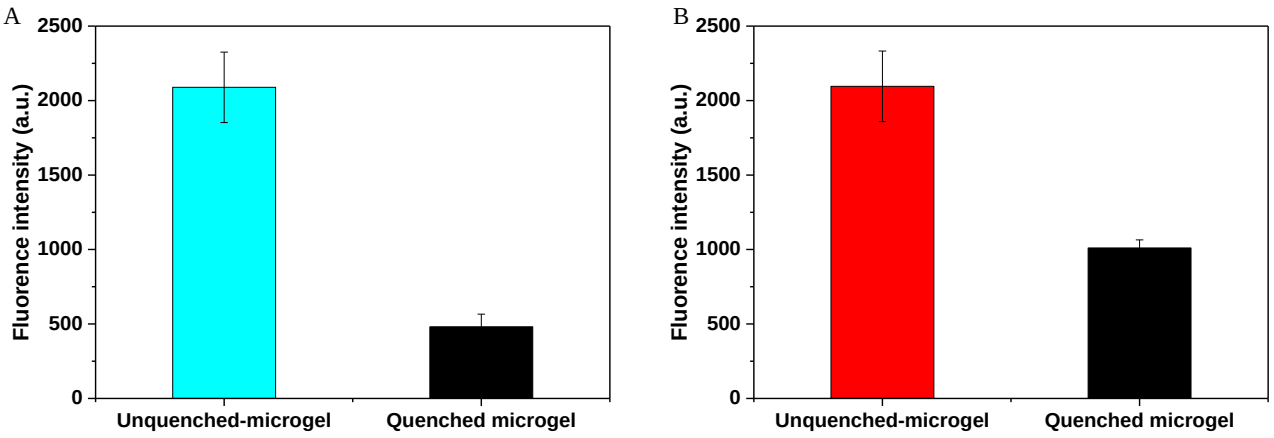

Figure 3 Fluorescence intensity measured by CLSM of quenched and unquenched probe P1 (A) and P2(B)

The assay is performed, as already described in chapter 2; by mixing the ds-microgels with the sample containing the target strand. The solution is incubated a room temperature until equilibrium is reached and then the fluorescence emission is measured collecting images by CLSM or recording the emission spectra by a spectrofluorometer. Previously manipulations of the sample are avoided, due to the antifouling properties, solution-like environment and signal concentrator capability of microgels, as already discussed in chapter 2 and 3.

The assay sensitivity has been estimated testing several target concentrations from µM to aM. The results indicate that the working range of the assay is comprised between 10^{-6} - 10^{-9}M for both ds-P1 and ds-P2-microgels (Figure 4). Microgels functionalized with ds-P1 reach LOD of 530.83 pM and LOQ of 1.6 nM while those coupled to ds-P2 achieve LOD 813.43 pM and LOQ 2.4 nM (Table 2).

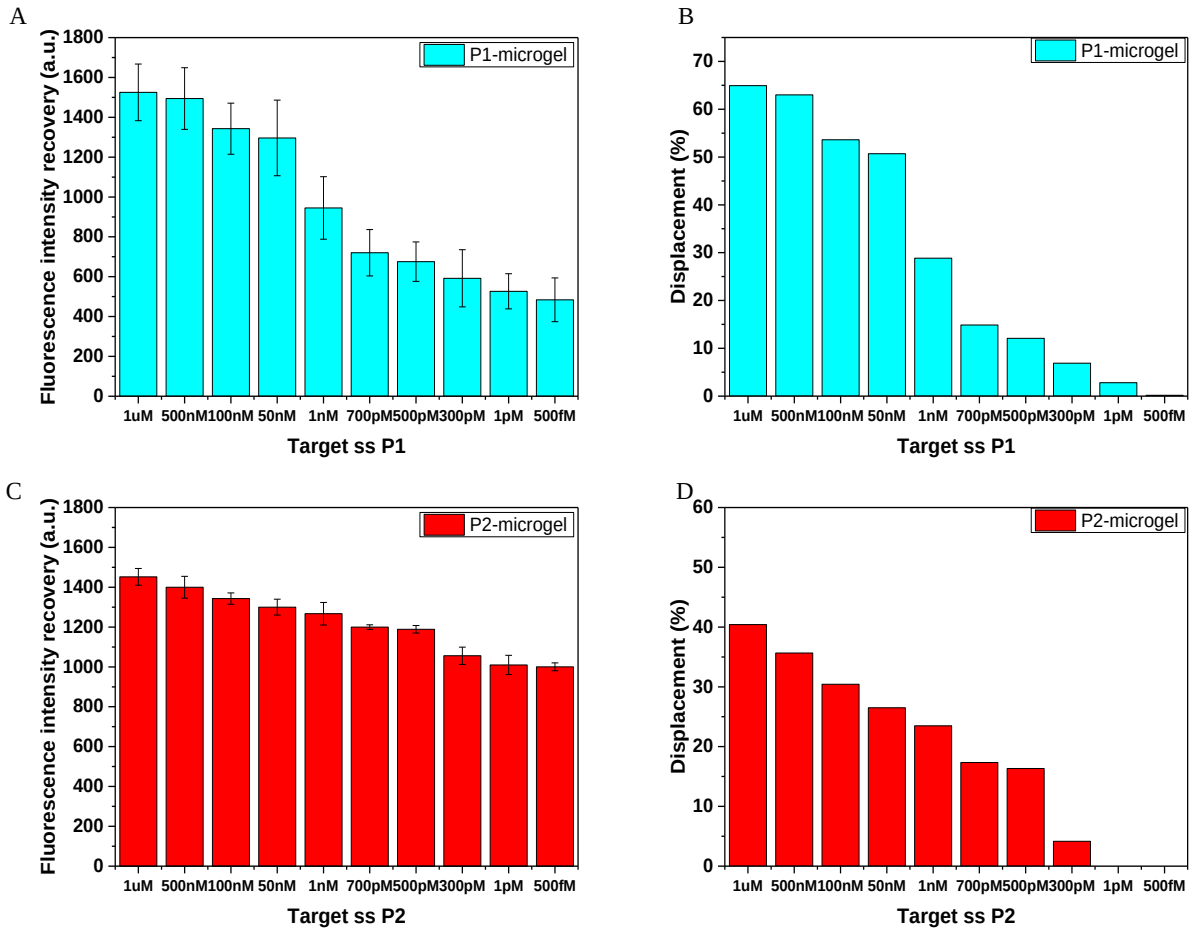

Figure 4 Double strand probe functionalized microgels performance. Fluorescence intensity recovery measure for P1- (A) and P2-microgel -(C) after addition of the target and their correlated percentage of displacement(P1-B/P2-D).

Table 2 Data analysis of ds-microgel assay

ds-microgel (5µg/mL)	**SE**	**SD**	**R-sq**	**Slope**	**LOD (fM)**	**LOQ (fM)**
P1-microgel 0.5nmol	28.1028	47.77	0.866	0.2970	530.83pM	1.6nM
P2-microgel 0.5nmol	49.69	84.47	0.857	0.347	813.43pM	2.46nM

The kinetics of displacement for both dsP1- and dsP2- functionalized microgels have been monitored by spectrofluorometer. The analysis confirms that a more efficient recovery of fluorescence is obtained by P1-microgels compared to P2-microgels in the same experimental condition (Figure 5). In particular, 50 µg/mL of P1-microgels achieve about 30% of recovery in 4 hours in presence of 10nM of target ss P1 while P2-microgels reach about 10% of fluorescence recovery spiking 10nM of Target ss P2.

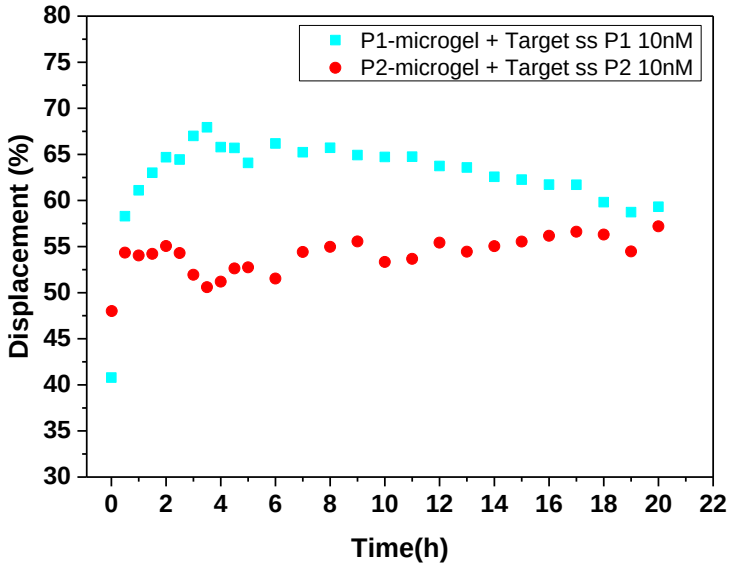

Figure 5 Kinetics of displacement of P1- and P2-microgels.

These results prove that microgel opportunely modified with double strand probes can be applied for the detection of long oligonucleotide sequence. The ds-microgels assay confirms enhanced specificity in target recognition, even in presence of high similar sequences. The assay allows the detection of biomarkers with length over 110nt, at last in 5 hours with working range comprises between 10^{-6} and 10^{-12} M. However, the sensitivity and assay time can be further improved to better meet the requirements of an amplification-free assay.

3.2. Molecular beacon-microgel assay

As discussed in chapter 3, the design of the molecular beacon has a great effect on the sensitivity, the hybridization time and the specificity of detection. In this study, the two molecular beacons MBP1 and MBP2 are firstly designed based on the folding prediction of the target. The portion of the target sequence characterized by lower self-hybridization and with a higher sequence variability (Figure 6 A-B) is chosen

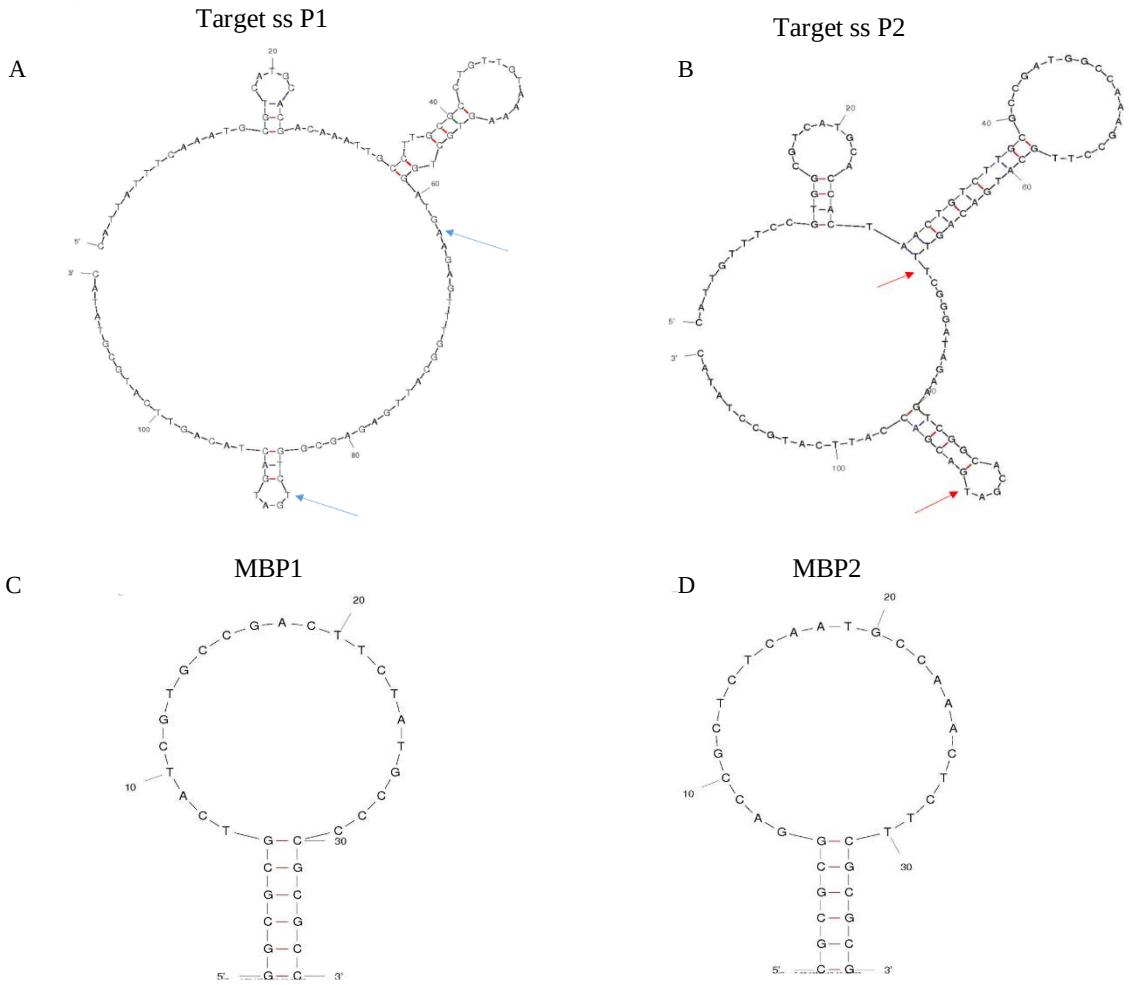

Figure 6 Folding simulation of the target ss P1 (A) and P2(B). The arrows indicate the target site complementary to the loop of the Molecular Beacon P1(C) and Molecular Beacon P2(D)

as the complementary sequence of the molecular beacon loop (Figure 6 C-D). Moreover, molecular beacons are designed with the stem of six nucleotides to guarantee a low fluorescence background and higher specificity, as already proved (chapter 3).

As for the double strand probes, molecular beacons are synthetized and studied in solution before the immobilization on the microgel shell. The melting profile reveals a temperature of melting significantly higher than that predicted by OligoAnalyzer. Melting temperatures of 75°C and 80.5°C have been measured for MBP1 and MBP2 (Figure 7 A-C), instead of 69.2°C and 70.6°C (Table 1). This gap can be explained as the OligoAnalyzer software do not take into account of the possible contribution of the fluorophore/quencher pair.

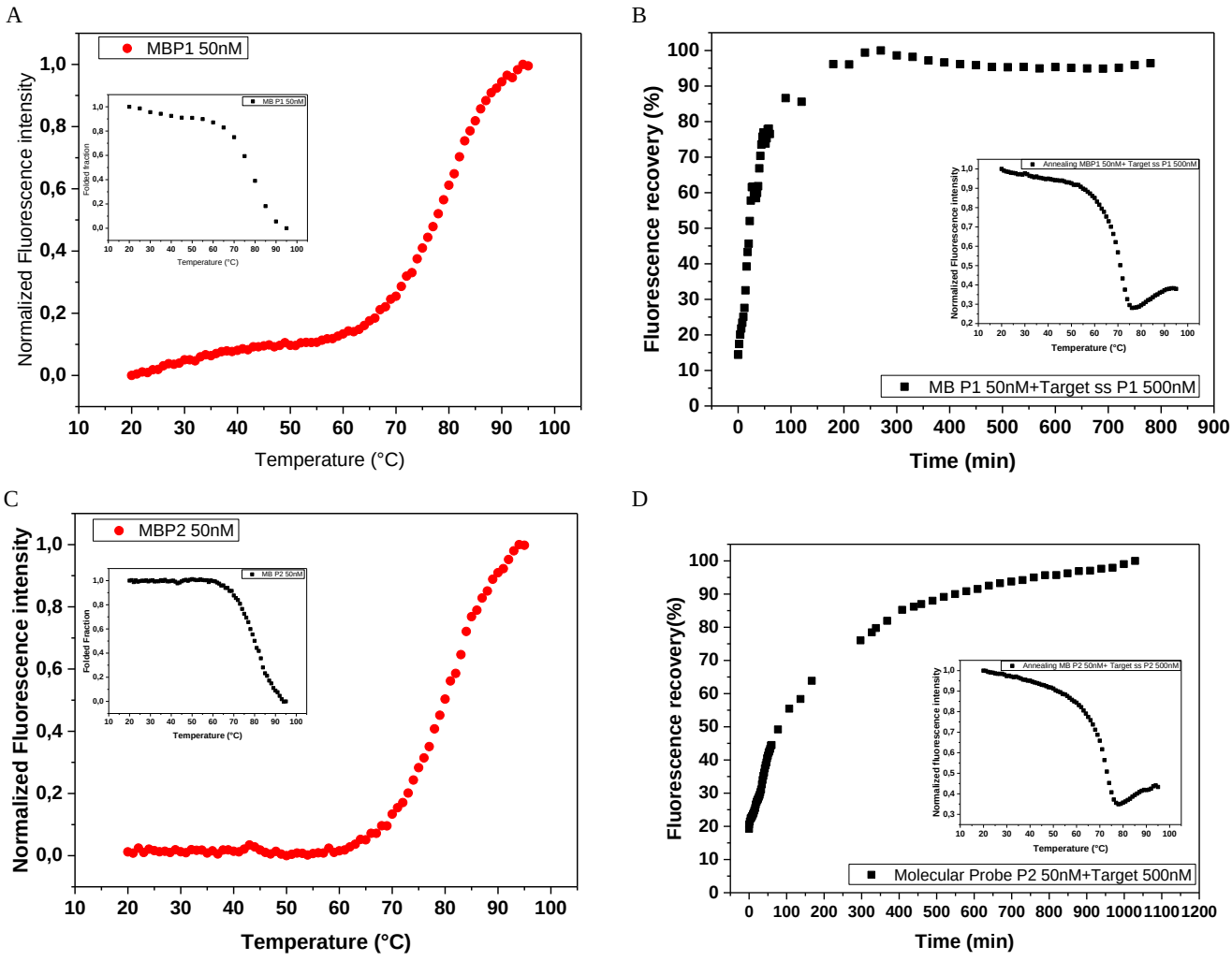

Figure 7 Melting curve and hybridization kinetics of molecular beacon used in this study. Melting profile of MBP1(A) and MBP2 (C) is obtained plotting the normalized fluorescence intensity as function of the temperature. In the inset is plotted the folded fraction vs the temperature. The melting point (Tm) is the inflection point of the curve. Kinetics of hybridization of MBP1 (B) and MBP2(D). in the inset the melting curve of the solution.

The kinetics of hybridizations prove that the hybridization between molecular beacons and long oligonucleotide targets occurs faster compared to ds-probe, in the same experimental condition. In the first 100 minutes of contact MBP1 recognizes the 87% of the target, while MBP2 captures the 56% of Target ss P2 (Figure 7 B-D).

Moreover, additional investigations about the thermodynamic properties of the probe have been carried out. For each MB the constant of dissociation (kd) is calculated by fluorescence titration and the curves are fitted by dose/response equation (Figure 8). From the analysis results that MBP1 and MBP2 have respectively kd of 42nM and 49nM (in line with those observed in other studies[31–33]).

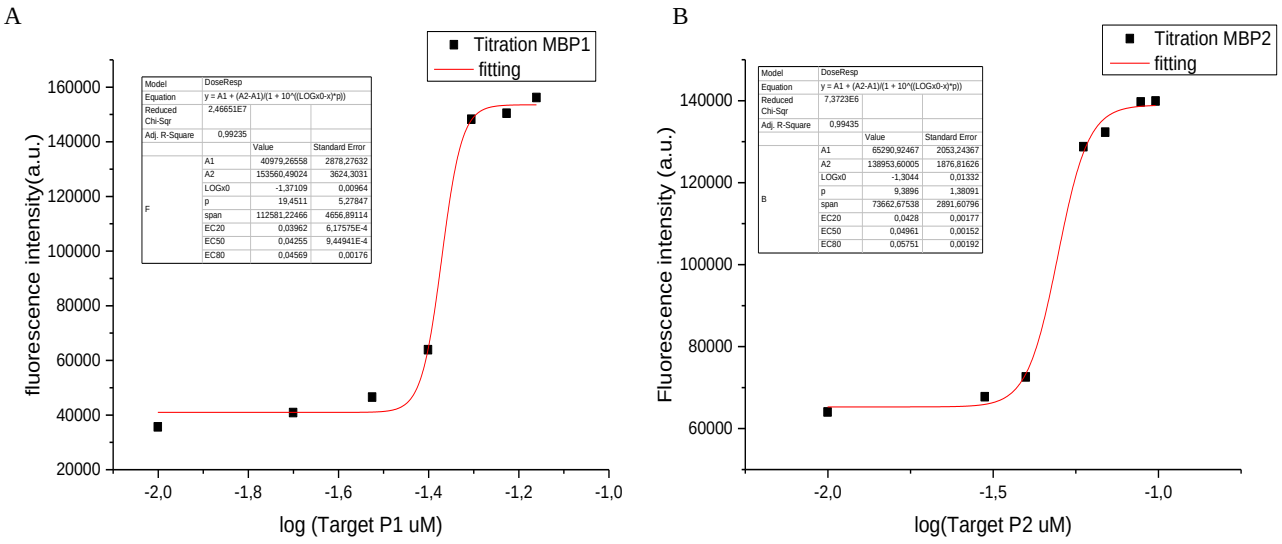

Figure 8 Titration curve of MBP1(A) and MBP2 (B). from the fitting of the curve is calculated the specific kd of each molecular beacon.

As done for ds-probe, cross-reactivity experiments have been carried out to prove the MB specificity towards the homologous target. Curves collected confirmed that both MBP1 and MBP2 in presence of high concentration of homologous sequence are very stable and fluorescence recovery is not recorded for 24 hours. A quick fluorescence intensity increment is recorded after the spiking the specific target into the solution (Figure 9A-B).

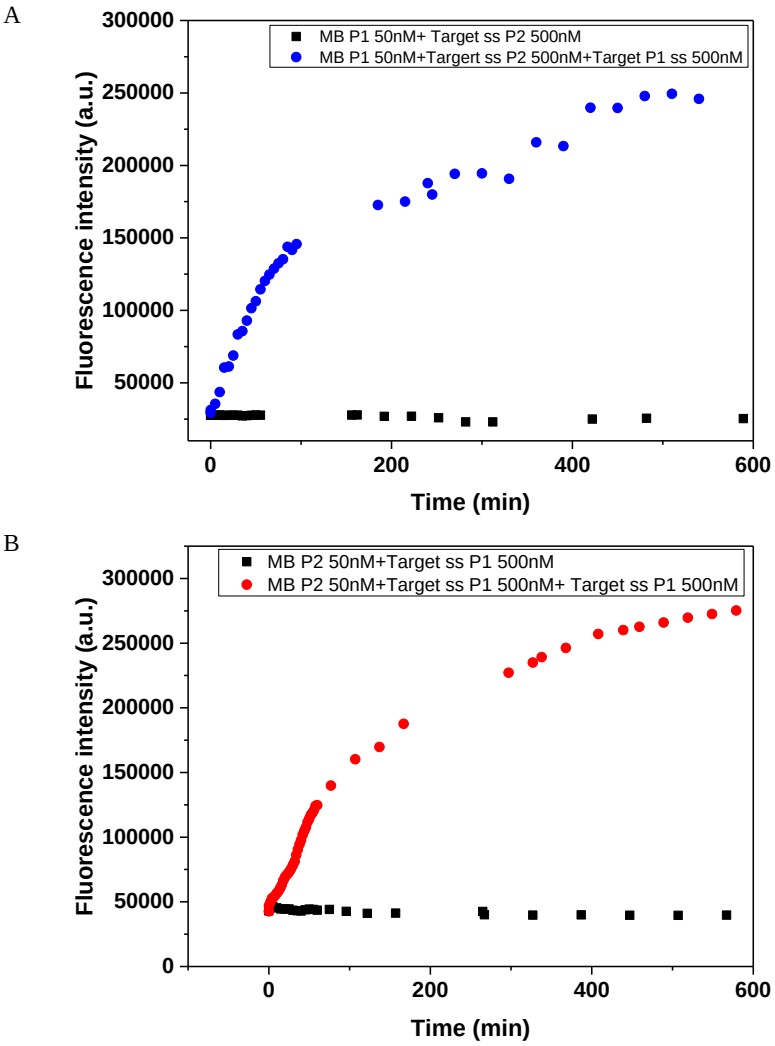

Figure 9 Cross-reactivity experiments: MBP1 (A) and MBP2 (B) probes were monitored in presence of the correspondent homologous Target ss P2 and P1(black square). After that, the specific target P1(blue dots) and P2 (red dots) is added and fluorescence emission collected for the following 24hours.

Subsequently, molecular beacons have been bioconjugated on microgels by carbodiimide chemistry. As widely discussed in chapter 1-3, when molecular beacons are immobilized on solid surfaces the probe density have a pivotal role on the sensitivity. For this reason, the analytical performances of microgels functionalized with 0.1nmol (L), 0.25nmol (M) or 0.5nmol (H) of MB probes have been tested. For each functionalization is measured the working range and the limit of detection and quantification. From the analysis of the data, MBP1 results more sensitive compared to MBP2, with working range comprises between 10^{-6}-10^{-15} M for MBP1-(L) and MBP1-(M) and 10^{-6}-10^{-12} M for MBP1-(H) (Figure 10 A-C-E). Regarding the assay sensitivity MBP1-(M) achieves LOD of 37.82 fM and LOQ of 114.6 fM while MBP-(L) reaches LOD of 76.14 fM and LOQ of 230.75 fM. Increasing the concentration of immobilized

probes the sensitivity decreases, indeed, MBP1-(H) has LOD of 1.32 and LOQ of 4.01 pM (Table). MBP2-microgel show generally less sensitive performance (Figure 10 B-D-F) with LOD of 274 pM, 5.09 pM and 1.06 pM and LOQ of 835 pM, 15,44 pM and 3,206 pM respectively for MBP2-(L) and MBP2-(M) and MBP2-(H) (Table).

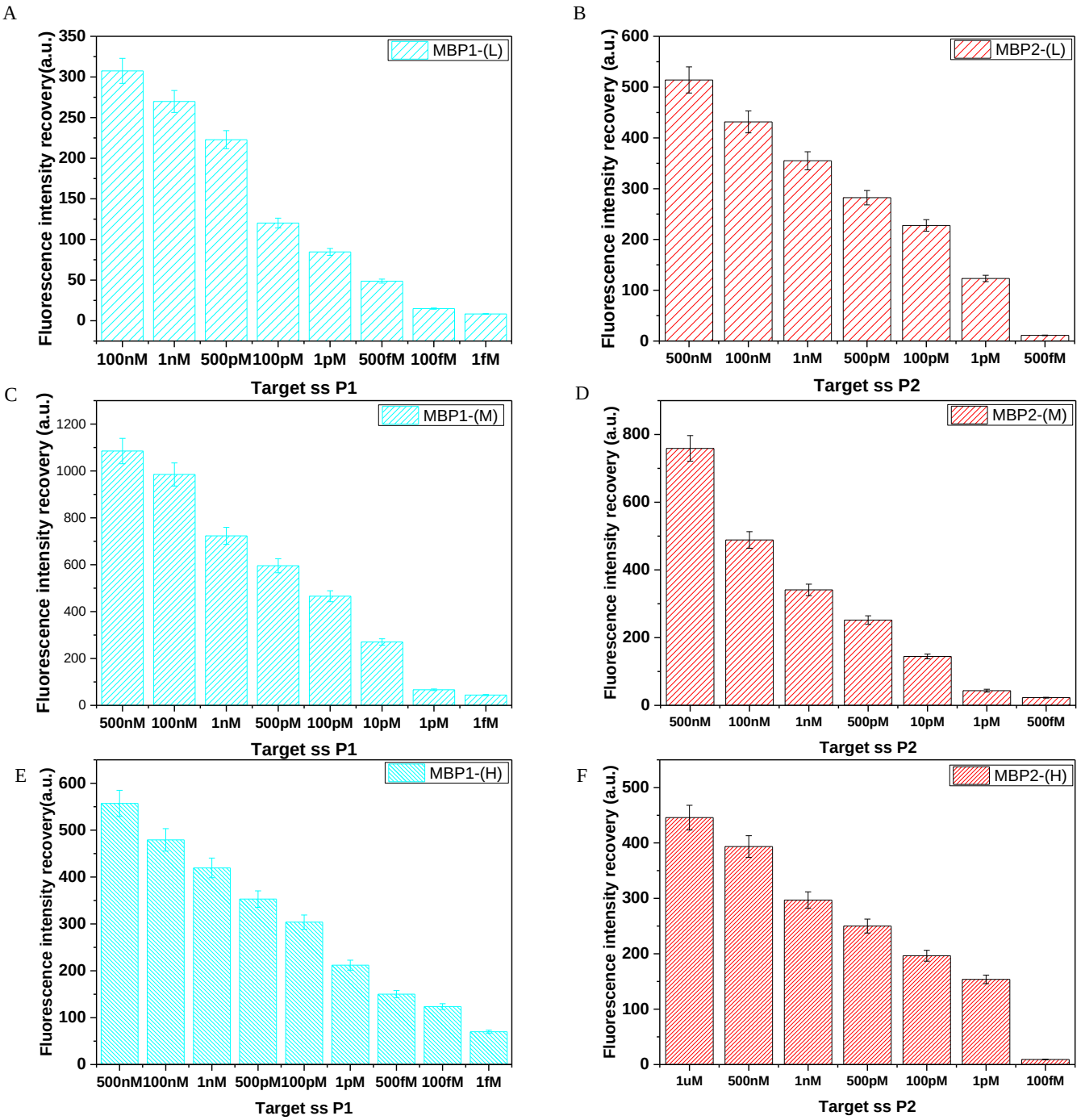

Figure 10 Molecular beacon bioconjugated microgels performances in long oligonucleotide target detection. MBP1- (A) and MBP2- (B) microgel with 0.1nmol functionalization (L); MBP1-(C) and MBP2- (D) microgel with 0.25nmol functionalization (M); MBP1- (E) and MBP2- (F) microgel with 0.5nmol of functionalization (H).

The mb-microgels show faster hybridization rate compared to ds-microgels (Figure 11). In particular, the medium (M) functionalization combines enhanced sensitivity and improved hybridization kinetics. MBP1-microgels with low and medium functionalization hybridize with the target (80% of effective recovery) at most in 100 minutes (Figure 11 A), while MBP 2 achieves 50% of target hybridization in the same experimental condition (Figure 11 B).

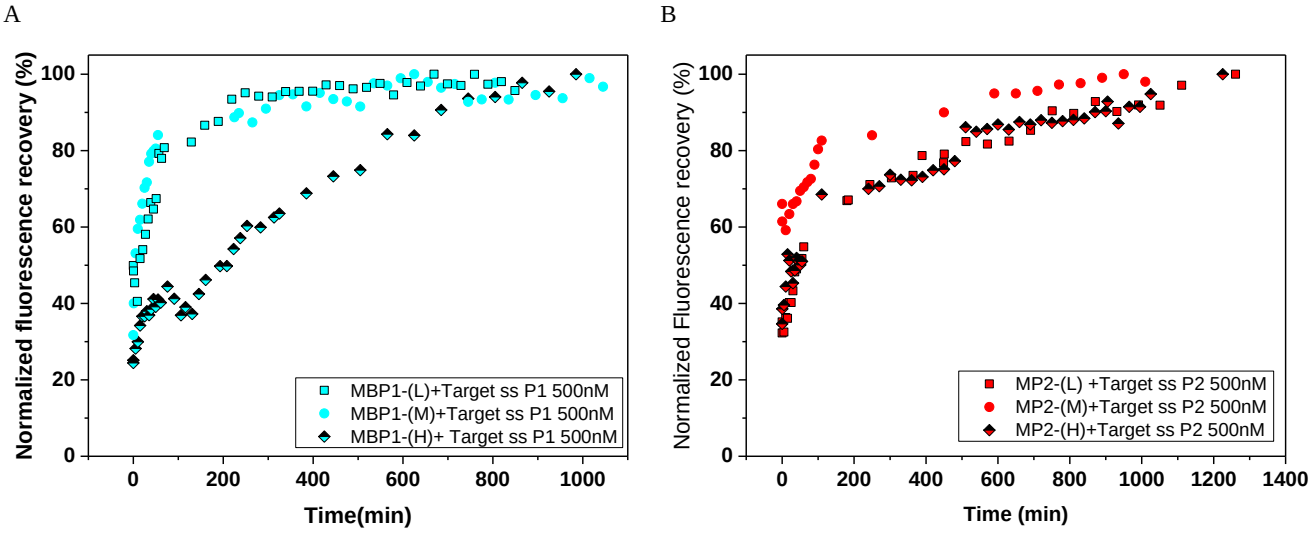

Figure 11 Kinetics of hybridization of MBP1 (A) and MBP2(B). Fluorescence recovery of low(L), medium(M) and high(H) functionalized microgels is recorder in the time, mixing 50ug/mL of microgels with 500nM of Target (111nt).

Considering all the data obtained it has been hypothesized that the less efficiency of MB2 probe could be ascribable to the folding of the target site. Hence, to prove our hypothesis and verify if mb-microgels are affected by the target structure or are independently capable to detect long oligonucleotide sequence

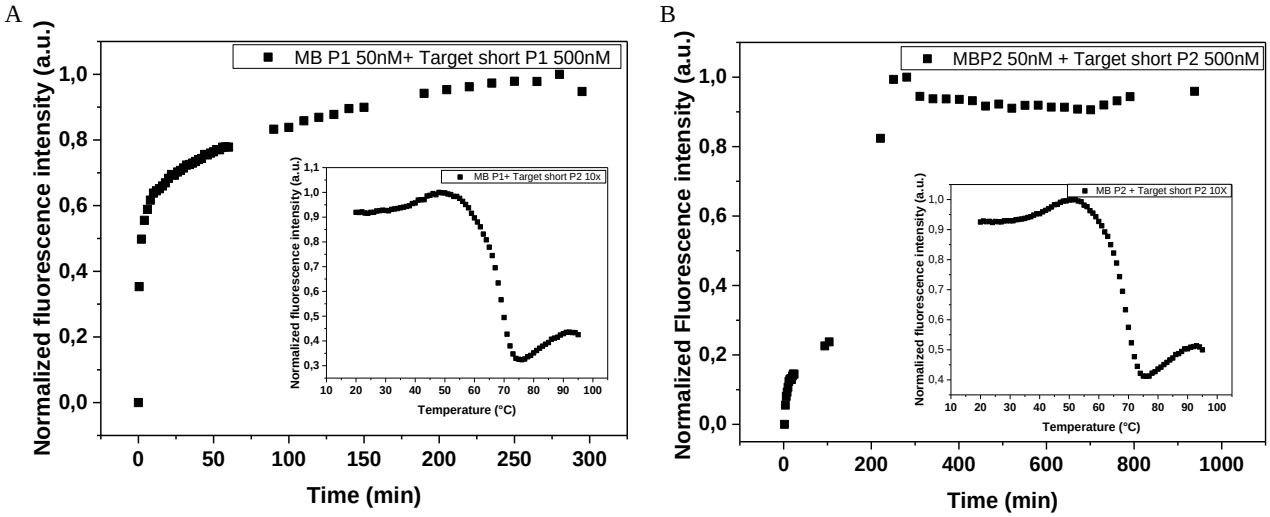

Figure 12 Hybridization kinetics and melting curve and of MBP1 and MBP2 in presence of the short Target P1 and P2

with the same sensitivity and specificity exhibited for miRNA targets, both MBP1 and MBP2 have been tested using short P1/P2 target (24 and 23n Table 1). The kinetics of hybridization of MBP1 and MBP2 with the short target results similar to those obtained for the long target in solution. In 200 minutes complete recovery is achieved by MBP1 (Figure 12A) and MBP2 (Figure 12B). As expected, their melting curves (Figure 12A-B inset) are also comparable.

Moreover, mb-microgels have been tested toward short target P1 and P2. As shown in Figure 13- and Figure 14-A, all the MBP1 and MBP2 functionalized microgels are very stable when mixed with the similar P2 and P1 short target. Their fluorescence background is equivalent to the mb-microgel control measured in absence of target. The specific target, instead, causes an increment of fluorescence distinguishable from the background. MBP1-microgels show working range (Figure 13 B-C-D), LOD and LOQ very similar to long oligonucleotide target P1, for all the functionalization tested (L-M-H)

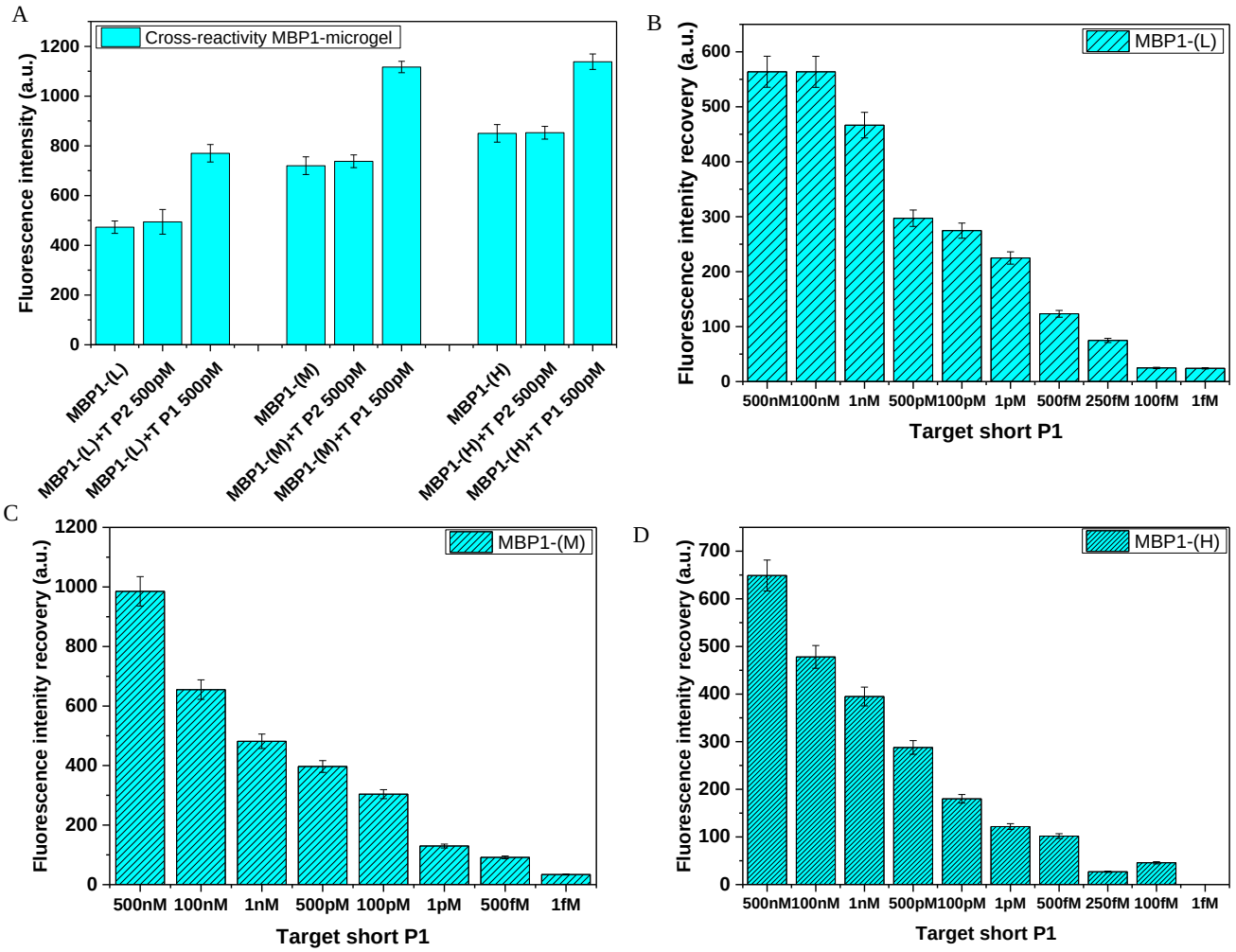

Figure 13 MBP1-microgels cross-reactivity experiment results (A). Molecular beacon bio-conjugated microgels performances in short oligonucleotide target detection measured for MBP1- (L) 0.1nmol of immobilized probes (B); MBP1- (M) 0.25nmol -(C); and MBP1- (D) 0.5nmol (H).

(Table 3). However, analysing the data collected for MBP2-microgels assay, the assay sensitivity results improved when the short P2 target is used (Figure 14B-C; Table 4). These results confirm that the sensitivity is correlated to the folding and in particular, to the self-hybridization of the target site. Analysing the portion of the target sequence that hybridizes with molecular beacon, we have calculated that only the 8.5% of this portion is self-hybridized in P1, while in P2 the 25% of the sequence is folded and not available for the hybridization. This explains the increased sensitivity observed in the case of the short P2 target. This short sequence, indeed, is not hindered or affected by stable secondary structures (Figure 14D) and it is completely free to hybridize with the MBP2 conjugated on the microgel surface. Hybridization kinetics are consistent with those observed for long oligonucleotide target P1 and P2 (Figure 15A-B)

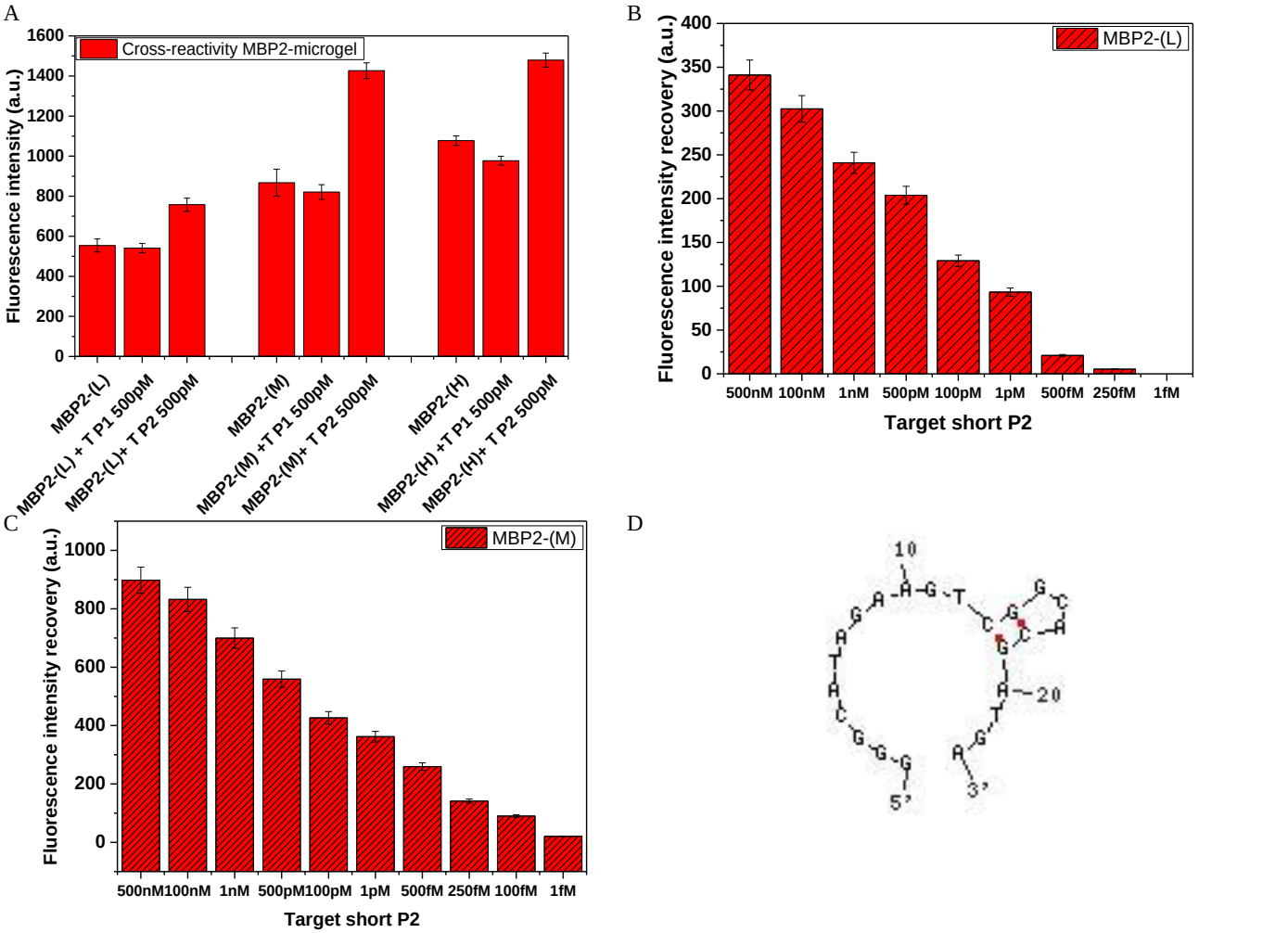

Figure 14 MBP2-microgels cross-reactivity experiment results (A).Molecular beacon bio-conjugated microgels performances in short oligonucleotide target detection measured for MBP1- (L) 0.1nmol of immobilized probes (B) and MBP1- (M) 0.25nmol -(C). D) Folding prediction of the short target P2

A

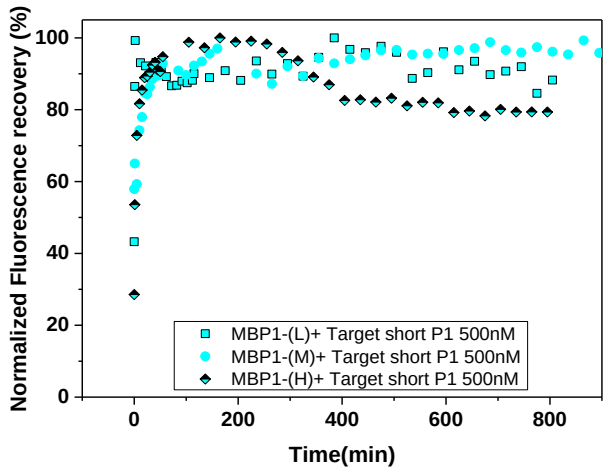

B

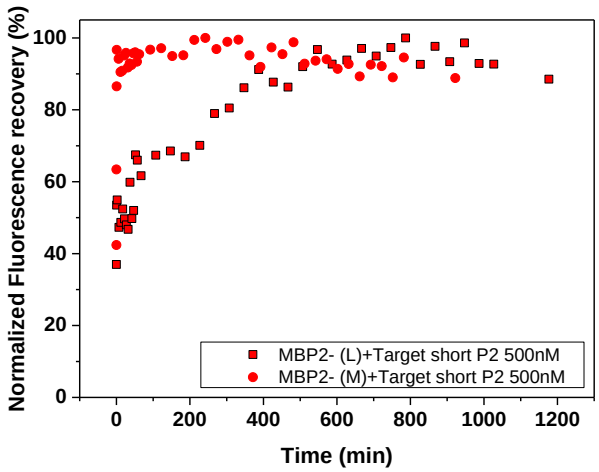

Figure 15 Kinetics of hybridizations of MBP1 (A) and MBP2(B). Fluorescence recovery of mb-microgels was recorder in the time, mixing 50ug/mL of microgels with 500nM of short Target (P1-24nt; P2 23nt).

Table 3 Data analysis of Molecular Beacon P1-microgel assay. MBP1-microgels (with 0.1nmol (L), 0.25nmol (M) and 0.5nmol (H) bioconjugation density) are tested in presence of long single strand oligonucleotide Target or the correspondent short target

	SE	SD	SLOPE	R2	LOD	LOQ
Target ss P1 (111nt)						
MBP1-L	1.1130	1.8921	0.082	0.998	76.14fM	230.75fM
MBP1-M	0.14833	0.2521	0.00226	0.9999	37.82fM	114.61fM
MBP1-H	29.44119	50.0500	0.1247	0.9158	1.32pM	4.01pM
Target short P1						
MBP1-L	0.69481	1.1811	0.1973	0.9999	19.75fM	59.86fM
MBP1-M	7.9914	13.5854	0.0958	0.9862	45.45fM	137.75fM
MBP1-H	18.11	30.80	0.0826	0.9	1.23pM	3.72pM

Table 4 Data analysis of Molecular Beacon P2-microgel assay. MBP2 microgels (with 0.1nmol (L), 0.25nmol (M) and 0.5nmol (H) bioconjugation density) are tested in presence of long single strand oligonucleotide Target or the correspondent short target.

	SE	SD	SLOPE	R2	LOD	LOQ
Target ss P2 (111nt)						
MBP2-L	78.651	133.71	0.0016	0.7357	274pM	835.6pM
MBP2-M	10.9908	18.6843	0.0121	0.9857	5.09pM	15.44pM
MBP2-H	61.965	105.34	0.3285	0.9335	1.06pM	3.206pM
Target short P2						
MBP2-L	10.9678	18.6454	0.1213	0.9727	507.25fM	1.537pM
MB21-M	17.44	29.65	0.4727	0.9585	207.005fM	627.28fM

This study has evidenced that molecular beacon bio-conjugated microgels are also efficient for the detection of long oligonucleotides sequences. The design of the probe must be opportunely tailored on the structural properties of the target and the probe density must be optimized on the microgel surface. Due to the enhanced properties of molecular beacons, high specificity is achieved as proved by cross-reactivity experiments. Moreover, the combination of these probes with the solution-like property of the hydrogel material and its capability of concentrating the fluorescence signal in a small volume allows to reach pM sensitivity in short time of analysis. Following these guidelines, specific and sensitive analytical assays based on microgels can be developed for a variety of target of interest.

4. CONCLUSION

In this chapter the guidelines to detect long oligonucleotide sequences by microgel-based assay have been investigated. The assay is developed using two oligonucleotides (111nt) with 70% of sequence similarity as targets. Microgels are functionalized with double strand or molecular beacon probes, specifically designed, and their performance in term of sensitivity and specificity are investigated.

This study has allowed to establish the instruction for the design of specific probes and we have demonstrated that the folding and alignment are fundamental parameters to take into consideration, during the design. In particular, we have proved that the target zone, comprises into the long oligonucleotide sequence, must not exceed the 8.5% of self-hybridization to obtain an assay with good sensitivity.

In conclusion, both double strand and molecular beacon-microgel probes ensure high specificity, however, molecular beacon-microgels achieve better sensitivity with LOD in fM order as observed for short oligonucleotide sequences in the *chapters 3*, in reduced time of analysis. By combining what we have learned on the design of probes with the enhanced properties of microgels, a simple assay for the detection of long-circulating oligonucleotide biomarkers such as mRNA and lncRNA may be further developed.

REFERENCES

1. Tong, Y.-K. & Lo, Y. M. D. Diagnostic developments involving cell-free (circulating) nucleic acids B. (2005). doi:10.1016/j.cccn.2005.05.048

2. Vlassov, V., Laktionov, P. & Rykova, E. Circulating Nucleic Acids as a Potential Source for Cancer Biomarkers. *Curr. Mol. Med.* **10,** 142–165 (2010).

3. Perakis, S. & Speicher, M. R. Emerging concepts in liquid biopsies. *BMC Med.* **15,** (2017).

4. Umu, S. U. *et al.* A comprehensive profile of circulating RNAs in human serum. *RNA Biol.* **15,** 242–250 (2018).

5. Dasí, F. *et al.* Real-Time Quantification in Plasma of Human Telomerase Reverse Transcriptase (hTERT) mRNA: A Simple Blood Test to Monitor Disease in Cancer Patients. *Lab. Investig.* **81,** 767–769 (2001).

6. Hsu, F.-M. *et al.* Circulating mRNA Profiling in Esophageal Squamous Cell Carcinoma Identifies FAM84B As A Biomarker In Predicting Pathological Response to Neoadjuvant Chemoradiation. *Sci. Rep.* **5,** 10291 (2015).

7. Zhou, J. *et al.* Maternal plasma levels of cell-free β-HCG mRNA as a prenatal diagnostic indicator of placenta accrete. *Placenta* **35,** 691–5 (2014).

8. Zhang, K., Wang, K., Zhu, X., Xu, F. & Xie, M. Sensitive detection of microRNA in complex biological samples by using two stages DSN-assisted target recycling signal amplification method. *Biosens. Bioelectron.* **87,** 358–364 (2017).

9. Dai, Q., Freire, J. & Zhang, T. Circulating long non-coding RNAs as biomarkers of acute myocardial infarction. *Non-coding RNA Investig.* 4–4 (2017). doi:10.21037/ncri.2017.08.03

10. Duan, W. *et al.* Identification of a serum circulating lncRNA panel for the diagnosis and recurrence prediction of bladder cancer. *Oncotarget* **7,** 78850–78858 (2016).

11. Yuan, W. *et al.* Circulating LncRNAs Serve as Diagnostic Markers for Hepatocellular Carcinoma. *Cell. Physiol. Biochem.* **44,** 125–132 (2017).

12. ANKER, P. & STROUN, M. Immunological Aspects of Circulating DNA. *Ann. N. Y. Acad. Sci.* **1075,** 34–39 (2006).

13. Shafiee, G., Heshmat, R. & Larijani, B. Circulating cell-free nucleic acids as potential biomarkers for sarcopenia: a step toward personalized medicine. *J. Diabetes Metab. Disord.* **16,** 19 (2017).

14. Quezada, M. S., Gil, M. M., Francisco, C., Oròsz, G. & Nicolaides, K. H. Screening for trisomies 21, 18 and 13 by cell-free DNA analysis of maternal blood at 10-11 weeks' gestation and the combined test at 11-13 weeks. *Ultrasound Obstet. Gynecol.* **45,** 36–41 (2015).

15. Bustamante, A. *et al.* Circulating cell-free DNA is a predictor of short-term neurological outcome in stroke patients treated with intravenous thrombolysis. *J. Circ. biomarkers* **5,** 1849454416668791 (2016).

16. Chang, C. P.-Y. *et al.* Elevated cell-free serum DNA detected in patients with myocardial infarction. *Clin. Chim. Acta* **327,** 95–101 (2003).

17. Gögenur, M., Burcharth, J. & Gögenur, I. The role of total cell-free DNA in predicting outcomes among trauma patients in the intensive care unit: a systematic review. *Crit. Care* **21,** 14 (2017).

18. Weerakoon, K. G. & McManus, D. P. Cell-Free DNA as a Diagnostic Tool for Human Parasitic Infections. *Trends Parasitol.* **32,** 378–391 (2016).

19. Gorgannezhad, L., Umer, M., Islam, M. N., Nguyen, N.-T. & Shiddiky, M. J. A. Circulating tumor DNA and liquid biopsy: opportunities, challenges, and recent advances in detection technologies. *Lab Chip* **18,** 1174–1196 (2018).

20. Cheng, F., Su, L. & Qian, C. *Circulating tumor DNA: a promising biomarker in the liquid biopsy of cancer*. **7,**

21. Diaz, L. A. & Bardelli, A. Liquid Biopsies: Genotyping Circulating Tumor DNA. *J Clin Oncol* **32,** 579–586 (2014).

22. Higuchi, R., Dollinger, G., Walsh, P. S. & Griffith, R. Simultaneous Amplification and Detection of Specific DNA Sequences. *Bio/Technology* **10,** 413–417 (1992).

23. Navarro, E., Serrano-Heras, G., Castaño, M. J. & Solera, J. Real-time PCR detection chemistry. *Clin. Chim. Acta* **439,** 231–250 (2015).

24. Gao, F. *et al.* Microdroplet Digital PCR: Detection and Quantitation of Biomarkers in Archived Tissue and Serial Plasma Samples in Patients with Lung Cancer. *J. Thorac. Oncol.* **10,** 212–217 (2015).

25. Vogelstein, B. & Kinzler, K. W. Digital PCR. *Proc. Natl. Acad. Sci. U. S. A.* **96,** 9236–41 (1999).

26. Diaz, L. A., Bardelli, A. & Bardelli, A. Liquid biopsies: genotyping circulating tumor DNA. *J. Clin. Oncol.* **32,** 579–86 (2014).

27. Ranasinghe, R. T. & Brown, T. Ultrasensitive fluorescence-based methods for nucleic acid detection: towards amplification-free genetic analysis. *Chem. Commun.* **47,** 3717 (2011).

28. Das, J. *et al.* An electrochemical clamp assay for direct, rapid analysis of circulating nucleic acids in serum. *Nat. Chem.* **7,** 569–575 (2015).

29. Mandli, J., Mohammadi, H. & Amine, A. Electrochemical DNA sandwich biosensor based on enzyme amplified microRNA-21 detection and gold nanoparticles. *Bioelectrochemistry* **116,** 17–23 (2017).

30. Bertucci, A. *et al.* Detection of unamplified genomic DNA by a PNA-based microstructured optical fiber (MOF) Bragg-grating optofluidic system. *Biosens. Bioelectron.* **63,** 248–254 (2015).

31. Hopkins, J. F. & Woodson, S. A. Molecular beacons as probes of RNA unfolding under native conditions. *Nucleic Acids Res.* **33,** 5763–5770 (2005).

32. Vijayanathan, V., Thomas, T., Sigal, L. H. & Thomas, T. J. Direct measurement of the association constant of HER2/neu antisense oligonucleotide to its target RNA sequence using a molecular beacon. *Antisense Nucleic Acid Drug Dev.* **12,** 225–33 (2002).

33. Tsourkas, A., Behlke, M. A., Rose, S. D. & Bao, G. Hybridization kinetics and thermodynamics of molecular beacons. *Nucleic Acids Res.* **31,** 1319–1330 (2003).

CHAPTER 5

"3D-Hydrogel Microparticles: mix-read bioassay for oligonucleotide detection. Case study of miR-143-3p detection as early biomarker in Amyotrophic lateral sclerosis"

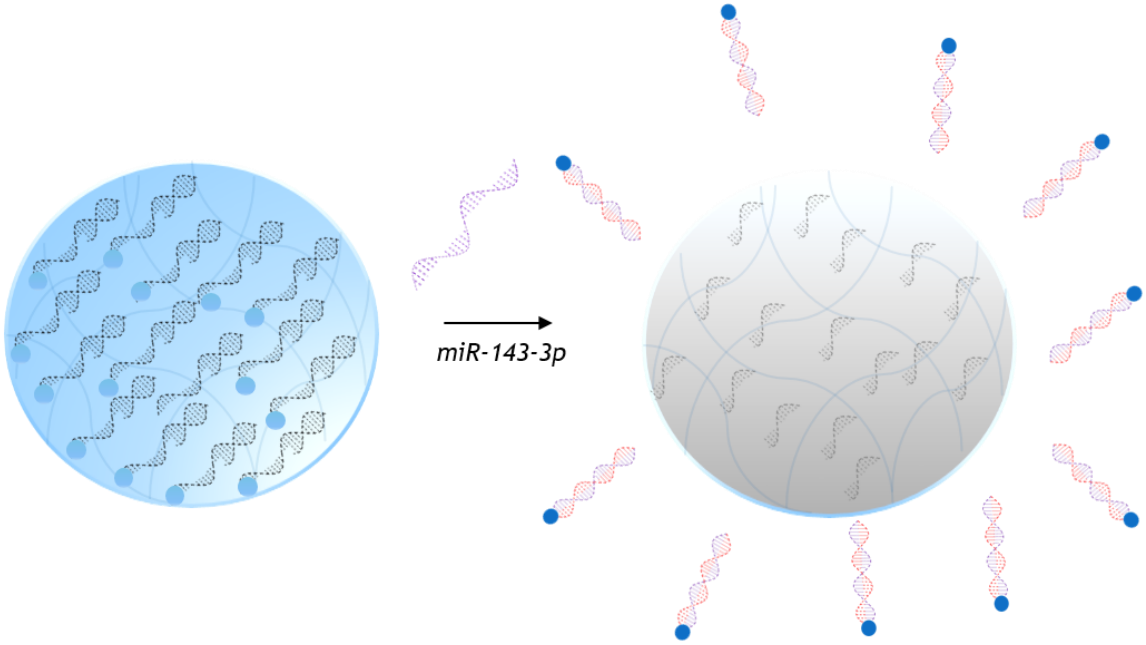

1. INTRODUCTION

In this chapter we have designed 3D one step functionalized hydrogel microparticles by microfluidic for microRNA (miRNA) detection. In biosensing application, three-dimensional (3D) functionalized materials represent the ideal choice since they combine the advantages of biorecognition in solution, as the faster kinetics of reactions and low signal background, with those observed on solid surface[1–4]. To achieve this goal, it is necessary to optimize the design and density of the capture probe, but above all, to fine tune the environment in which probes are immobilized.

Immobilization on solid surfaces[5–17] allow high-throughput analysis and parallel screening of several oligonucleotide sequences[18], however, immobilized probes suffer of same limitations[19,20]. In particular, on solid surfaces, the electrostatic repulsion between probe-probe[21,22], together with the steric hindrance between probe-target duplex[23,24] and the non-specific oligonucleotides adsorption[25] affect the hybridization efficiency. Regarding the hybridization rate, the design of the probe, its length and the GC content play a crucial role[1,26–28]. Furthermore, based on the immobilization methods biosensors suffer of inhomogeneous signal distribution and low conjugation reproducibility[29].

Contrariwise, 3D substrates offer higher capacity of immobilization compared to 2D surface. Considering similar probe concentrations for the conjugation, indeed, the crowding effects decrease in 3D and more target/probe complex are formed, increasing the sensitivity and reducing the background[30,31]. Furthermore, tailoring the probe design and the linkage chemistry, probes are homogeneously distributed into the whole volume and their density is finely tuned[32].

In this context, three-dimensional materials have demonstrated to be particularly suitable for the development of biosensors capable of detect oligonucleotides, small molecules and drugs. Biosensor made by three-dimensional (3D) nitrogen-doped graphene (NG) and Fe_3O_4 nanoparticles have been developed as sensing film and functionalized with oligonucleotide probes by Chen[33]. Compared to solid surfaces, the highly porous 3D NG had a large surface area, improved the sensitive detection of DNA with excellent selectivity, fast responses, and a low detection limit. Nanocube heads/TiO2 nanowire (NW) arms (PB-TiO2) have been developed for efficient three-dimensional interfacial sensing of small molecules and cellular activities[34]. Biocompatible 3D porous silica in which was immobilized the Acetylcholinesterase (AChE) has been used as matrix to develop biosensors for the detection of organophosphorus pesticide (OPs)[35]. Furthermore, hydrogels microparticles have been synthetized by flow lithography and functionalized using methacrylate probes obtaining a 3D functionalized network

by Doyle's group[36]. The particles are used to capture proteins and oligonucleotides[19,37,38] and the quantification is usually associated with optical amplification of the signal, after the hybridization assay.

Moreover, since the environment of the 3D network influences the biosensor sensitivity and specificity, it must be as far as possible similar to an ideal solution. Concerning this, the nature of the materials has a pivotal role, affecting both the diffusion of the molecules and the probe/target hybridization[39]. Polyethylene glycol (PEG) hydrogels are suitable materials due to their chemical flexibility, antifouling properties, biocompatibility[40-41], high water content and tuneable network structure[42]. The tuneable network confers size exclusion ability as the polymer mesh size can be finely tuned to specifically allow the diffusion and reaction of target molecules of different size, improving the assay sensitivity[43,44]. Furthermore, it has been proved that 3D functionalized polymer network offers not only enhanced sensitivity but also better specificity since probes spaced further apart hybridize less with mismatch sequences[26].

Among the various approaches for hydrogels synthesis, microfluidic technique represents the most promising methods for the production and functionalization of microparticles. Droplet microfluidics, in particular, reduces the costs, synthesis time and reagent consumption compared to the conventional techniques, achieving a large production of monodisperse microparticles per hours (10^5 particles)[38,45–47].

As proof, we have designed a specific double strand probe for the miR-143-3p detection and we have integrated it into the hydrogel microparticles produced by microfluidics. MiRNAs[48,49] are short non-coding RNA sequences, widely recognized as biomarkers in several diseases[50–52]. Recently, Waller et al. showed that miRNA-143-3p expression levels are increased in the serum of amyotrophic lateral sclerosis (ALS) patients, consequently[53], the miRNA has been validated as circulating biomarker for ASL early diagnosis. Amyotrophic lateral sclerosis (ALS) is one of the most common neurodegenerative diseases with a prevalence of 6-8 people per 100,000 per year. ALS is characterized by a selective degeneration of motor neutrons with a consequent progressive muscle wasting and leads to death within 2-5 from the symptom onset[54]. Unfortunately, until now, there is an average delay of 12 months from symptom onset to a confirmed diagnosis, typically midway through the patient's disease course. Actually, the main challenge is focused on the research of non-invasive diagnostic methods for the early disease diagnosis[55–57]. The diagnosis delay may exclude patients from enrolling in clinical trials, for this reason, ASL early diagnosis is fundamental to prolong survival and quality of life.

Three dimensional-hydrogels microparticles can be comprised into *mix-read* biosensor assays as they are capable to detect the miRNA directly in human serum, easily mixing them with the sample and reading the fluorescence turn-off. The enhanced properties showed, prior tested with miRNA-143-3p,

results to be useful for several biomarkers recognition, paving the ways for diagnosis and prognosis of many different diseases.

2. EXPERIMENTAL SECTION

2.1. Probe design and density

Oligonucleotide probes were designed for the selective and specific miRNA fluorescence detection according to a double strand (ds) displacement assay. Alignment, folding and thermodynamic studies were made using appropriate tools (BLAST, UNAfold, IDT-Integrated, D. N. A. "Technologies. OligoAnalyzer 3.1. Web." (2014)) in order to design probe with optimized properties and achieve enhanced target recognition capability, stability and appropriate difference in free energy of displacement. All the probes and synthetic target (DNA/RNA) were purchased from Metabion with HPLC purification and were re-suspended in water (Sigma Aldrich Molecular biology grade). The DNA probe was designed based on the miRNA-143-3p sequence (21 nt), and its length was properly improved to achieve higher stability, specificity and ΔG of displacement in presence of the target. The probes were tested in solution, in bulk-hydrogels and then in 3D-hydrogel microparticles.

Solution studies were carried out using a short DNA tail (*Fprobe) modified with a fluorophore with at 5'terminus and a longer DNA strand internally modified with a quencher (*Qprobe). Kinetic of hybridizations were performed mixing 50nM of the pre-hybridized *FQ-probe with 500nM and 50nM of target miR-143-3p in a 500uL of PBS enriched with 200mM NaCl (hybridization buffer). Melting curve of DNA double helix into separate random coils is monitored by fluorescence, heating 50nM of QF until 80°C and then annealing the solution to 10°C with scan rate 1 degree C/min. Constant of binding was calculated by titration of *F 50nM with Q* 2.5 μM in a final volume of 500 μL of PBS enriched with 200 mM NaCl (hybridization buffer). The titration curves were obtained by plotting α versus the Q concentration. The association constant Ka, expressed by the inverse of the molar concentration, was estimated from this plot by fitting the resulting curve to an independent and equivalent binding site model.

All solution fluorescence measurements were collected in a 1 cm path length cuvette with a Horiba JobinYvon model FluoroMax-4 fluorometer equipped with a Peltier temperature controller. The samples were excited at 647 nm with a slit width of 5 nm, and emission spectra were collected from 667 to 750 nm with a slit width of 5 nm

To simulate the diffusion and hybridization within the 3D polymer network studies were previously performed in bulk. Functionalized bulks were synthesized using UV free radical photopolymerization between PEGDA and fluorescent oligonucleotide, properly modified with methacrylamide moieties. Several bulks with different PEGDA and oligonucleotide concentrations were prepared and tested. The mixture composed of PEGDA (MW 700 Da) at different concentrations (10-15-20% w/v) in hybridization buffer, darocur as initiator and fluorescent methacrylate oligonucleotide (*Fb) at different concentrations (1µM-5µM) was strongly mixed and then purged with high purity nitrogen for 5 minutes to remove the excess of oxygen that may interfere with the free radical polymerization. Then, 100 µL of the mixture was carried out in 96-optiplate, illuminated with the UV lamp (λ = 365 nm and power-lamp = 21.7mW/cm^2) for 5 minutes leading to complete polymerization. Then the bulks were washed several times with hybridization buffer and fluorescence intensity was collected. Bulks were put in contact with 100 µL of partially complementary quencher strand (*Qb) both in equimolar or 5-fold excess concentration (1µM-5µM/5µM-25µM) and kinetics of quenching were recorded for 5 days. After the quenching step, bulks were washed several time to remove all the excess of quencher and resuspended in hybridization buffer. In the last step the target was added in final concentration of 10 µM and the kinetics of recovery recorder until 7 days. All fluorescence measurements were carried out by the means of a 2300 EnSpire multilabel reader (Perkin-Elmer, Waltham, MA). Fluorescence was measured from the top of the plate, with excitation wavelength of 647 nm, and emission wavelength at 667 nm, height 9 mm and 500 number of flash.

In 3D-hydrogel microparticles synthesis, probes sequences are the same used in solution with the exception of the fluorophore, which has been removed from the immobilized short DNA tail (T-DNA, 12 nt) sequence and added to the free to diffuse longer DNA sequence (F-DNA, 21 nt), complementary to the specific target. When the F-DNA and T-DNA partially hybridize into the 3D hydrogel network, the microparticles become fluorescent. In presence of the target, the F-DNA and the target hybridize so that low fluorescence background signal is registered. Fluorescence intensity was measured by Confocal laser scanning microscopy (CLSM) with λex 633 nm λem 650-700 nm, using water objective 25X.

Table 1 Sequence, length, modifications and thermodynamic parameters of the DNA probes and RNA targets used in solution and in 3D-hydrogel microparticles assay. All parameters are calculated by IDT-Integrated, D. N. A. "Technologies. OligoAnalyzer 3.1. Web setting respectively 50nM and 350mM as oligonucleotide and Na^+concentration. TF/QF*hyb represent the free energy gained from the partially complementary T-DNA/F-DNA or F*probe/Q*probe duplex; FTarthyb/*QTarhyb is the free energy gained from the fully complementary Target/F-DNA or Target/Q*probe duplex; Δdisplacement is the free energy gained after T-DNA/F-DNA de-hybridization and Target/F-DNA hybridization

Probe	5'-modification	sequence (5'-3')	Int	3'-modificati	nt	Tm	ΔG (Kcal/mol)	ΔH (kcal/mol)	ΔS cal/(K·mol)
F*probe	ATTO647N	GCA CTG TAG CTC		Acrydite	12	47.58	TF/QF^*_{hyb} = -13.39	-92.00	-253.45
T-DNA		GCA CTG TAG CTC		Acrydite	12				
Q*probe		GAG CTA CAG ***T***GT TTC ATC TCA	BHQ2		21	62.81	$FTar/^*QTar_{hyb}$ = -22.62	-160.80	-445.23
F-DNA		GAG CTA CAG TGC TTC ATC TCA-		ATTO647N	21				
Target		UGAGAUGAAG CACUGUAGCU C			21		ΔG_{disp}= -9.23		
Not-matching seq		UAGCUUAUCA GACUGAUGUU GA			22				

Table 2 Sequence, length, modifications and thermodynamic parameters of the DNA probes and RNA targets used in bulk assay. All parameters are calculated by IDT-Integrated, D. N. A. "Technologies. OligoAnalyzer 3.1. Web, setting respectively 50nM and 350mM as oligonucleotide and Na^+ concentration.

Probe	5'-modification	sequence (5'-3')	Int	3'-modificati	nt	Tm	ΔG (Kcal/mol)	ΔH (kcal/mol)	ΔS cal/(K·mol)
*Fb	ATTO647N	TGA AAT CGG TTA		Acrydite	12	39.9	$^*QFb_{hyb}$ = -11.01	-85.40	-239.84
*Qb		T AAC CGA TTT C***T**G ATG GTG CTA	BHQ2		21	64.73	$^*QTb_{hyb=}$ -24.05	-166.80	-460.27
*Tb		GAG CUA CAG UGC UUC AUC UCA					ΔG_{disp}= -13.04		

2.2. Microfluidic synthesis of 3D-hydrogel microparticles and characterization

The synthesis of microparticles was performed using a glass microfluidic device bought from Dolomite. The chip is made of two inputs for the continuous and disperse phase, a fine orifice where the two opposite channels converge, and an output. The sizes of the device are 22.5 mm × 15.0 mm × 4 mm (length × width × thickness) with wide channels cross-section of 100μm × 300 μm (depth × width) and channels cross-section at junction of 100 μm × 105 μm (depth × width). Microparticles were synthesized using light mineral oil (LMO, Sigma-Aldrich) mixed with non-ionic surfactant Span 80 (5 % v/v, Sigma-Aldrich) as a continuous phase and a water solution of poly(ethylene glycol) diacrylate (PEGDA, MW 700 Da, Sigma-Aldrich) (10-15-20 % w/v) with photoinitiator darocur (0.1% v/v with respect to the total

volume, Ciba) as dispersed phase. Methacrylate oligonucleotide probes were mixed in the dispersed phase to reach final concentration of 1μM. The reaction occurs by a UV free radical photopolymerization between PEGDA and oligonucleotide, properly modified with methacrylamide moieties. Droplet emulsions were achieved adding in the first channel water solution and continuous phase in the other. Solutions were injected using high-precision syringe pumps (neMesys-low pressure) to ensure stable flow and reproducibility. This system was mounted on an inverted microscope (IX 71 Olympus). The droplets formation was supervised using an objective with 5x magnification and 0.12 numerical aperture and recorded with a CCD camera ImperxIGV-B0620M that allow to record up to 259 frame per second. Once emulsion was formed, it was cross-linked outside the chip using an UV lamp at 365 nm wavelength at 6.38W/cm^2 power lamp for about 2 minutes obtaining a complete polymerization. Then, microparticles were collected in an eppendorf and washed several times with different solvents (diethyl ether, ethanol and milliQ water-tween solution (0.05 % v/v)) in order to remove all the residual oil and surfactant. After washing, microgels were stored at 4°C in buffer solutions until further use. Our buffer was obtained mixing 1x PBS (MP biomedicals), NaCl (Sigma-Aldrich) 200 mM and tween-20 (Sigma-Aldrich) at 0.05% v/v in milliQ water.

Hydrogels microparticles were characterized by scanning electron microscopy a FE-SEM Ultra Plus (Zeiss) microscope at 20 kV. For sample preparation, the microparticles solution was fixed on a microscope slide, air-dried and then sputtered with a 10 nm thin gold layer. Studies on the swelling of microparticles were carried out loading 20 μL of microparticles diluted solutions (about 100 microparticles) into μ-slide 18 well-flat (IBIDI, Martinsried, DE). Images in both swollen and dry conditions were collected with confocal laser scanning microscopy (CLSM Leica SP5- with an Objective HC PL FLUOROTAR 20x0.5 DRY and a scan speed of 8000 Hz). Then, images were analysed by ImageJ software to obtain diameter and calculate volume of microparticles in both conditions in order to apply equilibrium swelling theory[58]. Diffusion studies were carried out following by confocal laser scanning microscopy (CLSM). In particular, 10 μL of PEGDA 15% microparticles functionalized with 1 μM of methacrylate oligonucleotide (about 100 microparticles), were loaded onto μ-slide 18 well-flat. The microparticles were mixed with 10 μL of 2 μM of target miRNA-143-3p and 2 μM Albumin-fluorescein isothiocyanate conjugate (BSA Sigma-Aldrich) solution. Samples were illuminated at CLSM Leica SP5 using appropriate wavelength (Helium-neon λex 633, Helium-neon λex543, Argon λex 488 nm) and fluorescence images of microparticles were collected in the time.

2.3. Assay set up in buffer and Human serum

The 3D-hydrogel assay comprises two steps: (I) Tail hybridization and (II) Target hybridization step (fig1). All experimental steps were performed at room temperature in both hybridization buffer (1x PBS, NaCl 200 mM and tween-20 at 0.05% v/v) and human serum (Lonza). Regarding the first step (I) 100 µL of microparticles-Tail solution (~$25 \cdot 10^3$ particles and ~6 pmol of Tail), were put in contact with F-DNA 10x (~60 pmol) in 1.5mL DNA-low Bind tube (epperdorf). The solution was stirred until use for three days and then washed several times with hybridization buffer. Then 1 µL of this solution was diluted in 30 µL of buffer, added in µ-Slide VI 0.4 (IBIDI, Martinsried, DE) and therefore the fluorescence intensity was measured by CLSM. In the second step (II), 2µL of 3D-functionalized hydrogel microparticles (~330 particles and ~60 fmol of Tail), were mixed with different Target concentrations (from 10^{-4} M to 10^{-12}M in buffer solution) and incubated at room temperature to define the limit of detection (LOD) and quantification (LOQ).

Assays performances were also tested in human serum. The target 2 µM was spiked in 200 µL of serum and mixed with 300µL of hybridization buffer contain the 3D-hydrogel microparticles. Then 1 µL of this solution was diluted in 30 µL of hybridization buffer and fluorescence images collected by CLSM.

2.4. Specificity assay

3D-hydrogel microparticles were tested mixing 2µL of microparticles-Tail-F solution (~330 particles and ~60 fmol of Tail) with 500 nM of non-matching sequence miR-21 and 500nM of miR-21/miR-143-3p 1:1 and incubating at room temperature overnight.

2.5. Statistical analysis

All experiments were performed at least three times, reported as mean ± standard deviation and analysed statistically by paired Student's test. Significant difference was determined at P values smaller than 0.05. To estimate the Limit of detection and the Limit of quantification the values, subtracted of the background and reported as mean ± standard deviation. are fitted applying a linear regression The LOD values is calculated as three standard error (SE) above the slope, while the LOQ corresponds to ten standard deviation (SD) above the slope.

3. RESULTS AND DISCUSSION

3.1. Probe design and density optimization

To develop a sensitive fluorescence assay based on 3D functionalized hydrogels, three important parameters have been considered: the *design* of the probe, the *density* of immobilized molecules and the *diffusion* through the polymer network, as extensively described in chapter 1.

Firstly, the probe is accurately designed in order to specifically hybridize with the target and is tested in solution. Subsequently, three different concentrations of PEG-hydrogel bulk (10-15-20%) are synthetized and tested in order to optimize the probe density and tune the diffusion within the hydrogel network. Once these important parameters have been set, 3D functionalized hydrogel microparticles have been synthetized in one step by microfluidics. Firstly, probes are appropriately designed in term of alignment, folding and thermodynamics, then kinetics of hybridization and constant of binding (kb) are measured in solution. The mechanism of detection is based on double strand displacement assay. From the alignment studies is predicted that the probe has Evalue of $3E^{-3}$ for the hsa-miR143-3p and does not align with sufficient specificity with other human oligonucleotide sequences. The *ING5* mRNA (NM_032329.5) is the nearest in term of alignment obtaining Evalue of 48. From the folding simulation results that the probe is free from self-secondary structures that could decrease the hybridization ratio (Figure 1)

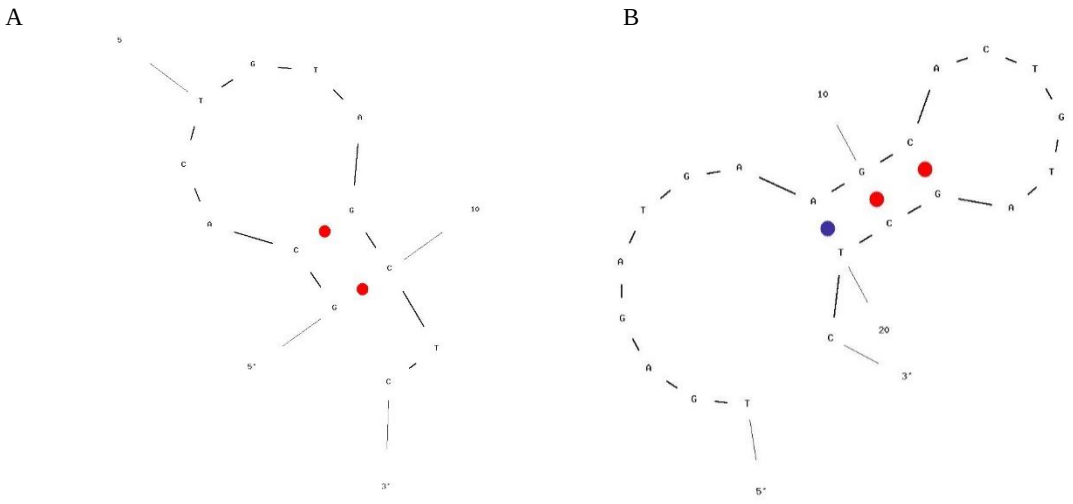

Figure 1 Folding simulation of the Tail(A) and Quenche(B)r strands using UNAFold and setting 50nM of oligonucleotide, 200mM of NaCl and 25°C as parameters.

Furthermore, the design of the probe is optimized on the free energy gained from the displacement assay (ΔG_{disp}) and is calculated as:

$$\Delta G_{disp} = \Delta G_{hyb*Q/Tar} - \Delta G_{hyb*QF} \qquad \text{Equation 1}$$

where ΔG_{hyb}*Q/Tar and ΔG_{hyb}*QF are respectively the free energy of hybridization of the duplex formed by the Q*/Target and Q*/F* strands. Probes are optimized in order to have favourable ΔG_{disp} to enhance the target displacement.

The performance of the probe has been prior tested in solution. To obtain this information, the strands are labelled with a fluorophore and a quencher as reported in table 1. In this case, the displacement event is associated to a fluorescence recovery after quenching (TURN-ON mechanism Figure 8). Kinetics of hybridizations have been performed in solution mixing QF*probe with equimolar or 10-fold excess of target. As showed in Figure 2 the kinetics of hybridization depends on the target concentration added and the maximum recovery of fluorescence, due to complete target displacement, is achieved in 3-6 hours when the equimolar or excess of target is added into the solution.

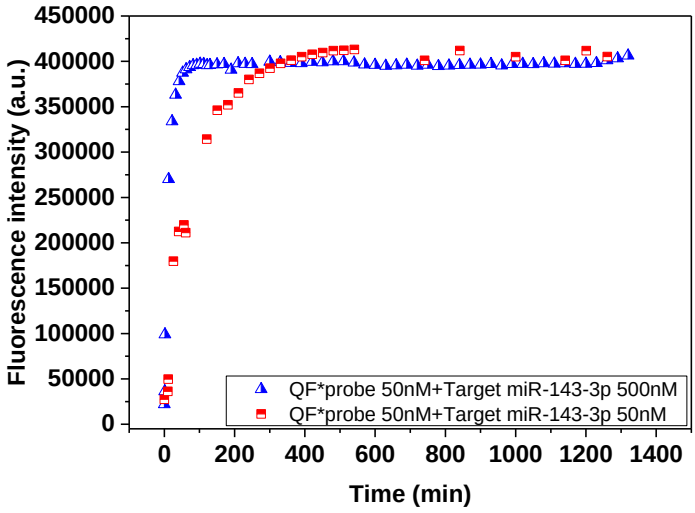

Figure 2 QF* probe/miR-143-3p kinetic of hybridizations

The binding curve is obtained by plotting the fraction of bound QF* probe (alpha) versus quencher (Q*) concentration (Figure 3 A). Assuming an independent and equivalent sites model, the curve fitting

provides the binding constant (kb) and stoichiometry. The data confirms that the strands association is very high kb about $1.6*10^{10}M^{-1}$ and 1:1 ratio stoichiometry.

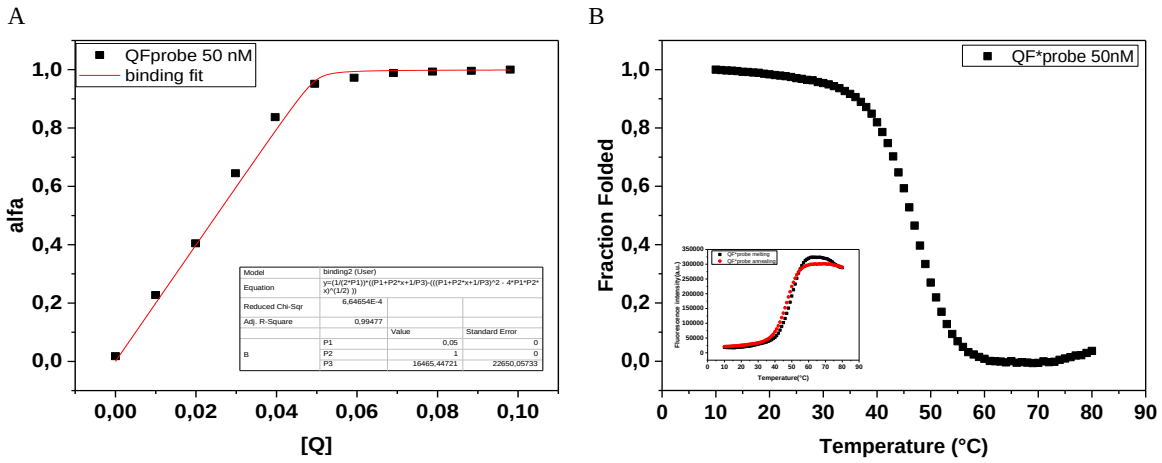

Figure 3 A)Fluorescence quenching titration to calculate kb of the probe. The stoichiometric ratio was determined by the intersection point of two straight lines extended, respectively, from the initial linear part and the plateau part of the titration curve. B) Melting profile, in the inset QF*probe annealing and melting curve

The melting profile is fully reversible at 50nM (Figure 3inset) and no significant hysteresis is observed between heating or cooling scans. The melting temperature is 47°C as predicted by OligoAnalyzer (Figure 3B; Table 1).

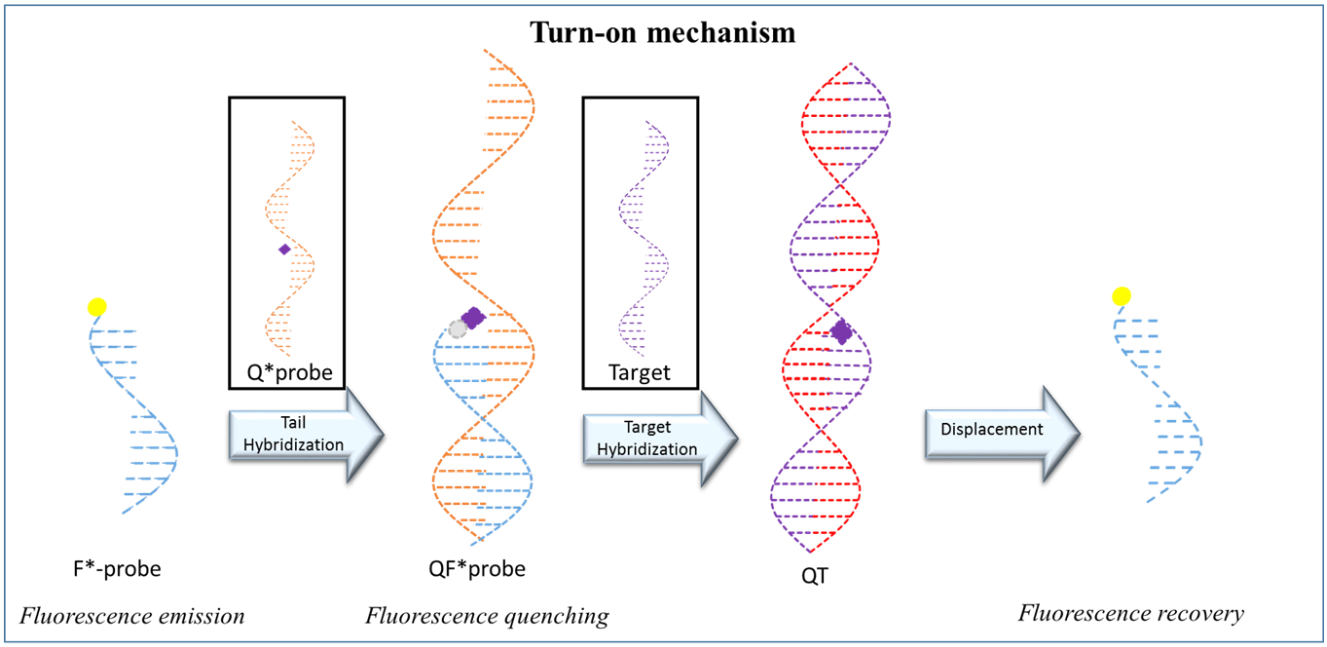

Figure 4 Mechanism of target detection used to analyse the probe in solution and in bulk

Bulk studies are carried out to optimize the probe density and to estimate the better PEGDA concentration capable to promote the free diffusion of oligonucleotides within the polymer network. These analyses confirm that the best analytical results are achieved using 1 μM of immobilized Tail and polymer concentration comprises between 10-15% of PEGDA. In particular, with the same amount of immobilized tails, the bulk with the highest concentration of PEGDA (narrower mesh size) allows a slow diffusion of *Qb strand and inefficient hybridization, as proved by the quick recovery of fluorescence following the quenching and the washing step (Figure 5). This event is ascribable to crowded environment into the bulk that obstacle the arrangement of a stable hybridization between the probe strands. By the contrast, in PEGDA 10%, the network is sufficiently wide to permit the formation of a stable complex between oligonucleotide strands, so that quenching is stable even after several washes. Increasing both probe density and polymer concentration, the hybridization kinetics, the quenching efficiency (Figure 6) and target detection (Figure 7) dramatically decrease due to the crowding effects and the hindered diffusion. This conclusion is also supported by additional studies made in our group. In particular, by swelling analysis and nuclear magnetic resonance (NMR) has been proved that increasing the PEGDA concentration the polymer mesh size decreases and diffusion is hindered (data not show). To sum up, these results obtained in bulk have allowed to set the best ratio between polymer and probe concentration in order to scale-down in microfluidics.

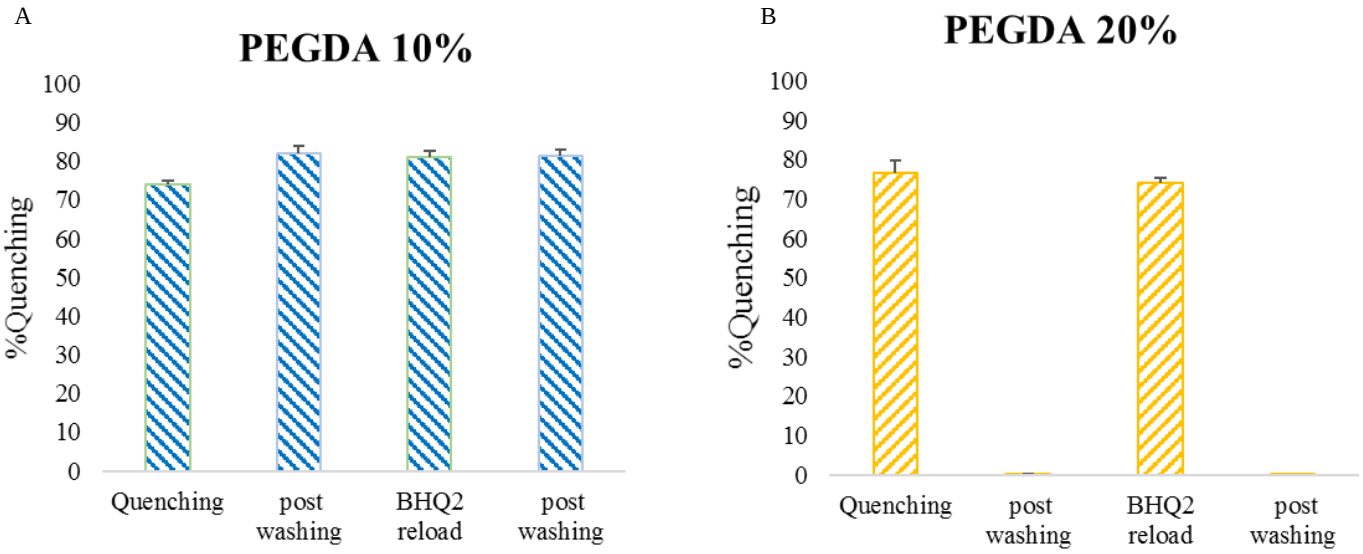

Figure 5 Quenching of fluorescence *QFb in PEGDA 10% (A) and 20% (B). Each step was collected after 3 days of incubation.

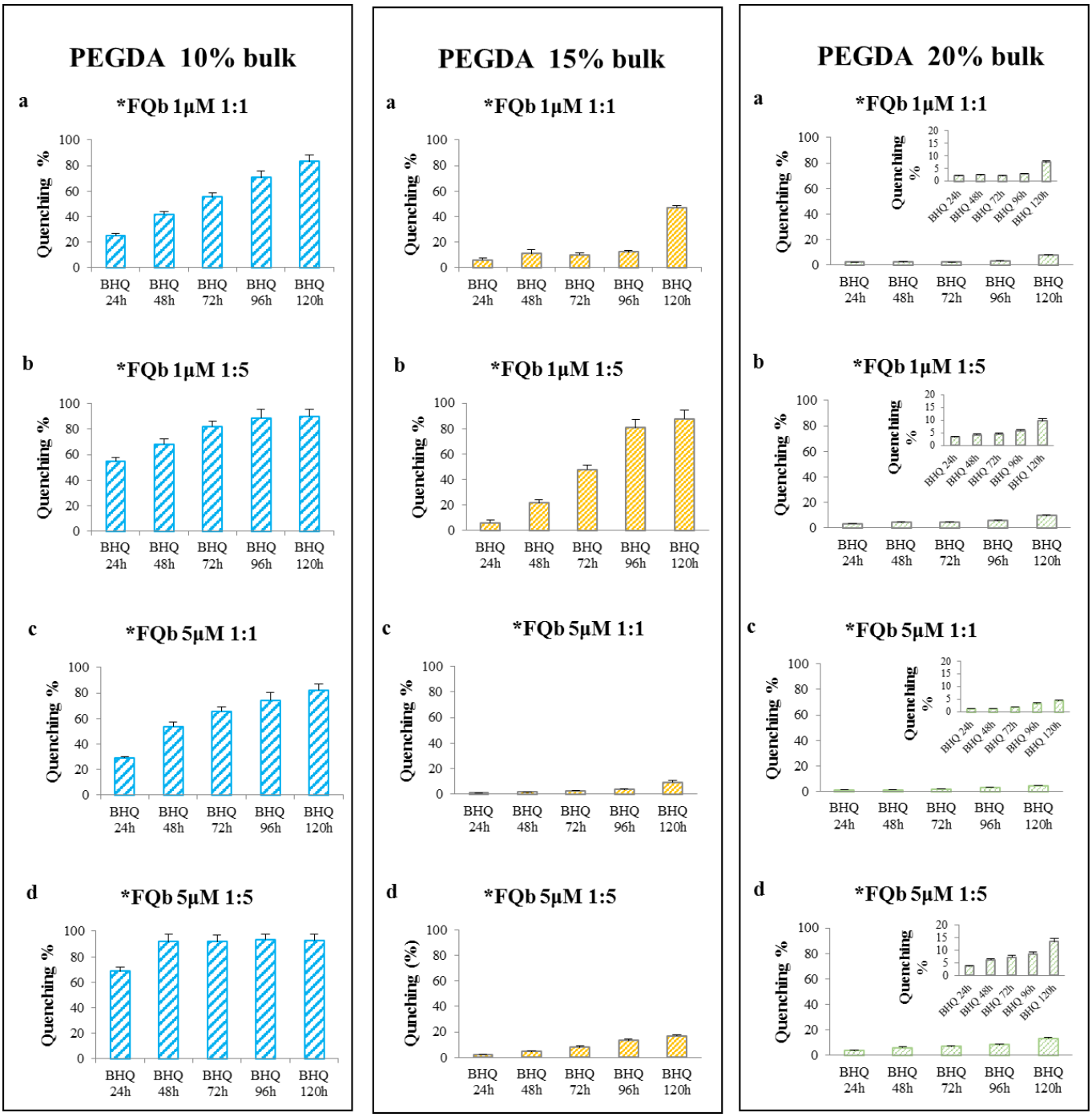

Figure 6 Kinetic of quenching in PEGDA 10%-15%-20% with several oligonucleotides concentrations: (a) F* 1µM- Q* 1x; (b) F* 1µM-Q* 5x; (c) F* 5µM-Q* 1x; (d) F* 5µM- Q* 5x.

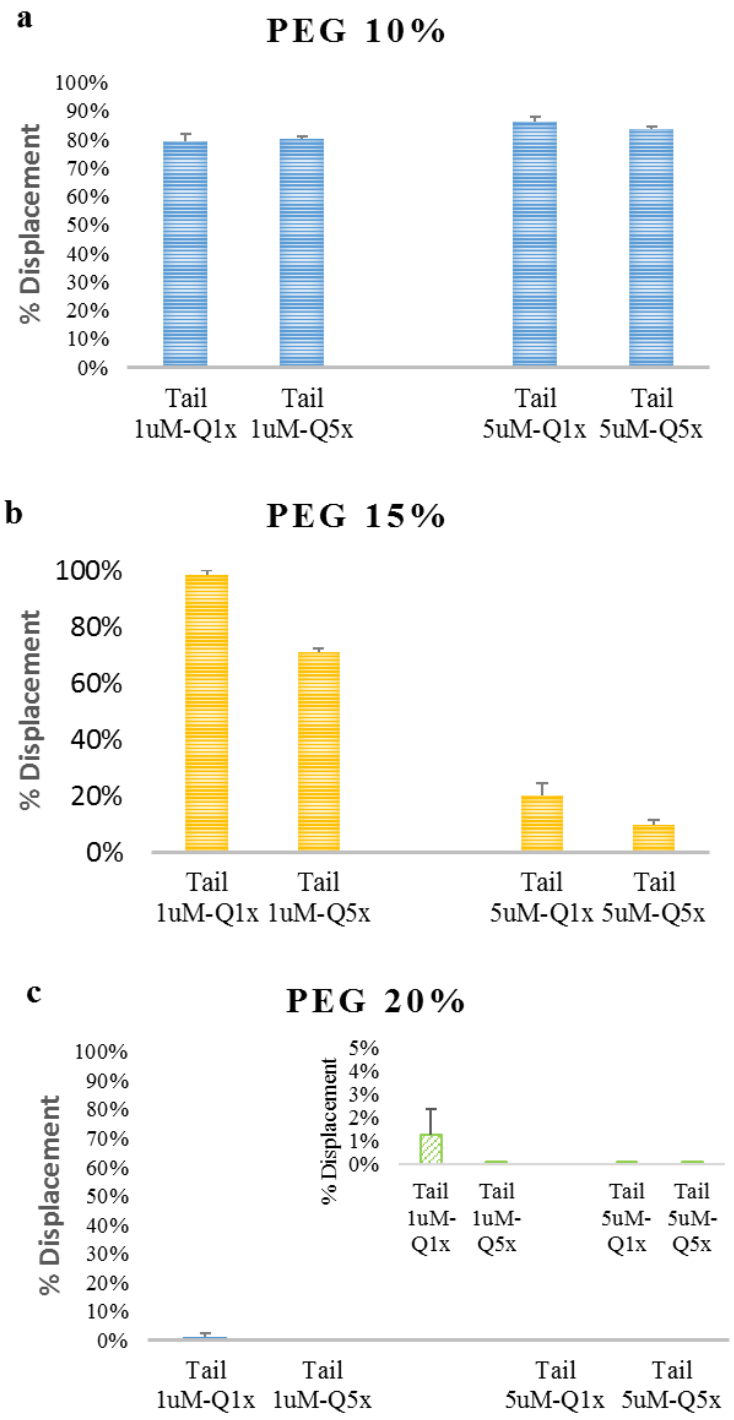

Figure 7 Bulk displacement efficiency

In Figure 8 is showed each single step of 3D hydrogel microparticles detection mechanism. In 3D-hydrogel microparticles, the target recognition is based on a double strand displacement assay integrating the probe sequence into the polymer network. However, in microparticles the target is quantified

measuring the depletion of fluorescence (TURN-OFF mechanism) (Figure 8B) instead of a recovery as already described. This is necessary, because of the UV- polymerization reaction in microfluidic induces a dramatically decrease of the reporter dye ATTO647N fluorescence. For this reason, in order to avoid mistake in target quantification, in 3D-hydrogel based assay the double strand probe consists of a short naked methacrylate DNA-Tail (T-DNA, 12 nt) covalently bound into the polymer networks during the polymerization and a longer partially complementary fluorescent DNA sequence (F-DNA, 21 nt), instead of *F- and Q*-probe respectively. In presence of target, the F-DNA strand hybridizes with it moving in the solution, with a consequent fluorescence decrease into the hydrogel.

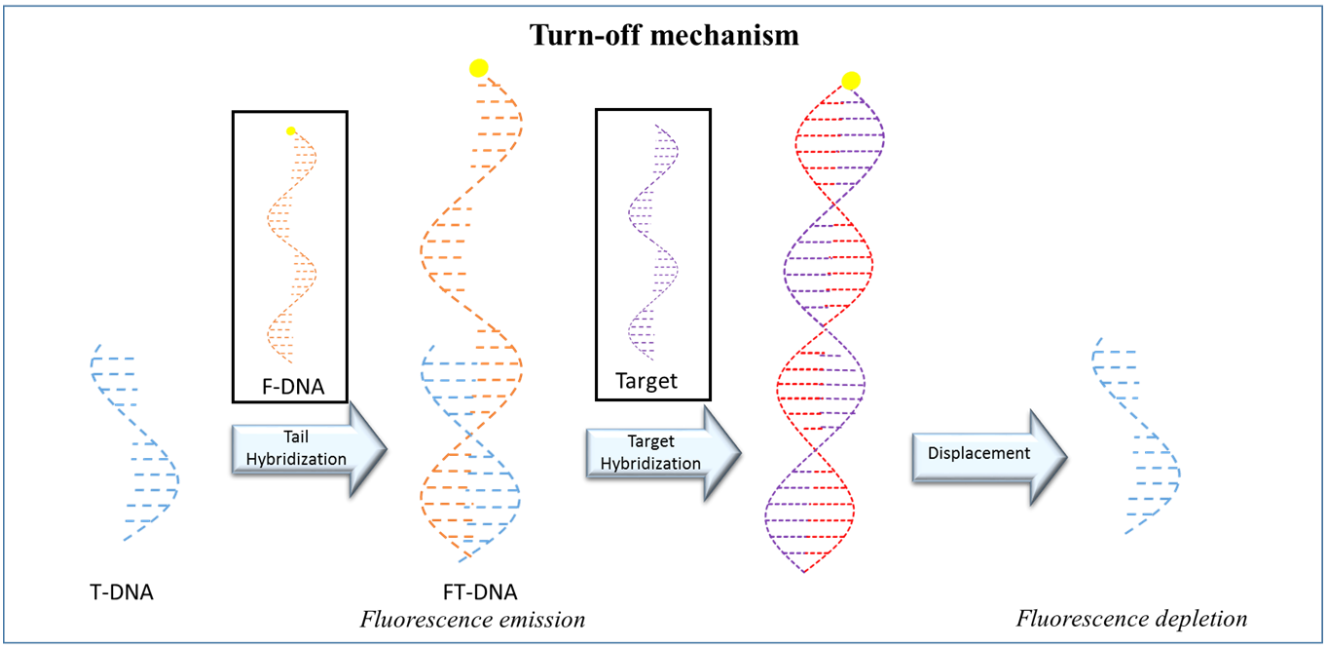

Figure 8 Target detection mechanism in 3D-hydrogel microparticles

3.2. Three-dimensional hydrogel microparticles synthesis

In Figure 9 A is showed an overview of the set-up used for the synthesis of 3Dhydrogel microparticles by microfluidics. The synthesis of hydrogels microparticles is performed using a T-junction microfluidic device (Figure 10 A-B). The LMO is injected as continuous phase, while the homogeneous water solution of PEGDA, methacrylate probes and photoinitiator is injected as dispersed phase.

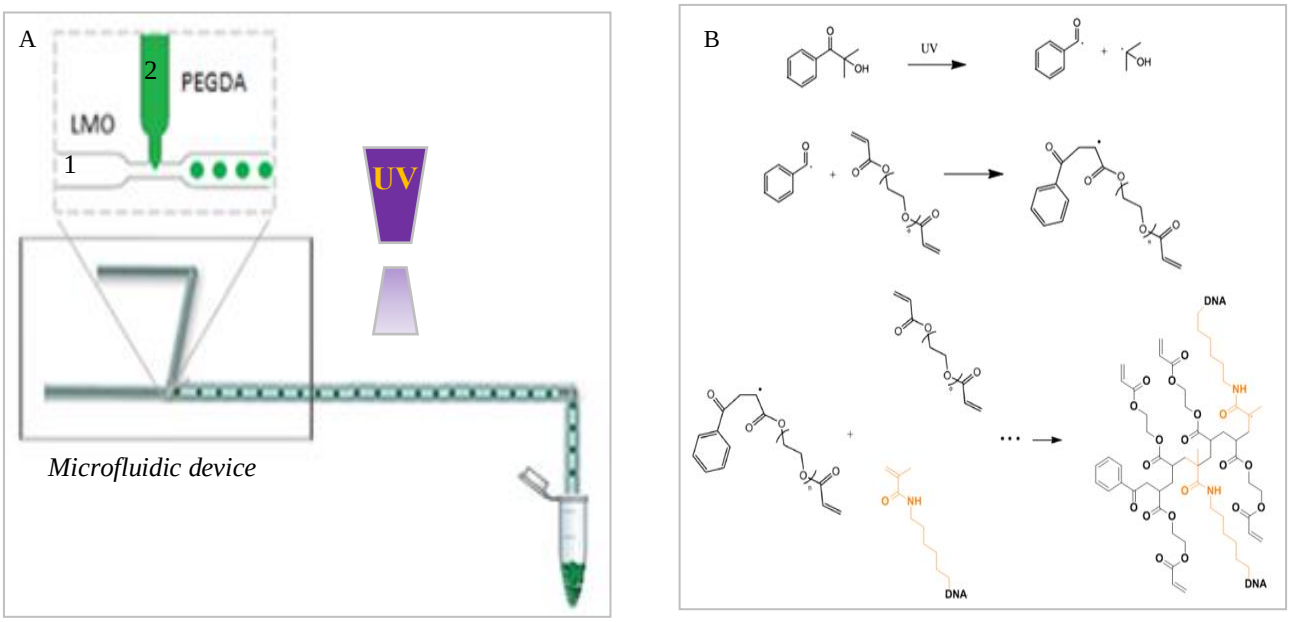

Figure 9 A) Schematic representation of microfluidic synthesis set-up for microparticles production; UV free radical photopolymerization between PEGDA and methacrylate oligonucleotide

Microfluidic parameters have been investigated and it has been found that a stable flow-rate regime is obtained when LMO flow rate (Qc) is between 6 and 10 μL/min and Capillary number (Ca) is in a limited range 0.05 ~ 0.20. In this condition the polymer phase is broken into a stable emulsion with sizes in the range of 46 to 110 μm (Figure 10 B). The droplets are then cross-linked by UV free radical polymerization reaction out of the chip (Figure 9 B). The reaction involves three basic steps. Firstly, in the *initiation reaction* step, darocur free radical is formed under UV light. Then, during the *propagation step*, the free radical comes into contact with the end of a PEGDA molecule and reacts with the carbon-carbon double bond in the acrylate functional group. This step produces a second free radical species,

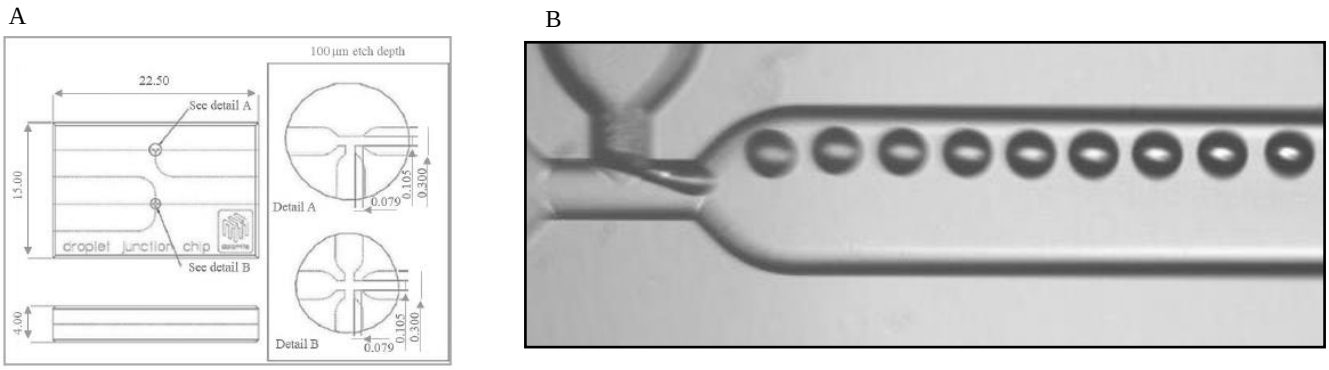

Figure 10 A) Geometry and size of the Dolomite chip; B)Droplet generation by microfluidic T-junction device

which can go on to react with more PEGDA polymers and/or methacrylate oligonucleotide species, propagating the crosslink until termination process occurs.

Morphological analysis confirms that microparticles are monodisperse and spherical, with a diameter of about 80 μm (Figure 11 A-B). Moreover, microparticles are homogeneously functionalized into the whole 3D polymer as is showed in the images collected by CLSM, after hybridization step with the complementary fluorescent strand (Figure 13 B-II).

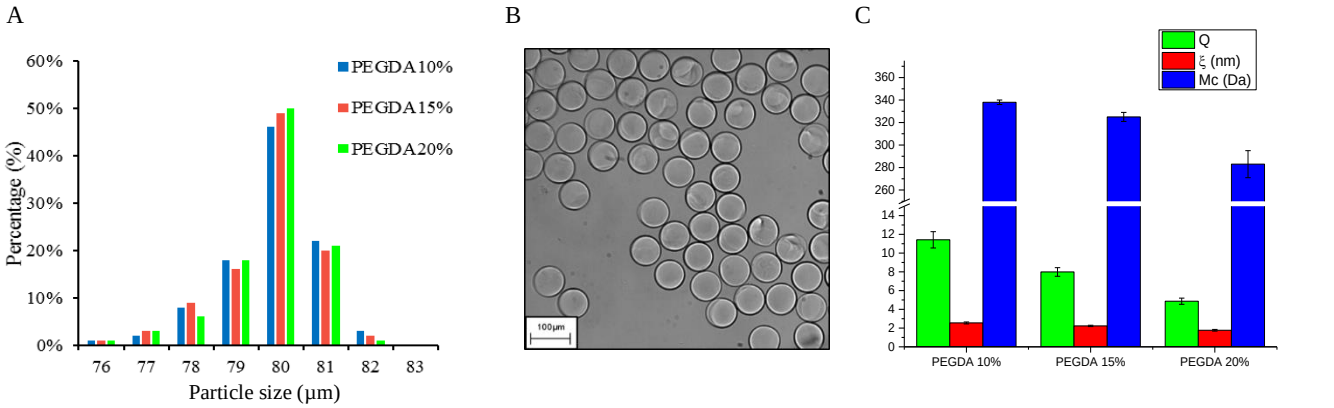

Figure 11 A)Size distribution of functionalized microparticles (PEGDA 10%, 15%, 20%) w/v); B) Optical image of monodisperse microparticles; Swelling parameters (Q, ξ, Mc) for different polymer concentrations

Microparticles swelling characterization proves that increasing the concentration of monomer the swelling ratio (Q) decreases from 11.42 to 4.87, the molecular weight (Mc) diminishes from 338 to 283 Da, while the mesh size(ξ) in the range of 2.55-1.77 nm is achieved. Diffusion studies on hydrogels microparticles have been carried out to simulate the behaviour and diffusion of biological molecules. In particular, here are showed the diffusion analysis of the target miR-143-3p and the proteins BSA, following the fluorescence intensity changes by CLSM images. In Figure 12 A is reported a plot profile of fluorescence intensities of the oligonucleotide. Probe diffusion is not hindered (Da>>1) and in few minutes the process is completed. The diffusion behaviour of probes is measured as ratio between fluorescence intensity (I) and maximum fluorescence reached in the microparticles (I_{MAX}) versus time and fitting following Equation 2.

$$\frac{I}{I_{MAX}} = 1 - e^{-\frac{t}{\tau}} \qquad \text{Equation 2}$$

where τ is the extrapolated value that represents the time required to achieve 67% of maximum intensity. In such a way, τ is calculated from the curves and corresponds to 5.7 ± 0.3 min for the oligonucleotide and 28.4 ± 1.0 for the BSA. Consequently, the oligonucleotide diffusion coefficient (D) into the hydrogel microparticle is $26.6 \cdot 10^{-8}$ cm^2/s. The value measured is comparable to that observed for free oligonucleotide in solution ($115 \cdot 10^{-8}$ cm^2/s for size of 23mer[59]). This result confirms that the 3D hydrogel structure is comparable to free solution and works as molecular filter hindering the diffusion of bigger molecules like proteins.

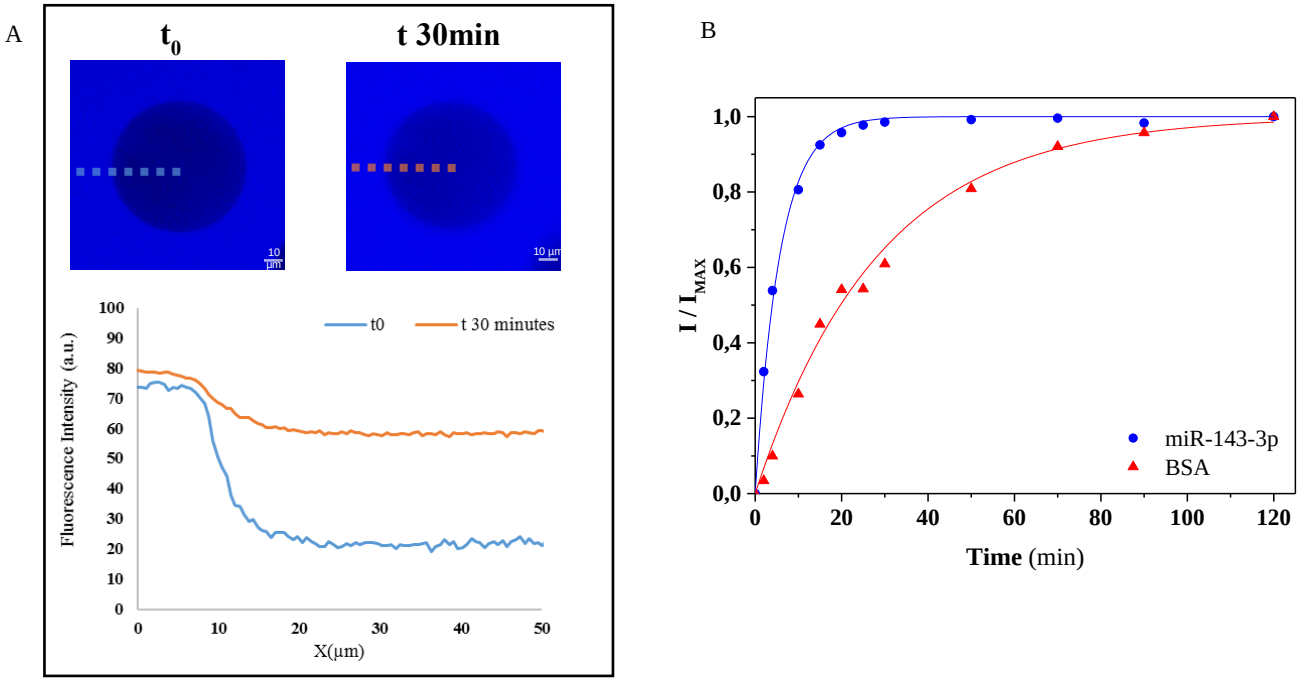

Figure 12 A) Plot profile of fluorescence intensity of Oligonucleotide diffusion in microparticles. B) Time lapse of fluorescence intensity (I/I_{max}) of miR-143-3p and BSA. All values reported show a standard deviation of 10%.

3.3. Assay set-up and human serum analysis

The assay is easily performed adding about 300 3D-hydrogel microparticles to the sample and incubating until equilibrium is reached. Then fluorescence depletion is measured and the target concentration is quantified based on the calibration curve.

Analysing the fluorescence images collected during the various preparation steps results that 3D-functionalized hydrogels have very low fluorescence background after microfluidic synthesis (Figure

133 A-B I). Moreover, the fluorescent signal significant increases after incubation with F-DNA (Figure 133-B II), this confirms that hybridization has occurred.

When the target is spiked into the solution, it quickly diffuses into the 3D hydrogel network and driven by the favourable ΔG of displacement, it hybridizes with the complementary F-DNA strand diffusing out of the hydrogel with consequent decrease of the hydrogel fluorescence (Figure 13A-B III). Furthermore, 3D-hydrogel microparticles can be directly added to the human sample without any previous oligonucleotide purification or amplification. The target is easily quantified reading the fluorescence depletion associated with the displacement event and as shown in Figure 13A-B IV the displacement in human serum is comparable to that in hybridization buffer.

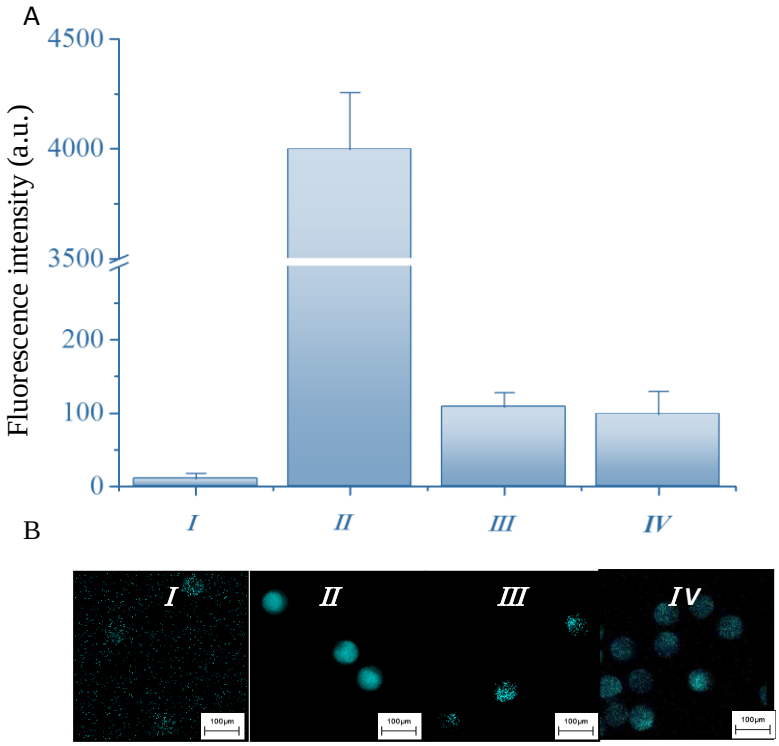

Figure 13:(a)Fluorescence intensity measured during the hydrogel based assay setup and (b) the corresponding CLSM images. In particular, the figure shows the fundamental steps involved in the target detection: (I) after the synthesis of functionalized hydrogel; (II) when the fluorescent DNA strand was added; (III) in presence of the target in hybridization buffer and (IV) in human serum.

3.4. Assay sensitivity and specificity

Under the optimized experimental conditions, the analytical performances of the proposed 3D-hydrogel microparticles are showed in Figure 14. The depletion of fluorescence in response to the miR-143-3p

concentration is shown in Figure 14A. For each target concentration images are collected (Figure 14C) and analysed. The fluorescence signal decreases gradually increasing the target concentration and the efficient working range is comprised between 10^{-6} to 10^{-12} M. Complete displacement, about 93.1±0.76%, is achieved testing 2 μM of mir-143-3p. Decreasing the target concentration to 500 pM, we reach 73±5.09% of displacement, which decreases until 3.6±1.08% at the lower concentration tested (Figure 14C). Moreover, the limit of detection (LOD) and limit of quantification (LOQ) are calculated and their values are respectively 30 pM and 91 pM. (Table 3).

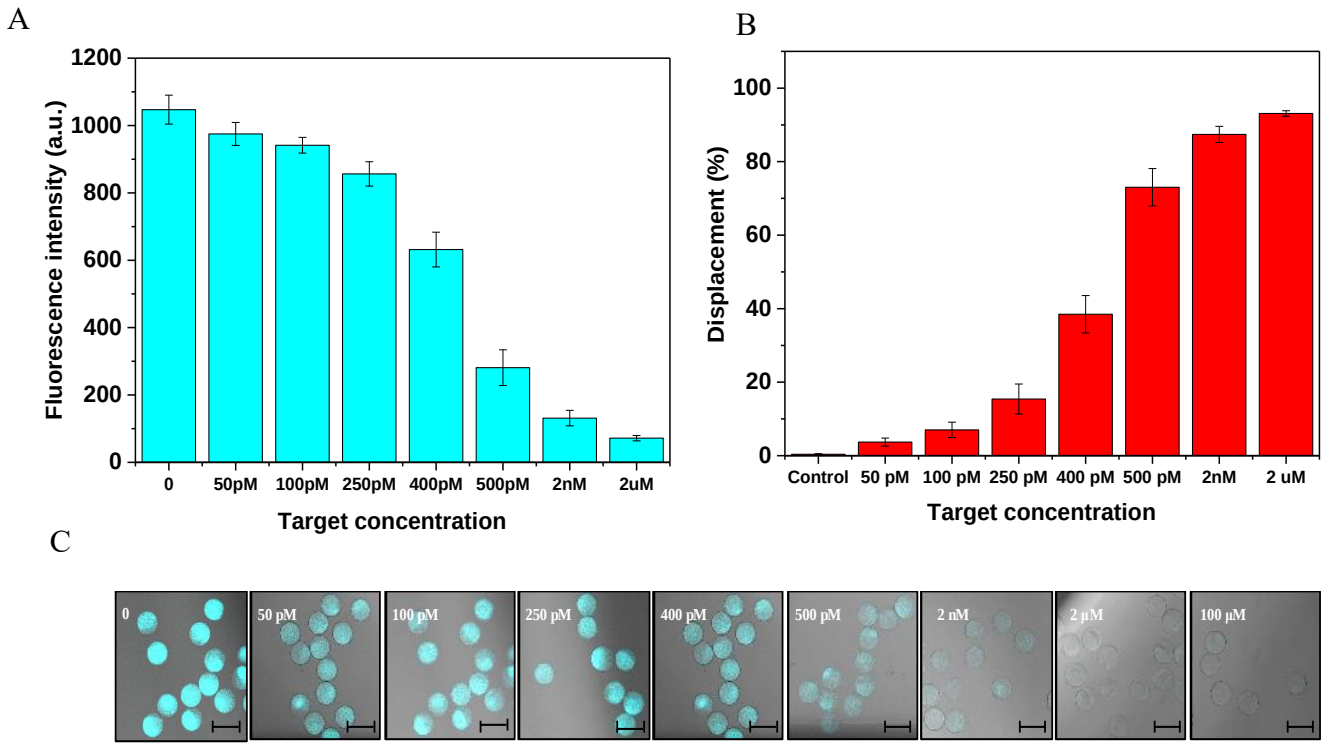

Figure 14 (A) MiR143-3p capture efficiency by Hydrogel beads assay and (B) corresponding fluorescence intensity turn-off (C) Images collected by CLSM for the target concentration analysed (Scale bars: 100 μm).

Table 3 Data analysis for 3D-hydrogel microparticles assay

	SE	**SD**	**R- sq**	**Slope**	**LOD (pM)**	**LOQ (pM)**
3D-hydogel microparticle	3.09598	5.3623	0.9987	0.5868	30.156	91.382

Additionally, specificity studies have been carried out on the 3D-hydrogels. To investigate the assay specificity, 3D-hydrogel microparticles are put in contact with 500nM of miR-21, then images are collected (Figure 15B) and analysed. From the fluorescence intensity measurements (Figure 15A) result that in presence of high concentration of non-specific microRNA (Table 1) a slight fluorescence intensity decrease is measured when compared with the control. Nevertheless, 500nM of miR-143-3p achieve a much stronger response compared to the blank. Furthermore, any interference in target displacement is observed when combined solutions of miR-143-3p/miR21 500nM (1:1) are tested. This suggests that the designed probe has good selectivity toward miR-143-3p and the hydrogel microparticles are capable to detect the target even in presence of crowded oligonucleotide solutions.

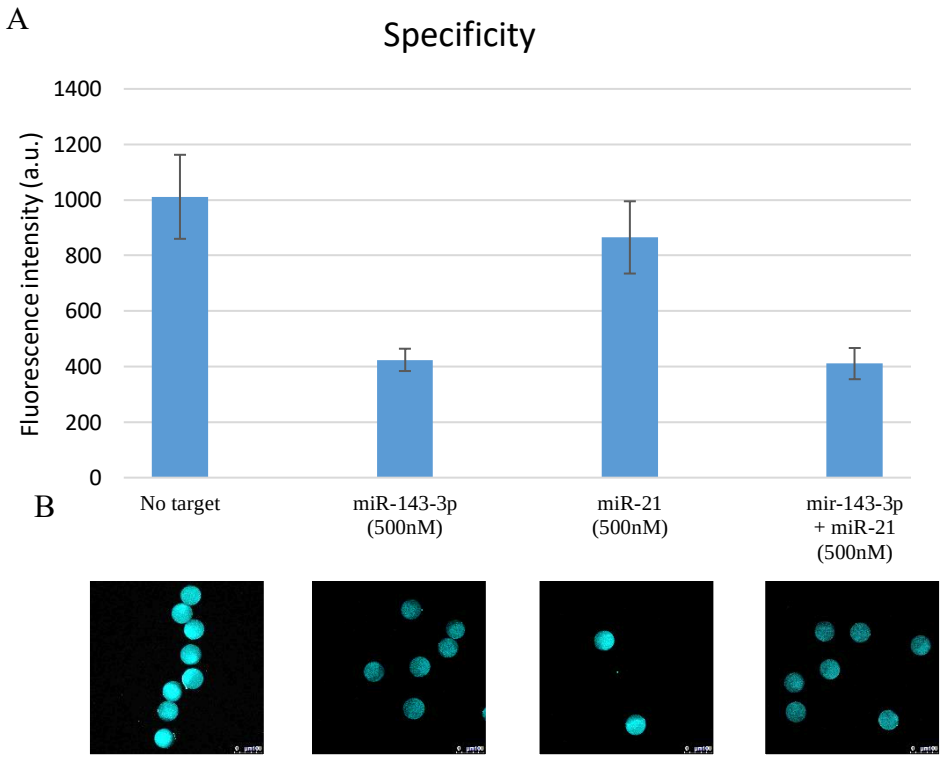

Figure 15 Specificity of 3D-hydrogel microparticles.

4. CONCLUSION

The purpose of this study is to combine the enhanced properties of 3D engineered hydrogel material with the necessity of the health field. In particular, we focused on the design of an assay for microRNA detection based on double strand displacement assay confined into a small hydrogel particle volume.

The parameters affecting the sensitivity and the diffusion have been studied both in solution and bulk, and the best ratio between probe and polymer concentration has been selected. Based on this consideration we have synthesized 3-D hydrogel microparticles with PEGDA 15% and T-DNA 1μM in microfluidics.

Tests in complex matrix as in human serum, fulfilled with CLSM, have demonstrated the capability of our microparticles to be used as a molecular filter allowing the target diffusion and excluding the majority of big molecules. Indeed, the detection system resulted to be very efficient with a displacement percentage of ~90%, comparable to that observed in buffer solution. The assay has also proved good sensitivity with LOD of 30 pM and good specificity.

The assay has shown several advantages compared to conventional techniques. Indeed, hydrogels are synthetized and functionalized in microfluidics in higher concentration reducing time and cost of production. They might be directly mixed into the human sample without any previous oligonucleotide purification or amplification resulting time saving and easy to manage. Furthermore, the target is easily quantified reading the fluorescence depletion associated with the displacement event avoiding complex analysis interpretations.

Therefore, 3D-hydrogel microparticles-based assay represents a highly promising method for developing low cost, sensitive routine test and non-invasive analytical tests.

REFERENCE

1. Irving, D., Gong, P. & Levicky, R. DNA Surface Hybridization: Comparison of Theory and Experiment. *J. Phys. Chem. B* **114,** 7631–7640 (2010).
2. Ariga, K., Mori, T., Nakanishi, W. & Hill, J. P. Solid surface vs. liquid surface: nanoarchitectonics, molecular machines, and DNA origami. *Phys. Chem. Chem. Phys.* **19,** 23658–23676 (2017).
3. Kannoujia, D. K., Ali, S. & Nahar, P. Single-step covalent immobilization of oligonucleotides onto solid surface. *Anal. Methods* **2,** 212 (2010).
4. Tjong, V., Tang, L., Zauscher, S. & Chilkoti, A. "Smart" DNA interfaces. *Chem. Soc. Rev.* **43,** 1612–1626 (2014).
5. Liu, C. *et al.* An electrochemical DNA biosensor for the detection of Mycobacterium tuberculosis, based on signal amplification of graphene and a gold nanoparticle–polyaniline nanocomposite. *Analyst* **139,** 5460–5465 (2014).
6. Gong, Q., Wang, Y. & Yang, H. A sensitive impedimetric DNA biosensor for the determination of the HIV gene based on graphene-Nafion composite film. *Biosens. Bioelectron.* **89,** 565–569 (2017).
7. Wang, J., Liu, G., Rasul Jan, M. & Zhu, Q. Electrochemical detection of DNA hybridization based on carbon-nanotubes loaded with CdS tags. *Electrochem. commun.* **5,** 1000–1004 (2003).
8. Hwang, B. H., Shin, H. H. & Cha, H. J. Optimization of DNA microarray biosensors enables rapid and sensitive detection. *Biotechnol. Bioprocess Eng.* **22,** 469–473 (2017).
9. Audrey Sassolas, Béatrice D. Leca-Bouvier, and & Blum*, L. J. DNA Biosensors and Microarrays. (2007). doi:10.1021/CR0684467
10. Kouassi, G. K. & Irudayaraj, J. Magnetic and Gold-Coated Magnetic Nanoparticles as a DNA Sensor. doi:10.1021/ac051621j
11. Ravalli, A. & Marrazza, G. Gold and Magnetic Nanoparticles-Based Electrochemical Biosensors for Cancer Biomarker Determination. *J. Nanosci. Nanotechnol.* **15,** 3307–3319 (2015).
12. Magnesphere, S., Particles, P. & Wi, M. Certificate of Analysis Instructions for use of this product can be found in the MagneSphere ® Magnetic Separation Products Technical Bulletin # TB246 , available online at : www.promega.com/tbs This lot passes the following Quality Control specifications. 5482 (2011).
13. Cao, Y. W. C., Jin, R. & Mirkin, C. A. Nanoparticles with Raman spectroscopic fingerprints for DNA and RNA detection. *Science (80-.).* **297,** 1536–1540 (2002).
14. Le Goff, G. C., Srinivas, R. L., Hill, W. A. & Doyle, P. S. Hydrogel microparticles for biosensing. *Eur. Polym. J.* **72,** 386–412 (2015).
15. Van Nguyen, K. & Minteer, S. D. DNA-functionalized Pt nanoparticles as catalysts for chemically powered micromotors: toward signal-on motion-based DNA biosensor. *Chem. Commun.* **51,** 4782–4784 (2015).
16. Sun, J. *et al.* DNA biosensor-based on fluorescence detection of E. coli O157:H7 by Au@Ag nanorods.

Biosens. Bioelectron. **70,** 239–245 (2015).

17. Yola, M. L., Eren, T. & Atar, N. A novel and sensitive electrochemical DNA biosensor based on Fe@Au nanoparticles decorated graphene oxide. *Electrochim. Acta* **125,** 38–47 (2014).
18. Klein, J. C. *et al.* Multiplex pairwise assembly of array-derived DNA oligonucleotides. *Nucleic Acids Res.* **44,** e43–e43 (2015).
19. Srinivas, R. L., Chapin, S. C. & Doyle, P. S. Aptamer-Functionalized Microgel Particles for Protein Detection. *Anal. Chem.* **83,** 9138–9145 (2011).
20. Daniel, C., Roupioz, Y., Gasparutto, D., Livache, T. & Buhot, A. Solution-Phase vs Surface-Phase Aptamer-Protein Affinity from a Label-Free Kinetic Biosensor. *PLoS One* **8,** e75419 (2013).
21. Wong, I. Y. & Melosh, N. A. An electrostatic model for DNA surface hybridization. *Biophys. J.* **98,** 2954–63 (2010).
22. Traeger, J. C. & Schwartz, D. K. Surface-Mediated DNA Hybridization: Effects of DNA Conformation, Surface Chemistry, and Electrostatics. *Langmuir* **33,** 12651–12659 (2017).
23. Peterson, A. W., Heaton, R. J. & Georgiadis, R. M. The effect of surface probe density on DNA hybridization. *Nucleic Acids Res.* **29,** 5163–5168 (2001).
24. Macedo, L. J. A., Miller, E. N. & Opdahl, A. Effect of Probe–Probe Distance on the Stability of DNA Hybrids on Surfaces. *Anal. Chem.* **89,** 1757–1763 (2017).
25. Kimura-Suda, H., Petrovykh, D. Y., Tarlov, M. J. & Whitman, L. J. Base-Dependent Competitive Adsorption of Single-Stranded DNA on Gold. *J. Am. Chem. Soc.* **125,** 9014–9015 (2003).
26. Schmitt, T. J. & Knotts, T. A. Thermodynamics of DNA hybridization on surfaces. *J. Chem. Phys.* **134,** 205105 (2011).
27. Steel, A. B., Levicky, R. L., Herne, T. M. & Tarlov, M. J. Immobilization of Nucleic Acids at Solid Surfaces: Effect of Oligonucleotide Length on Layer Assembly. *Biophys. J.* **79,** 975–981 (2000).
28. Monserud, J. H. & Schwartz, D. K. Mechanisms of Surface-Mediated DNA Hybridization Mechanisms of Surface-Mediated DNA Hybridization. *ACS Nano* **8,** 4488–4499 (2014).
29. Nimse, S. *et al.* Immobilization Techniques for Microarray: Challenges and Applications. *Sensors* **14,** 22208–22229 (2014).
30. Kumacheva, E., Kalinina, O. & Lilge, L. Three-Dimensional Arrays in Polymer Nanocomposites. *Adv. Mater.* **11,** 231–234 (1999).
31. Jang, J.-H., Dendukuri, D., Hatton, T. A., Thomas, E. L. & Doyle, P. S. A Route to Three-Dimensional Structures in a Microfluidic Device: Stop-Flow Interference Lithography. *Angew. Chemie Int. Ed.* **46,** 9027–9031 (2007).
32. Ravan, H., Kashanian, S., Sanadgol, N., Badoei-Dalfard, A. & Karami, Z. Strategies for optimizing DNA hybridization on surfaces. *Anal. Biochem.* **444,** 41–46 (2014).
33. Chen, M. *et al.* A sensitive electrochemical DNA biosensor based on three-dimensional nitrogen-doped

graphene and Fe3O4 nanoparticles. *Sensors Actuators B Chem.* **239,** 421–429 (2017).

34. Kong, B. *et al.* Bio-inspired porous antenna-like nanocube/nanowire heterostructure as ultra-sensitive cellular interfaces. *NPG Asia Mater.* **6,** 117 (2014).
35. Yang, Y., Asiri, A. M., Du, D. & Lin, Y. Acetylcholinesterase biosensor based on a gold nanoparticle–polypyrrole–reduced graphene oxide nanocomposite modified electrode for the amperometric detection of organophosphorus pesticides. *Analyst* **139,** 3055 (2014).
36. Appleyard, D. C., Chapin, S. C., Srinivas, R. L. & Doyle, P. S. Bar-coded hydrogel microparticles for protein detection: Synthesis, assay and scanning. *Nat. Protoc.* **6,** 1761–1774 (2011).
37. Choi, N. W. *et al.* Multiplexed detection of mRNA using porosity-tuned hydrogel microparticles. *Anal. Chem.* **84,** 9370–9378 (2012).
38. Chapin, S. C., Appleyard, D. C., Pregibon, D. C. & Doyle, P. S. Rapid microRNA profiling on encoded gel microparticles. *Angew. Chemie - Int. Ed.* **50,** 2289–2293 (2011).
39. Peppas, N. A., Hilt, J. Z., Khademhosseini, A. & Langer, R. Hydrogels in Biology and Medicine: From Molecular Principles to Bionanotechnology. *Adv. Mater.* **18,** 1345–1360 (2006).
40. Hoffman, A. S. Hydrogels for biomedical applications. *Adv. Drug Deliv. Rev.* **64,** 18–23 (2012).
41. Battista, E., Causa, F. & Netti, P. Bioengineering Microgels and Hydrogel Microparticles for Sensing Biomolecular Targets. *Gels* **3,** 20 (2017).
42. Zalipsky, S. & Harris, J. M. in 1–13 (1997). doi:10.1021/bk-1997-0680.ch001
43. Ulijn, R. V. *et al.* Bioresponsive hydrogels. *Mater. Today* **10,** 40–48 (2007).
44. Hagel, V., Haraszti, T. & Boehm, H. Diffusion and interaction in PEG-DA hydrogels. *Biointerphases* **8,** 1–9 (2013).
45. Wang, J.-T., Wang, J. & Han, J.-J. Fabrication of Advanced Particles and Particle-Based Materials Assisted by Droplet-Based Microfluidics. *Small* **7,** 1728–1754 (2011).
46. Celetti, G., Natale, C. Di, Causa, F., Battista, E. & Netti, P. A. Functionalized poly(ethylene glycol) diacrylate microgels by microfluidics: In situ peptide encapsulation for in serum selective protein detection. *Colloids Surfaces B Biointerfaces* **145,** 21–29 (2016).
47. Pregibon, D. C., Toner, M. & Doyle, P. S. Multifunctional encoded particles for high-throughput biomolecule analysis. *Science (80-.).* **315,** 1393–1396 (2007).
48. Hammond, S. M. An overview of microRNAs. *Adv. Drug Deliv. Rev.* **87,** 3–14 (2015).
49. Cai, Y., Yu, X., Hu, S. & Yu, J. A Brief Review on the Mechanisms of miRNA Regulation. *Genomics. Proteomics Bioinformatics* **7,** 147–154 (2009).
50. Wang, G.-K. *et al.* Circulating microRNA: a novel potential biomarker for early diagnosis of acute myocardial infarction in humans. *Eur. Heart J.* **31,** 659–666 (2010).
51. Wang, J., Chen, J. & Sen, S. MicroRNA as Biomarkers and Diagnostics. *J. Cell. Physiol.* **231,** 25–30 (2016).

52. Ferracin, M. & Negrini, M. Micromarkers 2.0: an update on the role of microRNAs in cancer diagnosis and prognosis. *Expert Rev. Mol. Diagn.* **15,** 1369–1381 (2015).
53. Waller, R. *et al.* Serum miRNAs miR-206, 143-3p and 374b-5p as potential biomarkers for amyotrophic lateral sclerosis (ALS). *Neurobiol. Aging* **55,** 123–131 (2017).
54. Rowland, L. P. & Shneider, N. A. Amyotrophic Lateral Sclerosis. *N. Engl. J. Med.* **344,** 1688–1700 (2001).
55. Brooks, B. R., Miller, R. G., Swash, M. & Munsat, T. L. El Escorial revisited: Revised criteria for the diagnosis of amyotrophic lateral sclerosis. *Amyotroph. Lateral Scler. Other Mot. Neuron Disord.* **1,** 293–299 (2000).
56. Costa, J., Swash, M. & de Carvalho, M. Awaji Criteria for the Diagnosis of Amyotrophic Lateral Sclerosis. *Arch. Neurol.* **69,** 1410 (2012).
57. Geevasinga, N. *et al.* Diagnostic criteria in amyotrophic lateral sclerosis: A multicenter prospective study. *Neurology* **87,** 684–90 (2016).
58. Peppas, N. A., Bures, P., Leobandung, W. & Ichikawa, H. Hydrogels in pharmaceutical formulations. *Eur. J. Pharm. Biopharm.* **50,** 27–46 (2000).
59. Zenk, J. *et al.* Stable DNA-based reaction-diffusion patterns. *RSC Adv.* **7,** 18032–18040 (2017).

CHAPTER 6

CONCLUSIONS AND FUTURE PERSPECTIVES

Throughout this thesis, we have developed and tested a hydrogel microparticles platform, that has proved to be attractive for biosensing applications.

In particular, we have demonstrated that superior materials and optimized oligonucleotide probe design are successfully combined to produce engineered hydrogel microparticles for circulating biomarker detection.

Compared to gold standard technologies, our hydrogels avoid all the sample preliminary manipulation steps as the purification, extraction or amplification, often cause of quantification errors in these assays. In addition, the limit of detection and the specificity are improved compared to the current amplification-free assay and the time of analysis are reduced, especially for molecular beacons-microgels assays.

Therefore, PEG-based hydrogels represent ideal materials for this purpose combining broad range of molecular weight, chemical functionalities and biocompatibility. Microparticles have been synthetized with different chemical strategy both in batch and microfluidics and their structural characteristics have been tuned for the purpose.

The hydrogel solution-like property enhances both the thermodynamic association constants and the kinetics (association rate k_{on}) for oligonucleotides, while its anti-fouling property imparts selectivity in biological fluids. Moreover, the fluorescent signal confinement of the specific probe into small volume allows to directly detect target with improved sensitivity compared to the common assay.

The design of specific oligonucleotide probe, in addition, consents to reach appealing sensitivity, single nucleotide specificity and rapid time of analysis. Moreover, all the hydrogels used in this thesis share the capability of work directly in human fluids due to the Poly(ethylene)glycol antifouling capability.

In this thesis we have highlighted the potentiality of hydrogel particles technologies and presented some proof of principle applications.

In particular, in *chapter 2* we have designed a heterogeneous assay by using PEG microgels armed with short fluorescent DNA double strand probes for the specific detection of viral microRNA biomarker by toehold-mediated strand displacement assay.

The assay is specific toward the selected target and the toehold mediated strand assay has improved the kinetics of recovery compared to perfect double strand probe.

The target has been detected with scalable sensitivity down to 150 aM and over a wide dynamic range (from nM to aM). Moreover, we have proved that microgel assay can be finely measured by the means of common laboratory equipment, as fluorimeter and flow cytometer, without loss in sensitivity.
Additionally, we have proved that our technology is very stable over a long period of storage, overcoming one of the main limitations that until now have delayed the marketing of hydrogel bioassay kits.

In *chapter 3* we have synthetized PEG-microgels functionalized with molecular beacons for the detection of miR-21. Molecular beacons have been immobilized into the hydrogel polymer network tuning the probe density and the length of the probe. Studies have proved that fluorescence background is reduced when molecular beacons are immobilized into solution-like environments as those generated in PEG hydrogel matrix, improving both the sensitivity and the specificity of the assay.
We have optimized the molecular beacon probe density and the concentration of microgels achieving down to fM sensitivity. The assay is specific toward single mutated target and the miR-21 is detected in 1 hour using only 20µL of sample. The solution-like environment within the microgel is capable to protect molecular beacons from the interfering proteins of the serum, indeed, the target detection results similar to those observed in PBS buffer.

In *chapter 4* the basis to detect long oligonucleotide sequences by microgel-based assay has been established. Microgels are functionalized with double strand or molecular beacon probes, specifically designed and tested versus two sequence with 70% of similarity.
Both probes have shown higher specificity in presence of the similar target free in solution and immobilized on the particle. The sensitivity is measured in pM order for ds-microgels, while mb-microgels have reached limit of detection down to pM. The assay time is additionally reduced for mb-microgels achieving complete target hybridization in 100 min.
The combination of the customized probes with the solution-like property of the hydrogel material and its capability to concentrate the fluorescence signal have allowed to develop sensitive and fast microgel assay for long oligonucleotide target.

In c*hapter* 5 3D engineered hydrogels for oligonucleotide detection have been developed by microfluidics. In particular, we have focused on the design of an assay for microRNA detection based on double strand displacement assay associated with fluorescence depletion event. The parameters affecting the sensitivity and the diffusion have been studied both in solution and bulk, and the best ratio between probe and polymer concentration has been selected.
The assay has proved good specificity and sensitivity with limit of detection of 30 pM. Tests in human serum have confirmed the capability of our microparticles to work as molecular filter allowing the target

diffusion and excluding interfering molecules. Moreover, the assay has shown several advantages compared to conventional techniques. Indeed, hydrogels are synthetized and functionalized in microfluidic in higher concentration reducing time and cost of production. They might be directly mixed into the human sample without any previous oligonucleotide purification or amplification resulting time saving and easy to manage, avoiding complex analysis interpretations.

This hydrogel based technology promises to be useful for *liquid biopsy* and *point-of-care* application widening the range of application not only in poor clinical settings. Furthermore, additional studies on real human samples and comparative analysis with gold standard techniques are still on-going to further validate the application in clinical routine of the hydrogel platform for oligonucleotide biomarkers detection.

Table 1 Technology properties of the hydrogel microparticles proposed in the thesis.

Technology	Probe	Target	LOD	Time	Sample volume	Complex fluid	Amplification
PEG-core/shell microgels	Double-strand probe	hcmv-miR-US4-5p	150aM	5 h	500µL	Yes	No
PEG-core/shell microgels	Molecular beacon	hsa-miR-21	10fM	1 h	20 µL	Yes	No
PEG-core/shell microgels	Double-strand probe	P1 P2	530pM 813pM	2-5 h	500 µL	Yes	No
PEG-core/shell microgels	Molecular beacon	P1 P2	1.32pM 1.06pM	1-2 h	20 µL	Yes	No
Microfluidics PEG-particles	Double strand probe	hsa-miR-143-3p	30pM	>5 h	500 µL	Yes	No

In the future, the possibility to detect also circulating DNA represents an appealing objective.

Therefore, the final goal of this project is the production of a microfluidic platform for in vitro, direct measurement of oligonucleotides circulating in biological fluids.

In particular, we foresee the possibility to accomplish a miniaturized system to directly analyze low volume of biological sample. Indeed, our major challenge is pointed toward the production of an integrated device for *liquid biopsy* application and *point-of-care* (POC) diagnostics.